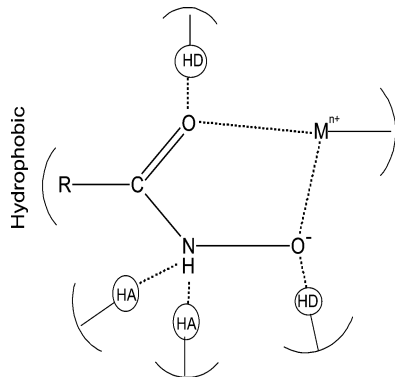


QSAR Studies on Hydroxamic Acids: A Fascinating Family of Chemicals with a Wide Spectrum of Activities

Satya P. Gupta*

Department of Applied Sciences, National Institute of Technical Teachers' Training and Research, Shamla Hills, Bhopal-462002, India



CONTENTS

1. Introduction	6427
2. Structure and Physicochemical Properties of Hydroxamic Acids	6427
3. Biological Activities of Hydroxamic Acids	6429
3.1. Inhibition of Highly Targeted Enzymes	6429
3.1.1. Urease	6429
3.1.2. Histone Deacetylases (HDACs)	6429
3.1.3. Lipoxygenases (LOXs)	6429
3.1.4. Matrix Metalloproteinases (MMPs)	6429
3.1.5. Tumor Necrosis Factor- α (TNF- α) Converting Enzyme (TACE)	6430
3.1.6. Carbonic Anhydrase (CA)	6430
3.2. Miscellaneous	6430
3.2.1. Ribonucleotide Reductase (RNR)	6430
3.2.2. Angiotensin-Converting Enzyme (ACE)	6430
3.2.3. Peptide Deformylase (PDF)	6430
3.2.4. Leukotriene A ₄ (LTA ₄) Hydrolase	6430
3.2.5. UDP-3-O-[R-3-Hydroxymyristoyl]-GlcNAc Deacetylase	6430
3.2.6. Procollagen C-Proteinase (PCP)	6430
3.2.7. Aggrecanase	6430
4. General Mechanism of Enzyme Inhibition	6431
5. Quantitative Structure–Activity Relationships (QSARs)	6431
6. QSAR Studies on Biological Activities of Hydroxamic Acids	6431
6.1. Urease Inhibition	6431
6.1.1. An Overview of Urease Inhibition	6438
6.2. HDAC Inhibition	6438
6.2.1. An Overview of HDAC Inhibition	6449
6.3. MMP Inhibition	6450
6.3.1. An Overview of MMP Inhibition	6460
6.4. TACE Inhibition	6461
6.4.1. An Overview of TACE Inhibition	6466
6.5. Clostridium Histolyticum Collagenase (ChC) Inhibition	6466
6.5.1. An Overview of ChC Inhibition	6467
6.6. 5-Lipoxygenase (5-LOX) Inhibition	6467
6.6.1. An Overview of 5-LOX Inhibition	6474
6.7. Miscellaneous	6474
6.7.1. Hydroxamic Acids as Anticancer Agents	6474
6.7.2. Hydroxamic Acids as Antibacterial Agents	6477
6.7.3. Hydroxamic Acids as Mineral Collectors	6477
6.7.4. An Overview of Mechanisms of Miscellaneous Activities of HAs	6479
7. An Overall View of Drug–Receptor Interactions of Multifarious Actions of Hydroxamic Acids	6479
Author Information	6480
Corresponding Author	6480
Notes	6480
Biography	6480
Acknowledgments	6480
References	6481

1. INTRODUCTION

Hydroxamic acids constitute a unique family of chemicals with multiple biological activities, because they act as potent and selective inhibitors of a large number of enzymes, such as matrix metalloproteinases,^{1–3} peroxidases,^{6–8} hydrolases,^{9–11} ureases,^{12–14} lipoxygenases,¹ cyclooxygenases,^{15,16} histone deacetylases,^{17,20} peptide deformylases,²¹ etc. The detailed role of hydroxamic acid derivatives as enzyme inhibitors has been well described by Muri et al.¹ and Lou and Kang.²² They have been developed as drugs against all of those diseases that can crop up by overactivation of these enzymes as described in a forthcoming section. Besides acting as enzyme inhibitors, hydroxamic acids have also been reported to act against hypertension,²³ cancer,^{24–27} malaria,^{28–32} tuberculosis and fungi,³³ HIV, Alzheimer's disease, and cardiovascular disorders.^{34,35} All of these biological activities of hydroxamic acids are due to their core structure, which enables them to form multiple hydrogen bonds with the receptor and the chelates with metal ions as described below.

2. STRUCTURE AND PHYSICOCHEMICAL PROPERTIES OF HYDROXAMIC ACIDS

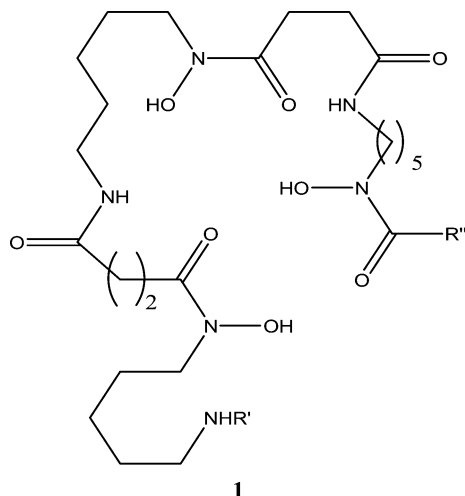
Hydroxamic acids are represented by a general formula RCONR'OH, where R, R' may be aryl or substituted aryl

Received: August 29, 2014

Published: May 29, 2015



moieties. They refer to a class of organic acids, which are much weaker than structurally related carboxylic acids.³⁶ These weak acids constitute one of the most important families of organic bioligands, and one of the first physiological roles of these compounds was associated with their use as siderophores, a class of low molecular weight iron-sequestering agents. Siderophores and their analogues have vast therapeutic potential; for example, trishydroxamate siderophore desferrioxamine B (Desferal, 1) is effectively used to deal with iron overload in transfusion-dependent patients, such as those suffering from thalassaemia.



A monohydroxamic acid, RCONHOH , which is formed when an O/N-protected hydroxylamine molecule is allowed to react with an activated acyl group as shown below, has been found to exist in two tautomeric forms as shown by Figure 1. Both forms exhibit the geometrical isomerism as shown by Figure 2a. These structures of hydroxamic acids resemble those of hydroxyureas or carbamylhydroxamic acids (Figure 2b).

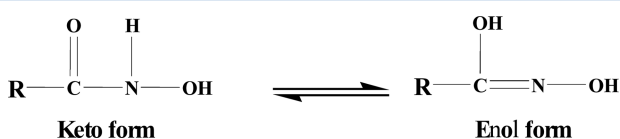


Figure 1. Two tautomeric (keto/enol) forms of monohydroxamic acid.

Because of the above structural properties, hydroxamic acids have strong chelating and H-bond forming abilities, responsible for their several biomedical applications. They can act as monodentate and as well as bidentate ligand through their deprotonated hydroxamate moiety and carbonyl oxygen atom as represented in Figure 3. As discussed by Scolnick et al.,³⁷ hydroxamic acid can also act as a monodentate ligand through its nitrogen atom (Figure 4). As apparent in Figure 3b, a hydroxamate can form a stable five-membered chelate, and, as can be seen in Figure 5, its chelating behavior can be enriched by incorporating secondary coordinating groups at adjacent sites in the molecule. Figure 5 shows the formation of a dinuclear complex of Cu(II) with an α -aminohydroxamate with two modes of hydroxamate coordination, O,O- as well as N,N-coordination, each giving a five-membered ring.^{38,39} However, a β -aminohydroxamic acid can also form a six-membered ring through its N,N-coordination, but only a five-membered ring

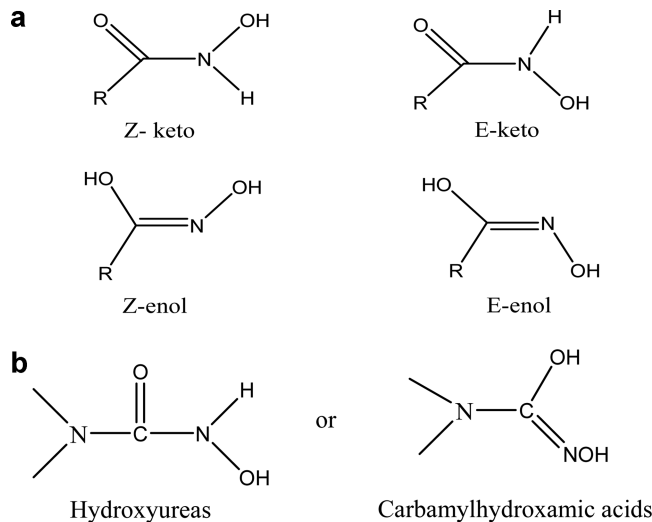


Figure 2. (a) Geometrical isomerism in hydroxamic acids. (b) Structures of hydroxyureas and carbamylhydroxamic acids.

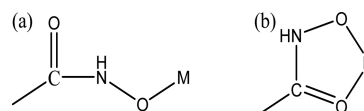


Figure 3. Representation of a monodentate (a) and a bidentate (b) complexation of a hydroxamate.

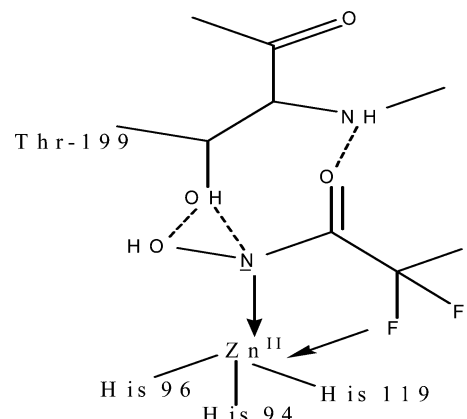


Figure 4. Monodentate N-bonded complex formation of a hydroxamate with carbonic anhydrase enzyme.

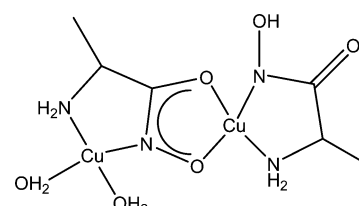


Figure 5. A Cu(II) complex of amino acid exhibiting two modes of hydroxamate coordination: O,O- and N,N-coordination.

through O,O-coordination⁴⁰ as shown in a complex with Cu(II) in Figure 6.

The ability of the H-bond formation of hydroxamic acids plays no less an important role than their chelating ability in their biomedical applications. As shown in Figure 4, a hydroxamic acid can form H-bonds through its OH group,

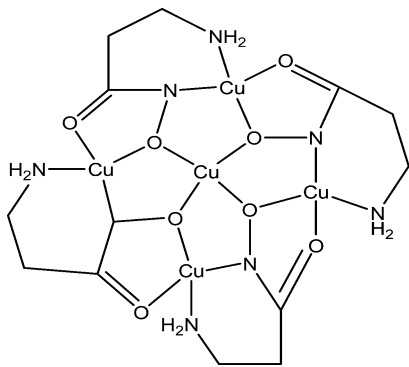


Figure 6. Structure of a complex of Cu(II) formed with a β -alaninehydroxamic acid showing the formation of a six-membered ring with N,N-coordination and a five membered ring with O,O-coordination of the hydroxamate.

NH group, and carbonyl oxygen. OH and NH groups can act both as H-bond donor and as H-bond acceptor and the carbonyl oxygen as an H-bond acceptor. Thus, depending upon the number of sites available in the receptor, hydroxamic acids can form 3–5 hydrogen bonds, strengthening drug–receptor interactions.

Besides their ability to form chelates and many hydrogen bonds, hydroxamic acids have one more property that is also of significant biological importance, and that is their ability to release nitric oxide. There are numerous pathological conditions where NO plays an important role.^{41–44} NO is of critical importance as a mediator of vasodilation in blood vessels. It also acts on cardiac muscle to decrease contractility and heart rate and thus saves from coronary artery disease. Marmion et al.³⁶ have shown that hydroxamic acids are effective NO donors and they readily transfer NO to ruthenium(III) to form highly stable ruthenium nitrosyls, Ru–NO, which cause vascular relaxation of rat aorta by NO-mediated activation of the Fe(II) haem-containing enzyme, guanylate cyclase. However, in this respect, only benzohydroxamic acid ($C_6H_5CONHOH$) has been found to be the best NO-releasing agent.

3. BIOLOGICAL ACTIVITIES OF HYDROXAMIC ACIDS

As was already discussed in the Introduction, hydroxamic acids have a wide spectrum of biological activities. Most of these activities depend on their ability to inhibit a large number of enzymes.^{1,45} Now we shall discuss here all of those enzymes that are inhibited by hydroxamic acids along with their biological roles and the effects of their overactivation that warrant their inhibition. We then shall discuss the importance of hydroxamic acids as biomedical ligands, NO donors, and other roles.

3.1. Inhibition of Highly Targeted Enzymes

Some of the important enzymes that have been targeted by hydroxamic acids to develop variety of drugs are as follows.

3.1.1. Urease. Urease is an enzyme that is produced by a bacterium called *Helicobacter pylori* (HP). Thus, the presence of urease in the body results from HP infections. In the body, this enzyme catalyzes the hydrolysis of urea to ammonia and carbamic acid, resulting finally in carbon dioxide and ammonia. This ammonia elevates the level of pH in the stomach and breaks the gastric mucosa,⁴⁶ and ammonia itself inhibits the consumption of oxygen and reduces the production of ATP in

gastric mucous cells or in mitochondria.⁴⁷ Thus, urease activity plays a critical role in the pathogenesis of several diseases, such as urinary tract infections, urolithiasis, pyelonephritis, hepatic encephalopathy, hepatic coma, cancer, etc. The urease activity in the soil leads to significant environmental and economic problems by releasing a large amount of ammonia into the atmosphere during nitrogen fertilization with urea. This release of ammonia induces plant damage by ammonia toxicity and increase in the pH of the soil.

3.1.2. Histone Deacetylases (HDACs). Enzymes histone deacetylases (HDACs) play an important role in the cell-cycle progression and differentiation. They catalyze deacetylation of lysine residues in the N-terminal tails of core histones and thus remove acetyl groups for the ϵ -amino groups of lysine residues clustered near the amino terminus of nucleosomal histones. The deregulation of their activity is associated with several types of cancer,⁴⁸ and therefore HDAC inhibitors are thought to have great potential to be developed as new anticancer drugs.⁴⁹ Some of them have already been found to act as potential anticancer drugs *in vivo*, and currently are in clinical trials in cancer patients. To date, at least 11 different isoforms of HDAC have been recognized,⁵⁰ and many of them have been exploited to develop the drugs for the treatment of cell proliferative diseases.^{17–20}

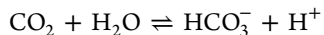
3.1.3. Lipoxygenases (LOXs). Lipoxygenases (LOXs) are a family of iron-containing enzymes that catalyze the dioxygenation of polyunsaturated fatty acids in lipids containing a *cis,cis*-1,4-pentadiene structure. They are of many types, but the most important of them has been the 5-lipoxygenase (5-LOX), which is involved in the biosynthetic pathway of leukotrienes (LTs) where it converts arachidonic acid to 5-hydroperoxy-6,8,11,14-eicosatetraenoic acid (5-HETE) leading to LTs. These oxygenated eicosanoids are implicated in inflammatory and allergic reactions,⁵¹ in which LTC₄, LTD₄, and LTE₄ are potent bronchoconstrictors and are involved in bronchial asthma, inflammation, tissue injury, liver diseases, and shock. LTs may also lead to arthritis and psoriasis. Therefore, 5-LOX inhibition represents potential approach for designing drugs against these diseases.⁵²

3.1.4. Matrix Metalloproteinases (MMPs). Matrix metalloproteinases (MMPs) are a class of enzymes whose inhibition hydroxamic acids have been the most widely studied. MMPs are zinc-containing enzymes that degrade and remodel essentially all of the components of extracellular matrix (ECM), such as membrane collagens, aggrecan, fibronectin, and laminin.^{53–60} To date, at least 26 MMPs are known, which have been classified into six groups based on their structural homology and substrate specificity: collagenases (MMP-1, -8, -13, and -18), gelatinases (MMP-2 and -9), stromelysins (MMP-3, -10, and -11), matrilysins (MMP-7 and -26), membrane types (MTs) (MMP-14, -15, -16, -17, -24, and -25), and others (MMP-12, -19, -20, -21, -22, -23, -27, and -29). MMPs are involved in a variety of physiological processes that require degradation of connective tissues, such as tissue remodeling or repair, bone remodeling, cervical dilation, embryonic development, wound healing, etc. However, over activation of these MMPs results in an imbalance between them and their endogenous regulators, called tissue inhibitors of matrix metalloproteinases (TIMMPs), which can lead to a wide array of disease processes, such as tumor metastasis,^{61,62} rheumatoid arthritis,⁶³ osteoarthritis,^{64,65} periodontal disease,⁶⁶ multiple sclerosis,⁶⁷ congestive heart failure,⁶⁸ etc. The development of MMP inhibitors as potential therapeutic agents

for the treatment of cancer and rheumatoid arthritis has recently been an area of intense interest among medicinal chemists.^{59,69}

3.1.5. Tumor Necrosis Factor- α (TNF- α) Converting Enzyme (TACE). TNF- α converting enzyme (TACE) is another member of the family of zinc-containing metalloproteinases, which cleaves a membrane bound protein (pro-TNF- α), releasing to the circulation a 17 kDa proinflammatory and immunomodulatory cytokine, TNF- α .^{70,71} The release of this cytokine in blood circulation may lead to inflammatory diseases, such as rheumatoid arthritis (RA), multiple sclerosis, and Crohn's disease.⁷² Therefore, there has been a great deal of interest in the design and development of TACE inhibitors to suppress the amount of circulating TNF- α .^{73,74}

3.1.6. Carbonic Anhydrase (CA). Carbonic anhydrase (CA) also is a zinc-containing enzyme. It is a ubiquitous enzyme, whose main physiological function is to catalyze the reversible hydration of carbon dioxide to bicarbonate ion as shown below.



Thus, by producing protons and bicarbonate ions, CA plays a key role in the regulation of pH and fluid balance in different parts of our body. The transport of the protons and bicarbonate ions produced in our kidney and eyes influences the water content of the cells at these locations. In our stomach lining, it plays a key role in secreting acid, while the same enzyme helps to make pancreatic juices alkaline and our saliva neutral. In humans and other higher vertebrates, a number of isozymes of CA have been investigated,⁷⁵ which perform different functions at their specific locations, and their absence or malfunction can lead to several diseased states, ranging from the loss of acid production in the stomach to kidney failure. Thus, the study of their inhibition has been found to be of great value in the development of the drugs acting as antiglaucoma agents, diuretics, and antiepileptics and in the management of mountain sickness, gastric and duodenal ulcers, neurological disorders, or osteoporosis.⁷⁵

3.2. Miscellaneous

3.2.1. Ribonucleotide Reductase (RNR). Ribonucleotide reductase (RNR) is the enzyme that is required for the conversion of ribonucleotides to 2'-deoxyribonucleotides and thus to provide the precursors needed for both synthesis and repair of DNA. There are three different classes of RNR enzymes, differing in their metal cofactors for the catalytic activity. However, all three classes have a conserved cysteine residue at the active site located on the tip of a protein loop in the center of an α/β -barrel structural motif. The inhibition of RNR blocks the formation of deoxyribonucleotides (building blocks of DNA), and thus this enzyme has been a good target for the development of anticancer drugs.⁷⁶

3.2.2. Angiotensin-Converting Enzyme (ACE). Angiotensin-converting enzyme (ACE) plays an important role in the renin–angiotensin system, where it converts a decapeptide, angiotensin I (AI), to an octapeptide, angiotensin II (AII), which stimulates G-protein coupled angiotensin II (type I) receptors, causing a potent vasoconstriction. Inhibition of ACE decreases the level of AII in the body, leading to a decrease in the blood pressure, and thus ACE inhibitors have been developed as antihypertensive agents. The design and development of ACE inhibitors have been extensively presented in some reviews.⁵⁹

3.2.3. Peptide Deformylase (PDF). Peptide deformylase (PDF) is a metalloproteinase that is found only in bacteria. Because there is no analogous human MMP, it is an attractive target for antibacterial drug discovery.⁷⁷ It is an essential enzyme in both gram-positive and gram-negative bacteria, where it helps the synthesis of protein for the bacteria. In eubacteria, the protein synthesis is initiated with *N*-formyl methionine, and the newly synthesized polypeptide is converted to mature protein by first removing the *N*-formyl group by PDF and then methionine by methionine amino peptidase. Thus, the activity of PDF may lead to bacterial infections. Its inhibitors are, therefore, developed as antibacterial drugs.

3.2.4. Leukotriene A₄ (LTA₄) Hydrolase. LTA₄ hydrolase also is a zinc-containing enzyme that catalyzes the hydrolytic conversion of LTA₄ to LTB₄ in the metabolic pathway of arachidonic acid. LTB₄ is a potent chemotactic factor and plays an important role in the inflammatory response by stimulating the adhesion of circulating neutrophils to the vascular endothelium and directing their migration toward the inflammation sites. Thus, the inhibition of LTA₄ hydrolase has drawn great attention of chemists for designing effective anti-inflammatory agents.^{78–80}

3.2.5. UDP-3-O-[R-3-Hydroxymyristoyl]-GlcNAc Deacetylase. This enzyme is involved in the second step of lipid A biosynthesis and therefore is a good target for the development of novel antibiotics.⁸¹

3.2.6. Procollagen C-Proteinase (PCP). The enzyme PCP is involved in the production of collagen, but its overactivity leads to excessive production of collagen, which can lead to many fibrotic diseases, including arthritis and adult respiratory distress syndrome. Hence, its inhibition has been studied to develop drugs for the treatment of these inflammatory conditions.

3.2.7. Aggrecanase. Aggrecanase is a proteolytic enzyme that acts on aggrecans, which are components of connective tissues such as cartilage. Its inappropriate activity leads to cartilage degradation in diseases such as arthritis,⁸² and therefore its selective inhibitors are thought to be useful in the prevention of joint destruction.

4. GENERAL MECHANISM OF ENZYME INHIBITION

Because almost all of the enzymes discussed above, except a few, contain Zn²⁺ ion and because hydroxamates can act as mono- and bidentate ligands with any metal ion, they form strong chelates with all of these enzymes, which are further strengthened by their ability to form the hydrogen bonds with residues of enzymes that may be hydrogen-bond donors or acceptors. In most of the zinc-containing enzymes, hydroxamates bind bidentately to their catalytic Zn²⁺ ion to create a distorted trigonal bipyramidal geometry around the Zn²⁺ as shown in Figure 7, representing a schematic diagram for the interactions of a hydroxamate with matrixin, as an example.⁸³ Figure 7 also shows that, in addition to the chelation, the hydroxamate anion (RCONH-O⁻) of the inhibitor can also form short but strong H-bonds with the neighboring residues, Glu219 and Ala182, of the enzyme. Additionally, the van der Waals and hydrophobic interactions are also possible that can stabilize the inhibitor–enzyme complex. Figure 7 also shows that the inhibitor interacts with the conserved water molecule.

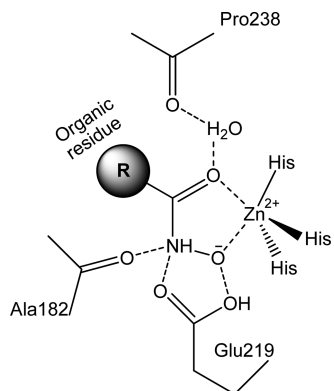


Figure 7. A schematic diagram showing the interaction of a hydroxamate with a representative zinc-containing enzyme (matrilysin) and conserved water molecule. Reprinted with permission from ref 83. Copyright 1995 American Chemical Society.

5. QUANTITATIVE STRUCTURE–ACTIVITY RELATIONSHIPS (QSARs)

Since the inception of the idea by Corwin Hansch in 1964⁸⁴ that biological activities of compounds can be the function of their structure defined by their physicochemical or topological properties, QSARs have gone a long way to become an important aspect of drug design. They provide deeper insight into the mechanism of drug–receptor interactions and rationalize the structural modification to design the potent drugs. It tries to explain the observed variations in biological activities of a group of congeners in terms of molecular variations caused by a change in the substituents. Among the various approaches initially developed for QSAR studies,⁸⁵ the most historical has been the parametric method developed by Hansch,^{84,86} which correlates the biological activity of molecules with their physicochemical, electronic, and steric properties. This parametric method by Hansch has been called Hansch analysis. However, this is also called the extrathermodynamic method or linear free energy-related approach as all of the molecular descriptors used in this method are linear free energy-related terms (i.e., derived from rate or equilibrium constants). Also, the biological activity terms, such as binding or inhibition constants, absorption, etc., are also linear free energy-related terms. However, as the QSAR study advanced, several topological parameters, such as Wiener index,⁸⁷ Hosoya index,⁸⁸ Randic's molecular connectivity index,⁸⁹ and many more defined by various authors, were developed⁹⁰ and successfully used not only in QSAR studies, but also in QSPR (quantitative structure–property relationships) studies.

Apart from the Hansch approach, there have been a few more approaches, such as the Free–Wilson⁹¹ or Fujita–Ban approach,⁹² discriminant analysis,⁹³ pattern recognition technique,⁹⁴ etc., that have been successfully applied to QSAR studies. Additionally, there have been some manual stepwise methods, such as Topliss operational scheme,⁹⁵ Craig plots,⁹⁶ Fibonacci search method,⁹⁷ and sequential simplex strategy,⁹⁸ but these approaches have been of limited use.

The simple Hansch approach adopts a linear multiple regression analysis fitted by least-squares to generate a mathematical model correlating a biological activity, the so-called dependent variable, with a few physicochemical or topological parameters, called independent variables. This simplistic approach, however, loses its meaning if the number of independent variables (descriptors) is relatively high as

compared to the number of data points (number of compounds in a given series) and several of the independent variables are mutually correlated. In such a situation, a partial least-squares (PLS) regression analysis, also known as projection to latent structures, technique is performed.⁹⁹ The PLS analysis generates latent variables from the linear combinations of the descriptors, which are then used to correlate the dependent variables. These latent variables are orthogonal to each other. The weighting coefficient of a descriptor in a latent variable shows its contribution to the dependent variable.

All of the above-mentioned QSAR approaches are related to 2D structures of the molecules. With the advent of the computer technologies came the era of 3D-QSAR studies, which led to the development of methods such as distance geometry approach,¹⁰⁰ comparative molecular field analysis (CoMFA),¹⁰¹ comparative molecular similarity indices analysis (CoMSIA),¹⁰² hypothetical active site lattice (HASL) technique,¹⁰³ de novo ligand design,¹⁰⁴ and docking,^{85d,105} etc.

In the QSAR studies on hydroxamic acids, most of the above approaches have been adopted, among which the Hansch approach, CoMFA, CoMSIA, and molecular modeling have been prevalent. The CoMFA calculates the steric and electrostatic interaction energies for a molecule binding with the receptor, and CoMSIA is simply a modified version of CoMFA, which not only calculates the steric and electrostatic interaction energies but also the hydrophobic and hydrogen-bond energies. In both of the methods, the different interaction energies calculated for a series of molecules at different grid points are correlated with the biological activity using the PLS method and are represented as a three-dimensional contour map in which contours of various colors represent locations on the molecular structure, where low or high steric, electrostatic, hydrophobic, hydrogen-bond donor, and/or hydrogen-bond acceptor interactions would take place. A detailed discussion of these methods can be found in refs 85d, 101, and 102. In molecular modeling, a mathematical simulation of drug–receptor interaction is done to predict a final most active drug molecule. It adopts graphical visualization techniques to provide a plausible three-dimensional representation of the drug molecule, their targets, and the interaction between them. After the advancement in the crystallographic studies, the 3D structures of several target molecules (proteins, enzymes) have been delineated, which have greatly facilitated the molecular modeling studies and the drug design.

6. QSAR STUDIES ON BIOLOGICAL ACTIVITIES OF HYDROXAMIC ACIDS

For most of the biological activities of hydroxamic acids as mentioned above, QSAR studies have been extensively made but not for all. Here, we mention only those systems on which any type of QSARs were available.

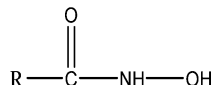
6.1. Urease Inhibition

The first structure–activity relationship on hydroxamic acids as urease inhibitors was qualitatively observed by Kobashi et al.¹⁰⁶ for a series of 11 *n*-aliphatic hydroxamic acids (**2**). These authors observed that their urease inhibition activity expressed in terms of $\log(1/IC_{50})$, where IC_{50} was the minimum concentration of the compound leading to 50% inhibition of the enzyme, was a function of the number of carbon atoms in their acyl moiety (R). An increase in the carbon number from 2 to 6/7 led to a gradual increase in their activity and beyond that to a decrease. Later, the same group of authors¹⁰⁷ performed a

QSAR study on different sets of these hydroxamic acids with varying R-moiety as shown in Tables 1–3. In each case, they

Table 1. *n*-Aliphatic Hydroxamic Acids and Their Urease Inhibition Activity

compd	R	π	log(1/IC ₅₀)		
			obsd	calcd, eq 1	diff
1	CH ₃	0.50	6.22	6.16	-0.06
2	<i>n</i> -C ₂ H ₅	1.00	6.25	6.30	0.05
3	<i>n</i> -C ₅ H ₁₁	2.50	6.34	6.49	0.15
4	<i>n</i> -C ₆ H ₁₃	3.00	6.50	6.48	-0.02
5	<i>n</i> -C ₇ H ₁₅	3.50	6.50	6.42	-0.08
6	<i>n</i> -C ₈ H ₁₇	4.00	6.40	6.33	-0.07
7	<i>n</i> -C ₉ H ₁₉	4.50	6.26	6.19	-0.07
8	<i>n</i> -C ₁₀ H ₂₁	5.00	6.08	6.02	-0.06
9	<i>n</i> -C ₁₁ H ₂₃	5.50	5.77	5.81	0.04
10	<i>n</i> -C ₁₃ H ₂₇	6.50	5.04	5.26	0.22
11	<i>n</i> -C ₁₅ H ₃₁	7.50	4.67	4.55	-0.12



found that the inhibitory activity of compounds had a parabolic correlation with the hydrophobic constant π of acyl residues or substituents. For compounds of Tables 1–3, the most significant correlations obtained by these authors were as shown by eqs 1–3.

$$\log(1/\text{IC}_{50}) = 0.407\pi - 0.080\pi^2 + 5.975 \quad (1)$$

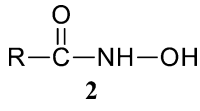
$$n = 11, r = 0.985, s = 0.119, \pi_0 = 2.54$$

$$\log(1/\text{IC}_{50}) = 0.260\pi - 0.134\pi^2 + 6.305 \quad (2)$$

$$n = 8, r = 0.942, s = 0.132, \pi_0 = 0.97$$

$$\log(1/\text{IC}_{50}) = -0.153\pi - 0.096\pi^2 + 6.414 \quad (3)$$

$$n = 9, r = 0.943, s = 0.239, \pi_0 = 0.80$$



In these equations, n refers to the number of data points, r the correlation coefficient, s the standard deviation, and π_0 the optimum value of π . In all three cases, no other physicochemical parameters were found to be relevant. Because in each case the activity had a parabolic correlation with π , it was suggested that the hydrophobic character of acyl residue played two kinds of role in urease inhibition: (1) it facilitated the random walk process of the compounds, and (2) it played a stereospecific role in binding of the substituent at the active site of the enzyme. However, because the activity was measured in vitro where there was no lipophilic–hydrophilic or blood–brain barrier, the role of π in random walk process was ruled out, and thus the substituents could be assumed to play only a stereospecific role, where the bigger substituents could produce steric hindrance in the interaction of the molecule with the receptor. In the case of substituted benzohydroxamic acids (Tables 2 and 3), the ring substituents seemed to play a position-specific role, as in the case of meta-substituted

Table 2. *m*-Substituted Benzohydroxamic Acids and Their Urease Inhibition Activity

compd	R	π	log(1/IC ₅₀)		
			obsd	calcd, eq 2	diff
1	-H	0	6.43	6.27	-0.21
2	-Cl	0.76	6.37	6.43	0.06
3	-NO ₂	0.11	6.43	6.33	-0.10
4	-CH ₃	0.51	6.20	6.40	0.20
5	-OCH ₃	0.12	6.27	6.33	0.06
6	-OC ₄ H ₉	1.62	6.44	6.37	-0.07
7	-OC ₆ H ₁₃	2.62	6.15	6.07	-0.08
8	-OC ₈ H ₁₇	3.62	5.44	5.49	0.05

Table 3. *p*-Substituted Benzohydroxamic Acids and Their Urease Inhibition Activity

compd	R	π	log(1/IC ₅₀)		
			obsd	calcd, eq 3	diff
1	-H	0	6.43	6.41	-0.02
2	-Cl	0.70 ± 0.03	6.52	6.26	-0.26
3	-NO ₂	0.24 ± 0.03	6.43	6.37	-0.06
4	-CH ₃	0.52 ± 0.05	5.96	6.31	0.35
5	-OH	-0.61 ± 0.01	6.37	6.47	0.10
6	-OCH ₃	-0.04 ± 0.01	6.64	6.42	-0.22
7	-OC ₄ H ₉	1.46	5.75	5.99	0.24
8	-OC ₆ H ₁₃	2.46	5.64	5.45	-0.18
9	-OC ₈ H ₁₇	3.46	4.68	4.73	0.05

analogues (Table 2) the π was shown to have a positive role up to a certain limit (eq 2) but in the case of para-substituted analogues it was shown to play throughout a negative role (eq 3), suggesting that para substituents would play only a steric role hindering drug–receptor interaction.

For another series of hydroxamic acids where R-substituents were araliphatic groups (Table 4), Kumaki et al. did not obtain any correlation but applied eq 1 to predict the activity of the compounds, and it was noted that for most of the compounds the predicted activity values were in good agreement with the observed ones. Thus, it was concluded that the hydrophobic property of the R-substituent of this series of compounds also played an important role.

In their further study,¹⁰⁸ these authors combined the first three series and added it to a new series having the structure R-CONHCH₂-CONHOH, and thus for this combined series (Table 5), they obtained the correlation as

$$\begin{aligned} \log(1/\text{IC}_{50}) &= 0.429(\pm 0.181)\pi - 0.083(\pm 0.024)\pi^2 \\ &\quad - 0.492(\pm 0.381)B_1 + 0.558(\pm 0.139)I \\ n = 64, r &= 0.890, s = 0.254, \pi_0 = 2.58 \end{aligned} \quad (4)$$

where π refers to the hydrophobic constant of R-substituent, B_1 is the STERIMOL parameter referring to the minimum width

Table 4. Araliphatic Hydroxamic Acids and Their Urease Inhibition Activity

compd	R	π^a	log(1/IC ₅₀)		
			obsd	calcd, eq 1	diff
1	CH ₂ — Ph	2.69	5.92	6.49	0.57
2	CH ₂ CH ₂ — Ph	3.15	6.70	6.47	-0.23
3	CH ₃ CH ₂ CH— Ph	3.49	4.96	6.43	1.47
4	CH ₃ CHCH ₂ — Ph	3.45	6.34	6.43	0.09
5	CH ₂ CH ₂ CH ₂ — Ph	3.68	6.00	6.40	0.40
6	CH ₃ (CH ₂) ₃ CH— Ph	4.49	5.05	6.20	1.15
7	CH ₃ (CH ₂) ₂ CHCH ₂ — Ph	4.45	5.92	6.21	0.29
8	CH ₂ — 1-naphthyl	3.83	5.07	6.37	1.30

^aThese π values were calculated according to Hansch's method: Hansch, C.; Anderson, S. N. *J. Med. Chem.* **1967**, *10*, 745.

of the substituent, and I is an indicator variable used with a value of 1 for $m = 1$ (R-CONHCH₂-CONHOH analogues) and 0 for $m = 0$ (R-CONHOH analogues). The figures with a “ \pm ” sign within the parentheses are 95% confidence intervals. In terms of π this equation is almost parallel to eq 1 with almost identical values of π_0 . Thus, eq 4 also suggested that R-substituents directly attached to CONHCH₂ or CONHOH would have a hydrophobic effect on the inhibition potency of the compounds, probably due to having hydrophobic interaction with the binding site of the enzyme. However, because also for this bigger series, the activity had parabolic correlation with π of substituents, the substituents would also have the stereospecific roles after their π -value reaches an optimum value. The negative coefficient of B_1 in eq 4 also suggested that the substituents with large minimum width would not be conductive to the activity, but the positive coefficient of the indicator variable I indicated that the presence of —CONHCH₂— moiety between the R-substituent and the hydroxamic acid moiety will be advantageous.

In the next communication, Kanoda et al.¹⁰⁹ calculated the electronic structures for a set of only 34 compounds of Table 5, as marked with an asterisk, and found that the charge density (Q_7) of the carbon atom (C_7) directly bonded to the —CONHOH group was an important factor controlling the activity. It was correlated with the activity as

$$\log(1/IC_{50}) = 3.581(\pm 1.258)Q_7 + 5.401 \quad (5)$$

$$n = 34, r = 0.717, s = 0.306, F_{1,32} = 46.93$$

In this equation, F is the Fischer ratio between the variances of calculated and observed activities. Equation 5 was further improved when the molar refractivity (MR) of the compounds was included (eq 6). Equation 6 thus suggested that while the C_7 atom might participate in some electronic interaction with the receptor, the bulk of the molecule might also have some dispersion interaction. However, because MR is usually found to be correlated with the hydrophobic property of compounds, the involvement of substituents, as suggested by eq 4, appears to be more plausible vis-à-vis the involvement of the whole molecule in the dispersion interaction. Now the indicator variable I of eq 4, which suggested an advantageous role of the presence of the CONHCH₂ group between the R-substituent and the —CONHOH moiety, might be interpreted to suggest the better electronic interaction of C_7 of CONHCH₂ than that of R-group. It was found that in compounds having a CONHCH₂ group, the Q_7 was positive, and in those not having this group Q_7 was negative.

$$\begin{aligned} \log(1/IC_{50}) &= 3.581(\pm 1.258)Q_7 + 0.0342(\pm 0.0341)MR \\ &\quad - 0.00051(\pm 1.258)MR^2 + 5.001 \\ n &= 34, r = 0.854, s = 0.236, F_{3,30} = 54.33 \end{aligned} \quad (6)$$

For a combine of compounds of Tables 1–4, Zaheer-ul-Haq et al.¹¹⁰ performed a CoMFA and CoMSIA study, where the CoMFA model had conventional $r^2 = 0.969$ and cross-validated $q^2 = 0.532$ and the CoMSIA model had $r^2 = 0.976$ and $q^2 = 0.665$. According to the CoMFA model, the steric field had a greater influence (70%) than the electrostatic field (30%) on urease inhibition by these compounds. On the other hand, the CoMSIA model, where five different fields were taken into account, steric, electrostatic, hydrophobic, H-bond donor, and H-bond acceptor, exhibited the steric field 43%, electrostatic 26.4%, hydrophobic 20.3%, H-bond donor 6.2%, and H-bond acceptor 4.2%. For compound 2 of Table 4 (Figure 8), which had the highest activity among all of the compounds, contour maps were obtained for both CoMFA and CoMSIA.

In the CoMFA contour, sterically favored regions were found near C3 and C4 atoms of phenyl ring extending to the C_α of the side chain where bulkier substituents might increase the activity, and two sterically unfavorable regions, one above C6 of the phenyl ring and the other away from the phenyl ring, were found where the bulkier substituents might decrease the activity. For electrostatic interaction, a region near C2 indicated the region where the negatively charged groups could increase the activity; that is, electron-donating groups at this position might increase the activity, and some areas near the meta-position of the phenyl ring referred to the regions where positively charged groups could increase the activity, meaning electron-withdrawing groups there could be favorable.

In CoMSIA contour maps, the steric regions were almost identical to those in CoMFA. Regarding the electrostatic interactions, the favorable regions for negatively charge groups were identical to those in CoMFA, but the areas favorable for positively charged groups were found above C_α .

The CoMSIA countour maps were also obtained for hydrophobic interactions, which exhibited that hydrophobically favored and disfavored regions were around the side chain in up and down positions. In H-bond donor and acceptor contour maps of CoMSIA, the favorable H-bond donor region was found near the amido nitrogen and the favorable H-bond

Table 5. Hydroxamic Acids, R-(CONHCH₂)_m-CONHOH, and Their Urease Inhibition Activity

compd ^a	R	<i>m</i>	π	<i>I</i>	log(1/IC ₅₀)		compd ^a	R	<i>m</i>	π	<i>I</i>	log(1/IC ₅₀)	
					obsd	calcd, eq 4						obsd	calcd, eq 4
1*	Me(CH ₂) ₁₀ -	1	5.50	1	5.82	5.30	35*	Me-	0	0.50	0	5.25	5.08
2*	Me(CH ₂) ₈ -	1	4.50	1	5.68	5.70	36*	Et-	0	1.00	0	5.28	5.23
3*	Me(CH ₂) ₇ -	1	4.00	1	5.89	5.84	37*	Me(CH ₂) ₄ -	0	2.50	0	5.37	5.44
4*	Me(CH ₂) ₆ -	1	3.50	1	5.80	5.93	38*	Me(CH ₂) ₅ -	0	3.00	0	5.53	5.43
5*	Me(CH ₂) ₅ -	1	3.00	1	5.82	5.98	39*	Me(CH ₂) ₆ -	0	3.50	0	5.53	5.37
6*	Me(CH ₂) ₄ -	1	2.50	1	5.89	6.00	40*	Me(CH ₂) ₇ -	0	4.00	0	5.43	5.28
7	(Me) ₂ CH(CH ₂) ₂ -	1	2.37	1	5.72	5.99	41*	Me(CH ₂) ₈ -	0	4.50	0	5.29	5.14
8	(Me) ₂ CHCH ₂ -	1	1.87	1	5.82	5.95	42*	Me(CH ₂) ₉ -	0	5.00	0	5.11	4.96
9	(Et) ₂ CH-	1	2.37	1	6.10	5.70	43*	Me(CH ₂) ₁₀ -	0	5.50	0	4.80	4.74
10	EtCH(Me)-	1	1.87	1	5.89	5.77	44*	Me(CH ₂) ₁₂ -	0	6.50	0	4.07	4.18
11	(Me) ₃ C-	1	1.68	1	5.36	5.40	45	Me(CH ₂) ₁₄ -	0	7.50	0	3.70	3.45
12	C ₆ H ₁₁ -	1	2.39	1	5.68	5.74	46	PhCH ₂ -	0	2.69	0	4.95	5.44
13	Ph(CH ₂) ₂ -	1	3.19	1	6.05	5.97	47	Ph(CH ₂) ₂ -	0	3.19	0	5.73	5.41
14	PhCH ₂ -	1	2.69	1	5.89	6.00	48	Ph(CH ₂) ₃ -	0	3.69	0	5.03	5.34
15*	Ph-	1	2.13	1	6.11	5.89	49*	Ph-	0	2.13	0	5.46	5.33
16*	4-Cl-Ph	1	2.87	1	6.0	0	50*	3-Cl-Ph-	0	2.84	0	5.40	5.30
17*	4-Me-Ph-	1	2.69	1	5.82	5.91	51*	3-NO ₂ -Ph-	0	1.85	0	5.46	5.31
18*	4-NO ₂ -Ph-	1	1.85	1	5.54	5.86	52*	3-Me-Ph-	0	2.69	0	5.23	5.35
19	4-MeSO ₂ -Ph-	1	0.50	1	4.96	5.34	53*	3-MeO-Ph-	0	2.11	0	5.30	5.33
20*	4-MeO-Ph-	1	2.11	1	5.77	5.89	54	3-n-BuO-Ph-	0	3.68	0	5.47	5.25
21	4-EtO-Ph-	1	2.51	1	5.82	5.91	55	3-n-Me(CH ₂) ₅ -O-Ph-	0	4.68	0	5.18	4.99
22	4-n-PrO-Ph-	1	3.18	1	5.82	5.88	56	3-n-Me(CH ₂) ₇ -O-Ph-	0	5.68	0	4.47	4.57
23	4-n-BuO-Ph-	1	3.68	1	5.89	5.81	57*	4-Cl-Ph-	0	2.84	0	5.55	5.30
24*	3-Cl-Ph-	1	2.82	1	6.19	5.85	58*	4-NO ₂ -Ph-	0	1.85	0	5.46	5.31
25*	3-Me-Ph-	1	2.69	1	6.34	5.91	59*	4-Me-Ph-	0	2.69	0	4.99	5.35
26*	3-MeO-Ph-	1	2.11	1	5.92	5.89	60	4-HO-Ph-	0	1.46	0	5.40	5.24
27*	3-NO ₂ -Ph-	1	1.85	1	5.92	5.86	61*	4-MeO-Ph-	0	2.11	0	5.67	5.33
28	3-(Me) ₂ N-Ph-	1	2.31	1	5.60	5.90	62	4-n-BuO-Ph-	0	3.68	0	4.78	5.25
29	3-MeCONH-Ph-	1	1.16	1	5.70	5.74	63	4-Me(CH ₂) ₅ O-Ph-	0	4.68	0	4.67	4.99
30	3-EtCONH-Ph-	1	1.66	1	5.50	5.84	64	4-Me(CH ₂) ₇ O-Ph-	0	5.68	0	3.71	4.57
31	3-n-PrCONH-Ph-	1	2.16	1	5.85	5.89							
32	3,4-di-Cl-Ph-	1	3.38	1	5.77	5.81							
33	3,4-OCH ₂ O-Ph-	1	2.08	1	5.85	5.78							
34	2-thienyl-	1	1.81	1	6.19	5.88							

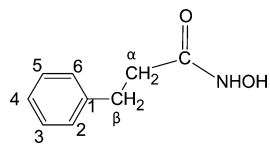


Figure 8. Structure of compound 2 of Table 4 for which CoMFA and CoMSIA contours maps were drawn.

acceptor near the carbonyl oxygen of the hydroxamic group, which were true for most of the compounds.

In the next communication, Zaheer-ul-Haq and Wadood¹¹¹ performed 3D QSAR studies on a set of 27 compounds belonging to the series of R-CONHCH₂-CONHOH and taken from Zareen et al.,¹¹² in which the most important was their docking study that determined the binding mode of these compounds with the urease extracted from the bacteria *Bacillus pastrurii* (BP). The docking software FlexX implemented in SYBYL was applied. The structure of the enzyme complexed with acetohydroxamic acid (CH₃CONHOH) (PDB entry 4UPB) was taken from the protein databank (PDB). The three-dimensional structure of each compound was constructed, and the structural minimization was performed using a standard Tripos force field.¹¹³

The ureas active site contains two Ni²⁺ ions linked to each other by a carbamate bridge. Two imidazole nitrogen atoms are bound to each nickel ion, and a carboxylate group and a water molecule fill the remaining coordination site of the metal ion.¹¹⁴ The docking result showed a common mechanism of binding for almost all of the compounds, where the carbonyl and hydroxyl oxygens of hydroxamic group in each compound are coordinated to Ni²⁺(2) and Ni²⁺(1), respectively, as well as each of them forms two hydrogen bonds, the former with His137 and His139 and the latter with His249 and His275. Additionally, the carbonyl oxygen of amido group was also found to form a hydrogen bond with Arg339. All of these bindings for a representative compound (3) can be diagrammatically shown as in Figure 9.

Zaheer-ul-Haq and Wadood¹¹¹ had also performed COMFA and COMSIA studies on these compounds in which the contour plots were drawn for the representative compound (3). The COMFA contour plots obtained for steric and electrostatic interactions exhibited that sterically favored regions were near C2 and C3 atoms of the phenyl ring and that sterically unfavorable regions were at C5 and at a distance away from C3. For electrostatic interactions, the favorable region for a positive charge was shown above C2 and for the negative charge above the carbonyl oxygen of the hydroxamate moiety.

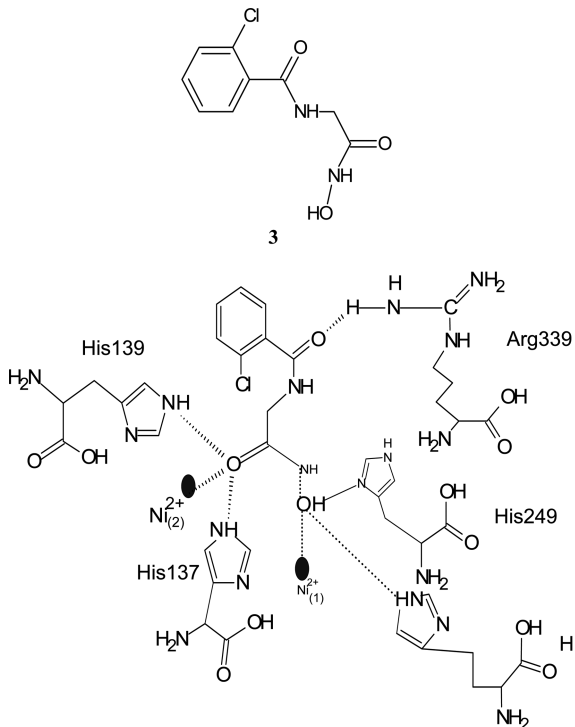


Figure 9. A schematic diagram of the interaction of an urease inhibitor (3) with BP urease, where the carbonyl oxygen of amide moiety is shown to form an H-bond with Arg339 and the two oxygens of hydroxamic acid moiety to have interactions with Ni^{2+} ions and with amino acid residues.

In COMSIA contour maps, the steric regions were in accordance to those in COMFA, but the electrostatic regions were slightly different. The electropositive favorable region was found near C5, and the electronegative favorable region was observed to be near C2 and C3 of the phenyl ring. However, the hydrophobically favored regions were also indicated near these two atoms, C2 and C3, which might refer to sterically favored regions of COMFA. COMFA also showed two hydrogen-bond favorable regions, one near NH of amido group and one near hydroxamic group. The hydrogen-bond acceptor favorable regions were shown near C5 and C6 of the phenyl ring.

Much attention has been paid to the inhibition of urease of *Helicobacter pylori* (*H. pylori*), because *H. pylori* infection is etiologically associated with chronic active gastritis, peptic ulcer diseases, mucosa-associated lymphoid tissue-type gastric carcinoma, and other gastric cancers.¹¹⁵ Ureases are ubiquitous in nature and are inhibited, in general, by a variety of agents including fluorides,¹¹⁶ thiols,¹¹⁷ and hydroxamic acids.¹¹⁸ While studying the role of hydroxamic acids in the inhibition of *H. pylori* urease, Odake et al.¹¹⁹ studied the urease inhibition activity of some dipeptide hydroxamic acids as shown in Table 6. For these dipeptide hydroxamic acids, Mishra et al.¹²⁰ made a 3D-QSAR study, in which they first developed a homology model of *H. pylori* urease using the crystal structure of urease obtained from *Klebsiella aerogene* as a template. The acetohydroxamic acid moiety then was docked into the active pocket of the enzyme model, using the docking protocol of MOE (molecular orbital environment) software package. The resulting conformation was used as a template to construct the potential dipeptide hydroxamic acid inhibitors. For these compounds then a COMFA model was obtained with $q^2 =$

Table 6. Dipeptide Hydroxamic Acids (R-X-Gly-NHOH) and Their Urease Inhibition Activity^a

no.	compd	R ^b	X ^c	IC ₅₀ (μM) ^d
1	DP-1	H	Ile	0.20
2	DP-2	H	Leu	0.22
3	DP-3	H	Phe	0.71
4	DP-4	H	Met	0.31
5	DP-5	H	Gly	0.78
6	DP-6	H	Ala	0.79
7	DP-7	H	Arg	0.97
8	DP-8	H	Pro	1.1
9	DP-9	H	Ser	1.3
10	DP-10	H	Tyr	1.6
11	DP-11	H	Lys	7.0
12	DP-12	H	Glu	37.0
13	DP-14	Boc	Ile	95.0
14	DP-15	Boc	Leu	21.0
15	DP-16	Boc	Met	20.0
16	DP-17	Boc	Gly	41.0
17	DP-18	Boc	Ala	32.0
18	DP-19	Boc	Pro	87.0
19	DP-20	Boc	Ser	36.0
20	DP-21	Boc	Tyr	110.0
21	DP-27	Ac	Phe	16.0
22	DP-28	Z	Phe	29.0
23	DP-30	H	Ser(Bzl)	0.21
24	DP-31	H	Tyr(Bzl)	1.2
25	DP-25	Boc	Phe	28.0
26	DP-26	Bz	Phe	14.0

^aAbbreviations: Boc, *tert*-butoxycarbonyl; Bz, benzoyl; Ac, acetyl; Z, benzyloxycarbonyl. ^bProtecting groups. ^cAn amino acid. ^dTaken from ref 119.

0.610, $r^2 = 0.988$, and $F = 294.88$. The COMFA contour maps indicated the favorable and unfavorable electrostatic and steric regions. A field around the Ni^{2+} ion was found to constitute an electropositive region where any negative portion of the ligand could bind and large negative field was found to be constituted by three amino acid residues, which required a positively charged group on the ligand to interact, and thus NH_2 of the compound seemed to be crucial for the activity. The presence of Asp223 itself in the active pocket warranted the NH_2 group to be in the ionized state. In the steric map, a cavity in the receptor surrounded by the residues Met366, Met316, and Ala365 was observed that warranted an interaction with a large steric (hydrophobic) group on the ligand. In fact, the most active ligands are those that possess hydrophobic substituents, properly oriented to interact with this cavity. A polyhedra surrounding the NH_2 group had indicated an area of the pocket where there could be a steric hindrance and no large group of ligand could have any effective interaction. Such a steric hindrance was also indicated by Munakata et al.¹⁰⁸ (eq 4). Thus, the contour maps were in agreement with the observations.

In urease inhibition, the hydrophobic interaction has been found to play a special role because the enzyme has in its active region a cavity surrounded by hydrophobic amino acid residues. Thus, the hydrophobic portion of the compounds may be engulfed in this cavity and have a hydrophobic interaction.¹²¹ Zaheer-ul-Haq et al.¹²² performed a COMFA study on a series of bis-coumarine analogues (4) as urease inhibitors in which the COMFA electrostatic plots (Figure 10) indicated the

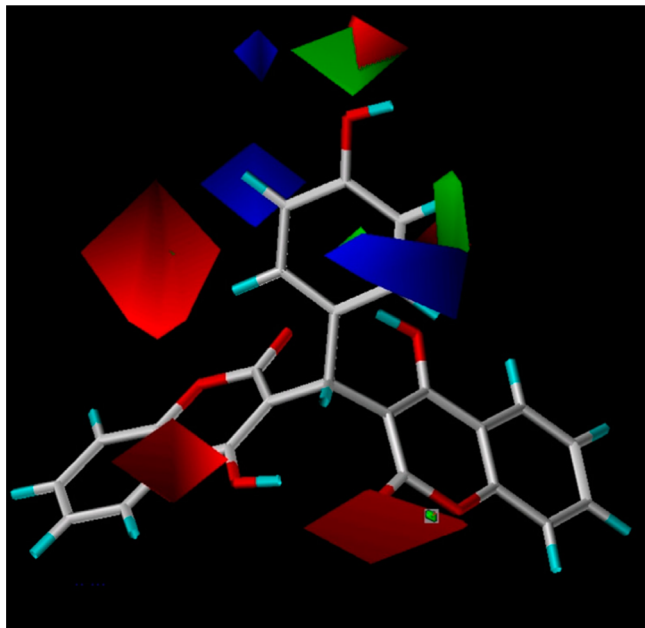
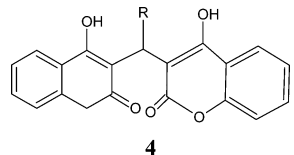


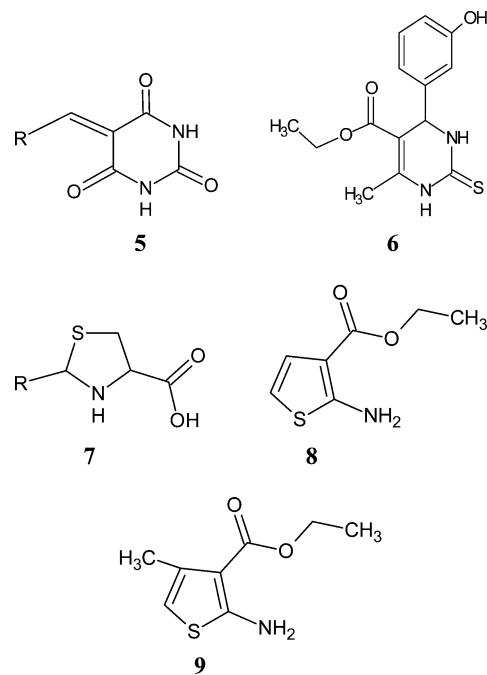
Figure 10. CoMFA electrostatic contour maps, where red regions indicate the areas where biological activity is improved by a negative charge and the blue regions indicate the areas where electropositively charged moieties can enhance the activity. Reprinted with permission from ref 122. Copyright 2008 Elsevier.

favorable and unfavorable electrostatic fields. In this figure, the red contours indicated the regions of the compounds that can interact with the Ni^{2+} ions, and, as can be seen, these regions cover both hydroxyl moieties and both lactones moieties. These results are in accordance with the findings of a previous study of these authors.¹²³ The blue contours indicated the regions where the positively charged group can increase the activity. These regions are indicated to be in R-substituents. This also supported previously published results.¹²⁴ In the steric map (not shown), a small green contour had indicated the presence of a small hydrophobic site in the receptor, where a small hydrophobic R-substituent of the size of CH_3 to *p*-isopropylphenyl might interact. However, a very bulky hydrophobic group might decrease the activity. Such steric and hydrophobic interactions in urease inhibition by different kinds of inhibitors have been previously discussed by Amtul et al.¹²⁵



In urease inhibition, the nickel coordination might be one of the important determinants for the activities of the compounds. Acetohydroamic acid (CH_3CONHOH) is a drug that is a potent and irreversible inhibitor of bacterial and plant urease and is usually used for urinary tract infection. A model of binding of this compound with 4UBP is shown in Figure 11 by Rashid et al.¹²⁶ In this figure, the most important interaction is the coordination of hydroxyl oxygen with both the Ni^{2+} ions and a steric or hydrophobic interaction of CH_3 group with Ala170 residue. Mostly, all known urease inhibitors interact with nickel ions,^{127–130} where the activity of the compounds can be further increased by hydrophobic interaction and/or hydrogen

bonding with the active sites of the enzyme. This could be verified by various authors studying the urease inhibition by different kinds of compounds; for example, for a series of arylidene barbiturates (**5**), Khan et al.¹³¹ found the most active compound (**5**, $\text{R} = p\text{-F-C}_6\text{H}_4$) to bind as shown in Figure 12, and Rashid et al.¹²⁶ showed one of the monastrol derivatives (**6**) to bind with 4UBP as in Figure 13. Similarly, Khan et al. in their further two communications^{132,133} showed the bindings of sulfur-containing compounds. In their first communication,¹³² they studied the binding of 2-substituted (*4R*)-thiazolidine carboxylic acids (**7**) and in the next communication¹³³ the binding of 2-aminothiophene (**8**) derivatives. For a representative compound in the series of **7** ($\text{R} = \text{H}$), the binding with *Bacillus pasteurii* (BP) urease was as shown in Figure 14 and for the most active compound (**9**) in the series of **8** as shown in Figure 15.



Most of the urease inhibitors bind to urease almost in the same way as does the urea (H_2NCONH_2), the substrate of urease. In fact, the active site of urease is located in the domain of α -subunit of the enzyme and contains two nickel ions: $\text{Ni}^{2+}(1)$ legated by His272 and His246 and $\text{Ni}^{2+}(2)$ legated by Asp360, His134, and His136. The two nickel ions are bridged by carboxylated Lys217 (Figure 16). When urea binds to urease, it is ligated to $\text{Ni}^{2+}(1)$ through its carbonyl oxygen and to $\text{Ni}^{2+}(2)$ through one of its NH_2 moieties as shown in Figure 16. Three of the water molecules observed in the native structure of urease are displaced, leaving only a hydroxyl moiety that bridges the two nickel ions. The nucleophilic attack by this Ni^{2+} -bridging hydroxide onto the sp^2 carbon atom of urea yields a tetrahedral transition state with a sp^3 carbon.¹³⁴

The binding of the urea N to $\text{Ni}^{2+}(2)$ is favored by the change of “pseudo” sp^2 state of N to pure sp^3 state, where the loss of resonance delocalization energy of urea is compensated for by the formation of urea N– $\text{Ni}^{2+}(2)$ bond.¹³⁴

The binding of urea with the enzyme is further stabilized by hydrogen bondings between its both NH_2 groups to the oxygen of Ala366. The active site of urease is surrounded by hydrophilic amino acid residues and is roughly the size of the urea molecule. It is flexible in nature and undergoes an induced

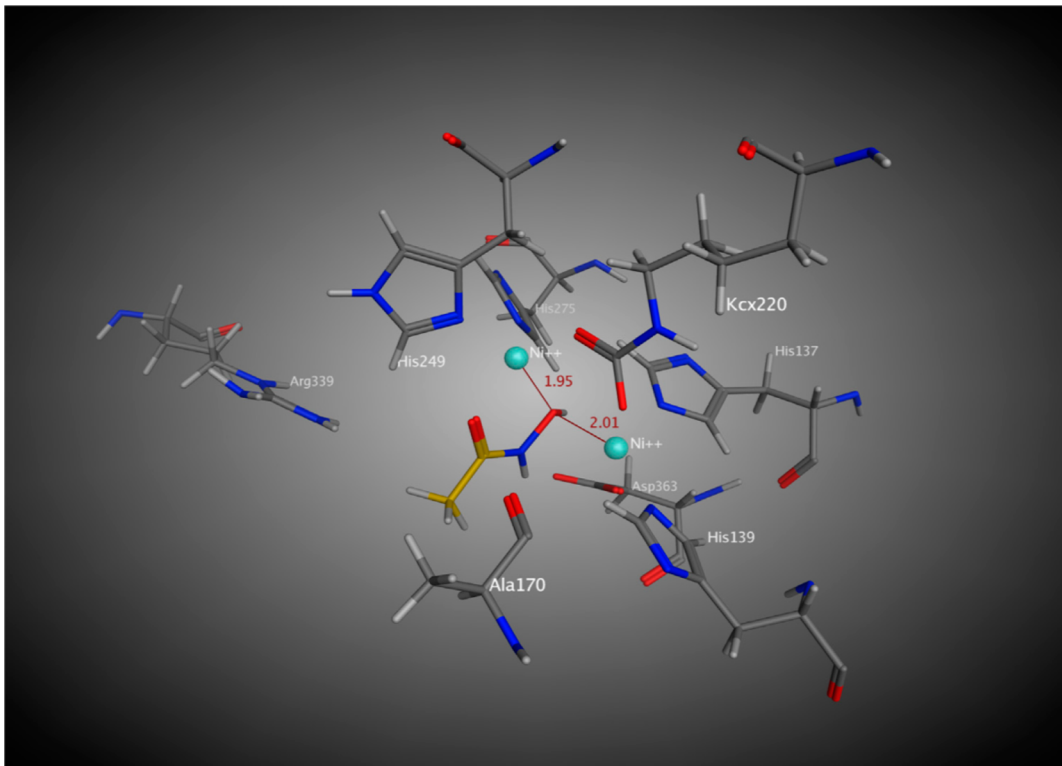


Figure 11. Modeled mode of binding of acetohydroxamic acid (HAE800) in 4UBP active site. Most important interaction is the coordination of hydroxyl oxygen with both the nickel ions and a steric or hydrophobic interaction of CH_3 group with Ala170 residue. Reprinted with permission from ref 126. Copyright 2013 Elsevier.

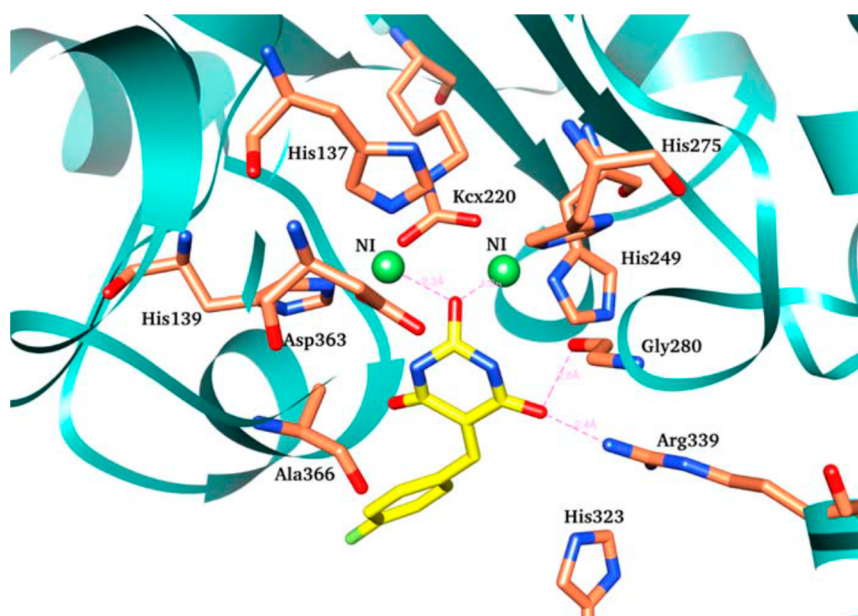


Figure 12. Predicted binding mode of compound 5 (carbon atoms depicted in yellow) to urease. The carbon atoms in several key residues in urease are colored gold, while nitrogen and oxygen atoms are colored in blue and red, respectively. One of the carbonyl groups is shown to bind with both of the nickel ions and one to form the hydrogen bonds with two amino acid residues of the active sites, Gly280 and Arg339. Reprinted with permission from ref 131. Copyright 2011 Elsevier.

fit. When urea enters the active site cavity, the highly mobile flap is in the open conformation to have the best fit of the substrate or inhibitor. This allows the extensive access of the substrate or inhibitor to the active site replacing three of four water molecules located in positions matching its molecular shape and dimensions.

Amtul et al.¹²⁵ have discussed that the urease has high substrate (urea) specificity; hence only a few classes of inhibitors may have a binding mode similar to that of urea. In urease binding, several noncovalent interactions, such as hydrogen bondings and hydrophobic contacts, also take place and stabilize the enzyme–inhibitor complex. Compounds with

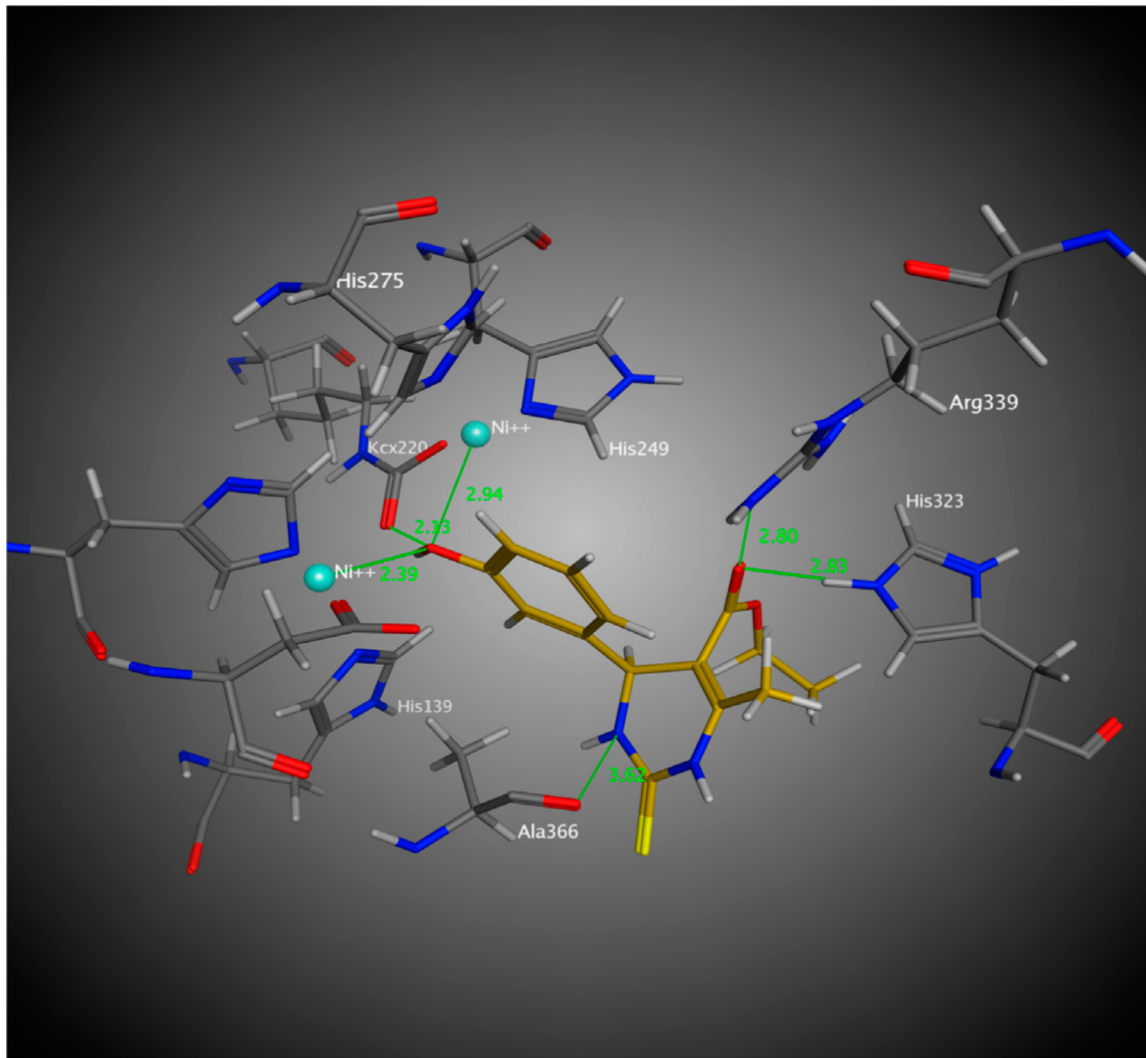


Figure 13. Molecular level interactions of a monastrol (**6**) in the active site of 4UBP. The coordination pattern of this compound via its 3-hydroxyphenyl group at C4 is shown to mimic the coordination of HAE (Figure 11). Also, the active site residues similar to those in HAE are shown to stabilize the enzyme ligand binding. Reprinted with permission from ref 126. Copyright 2013 Elsevier.

electronegative atoms, such as oxygen, nitrogen, and sulfur, can act usually as bidentate ligands to form slightly distorted octahedral complexes with Ni^{2+} ions. The bulky groups present in the pharmacophore of the molecules may, however, create the steric problem for the molecules to enter the active pocket of the enzyme and interact with amino acid residues of the cavity.

6.1.1. An Overview of Urease Inhibition. Because the active site of urease contains two Ni^{2+} ions, these nickel ions generate electropositive fields around them, where the negatively charged portions of any inhibitor can interact. The above-discussed docking studies have shown a common mechanism of binding of hydroxamic acids where the carbonyl and hydroxyl oxygen atoms of hydroxamic group (CONHOH) are coordinated with $\text{Ni}^{2+}(2)$ and $\text{Ni}^{2+}(1)$, respectively (Figure 9), and simultaneously CO and NH moieties of this group participate in H-bond acceptor and donor interactions with the enzyme. Further, if there was any H-bond acceptor moiety in the R group of R-CONHOH, as shown in **3**, it also had the opportunity to form the H-bond with some residue of the enzyme.

For the compounds such as **3**, the ortho and meta positions of the phenyl ring have been found to be sterically and hydrophobically favorable positions. In urease inhibition, the hydrophobic interaction has been found to play a special role, because enzyme has in its active region a cavity surrounded by hydrophobic amino acid residues, Met366, Met316, and Ala365, that warrants an interaction with a large steric (hydrophobic) group on the ligand. Such a hydrophobic interaction, of course with a steric problem of very bulky R-substituent, has also been clearly indicated by 2D QSAR models (eqs 1–4).

6.2. HDAC Inhibition

There are many kinds of HDAC inhibitors,^{135–139} which can be divided into several structural classes, such as small molecular hydroxamic acids, carboxylates, benzamides, electrophilic ketones, and cyclic peptides. Among them, the hydroxamic acids have been widely studied for HDAC inhibition, and the two members belonging to this class, Trichostatin A (TSA, **10a**) and suberoylanilide hydroxamic acid (SAHA, **10b**), have been established to be potent HDAC inhibitors. Great attention has been paid to the study of interactions of these two prototype compounds with HDAC.

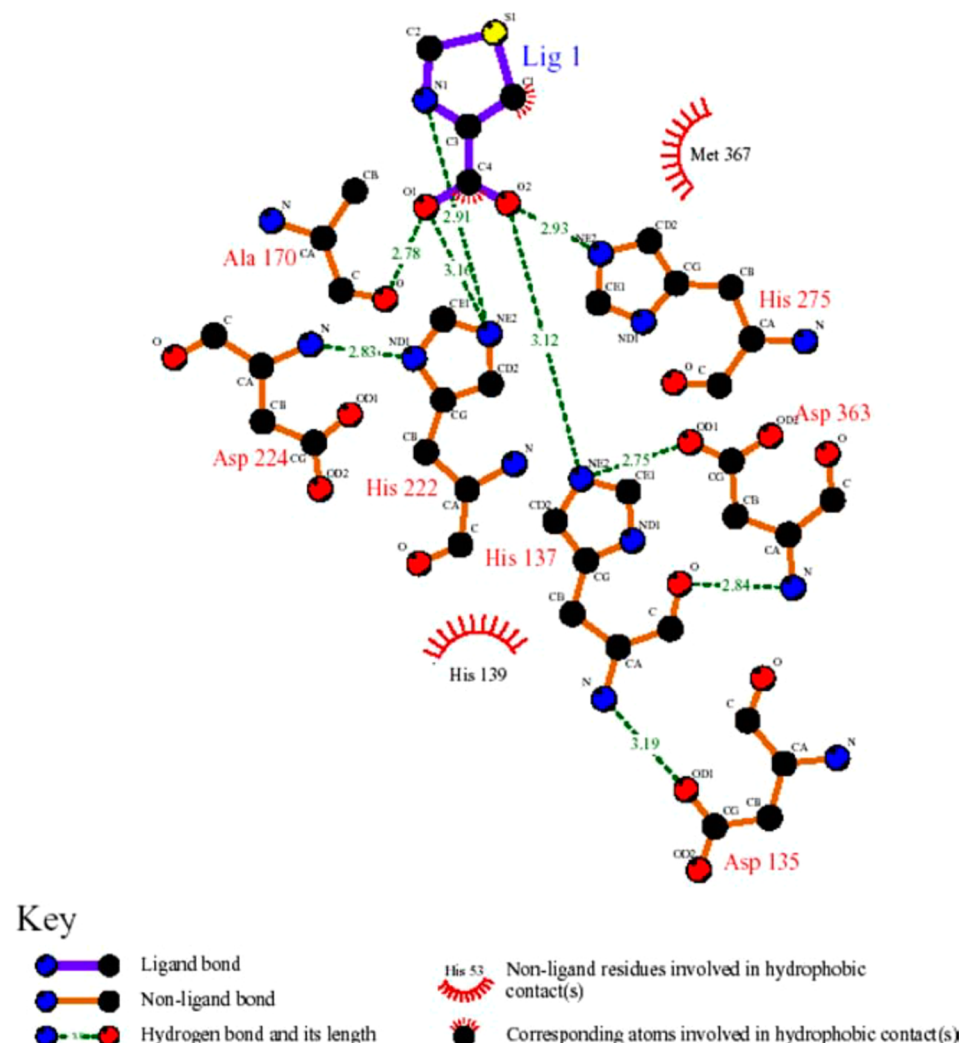
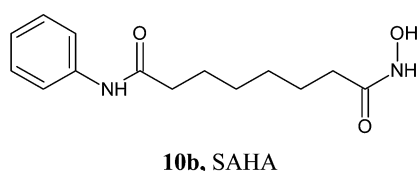
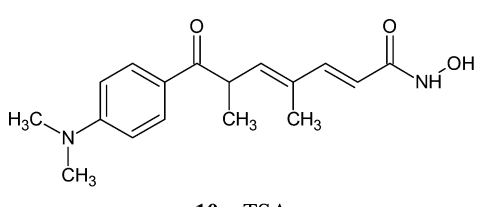


Figure 14. Molecular docking simulations of 7 obtained at lowest energy conformation, highlighting potential hydrogen bondings, mainly with Ala170, His222, His275, and His137 and hydrophobic contacts with His139 and Met367. Reprinted with permission from ref 132. Copyright 2006 Springer.



The X-ray crystal structure of a histone deacetylase like protein (HDLP), a bacterial HDAC homologue, complexed with TSA has been resolved, revealing a distinctive mode of protein–ligand interactions.¹⁴⁰ The catalytic domain of HDAC has been observed to consist of a narrow tube-like pocket with a depth of 4–6 carbon straight chain and a Zn²⁺ ion at the bottom (Figure 17).¹⁴¹ Additionally, there are certain hydrophobic residues. Therefore, potent HDAC inhibitors must

possess a hydrophobic group, which may be called a cap group that might have hydrophobic interaction at the entrance of the catalytic domain, an aliphatic chain, usually consisting of five or six carbons, and a zinc-binding group (ZBG), which can interact with Zn²⁺ ion at the bottom. These three requirements, in fact, constitute a well-accepted pharmacophore model of HDAC inhibitors.

The family of HDAC enzymes is comprised of 18 isoforms, broadly grouped into four classes: Class I (HDAC1, 2, 3, and 8), Class II (HDAC4, 6, 7, 9, and 10), and Class IV (HDAC 11) HDACs, which are zinc-dependent enzymes, and Class III HDACs that are sirtuin proteins dependent on NAD⁺ for their activity.^{142,143} However, among all of these HDACs, only HDAC8 is functionally active. A highly malignant childhood cancer, neuroblastoma, derived from sympathetic nervous system,¹⁴⁴ is highly correlated only with the expression of HDAC8. An RNA interference study showed that HDAC8 is involved in the regulation of proliferation, clonogenic growth, and neuronal differentiation of neuroblastoma cells. Therefore, the attention has been widely paid to the inhibition of HDAC8 and consequently to its structural elucidation. Now the crystal structures of HDAC8 (PDB entry code 1T64) and histone deacetylase-like protein (PDB entry code 1C3R) are available.

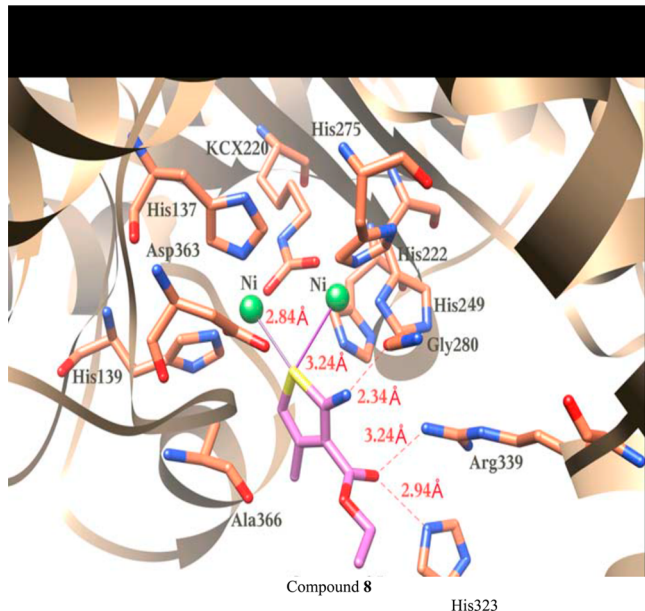


Figure 15. Docking of compound 8 in the active site of BP urease. The purple line indicated coordination between nickel ions and ligand atoms, whereas the red dotted line represented hydrogen bonding between ligand atoms and active site residues. Reprinted with permission from ref 133. Copyright 2010 Elsevier.

Some authors, however, attempted to present homology models of HDAC1, HDAC2, and HDAC3, which were validated by comparison with the X-ray structure of HDAC8.¹⁴⁵

For the design of potent HDAC inhibitors, many authors attempted to develop pharmacophore models particularly for HDAC8 inhibitors. Sundrapandian et al. built the pharmacophore model with a diverse training set containing 20 compounds.¹⁴⁶ This model was shown to have one hydrogen-bond acceptor (HBA) group, two hydrogen-bond donor (HBD) groups, and a hydrophobic (HYP) group with distance constraints (Figure 18). This model was called Hypo1 model.

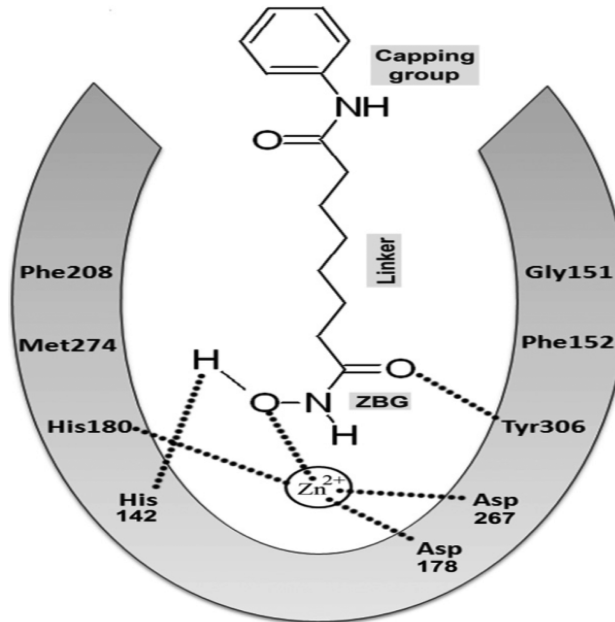


Figure 17. Schematic representation of basic pharmacophore model and binding of hydroxamic acid-based HDAC inhibitors. Reprinted with permission from ref 141b. Copyright 2010 Elsevier.

Although this model misses the hydrophobic cap group, it was selected as the best model for further analysis. Figure 19 shows the mapping of the most and least active compounds (**11**, **12**) of the training set on this pharmacophore model. On the basis of this model, three new compounds with high potency, HTS 09035, BTB 08560, and RF 02863 (Figure 20), were identified, whose overlay on the pharmacophore model is shown in Figure 21 and their interactions with HDAC8 in Figure 22. The estimated activity values of these three compounds were 0.807, 0.49, and 0.004 μM , respectively. The HTS 09035, with lowest activity, is a derivative of 1,2,4-thiazole-3-thione with a long alkyl chain. Its low activity was supposed to be due to the lack

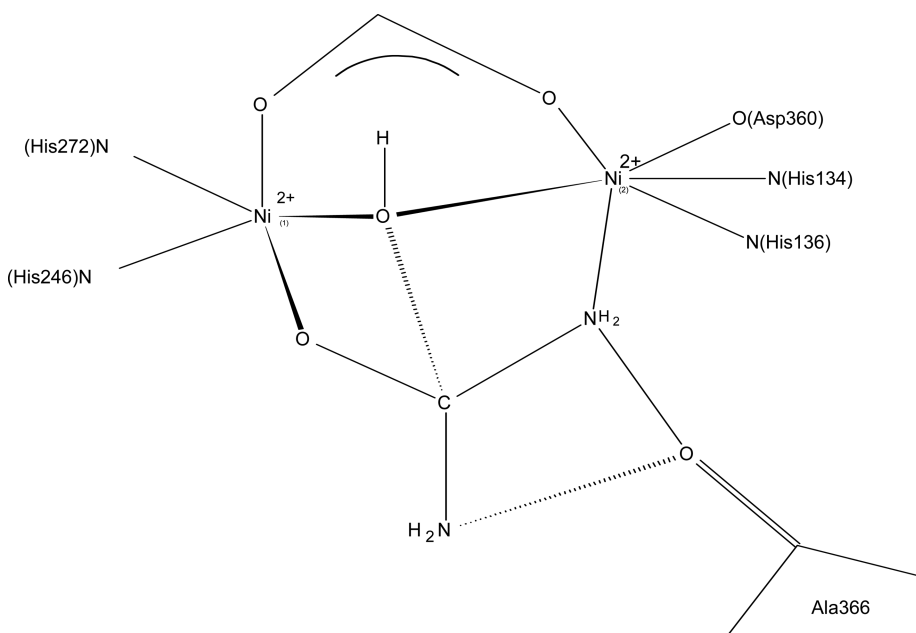


Figure 16. A schematic representation of the binding of urea (substrate) to urease.

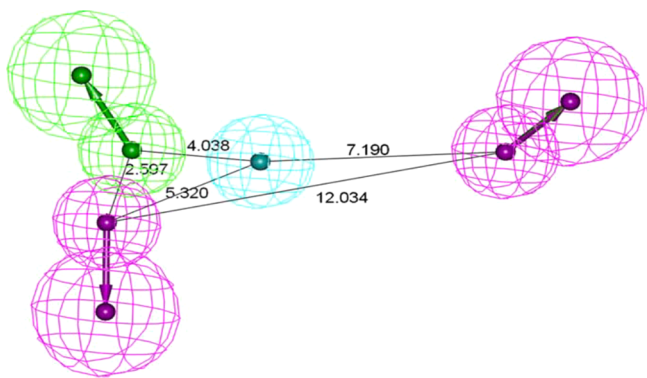
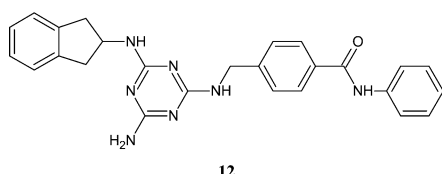
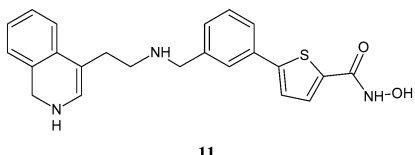


Figure 18. Best pharmacophore model Hypo1 represented with distance constraints and pharmacophoric features as hydrogen-bond acceptor (green), hydrogen-bond donor (magenta), and hydrophobic (cyan). Reprinted with permission from ref 146. Copyright 2010 Elsevier.

of the hydrophobic cap group. A replacement of its thiocarbonyl group with an indole (OPT 15, Figure 20) improved the binding and exhibited a better estimated activity ($0.11 \mu\text{M}$). No other substitution was found to be as fruitful.



Bozorgi et al.¹⁴⁷ and some other authors¹⁴⁸ pointed out that a potent HDAC inhibitor must have a zinc binding group to chelate the Zn^{2+} ion in the active site of the enzyme, a linker to access the active site, and a cap group for interactions with the external surface of the enzyme. Vanommeslaeghe et al.¹⁴⁹ pictured more specifically the following structural features in an HDAC inhibitor.

- (a) A group A, which may be a soft nonbonding electron pair donor that can coordinate with the Zn^{2+} ion and accept an H-bond from the phenolic OH of Tyr297 residue or/ and donate an H-bond to the phenolic O of the same.
- (b) A group B that can link the zinc-chelating moiety to the spacer and hence be at least trivalent.
- (c) A group C, which can donate an H-bond to His132. This can also be at least a trivalent.
- (d) A group D, which can be a proton donor to protonate His131 and subsequently accept an ionic H-bond from it and have strong interaction with the zinc ion.

All of the above features are well depicted in Figure 23. In their QSAR study on a large set of 313 compounds of diverse structures, Bozorgi et al.¹⁴⁷ had derived a model as shown by eq 7, where SP20 is the Randic molecular profile for most distant pairs of atoms, piPC09 is a parameter that shows the effect of ninth distanced atomic environment, HATS8v refers to atomic van der Waals volume, AlogP is hydrophobic parameter calculated on the basis of hydrophobic atomic constants, and nR06 refers to the number of six-membered rings. This model has been of only predictive value and not of much mechanistic value. It, however, showed that highly hydrophobic molecule or a molecule that may have large number of six-membered rings may not be very active, probably because of the steric region.

$$\begin{aligned} \log(\text{IC}_{50}) = & -0.08 \text{ SP20} - 0.07 \text{ piPC09} - 78.42 \text{ HATS8v} \\ & + 0.04 \text{ A log } P + 0.61 \text{ nR06} + 4.71 \end{aligned} \quad (7)$$

$$n = 313, r^2 = 0.75, r^2_{cv} = 0.75, s = 0.52, F = 1207$$

Chen et al.¹⁵⁰ had derived a pharmacophore for HDAC1 inhibitors using Catalyst 4.10 software (Accelrys Inc., San Diego, CA) from a series of 30 hydroxamic acids. The best pharmacophore was found to consist of five features: a hydrogen-bond donor, a hydrogen-bond acceptor, and three hydrophobic (HY) features. This model was named as the Hypo1 model. One of the three hydrophobic features, HY1, can interact with the two juxtaposed phenyl moieties of Phe141 and Phe198 of the enzyme. The other two hydrophobic features FY2 and FY3 mapped to the cap group of HDAC inhibitors make contacts at the pocket entrance. The carbonyl oxygen of CO group of the hydroxamic acid serves as an H-bond acceptor and the OH of the NHOH moiety as the H-bond donor. The most active compound (13a) of the training

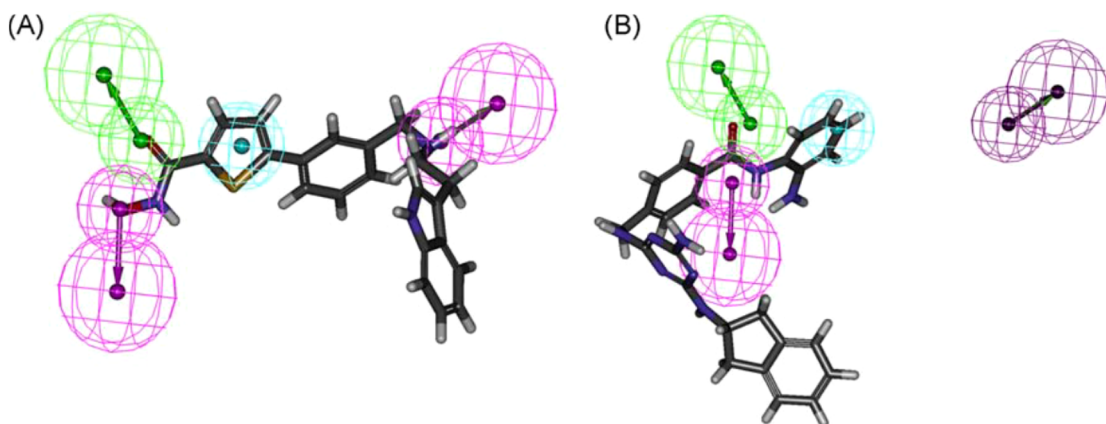


Figure 19. Overlay of most active (A) and least active (B) compounds in the training set upon the best pharmacophore model Hypo1. Pharmacophoric features: hydrogen-bond acceptor (green), hydrogen-bond donor (magenta), and hydrophobic (cyan). Dark magenta color represents the missing hydrogen-bond donor feature. Reprinted with permission from ref 146. Copyright 2010 Elsevier.

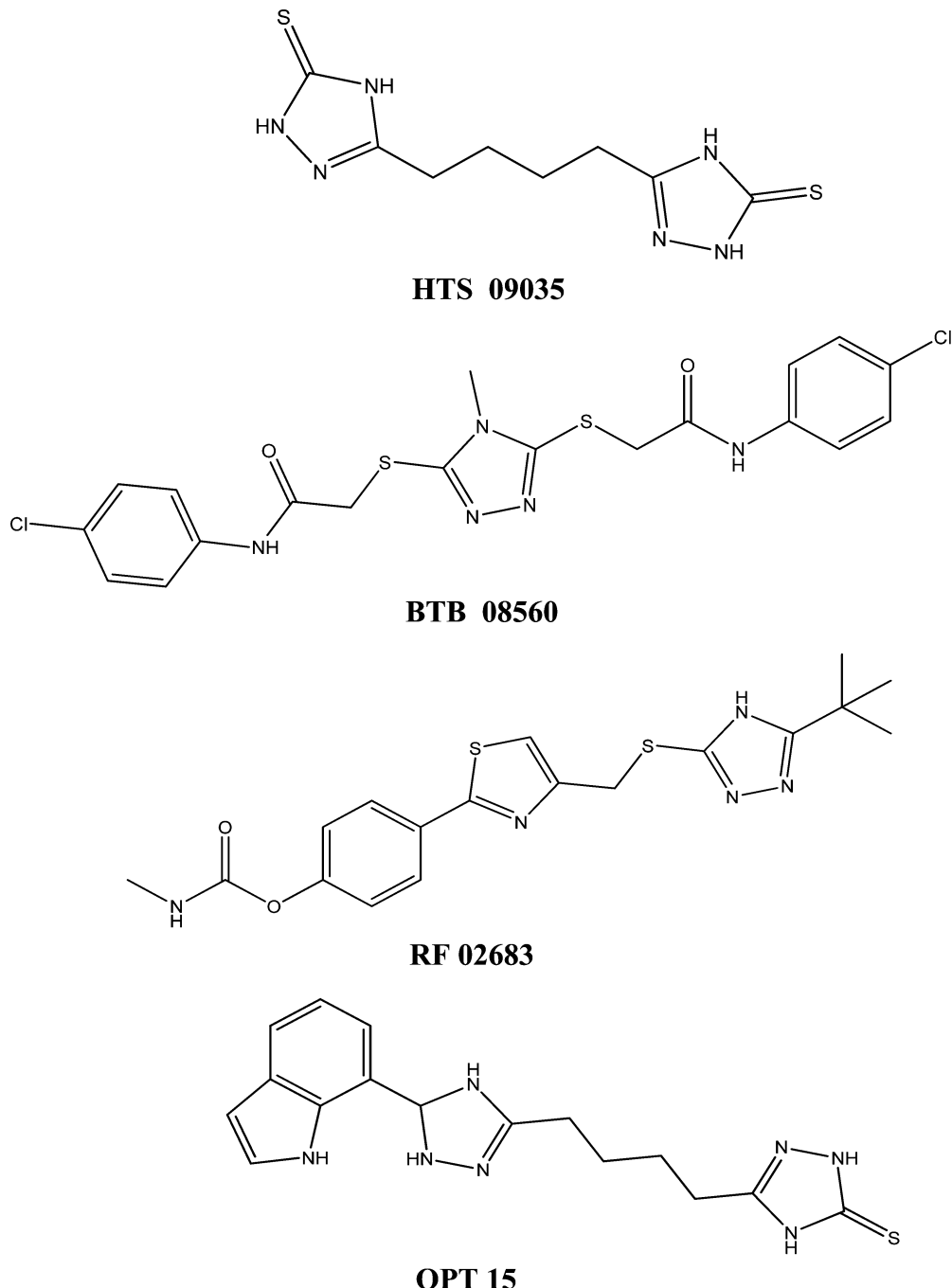
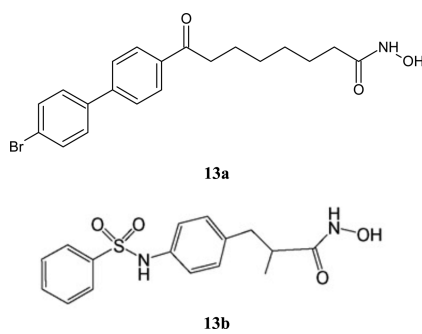


Figure 20. 2D representations of the final hit compounds.¹⁴⁶

set was found to closely map this pharmacophore model (Figure 24). Figure 24 also showed, as an example, the mapping on Hypo1 of a training set compound (**13b**), for which two oxygen atoms of CONHOH moiety served as HBA and HBD features, respectively. This pharmacophore model was found to be in good agreement with structural information derived from the binding domain of HDLP by X-ray. The conformation of TSA (**10a**) bound with HDLP was found to successfully fit all chemical features of the Hypo1 model (Figure 25).

Several pharmacophore models for HDAC inhibitors have been defined by different authors with a slight difference from each other. Chen et al.¹⁵¹ built a pharmacophore model manually by mapping the chemical features on the corresponding groups of TSA in its bound conformation. TSA contains 22



features to bind with HDACs. Chen et al. selected a subset of these features including two hydrogen-bond acceptors and

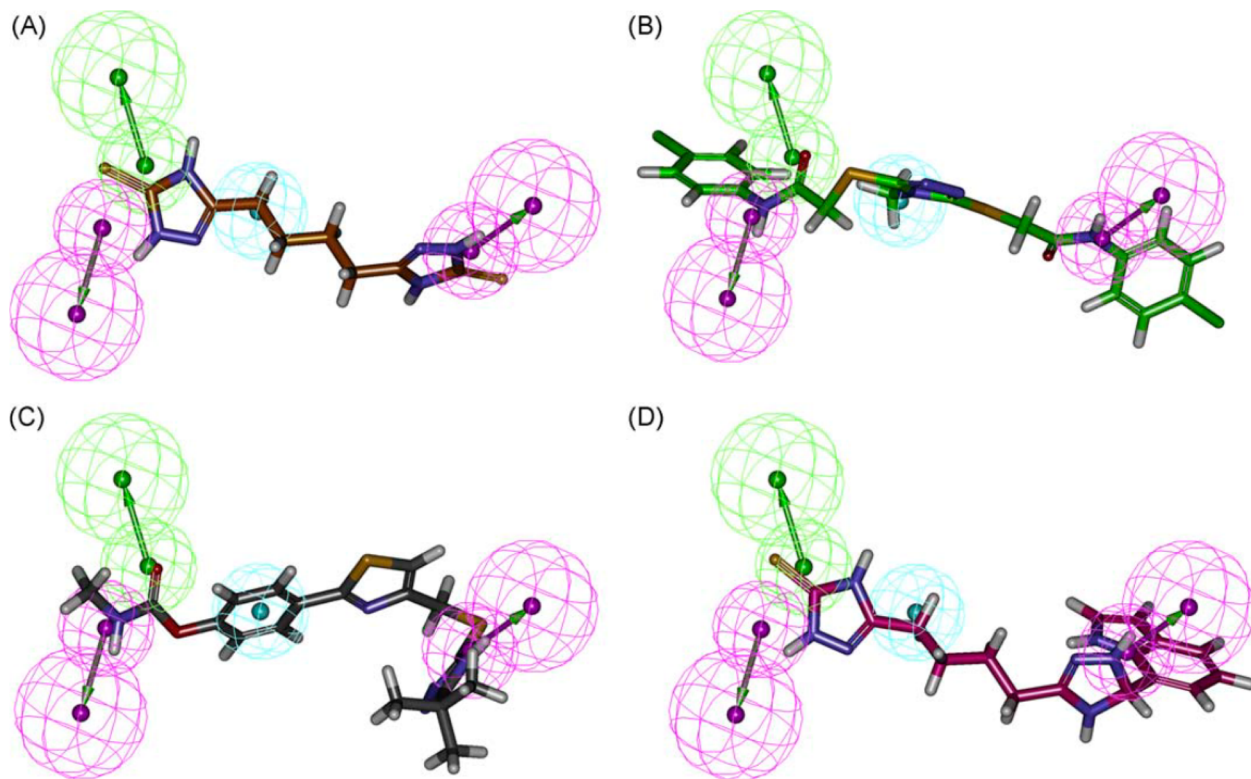


Figure 21. Pharmacophore overlay of hit compounds. (A) HTS 09035, (B) BTB 08560, (C) RF 02863, and (D) OPT-15. Reprinted with permission from ref 146. Copyright 2010 Elsevier.

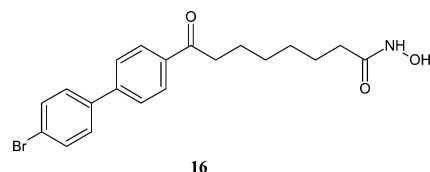
three hydrophobic features. The important features of the pharmacophore model could be identified from the interaction information of the TSA–HDLP complex, which reflect the primary interactions between the protein and the ligand. An essential part of the pharmacophore is the ZBG that is constituted of two hydrogen-bond acceptors. Another essential part may be a hydrophobic region, which may have effective hydrophobic interactions with the enzyme.

Vadivelan et al.¹⁵² had developed a HypoGen (Hypo-1) model that consisted of four pharmacophore features: one hydrogen-bond acceptor, one hydrophobic aliphatic, and two ring aromatic centers. This model was validated against 378 known HDAC inhibitors with a correlation coefficient of 0.897. This model, as shown in Figure 26 with its distance constraints, was mapped to the most and the least active compounds of the training set (14 and 15 with $IC_{50} = 0.02$ nM and 1500 μ M, respectively) (Figure 27).

Nair et al.¹⁵³ had proposed a pharmacophore model (AAPR) that consisted of five structural features: three H-bond acceptors (AAA), one positive ionic group (P), and one aromatic feature (R).

All of the above models proposed by various authors differ only slightly. Any set of compounds following any pharmacophore model would further require modifications in terms of their steric, physicochemical, and electronic properties to have the optimum interactions with the receptor. For this purpose, many authors reported COMFA and CoMSIA studies on different classes of HDAC inhibitors. For a large series of TSA analogues, Juvale et al.¹⁵⁴ performed CoMFA and CoMSIA studies that produced steric and electrostatic contour plots for CoMFA and the steric, electrostatic, hydrophobic, and H-bond donor and acceptor contour plots for CoMSIA. For each

contour plot, the most active compound in the series ($pIC_{50} = 8.70$), as represented by **16**, was taken.



In the COMFA steric contour plot, the phenyl ring of the molecule was shown to sterically favor the activity, and a substitution on the spacer atoms adjacent to the phenyl ring was also shown to favor the activity, but any substitution on the carbon next to the hydroxamic acid moiety was shown to be unfavorable. In the electrostatic plot, a red contour near the phenyl ring of the compound suggested that a high electron density in this region might increase the activity and a large blue contour surrounding the spacer chain emphasized the necessity of a positively charged group. Thus, hydroxamate moiety seems to be essential for HDAC inhibition activity.

The steric contour maps of CoMSIA were almost similar to those of CoMFA. However, in electrostatic contour plots of CoMSIA, the blue contours over the hydroxamic acid group signified the importance of this group. A red polyhedra over the phenyl ring had indicated that the presence of electron-rich functional groups at this position would increase the activity. In CoMSIA hydrophobic plots, a lipophilic favorable region was indicated to be near the aromatic ring, suggesting that the lipophilicity of the cap portion of the molecule was important for the activity. A hydrophilic favorable region was shown to surround the hydroxamate functional group.

In H-bond acceptor and donor plots of CoMSIA, the H-bond acceptor fields exhibited the importance of positively

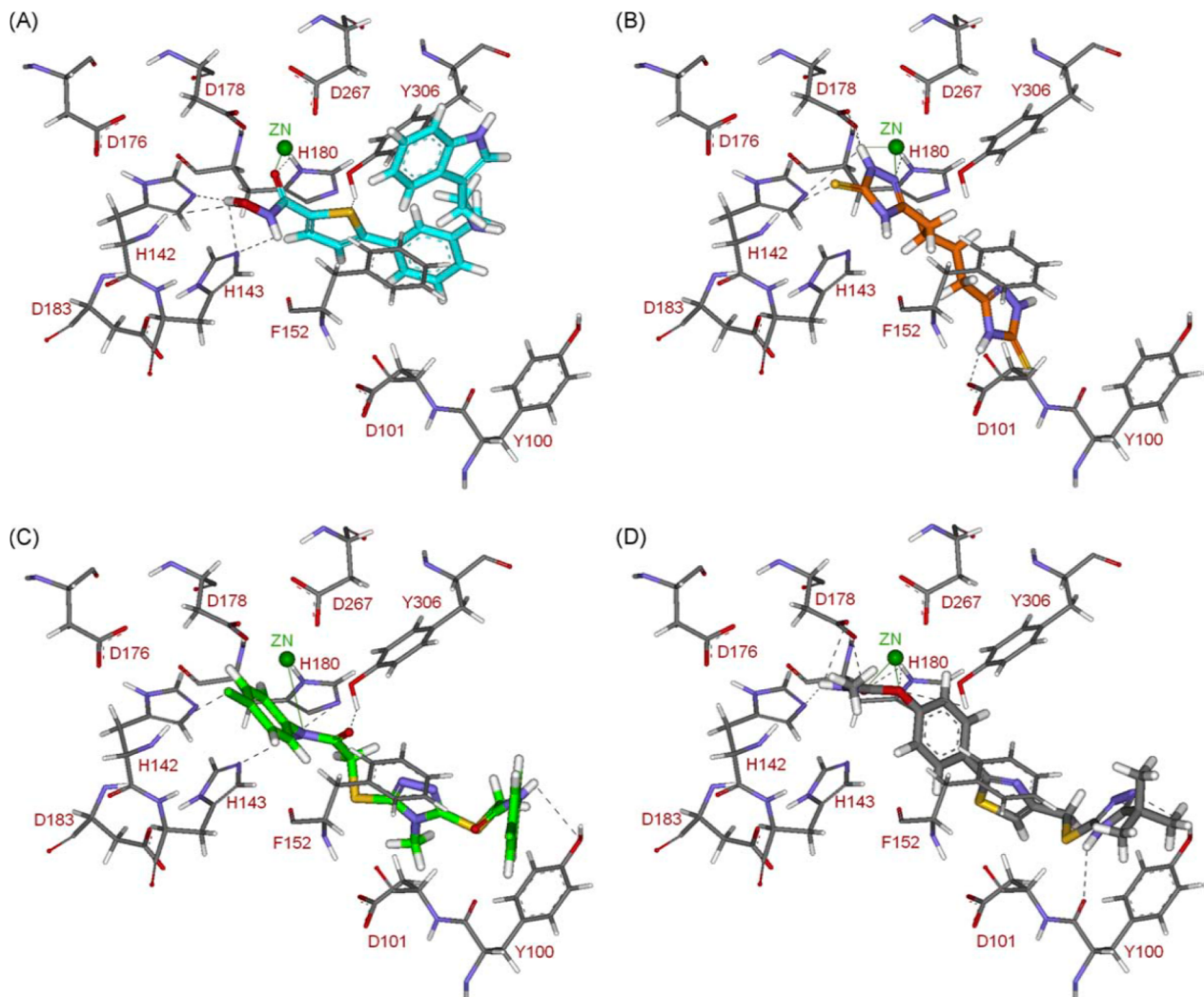


Figure 22. Molecular docking results. Docked orientations of (A) compound 11 of training set (cyan color), (B) HTS 09035 (orange color), (C) BTB 08560 (green color), and (D) RF 02683 (gray color). Active site residues are shown in stick form and metal (Zn^{2+}) ion in green sphere. Hydrogen-bond networks with protein residues and metal ions are represented in black dotted and green straight lines, respectively. Reprinted with permission from ref 146. Copyright 2010 Elsevier.

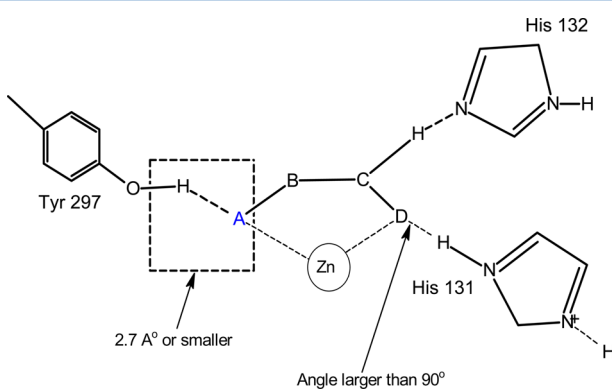


Figure 23. Common framework for bideterminate chelating group. Reprinted with permission from ref 147. Copyright 2013 Elsevier.

charged hydroxamate group, and the H-bond donor plots showed the necessity of hydroxyl group of hydroxamic acid moiety. All of these findings of the authors were in accordance with the pharmacophore models defined by various authors.

For the same set of compounds, however, Wagh et al.¹⁵⁵ had also reported a QSAR model (eq 8), using genetic function

approximation (GFA). This model indicated that molecular shape analysis (MSA), thermodynamic, and structural descriptors are important for HDAC inhibition.

$$\begin{aligned} \log(1/IC_{50}) = & 0.1098 \log P + 0.1624 \text{Molref} - 0.0017 \text{NCOSV} \\ & - 0.0521 \text{DIFFV} - 11.842 \\ n = 40, r^2 = 0.72, r^2_{cv} = 0.611, s = 0.16, r^2_{\text{pred}} = 0.585, F = 15.81 \end{aligned} \quad (8)$$

In eq 8, $\log P$ refers to the hydrophobic character of the molecule, Molref stands for the molar refractivity of the molecule, NCOSV is an MSA descriptor defining the difference between the steric volume and the common overlap steric volume of a molecule, and DIFFV is a shape descriptor referring to the differential volume, the difference between the volumes of individual molecule and shape reference molecule. Thus, the coefficients of these parameters indicate that while the hydrophobicity and the molar refractivity, which refers to the polarizability of the molecule, would be favorable to the activity, the bulk of the molecule may have the negative effect.

For a larger set of hydroxamic acid analogues that included all TSA analogues treated by Wagh et al. and several SAHA

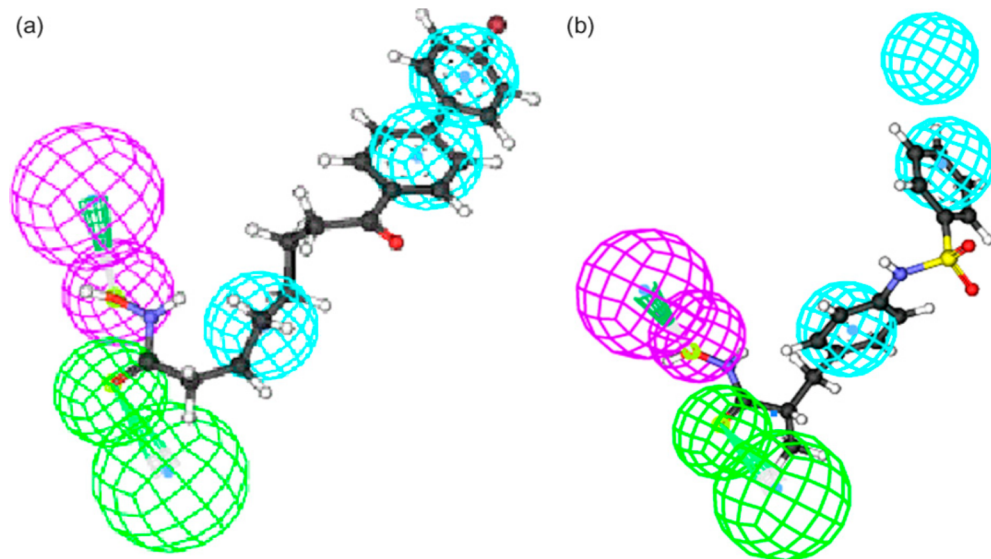


Figure 24. Training set compound (**13a**) and a test compound (**13b**) mapped to Hypo1. Hypothesis features are color-coded as follows: hydrophobic aromatic, light blue; hydrogen-bond donor, violet; and hydrogen-bond acceptor, green. Reprinted with permission from ref 150. Copyright 2008 Elsevier.

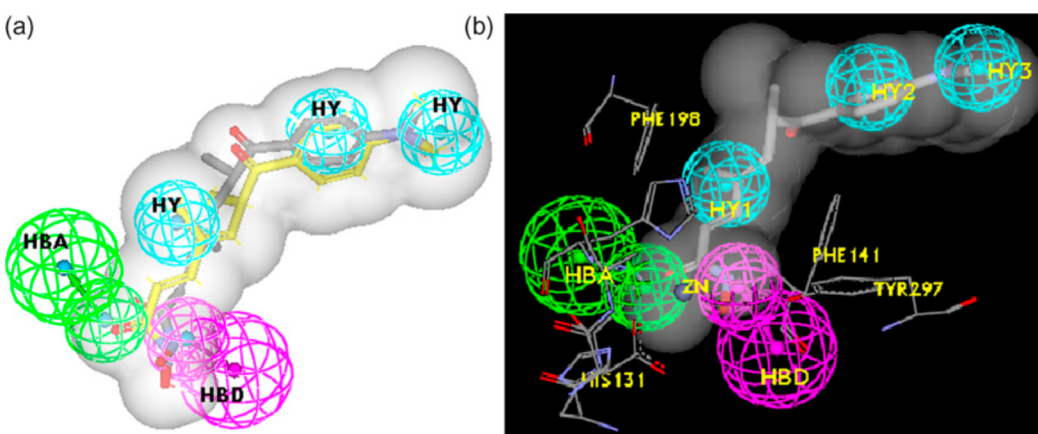


Figure 25. (a) Catalyst conformation from 3D mapping of TSA onto pharmacophore Hypo1: the bound conformation from X-ray crystal structure and integrated shape are presented, with the catalyst conformation in gray and bound conformation in yellow (HBA, hydrogen-bond acceptor; HBD, hydrogen-bond donor; HY, hydrophobic region). (b) The pharmacophore Hypo1 mapped to a HDLP crystal structure: the hydrogen-bond acceptor feature is shown in green, the hydrogen-bond donor feature in purple, and the hydrophobic features in light blue. The carbon atoms of the HDLP residues are shown in gray. Zinc ion is shown in sphere. The ligand TSA is shown in stick. The shaded part that surrounds the molecule shows the shape. Reprinted with permission from ref 150. Copyright 2008 Elsevier.

analogues, Xi et al.¹⁵⁶ had derived a QSAR model as shown by eq 9, where PEOE_VSA-O stands for the sum of the van der Waals surface area (ν_i) of each atom, where the partial charge q_i of each atom calculated by the Partial Equalization of Orbital Electro negativities (PEOE) method is in the range of 0–0.05, Q_VSA_NEG stands for total negative van der Waals surface area, where each q_i is negative, Slog_VSA8 stands for the sum of ν_i such that contribution to $\log P$ of each atom (L_i) is in the range of 0.3–0.4, and E_sol stands for salvation energy. Thus the correlation suggested that the major role in HDAC inhibition activity of compounds was of van der Waals surface area of atoms, where the salvation energy of the compounds might play a negative role.

$$\begin{aligned} \log(1/\text{IC}_{50}) = & 0.0114(\text{PEOE_VSA-O}) \\ & + 0.0114(\text{Q_VSA_NEG}) + 0.0245(S \log P_{\text{VSA8}}) \\ & - 0.00699(E_{\text{sol}}) + 2.699 \end{aligned}$$

$$n = 94, r^2 = 0.76, r^2_{\text{cv}} = 0.73, s = 0.63, F = 70.03 \quad (9)$$

Kalyaanmurthy and Phoebe Chen¹⁵⁷ recently made an interesting study to investigate the significance of protonation states of HDAC inhibitors. A TSA-like HDAC inhibitor can exist in protonated and deprotonated states as shown in Figure 28. The significance of protonated states of HA inhibitor has been reported earlier also by some authors^{158–161} but with some contradictions; for example, Wang et al.'s density functional theory (DFT)-based study¹⁵⁹ showed that deprotonation of hydroxamic acids (HAs) leads to strong bidentate coordination with the Zn^{2+} of HDACs, while the neutral forms

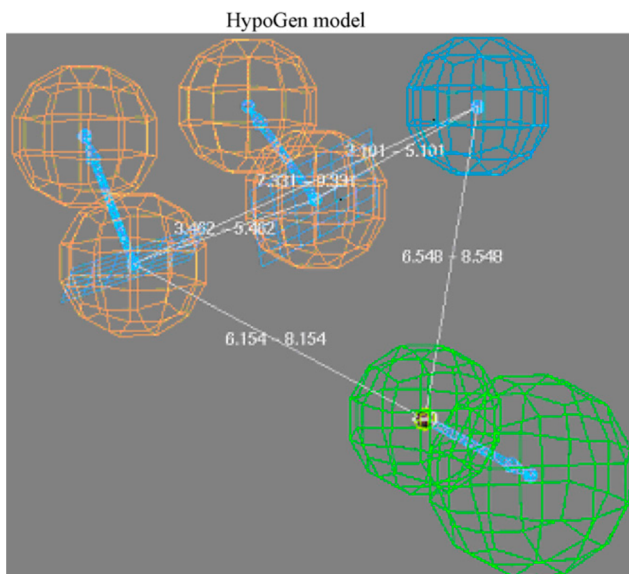
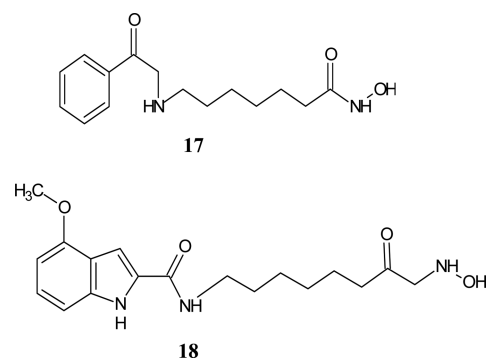


Figure 26. Histone deacetylase inhibitor pharmacophore model with its distance constraints and features: green, one hydrogen-bond acceptor; light blue, one hydrophobic aliphatic; and orange, two aromatic rings. Reprinted with permission from ref 152. Copyright 2008 Elsevier.

exhibit only monodentate coordination vis-a-vis Tavakol's DFT finding¹⁶⁰ that the neutral or protonated form of HAs are the most stable structures. A recent study on SAHA reported that its deprotonated form is less stable than its neutral or protonated form.¹⁶¹ To overcome these contradictions, Kalyaanmurthy and Phoebe Chen¹⁵⁷ made a quantum polarized ligand docking (QPLD) and molecular mechanics-generalized Born surface area (MM-GBSA) study on some HA inhibitors. Their QPLD results showed that the protonated states of inhibitors exhibit a better role than the deprotonated ones with Class I HDACs. With this class of HDACs, the hydrogen-bond analyses exhibited more favorable binding modes and interactions. The molecular electrostatic potentials and other physicochemical descriptors were found to support these findings, and also a MM-GBSA study of these authors predicted the higher (more negative) binding free energies of protonated states than the neutral forms and that of

deprotonated forms quite erroneous and unrealistic (Figure 28).

Guo et al.¹⁶² performed CoMFA, CoMSIA, and FlexX docking studies on a series of indole amide analogues having general structures as **17**, where Ar can be a substituted or unsubstituted amide ring attached through different positions. The activity of these compounds was assayed predominantly against HDAC1 and HDAC2. Selected ligands were docked into the active site of human HDAC1. Human HDAC1 and HDAC2 are highly homologous to HDAC8, especially on the binding site of Zn²⁺. Therefore, the homology structure of HDAC1 based on human HDAC8 in complex with TSA and SAHA (PDB entries 1T64, 1T67) was applied. The docking results showed a novel binding mode of indole amide analogues in human HDAC1 catalytic core, where the indole amide group was located in the open pocket and anchored to the protein through a pair of H-bonds between Asp99 oxygen atom and amide NH group on the ligand. Figure 29 shows the mode of interaction with HDAC1 of the most potent compound in the series, whose structure was as **18**. The figure shows that the hydroxamic acid moiety of the compound is located in the active site and interacts with the catalytic Zn²⁺ through its CO and OH. Further, NH's of amide as well as of indole ring are shown to interact with COO of Asp99 through the formation of potential hydrogen bonds, which perhaps affects the orientation of all indole amide hydroxamic acid-based inhibitors.



In COMFA and CoMSIA studies made by Guo et al.,¹⁶² the CoMFA steric countour plots suggested that any bulkier

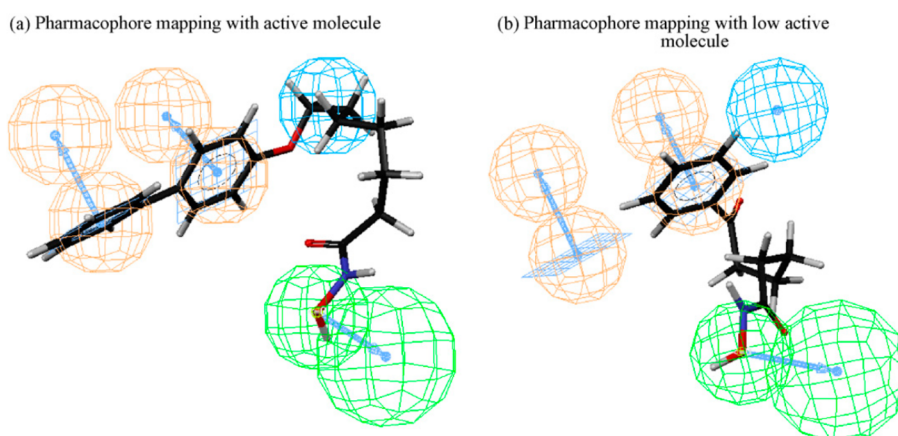


Figure 27. Hypo-1 mapped to the most active molecule (**14**, IC₅₀ = 0.02 nM) (a) and also to the least active one (**15**, IC₅₀ = 1500 nM) (b) in the training set. Pharmacophore features are color coded with green, hydrogen-bond acceptor; light blue, hydrophobic aliphatic; and orange, aromatic rings. Reprinted with permission from ref 152. Copyright 2008 Elsevier.

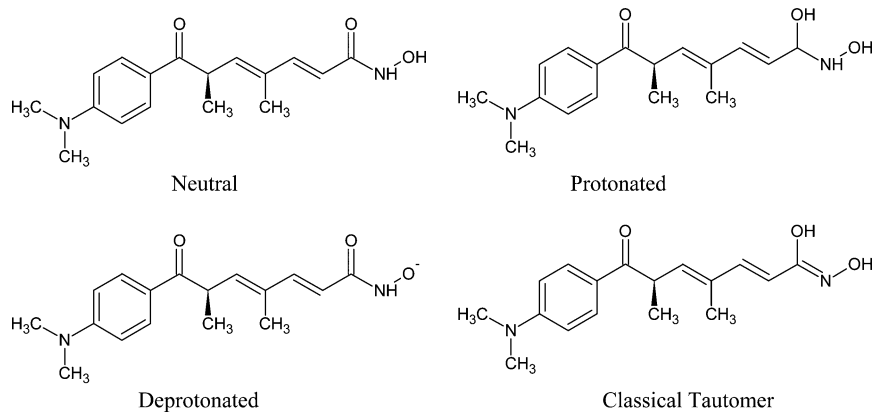


Figure 28. Different structural states of a TSA-like HDAC inhibitor.

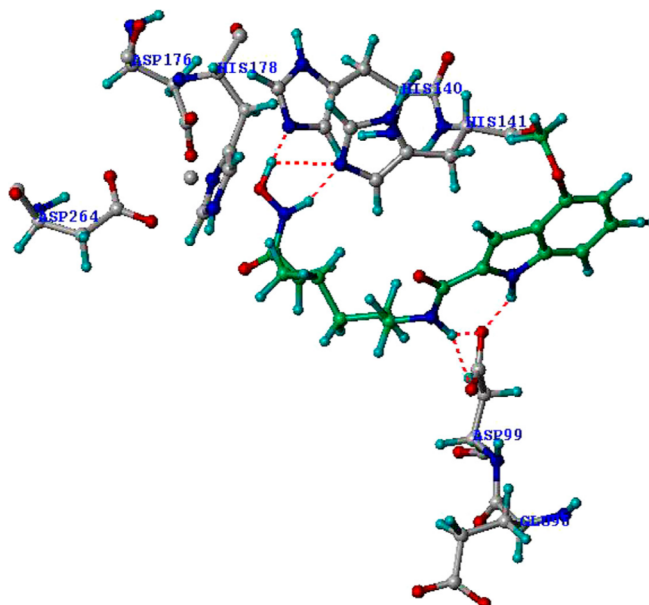


Figure 29. Highest score docking result in the FlexX docking of compound 18 (docked into the HDAC1 catalytic core). Compound 18 is in green, and some residues are shown in the tube/ribbon graphic. Reprinted with permission from ref 162. Copyright 2005 Elsevier.

substituent would be preferred at the 4 position of the indole ring, and thus compounds with bulkier substituents, such as OCH_3 , were found to have better activity than those having no substituent at this position. This is probably due to the involvement of bulkier substituent at this position in hydrophobic interaction. Likewise, the CoMFA electrostatic contour plots suggested that the negative charges in the 4- and 5-positions of the indole ring would be important to the ligand binding, and thus a charge-withdrawing group linked to these position may enhance the activity. Examples were cited of the compounds having Br or F at 5-position to be more potent than those having only H at this position. These two CoMFA contour plots are shown in Figure 30.

The CoMSIA contour plots are shown in Figure 31 where steric and electrostatic contours (Figure 31A,B) are almost similar to those of CoMFA. The hydrogen-bond donor contours in Figure 31C highlight the areas near which the H-bond donor on the ligands can form H-bonds. The cyan-colored contour near the NH of amide indicated that an H-

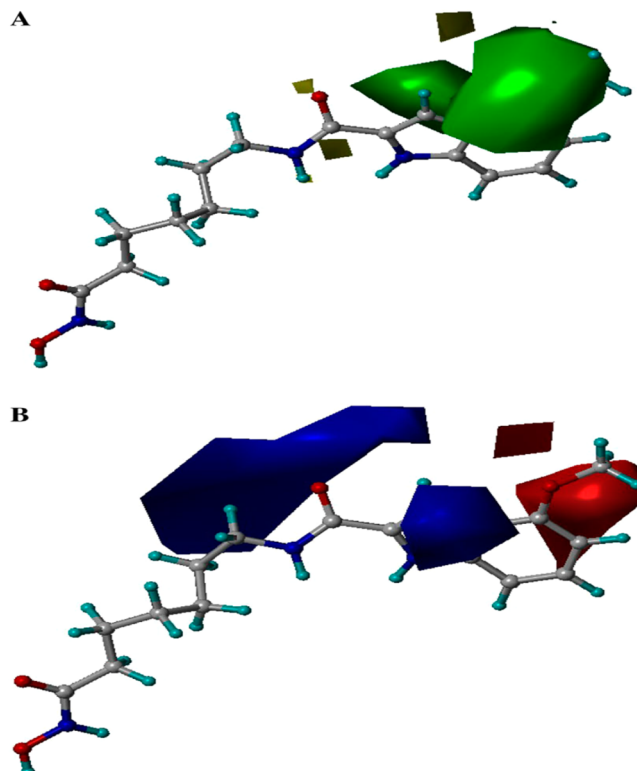


Figure 30. Stereoview of the contour plots (SD^*coeff) of the CoMFA. (A) Steric fields: green contours indicate regions where bulky groups can increase activity, whereas yellow contours indicate regions where bulky groups can decrease activity. (B) Electrostatic fields: blue contours indicate regions where electropositive groups can increase activity, whereas red contours indicate regions where electronegative groups may increase activity. Potent HDAC inhibitor 18 is displayed in the background for reference. Reprinted with permission from ref 162. Copyright 2005 Elsevier.

bond donor substituent at this position can enhance the HDAC inhibitory activity.

Xiang et al.¹⁶³ made CoMFA, CoMSIA, and docking studies on a series of 65 compounds with diverse structures, but containing the hydroxamic acid moiety. Their CoMFA and CoMSIA studies also suggested almost similar structural modifications for hydrophobic, electrostatic, and H-bond interactions. Their docking study showed how a compound such as 19 of the series that had the highest activity could interact with HDAC8 (PDB entry 1T64). The hydroxamic acid

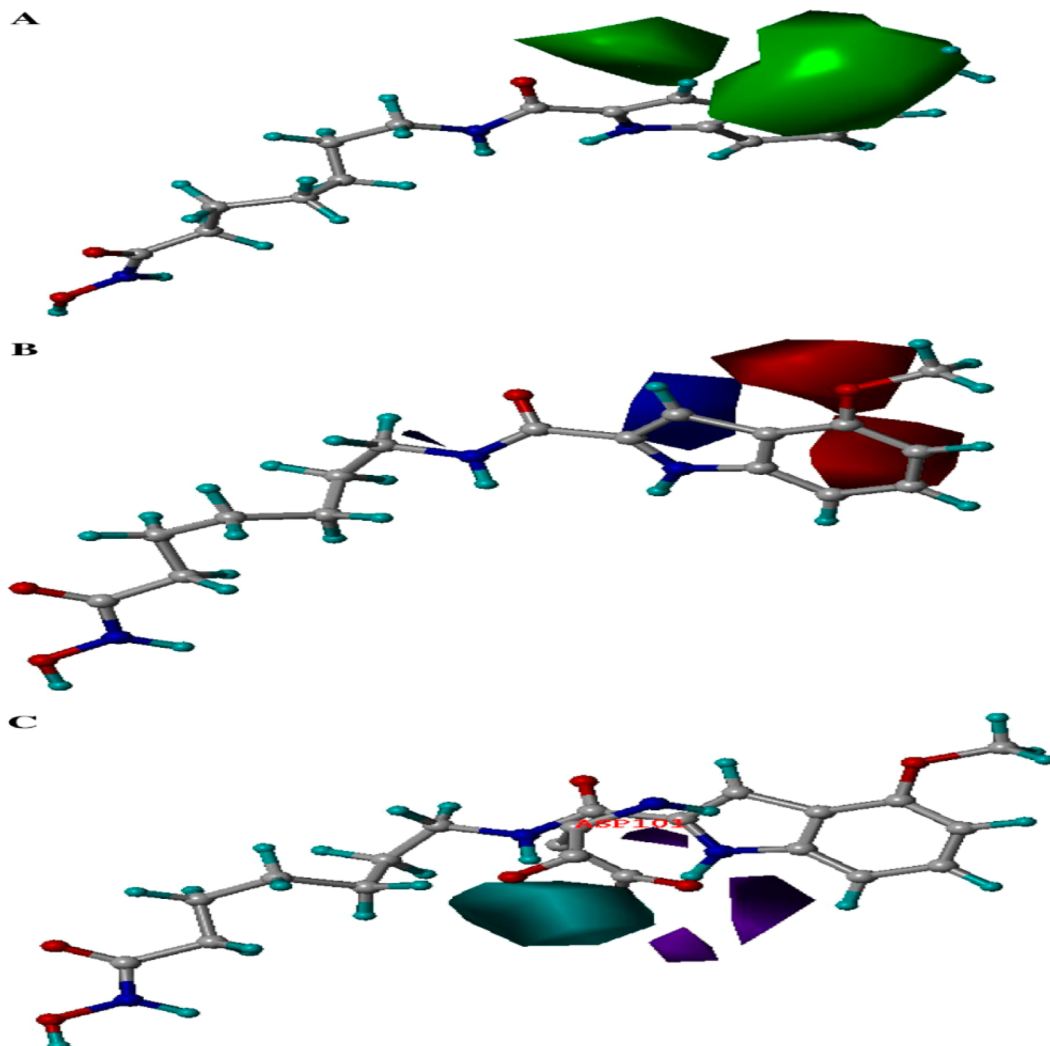
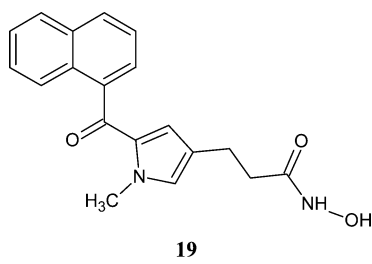


Figure 31. Stereoview of the contour plots of the CoMSIA: (A) steric fields (green, bulky substitution favored; yellow, bulky substitution disfavored), (B) electrostatic fields (blue, electropositive group favored; red, electronegative group favored), and (C) hydrogen-bond donor fields (cyan, favored; purple, disfavored). Potent HDAC inhibitor 18 is displayed in the background for reference. Reprinted with permission from ref 162. Copyright 2005 Elsevier.

moiety was found to interact with two nitrogen atoms of His143 and His142 through H-bond, carbonyl oxygen to interact with hydroxyl of TVR306, and other carbonyl oxygen to form the H-bond with H₂O657. The hydroxamic acid moiety was also observed to be ligated with Zn²⁺ through both the oxygen atoms and the nitrogen. The hydrophobic parts of the molecule were shown to fall into the hydrophobic pocket at the bottom of the active site of the enzyme and have hydrophobic interaction with it. A tube-like hydrophobic pocket at the bottom of the active site is formed by the amino acid residues Lys33, Ile32, Ile34, Pfo35, and Ala32 and is too narrow to accommodate any bulky substructure.



All of the above 3D QSAR studies discussed so far provided enough structural information about the ligands to have the best interaction with HDACs. Supporting details, however, could be had from 2D QSAR studies. We have already discussed a 2D QSAR model derived by Xi et al. for a large set of hydroxamic acid analogues (eq 9). Ponitiki and Hadjipavlou-Litina¹⁶⁴ reported several QSAR models comprehensively on several small sets of HDAC inhibitors just to find the same information as eq 9 provides. Their entire study revealed that the lipophilicity is one of the most important properties of the molecules that govern the HDAC inhibition activity of the hydroxamic acids. Additionally, steric factors such as molar refractivity or molar volume of the molecules and the sterimol parameters like B_1 and L of substituents were also found to affect the activity.

Kozikowski et al.¹⁶⁵ studied the HDAC inhibitory activity of some biphenyl-bearing hydroxamates (**20a**), mercaptoacetamides (**20b**), and phenylthioazole-bearing hydroxamates (**20c**) and performed a 2D QSAR on a combination of them to derive the correlations for some HDACs as shown by eqs 10–13.

$$\log(1/\text{IC}_{50})_{\text{HDAC}1} = 0.983(\pm 0.149)I_{\text{thiazole}} - 1.844(\pm 0.248)I_{\text{NHCOCH}_2\text{SH}} + 7.299(\pm 0.114)$$

$n = 23, r^2 = 0.920, s = 0.322, p < 0.0001 \quad (10)$

$$\log(1/\text{IC}_{50})_{\text{HDAC}2} = 0.606(\pm 0.151)I_{\text{thiazole}} - 2.127(\pm 0.195)I_{\text{NHCOCH}_2\text{SH}} + 6.183(\pm 0.112)$$

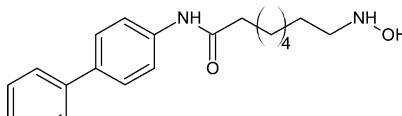
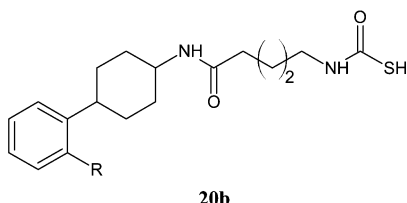
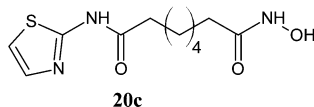
$n = 22, r^2 = 0.918, s = 0.318, p < 0.0001 \quad (11)$

$$\log(1/\text{IC}_{50})_{\text{HDAC}10} = 1.007(\pm 0.153)I_{\text{thiazole}} - 2.029(\pm 0.222)I_{\text{NHCOCH}_2\text{SH}} + 7.192(\pm 0.112)$$

$n = 22, r^2 = 0.918, s = 0.318, p < 0.0001 \quad (12)$

$$\log(1/\text{IC}_{50})_{\text{HDAC}6} = 0.711(\pm 0.184)I_{\text{thiazole}} - 1.429(\pm 0.246)I_{\text{NHCOCH}_2\text{SH}} + 0.046(\pm 0.023)(C \log P)^2 + 27.799(\pm 0.163)$$

$n = 23, r^2 = 0.918, s = 0.318, p < 0.0001 \quad (13)$

**20a****20b****20c**

In these equations, mostly indicator parameters have been used, and no role of any physicochemical parameter has been shown, except in eq 13 where a slight role of $C \log P$ has surfaced. The parameter I_{thiazole} has been used with a value of 1 for a thiazole and $I_{\text{NHCOCH}_2\text{SH}}$ with a value of 1 for a mercaptoacetamide. Both of the variables have a value of zero for other compounds. All four equations thus suggest that phenylthiazole derivatives (**20c**) will have better activity than other hydroxamates, and, on the other hand, mercaptoacetamides (**20b**) will have less activity as compared to other compounds. The better activity of phenylthiazole derivatives may be due to the involvement of their thiazole ring in some electronic or hydrogen-bond interaction with some residues in the active site of the HDACs, and the inferior activity of mercaptoacetamides may be due to the inability of the mercapto (SH) group to have any interaction with the receptor. In eq 13, the occurrence of only square term of $C \log P$ with a small positive coefficient might simply suggest that a hydrophilic–lipophilic balance may be better for HDAC6 inhibition activity.

The PC3 cell line antiproliferation activity reported by Lan-Hargest et al.¹⁶⁶ for some TSA analogues was, however, found

to be correlated with some physicochemical parameters by Wang et al.¹⁶⁷ as

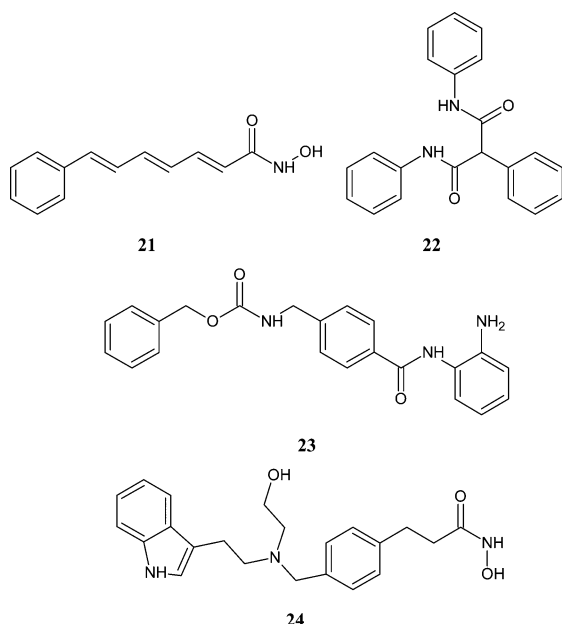
$$\log(1/\text{IC}_{50}) = 1.96 + 14.08 \text{Qco} - 15.73 \text{Glob} + 0.05 \text{FISA}$$

$n = 19, r = 0.96, F = 59.25, t\text{-value: Qco, } 4.33; \text{ Glob, } -4.02; \text{ FISA, } 9.70 \quad (14)$

where all of the statistical parameters show that the correlation is quite significant. In this equation, the Qco refers to atomic partial charge on the carbon atom of CONHOH moiety, Glob refers to the globularity of the compound, and FISA refers to the hydrophilic component of the solvent-accessible surface area of the compound. Thus, the high charge on the carbon atom will refer to the polarity of C=O bond, which may be involved in some polar interaction with the active site. However, the globularity of the molecule does not appear to be conducive to the activity. If the molecule is more globular, the solvent-accessible area would be reduced. The correlation shows that an increase in FISA would be advantageous to the activity, and this FISA, which refers to the hydrophilic component of the solvent-accessible surface area of the compound, would increase only when the molecule reduces its globularity and becomes more open.

From the molecular dynamics simulation of HDAC–inhibitor complexes, Wang et al.¹⁶⁸ had found that the interaction between the protein surface and inhibitor was playing an important role. These authors also found that some active site residues in the protein have some flexibility, which is usually not included in docking protocols. To investigate the differences between the four isoforms of Class 1 HDACs, that is, HDAC1, 2, 3, and 8, Wang et al.¹⁶⁸ made three-dimensional models of these isoforms using homology modeling. The excellent agreement between the homology model of HDAC8 with its X-ray structure, which was by then obtained, had validated the approach. In these homology models were docked three widely studied HDAC inhibitors TSA (**10a**), CG-1521 (**21**), and SK-683 (**22**). Three more HDAC inhibitors that are in clinical trials, SAHA (**10b**), MS-275 (**23**), and NVP-LAQ824 (**24**), were docked to the models of these HDACs, except for HDAC2. There were found too little differences in active site regions and 11 Å deep channels of these HDACs to be exploited to achieve any isoform selectivity, but small differences in the shape and charge distribution around the opening of the active site hold some promise for differentiation between HDAC1, HDAC3, and HDAC8, but not between HDAC1 and HDAC2.

6.2.1. An Overview of HDAC Inhibition. Because among all of the isoforms of HDAC, HDAC8 was found to be functionally most active, the greatest attention has been paid to the structure and inhibition of this isoform. Therefore, crystal structures of human HDAC8 complexed with TSA and SAHA (PDB entries 1T64 and 1T67) were determined, and also the X-ray crystal structure of a histone deacetylase like protein (HDLP), a bacterial HDAC homologue, complexed with TSA was resolved. As shown in Figure 17, the catalytic domain of HDAC was observed to consist of a narrow tube-like pocket with a depth of 4–6 carbon atoms straight chain and a Zn²⁺ ion at the bottom. Additionally, there are hydrophobic residues. Therefore, potent HDAC inhibitors must possess a hydrophobic group (may be called cap group) to have hydrophobic interaction at the entrance of catalytic domain, a zinc binding group (ZBG) at the other end to interact with Zn²⁺ ion, and between them an aliphatic chain, large enough (5–6 carbon



atoms) to push the ZBG near the Zn^{2+} ion. These three requirements constitute a well-accepted pharmacophore model of HDAC inhibitors. However, many authors attempted to develop some different pharmacophore models.^{146,150,152} A model developed by Sundarapandian et al.¹⁴⁶ was devoid of cap group but had an H-bond acceptor (HBA) group, two H-bond donor (HBD) donor groups, and a hydrophobic (HYP) group (Figure 18). Another model developed by Chen et al.¹⁵⁰ (Figure 25), on the other hand, had three hydrophobic features and only one HBA and one HBD donor feature. A similar model was developed by Vadivelan et al.¹⁵² (Figure 26), but it had no HBD feature. This model does not seem to be of much importance as HBD is an essential feature of potent HDAC inhibitors. However, this and the other two models also require further modifications in terms of steric, physicochemical, and electronic properties to have optimum interactions with HDACs. This is because many CoMFA and CoMSIA studies^{154,162} have suggested that the cap group and also the aliphatic chain may have steric as well as electrostatic interactions with the receptors. Equation 8 derived by Wagh et al.¹⁵⁵ also suggested the involvement of steric and electrostatic interactions between the inhibitors and HDACs. Equation 9 suggested the major role of van der Waals surface area of atoms of inhibitor molecules in HDAC inhibition, where the salvation energy of molecules might play a negative

role. For the data treated by Guo et al.,¹⁶² Bajpai et al.¹⁶⁹ had derived a simple 2D QSAR model (eq 15), which suggested the involvement of strong dispersion interaction between the inhibitors and HDACs, where the global topological charge index of the molecule might play a major role.

$$\begin{aligned} pIC_{50} &= 2.145(\pm 1.441)MR - 0.100(\pm 0.076)MR^2 \\ &\quad + 6.223(\pm 4.731)GTCI + 0.391(\pm 0.238)I - 5.870(\pm 5.709) \\ n &= 23, \quad r = 0.944, \quad r_{cv}^2 = 0.740, \quad r_{pred}^2 = 0.775, \\ s &= 0.23, \quad F_{4,18} = 36.88(4.58), \quad MR_{op} = 10.66 \end{aligned} \quad (15)$$

Equation 14 derived by Wang et al.¹⁶⁷ for TSA analogues for their antiproliferation activity also suggested the involvement of some polar interaction between the compounds and the receptors.

A TSA-like inhibitor can exist in protonated and deprotonated states (Figure 28), where the protonated state has been found to be of great importance. Kalyaanmurthy and Phoebe Chen¹⁵⁷ reported that protonated states of HAs exhibit better role than the deprotonated states with class I HDACs. A few more authors¹⁵⁸⁻¹⁶¹ have also reported the significance of protonated states of HAs in HDAC inhibition.

6.3. MMP Inhibition

Inhibitors of matrix metalloproteinases have been widely studied from the point of view of their structure-activity and quantitative structure-activity relationships. In this connection, several reviews¹⁷⁰⁻¹⁷³ and a recent book edited by Gupta¹⁷⁴ and some excellent chapters in it¹⁷⁵⁻¹⁷⁷ present a wide coverage of SAR and QSAR of MMP inhibitors (MMPIs) along with the description of different families of MMPs, their physiological roles, and the implication of their overactivation. We therefore want to focus in this Review only on 3D QSAR studies of MMP inhibition, where we take into account the 3D structures of both the enzymes and the inhibitors. Knowledge of 3D structures of MMPs can provide valuable insights into the structural determinants of selective inhibition of a particular MMP. In their recent article,^{176a} Gupta and Patil presented the results of X-ray crystallographic and NMR studies on three-dimensional structures of a number of MMPs, revealing their catalytic sites, subsites, specificity of binding with substrate and inhibitors, and catalytic mechanism. In addition to catalytic site, MMPs possess, as shown in Figure 32,¹⁷⁸ some subsites designated by unprimed and primed S, for example, S1, S2, S3 and S'1, S'2, S'3'. Among these, the S1' pocket varies the most among the different MMPs in terms of both the amino acid

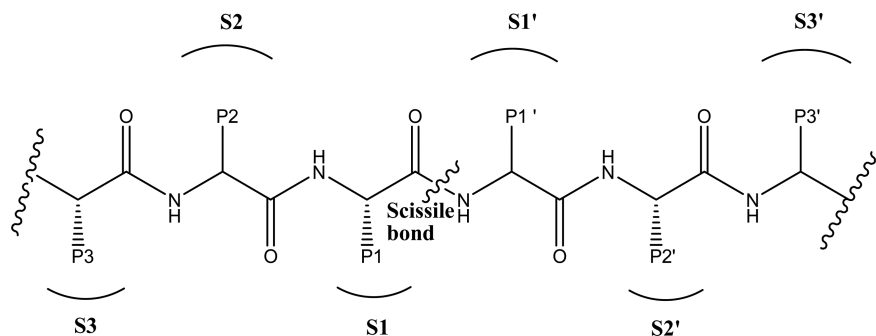


Figure 32. Standard nomenclature of amino acid residues of a peptide substrate and the corresponding binding sites in a protease enzyme. P_n and P'_n ($n = 1, 2, 3, \dots$) refer to the residues of the substrate, and S_n and S'_n refer to the corresponding binding sites in the enzyme. Reprinted with permission from ref 178. Copyright 1997 American Chemical Society.

makeup and the depth of the pocket (shallow, intermediate, and deep).

The catalytic domain of MMPs consists of five stranded β -pleated sheets, three α -helices and connecting loops, two zinc ions (structural and catalytic), and three calcium ions, which stabilize the structure. A hydrophobic S1' pocket is found to be present in the substrate-binding site, which contributes to MMPs substrate specificity.¹⁷⁹

The requirements for a molecule to be an effective MMP inhibitor are: (1) the presence of a functional group, such as carboxylic acid group (COOH), hydroxamic acid group (CONHOH), and sulfhydryl group (SH), which may be able to chelate the active site Zn²⁺ ion of the enzyme (such group is referred to as a zinc binding group, ZBG); (2) at least one functional group capable of hydrogen bonding with the enzyme backbone; and (3) one or more side chains that can have van der Waals interactions with the enzyme subsites. In a substrate-based design, which has been the principal approach for the identification of synthetic inhibitors fulfilling the above requirements, a ZBG has been found to be attached to peptide derivatives that mimic the sequence of collagen substrate cleavage site. Three classes of compounds have been developed depending upon on which side of ZBG the compounds have the amino acid residues. If they have amino acid residues on the right-hand side, for example, ZBG-A1'-A2'-A3', they are called right-hand side inhibitors, and if on the left-hand side, for example, A₃-A₂-A₁-ZBG, they are called left-hand side inhibitors. The third category of compounds may have amino acid residues on both sides of ZBG, such as A₃-A₂-A₁-ZBG-A1'-A2'-A3'. In all of these compounds A's and A's refer to amino acid residues that can interact with S and S' subsites of the enzyme, respectively. Of all three types of inhibitors, the right-hand side ones were reported to be more potent.¹⁷⁰ A model of interaction of right-hand side inhibitors is shown in Figure 33.

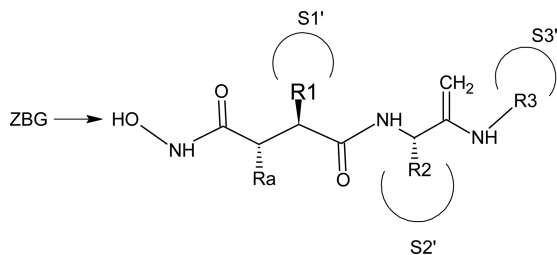


Figure 33. A model of interaction of a right-hand side MMP inhibitor with the enzyme. R1, R2, and R3 are the substituents of the amino acid residues, which can be referred to as P1', P2', and P3' substituents that may interact correspondingly with S1', S2', and S3' subsites of the enzyme. Reprinted with permission from ref 170. Copyright 1999 American Chemical Society.

In MMPs, the main subsites for substrate recognition are the specificity pocket S1' and to the lesser extent S2'.^{180,181} The S1' pocket varies the most among the different MMPs in both the amino acid makeup and the depth of the pocket, and the MMPs can be classified on the basis of the depth of this pocket into shallow, intermediate, and deep pocket MMPs.^{182–184} The shallow S1' pocket is found in MMP-1 and MMP-7; the intermediate one in MMP-2, MMP-8, and MMP-9; and the deep one in MMP-3 and MMP-11–14.^{182,185,186} The S1' pocket is generally characterized as being large and an open channel.

The substrate-based right-hand side MMP inhibitors have been put basically into four broad classes:¹⁸⁷ (1) carboxylic-acid-based inhibitors; (2) hydroxamic-acid-based inhibitors; (3) thiol-based inhibitors; and (4) phosphorus-based inhibitors, of which hydroxamic-acid-based inhibitors (hydroxamates) have been most widely studied. We shall be concerned here only with this class of inhibitors.

In all of the above classes of synthetic inhibitors, there has been found, in addition to a zinc binding group, a peptidic or peptidomimetic moiety, mimicking peptide substrate binding to the substrate recognition site. In the majority of such inhibitors, this peptidic moiety has been found to interact in an extended manner with the right-hand S' subsites with an L-configured P1' side chain substituent, perfectly arranged to extend into the hydrophobic bottleneck of S1' pocket. In case of hydroxamates, the steric bulk (sulfonamide group) was added as it favors the large opening of S1' pocket in MMP-3 and thus selectivity over MMP-1, MMP-2, MMP-9, and MMP-14. However, it has been emphasized that the structure of catalytic domain is maintained in the full-length protein.¹⁸⁸ This is an important observation as only the structure of catalytic domain is available for most of the MMPs.

Regarding the importance of subsites S and S', Terp et al.¹⁸⁹ computed GRID molecular interaction fields (MIFs) for the binding sites of 10 aligned MMPs, where five had X-ray structures and five were homology models, and then applied consensus principal component analysis on the matrix of GRID MIFs. This work of Terp et al.¹⁸⁹ highlighted the importance of unprimed pockets S2 and S3 for selective interactions along with that of the S1' pocket. Lukacova et al.¹⁹⁰ used force field interaction energies to compare the structures of 24 MMPs, including 9 X-ray structures and 15 homology models, and ranked the MMP pockets in decreasing order of similarity as S1' (most similar) > S2 > S3' > S1 ≈ S3 > S2' (least similar).

The sulfonamide group in MMPs generally improves the enzyme–inhibitor binding, not only by the formation of hydrogen bond with the enzyme but also by directing the hydrophobic substituent to S1' pocket and enabling it to push deeply. An overview of SAR of β -N-biaryl ether sulfonamide hydroxamates studied for the inhibition of MMP-2 and MMP-9 by Yang et al.¹⁹¹ is presented in Figure 34. This figure shows the flexibility of the S1' pocket, which can be pushed down to accommodate the bulky hydrophobic group of the inhibitors.

In a receptor-based 3D-QSAR study performed by Tuccinardi et al.¹⁹² for the analysis of MMP-2, MMP-3, and MMP-9 inhibitors, it was pointed out that the activity of MMP-2 inhibitors is determined by both electrostatic and hydrophobic interactions, while the selectivity appeared to be correlated primarily with lipophilic interactions. The surface analysis of the crystallographic structure of the three MMP subtypes revealed that the S1' cavity, where the not conserved residues supposed to be important for the MMP selectivity are located, possessed a different shape due to the presence of different residues. In MMP2, this cavity was mainly delimited by Pro417, Gly 418, Ala422, Ile424, and Thr426 with a large aperture at the end of the pocket, and in MMP-3 by Thr232, Glu233, Tyr237, Leu239, and His241 with a small aperture at the end of the cavity. The S1' of MMP-9 was totally different from the other two MMPs capped by the presence of the not conserved residue Arg424.

MMP-2 and MMP-9 are known as gelatinases. Xi et al.¹⁹³ performed a combined molecular modeling study on a large series of β -N-biaryl ether sulfonamide hydroxamates (25) to

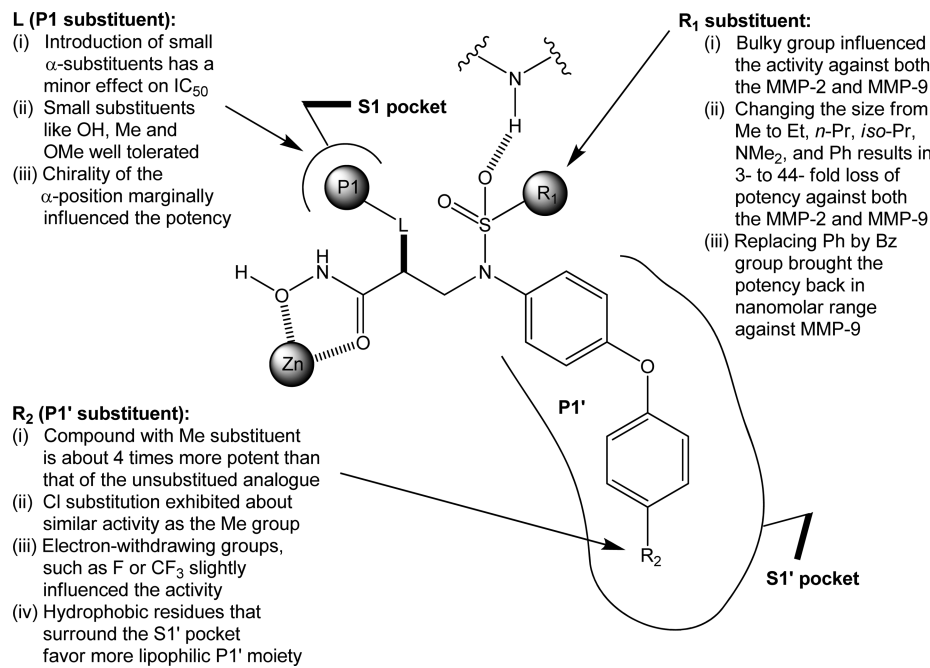
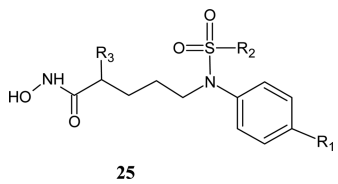


Figure 34. Summary of structure–activity relationships for the inhibition of MMP-2 and MMP-9 by β -N-biaryl ether sulfonamide hydroxamates. Reprinted with permission from ref 191. Copyright 2008 Elsevier.

find the nature of binding of these compounds with these gelatinases. In this study, the authors first analyzed the similarities and differences between the binding sites of MMP-2 and MMP-9 by sequence alignment and structural superimposition and then, to extract structural features of inhibitors influencing their activity, developed QSAR models using GA-MLR and performed CoMFA and CoMSIA studies. Thereafter, docking study was employed to further explore the binding mode of compounds with the enzyme.



In the sequence analysis, Xi et al.¹⁹³ found the high similarity between the two gelatinases. Six important pockets were found in each protein, where S2 and S2' were catalytic domain with three histidine residues coordinated to Zn²⁺. The hydrophobic S1' that is considered to be a critical and primary site for selective MMP inhibition^{188,194} was also observed. S1' interacts with P1' of the ligand and has little difference in MMP-2 and MMP-9, except that its hydrophobic property in MMP-9, where it has more hydrophobic residues, is slightly stronger than that in MMP-2.

The secondary pockets S1, S3, S3', and S2+S2' (catalytic domain) were observed to be almost the same. In the catalytic domain, S2+S2', three histidine residues were seen to adopt similar conformations toward Zn²⁺.

The GA-MLR models for both MMP-2 and MMP-9 were found to be almost parallel (eqs 16a, 16b), except that eq 16a obtained for MMP-2 had an additional parameter H5m and eq 16b obtained for MMP-9 an additional parameter RDF075m. H5m is a GETAWAY descriptor¹⁹⁵ based on the spatial autocorrelation and encodes information on the effective

position of substituents and fragments in the molecular space. To some extent, it accounts for the information of molecular size. RDF075m is a parameter that is based on radial distribution function (RDF), but weighted by atomic mass. Both H5m and RDF075m are 3D descriptors, which are weighted by atomic mass and thus both reflect the size of the molecule. Therefore, their positive coefficients in both of the models indicated the importance of shape and size of molecules in inhibition of both MMP-2 and MMP-9.

$$\begin{aligned} \log(1/IC_{50})_{\text{MMP-2}} &= 12.792 - 2.221 \text{ EEig11r} - 0.190 \text{ RDF085v} \\ &\quad - 2.221 \text{ Mor17v} + 4.885 \text{ H5m} - 76.604 \text{ R4u+} \\ r^2 &= 0.838, r^2_{cv} = 0.781, s = 0.349, r^2_{boot} = 0.768 \end{aligned} \quad (16a)$$

$$\begin{aligned} \log(1/IC_{50})_{\text{MMP-9}} &= 15.000 - 1.862 \text{ EEig11r} \\ &\quad + 0.115 \text{ RDF075m} - 0.210 \text{ RDF085V} \\ &\quad - 1.919 \text{ MOR17V} - 98.984 \text{ R4u+} \\ r^2 &= 0.821, r^2_{cv} = 0.771, s = 0.414, r^2_{boot} = 0.754 \end{aligned} \quad (16b)$$

The other variables in eqs 16a, 16b have the following meanings: EEig11r, eigenvalue 11 from edge adj. matrix weighted by resonance integral; RDF085v, radial distribution function-8.5/weighted by atomic van der Waals volume; Mor17v, 3D Morse-signal17/weighted by atomic van der Waals volumes; R4u+, R matrix autocorrelation of lag 4/unweighted.

All of these parameters are usually related to molecular size and shape of the molecule. The negative coefficients of all of these parameters in both of the equations, in fact, suggest that while molecular size may be important in drug–receptor interaction, there can be a steric effect, too, influencing the inhibition of both of the enzymes.

Table 7. CoMFA and CoMSIA Results for MMP-2 and MMP-9

model	ONC ^a	q^2	r^2	s	F	r^2_{test}	field contribution
MMP-2							
CoMFA (S+E)	4	0.648	0.933	0.239	138.56	0.716	S = 58.20% E = 41.80%
CoMSIA (S+E+H+A)	6	0.641	0.955	0.200	134.20	0.767	S = 24%, E = 35.5% H = 25.9%, A = 14.6%
MMP-9							
CoMFA (S+E)	5	0.587	0.955	0.222	166.72	0.744	S = 56.2%, E = 43.8%
CoMSIA (S+E+H)	6	0.568	0.954	0.230	129.88	0.784	S = 27.4%, E = 40.2% H = 32.4%

^aONC = optimal number of components.

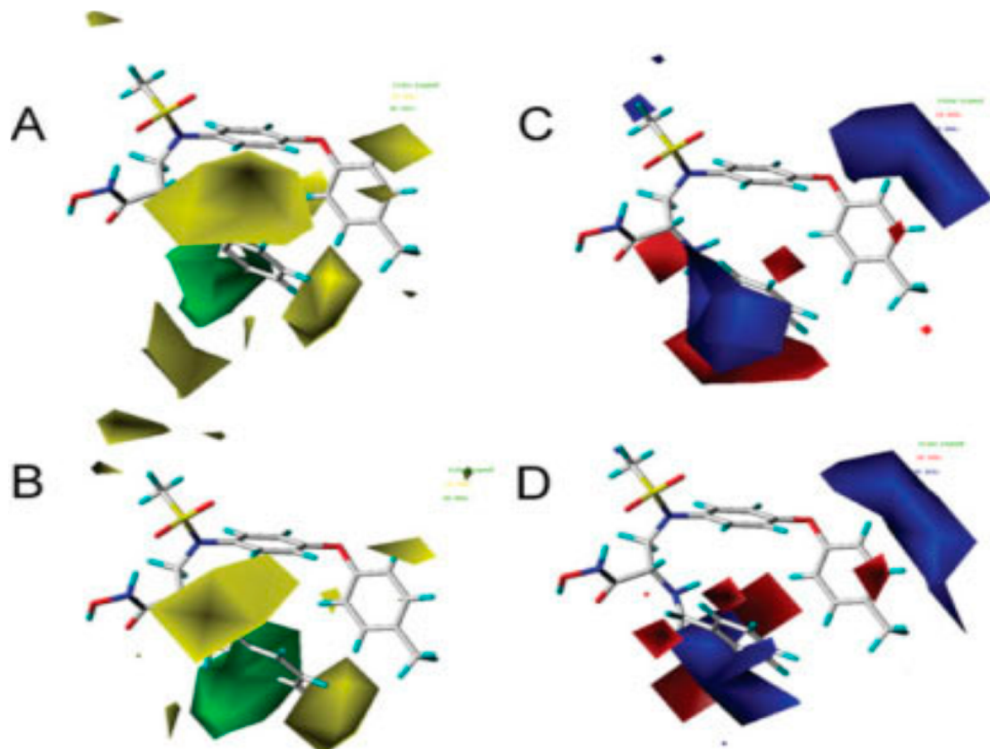
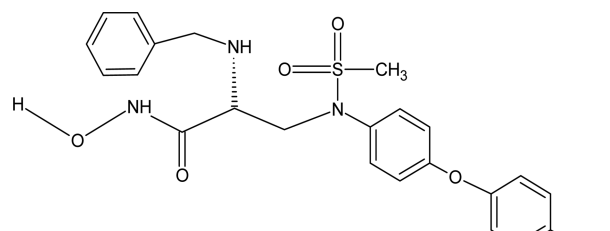


Figure 35. CoMFA contour maps of potent MMP-2 and MMP-9 inhibitors, where (A) and (C) represent the steric and electrostatic fields of MMP-2 and (B) and (D) those of MMP-9. Compound 26 is shown in sticks. Reprinted with permission from ref 193. Copyright 2010 Wiley Periodicals, Inc.

In their CoMFA and CoMSIA studies, Xi et al.¹⁹³ found the results as shown in Table 7. This table shows that all statistical parameters are almost identical and significant for both models as well as for both of the enzymes MMP-2 and MMP-9. However, while for both MMPs, CoMFA described only the steric (S) and electrostatic (E) fields, CoMSIA described four fields for MMP-2, S, E, H (H-bond acceptor), and A (hydrophobic), and only three fields for MMP-9, S, E, and H, and these were the best results. In the contour maps of CoMFA and CoMSIA (Figures 35 and 36) for both MMP-2 and MMP-9 for a representative compound (26), Xi et al.¹⁹³ noticed that the steric field had the same influence on MMP-2 and MMP-9. Large substituents in R₁ (25) might have an adverse effect on both of the enzymes. Blue contours in Figures 35D and 36D at the phenyl ring suggested the importance of electropositive substituents at the phenyl ring for the inhibition of both MMP-2 and MMP-9. Further, the para and meta positions of the phenyl ring linked to oxygen atom are

electronegative and favorable to the inhibition of both MMP-2 and MMP-9.



26

The docking study by Xi et al.¹⁹³ on compound 26 in MMP-2 and MMP-9 was performed to see the nature of interactions of inhibitors with the proteins. Compound 26 was selected because it had significant difference in its activities against MMP-2 and MMP-9. The docking showed that inside MMP-2, the ZBG of compound was coordinated to Zn²⁺ along with

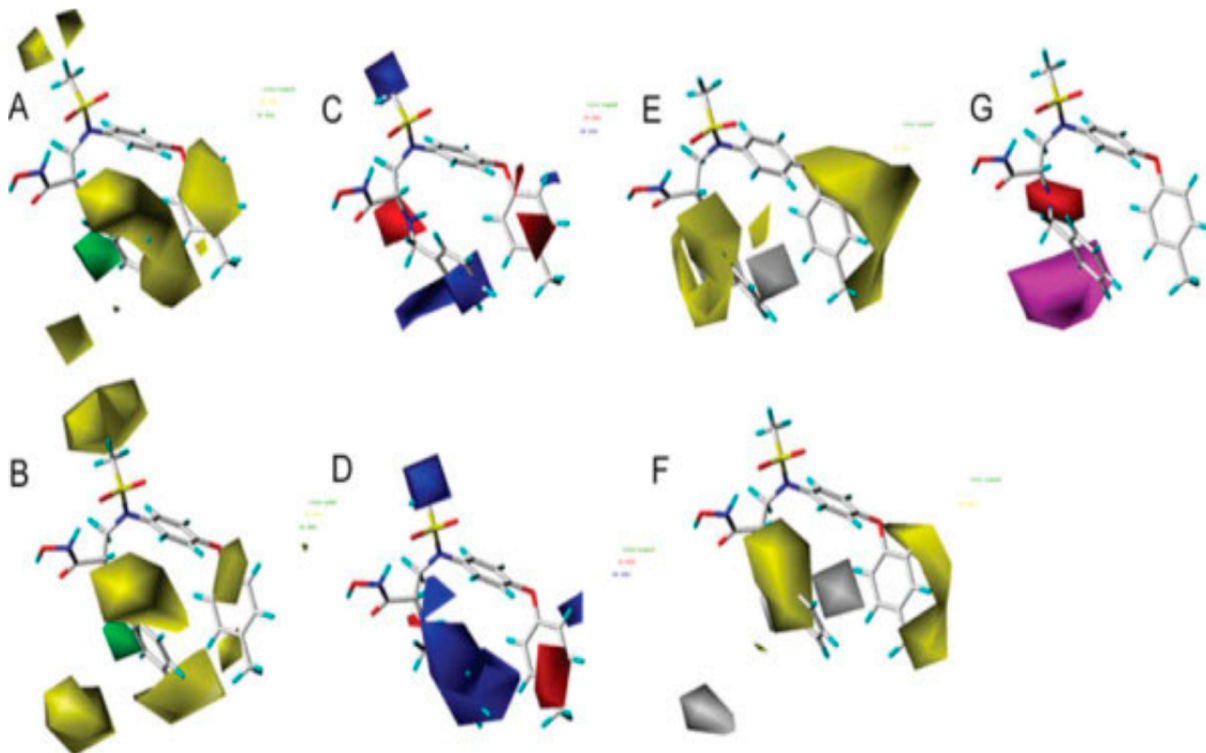


Figure 36. CoMSIA contour maps of MMP-2 and MMP-9 potent inhibitors, where (A), (C), (E), and (G) represent the steric, electrostatic, hydrophobic, and H-bond acceptor fields of MMP-2, respectively, and (B), (D), and (F) the steric, electrostatic, and hydrophobic fields of MMP-9, respectively. Compound 26 is shown in sticks. Reprinted with permission from ref 193. Copyright 2010 Wiley Periodicals, Inc.

three histidine residues, His201, His205, and His211. Simultaneously, the hydroxamate group was observed to form two hydrogen bonds with side chain of Glu202, and the NH one hydrogen bond with Ala165. The R₃-substituent was also found to form the H-bonds with all three histidine residues as well as with Ala165, His166, and Ala167 of the S1 pocket, and the sulphonamide group not only formed the H-bond with the enzyme but also directed properly the hydrophobic substituents to the S1' pocket, enabling it to plunge deep in the pocket.¹⁹⁶ P1' group had only hydrophobic interaction with the S1' pocket. The R₁-substituent had the hydrophobic interaction with two hydrophobic residues, Pro221 and Ile222.

In MMP-9 also the inhibitor had almost similar interactions, where the hydroxamate group was coordinated with Zn²⁺ ion along with three histidine residues, His401, His405, and His411, and the NH group was involved in the formation of H-bond with Ala189. The sulfonamide group formed the H-bond through its oxygen with Tyr423, and there was a hydrophobic interaction of the ligand with Pro421, Met422, and Tyr423 of the S1' pocket.

However, the difference in the activities of this compound against MMP-2 ($pIC_{50} = 6.69$) and MMP-9 ($pIC_{50} = 8.15$) was attributed to the fact that while in MMP-9, Leu187 located in the S3' pocket formed an H-bond with the ligand, no such bond was formed in the MMP-2, and that in MMP-9 the OH group of hydroxamate formed an H-bond with Gln402 but not in MMP-2. Besides, the hydrophobic interaction of P1' of the ligand with S1' of the enzyme in MMP-2 slightly differed from that in MMP-9.

Amin and Welsh¹⁹⁷ made a CoMFA study on a few sets of piperazine-based stromelysin-1 (MMP-3) inhibitors as shown in Figure 37, and then later CoMFA as well as CoMSIA studies on a set of arylsulfonyl isoquinoline-based and a series of

thiazine/thiazepine-based stromelysin-1 (MMP-3) inhibitors (Figure 38).¹⁹⁸

Regarding the piperazine-based MMPIs as given in Figure 37, the inspection of experimental binding data reported by Cheng et al.¹⁹⁹ had led the authors to suggest that steric bulk did not significantly alter the in vitro profile of the compounds and that a basic nitrogen adjacent to piperazine ring was not well

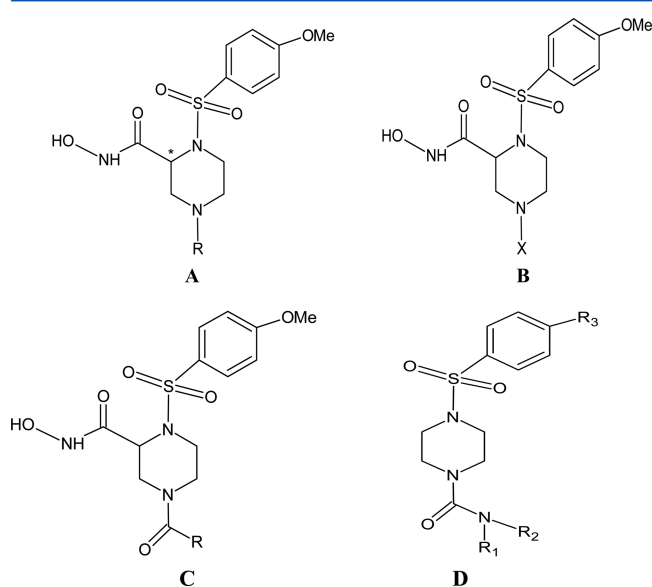


Figure 37. Piperazine-based stromelysin-1 inhibitors. (A) N-Alkyl and heterocyclic substituted analogues, (B) sulfonamide and carbamide substituted analogues, (C) amide substituted analogues, and (D) urea substituted analogues.

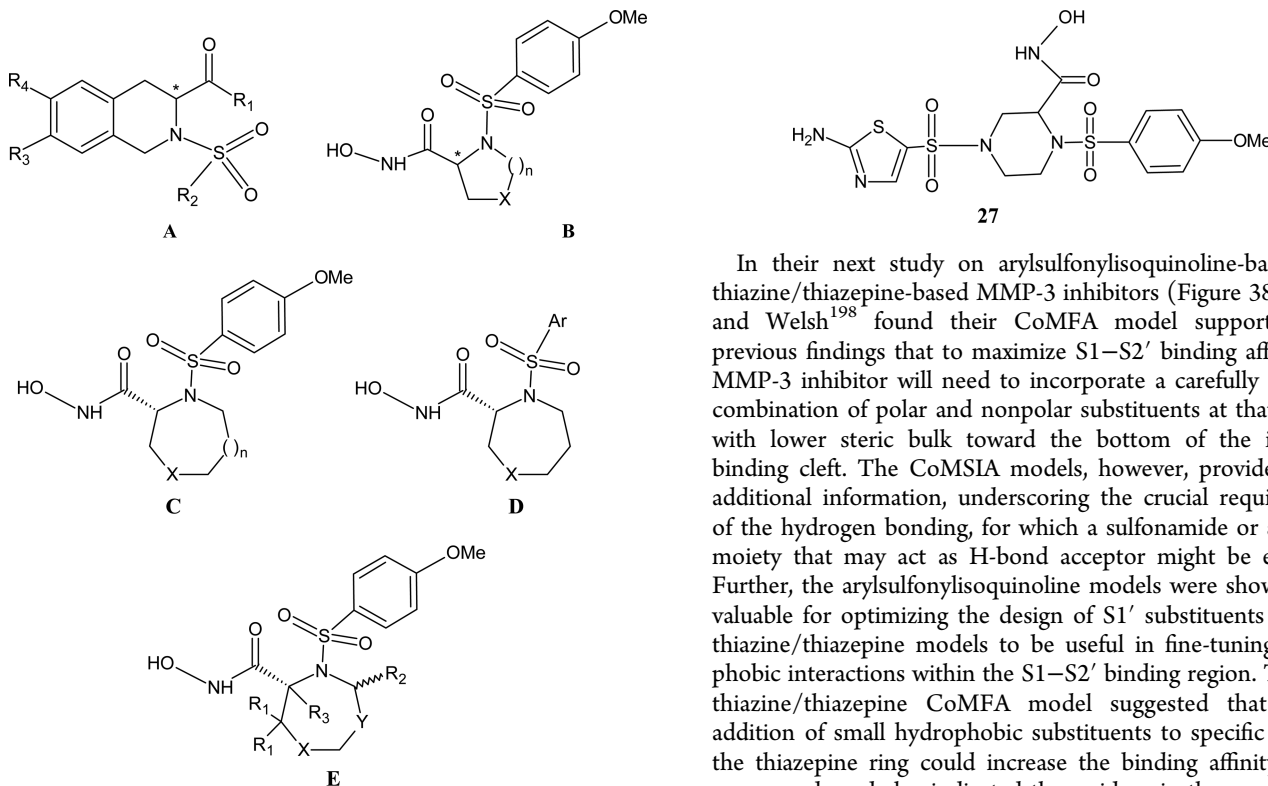


Figure 38. Arylsulfonylisoquinoline-based and thiazine/thiazepine-based stromelysin-1 inhibitors. (A) Aryl sulfonylisoquinolines, and (B)–(E) thiazine/thiazepine-based analogues.

tolerated. Further, according to Cheng et al., the orientation and electrostatic properties of 4N-substituents were important. In an enzyme–ligand crystal structure, where ligand was an analogue of **B** (Figure 37), containing a cbz moiety at 4N ($X = \text{cbz}$), the cbz moiety was observed to be oriented approximately midway between S1 and S2' pockets to have hydrophobic interactions with two phenyl alanine residues, Phe210 and Phe186, located at the edge of MMP binding cleft. Because S1–S2' area is partly exposed to solvent, the polar substituents were not expected to orient toward this area. The CoMFA study of Amin and Welsh almost supported all of these observations and pointed six major areas on and around the inhibitors whose steric and electrostatic properties may be crucial for the activity of the compounds. In a contour map of CoMFA, plotted for the most active compound in the series (**27**, $\text{pIC}_{50} = 8.60$), the distal nitrogen substituents were found to be surrounded by a large blue region, indicating a strong preference for hydrophobic group facing the two phenylalanine residues (Phe201 and Phe186) near the bottom of the binding cleft. In some cases, this blue region had included the 4N-substituents as well. The two yellow areas below the large blue region had indicated the modest intolerance of bulky substituents at these positions. At the bottom of the 4N-substituents, the two adjacent broad red areas had indicated a preference for negative electrostatic potential. All of these observations led Amin and Welsh¹⁹⁷ to conclude that an MMP-3 inhibitor with strong binding affinity at S1–S2' site should have a medium-size polar group oriented toward the solvent/top of the binding cleft of the enzyme and a hydrophobic moiety directed toward the bottom of the cleft, with minimal, carefully oriented areas of the steric bulk.

In their next study on arylsulfonylisoquinoline-based and thiazine/thiazepine-based MMP-3 inhibitors (Figure 38), Amin and Welsh¹⁹⁸ found their CoMFA model supporting the previous findings that to maximize S1–S2' binding affinity, an MMP-3 inhibitor will need to incorporate a carefully oriented combination of polar and nonpolar substituents at that region, with lower steric bulk toward the bottom of the inhibitor binding cleft. The CoMSIA models, however, provided some additional information, underscoring the crucial requirements of the hydrogen bonding, for which a sulfonamide or a similar moiety that may act as H-bond acceptor might be essential. Further, the arylsulfonylisoquinoline models were shown to be valuable for optimizing the design of S1' substituents and the thiazine/thiazepine models to be useful in fine-tuning hydrophobic interactions within the S1–S2' binding region. The best thiazine/thiazepine CoMFA model suggested that careful addition of small hydrophobic substituents to specific sites on the thiazepine ring could increase the binding affinity of the compounds and also indicated the residues in the enzyme that could interact with these substituents. The S-isomer compounds in thiazine/thiazepine-based MMPIs were found to exhibit broad-spectrum affinity against MMPs, regardless of structure/polarity of P1' substituent, and this emphasized the important contribution of the ill-defined S1–S2' pocket of the enzyme. The best CoMFA model obtained for arylsulfonylisoquinoline-based MMPIs confirmed the narrow hydrophobic nature of S1' pocket and the necessity to avoid the steric bulk near the zinc-binding group, facts that were observed in X-ray and NMR structural studies.

Tsai and Linn²⁰⁰ made a CoMFA and CoMSIA study on a series of 84 proline-based compounds with general structure as **28** plus some structurally diversified nonproline compounds acting as MMP-1 inhibitors. Their CoMFA study prominently described the favorable steric (S) and electrostatic (E) regions, while CoMSIA described favorable hydrophobic (H), steric (S), and H-bond acceptor (A) regions. For the former, q^2_{cv} was 0.649, and for the latter 0.730. The contour maps for both CoMFA and CoMSIA were obtained for the most active compound (**29**, $\text{pIC}_{50} = 8.52$) in the proline-based series. Both CoMFA and CoMSIA contour maps (Figure 39) showed that there were disfavor regions for steric interactions somewhere around the tip of the bulky diphenyl substituent (shown by yellow regions). The favorable regions for steric interactions were shown by both of the models around the diphenyl substituent or around the tip of the hydroxamic acid (green contours).

The favorable regions for electrostatic interactions in CoMFA plots were shown around the oxime substituent on pyrrolidine ring or the hydroxamic acid group (blue regions, Figure 39a), which can tantamount to disfavorable regions for hydrophobic interactions identified by CoMSIA with white in Figure 39b. The favorable hydrophobic region is expressed by purple contours around the oxime group.

The favorable or disfavorable regions for H-bond acceptor were shown only in CoMSIA contour plots (Figure 39b), which

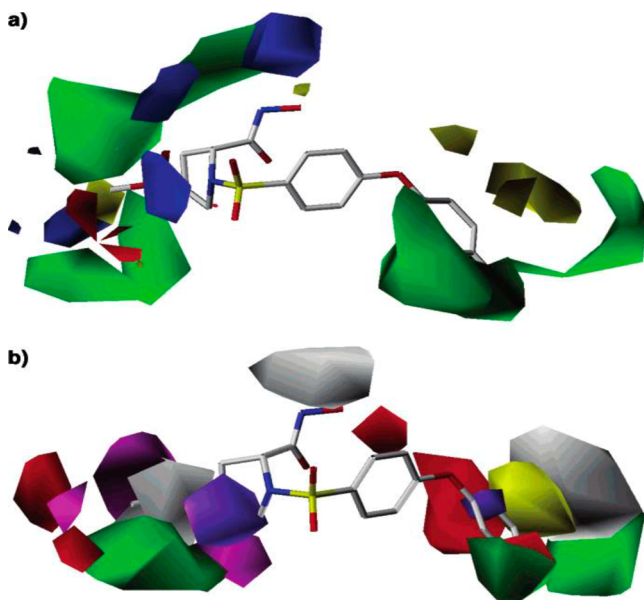
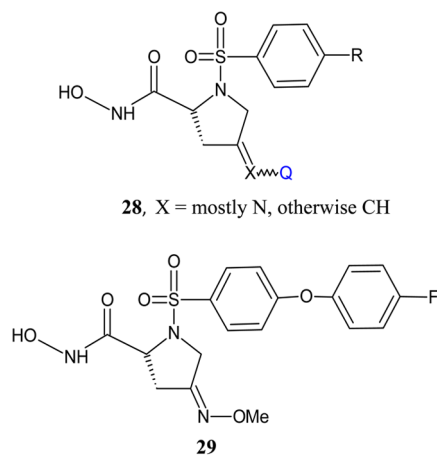


Figure 39. (a) The CoMFA contours obtained from the aligned structures of 60 proline-based inhibitors of the training set mapped onto compound **29**. Green contours represent favor, while yellow ones represent disfavor regions for steric interactions. Blue contours represent favor, while red contours represent disfavor regions for electrostatic interactions. (b) The CoMSIA contours obtained from the aligned structures of 60 proline-based inhibitors of the training set mapped onto compound **29**. Green contours represent favor, while yellow contours represent disfavor regions for steric interactions. Purple contours represent favor, while white contours represent disfavor regions for hydrophobic interactions. Magenta contours represent favor, while red contours represent disfavor regions for H-bond acceptor. Reprinted with permission from ref 200. Copyright 2004 American Chemical Society.

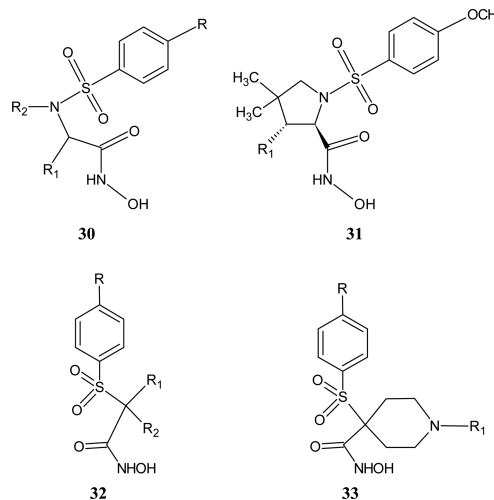


were around hydroxamic acid group. Magenta contours represented favorable, while red contours represented unfavorable regions for H-bond acceptor.

The C-4 substituent, that is, C=X bond, on the proline is actually flat (sp^2 orientation) and is extended into the S2' surface pocket of MMP-1 where it can have hydrophobic interaction.^{201–203}

Fernández et al.^{204,205} reported some linear and nonlinear QSAR studies first on a series of *N*-hydroxy-2-[*(phenylsulphonyl)amino*]acetamide derivatives (HPSAAs) with general structures as **30** and **31** acting against MMP-1, MMP-2, MMP-3, MMP-9, and MMP-13, and then on a series

of *N*-hydroxy- α -phenylsulfonamide acetamide derivatives (HPSAs) with general structures as **32** and **33**, acting against only MMP-1, MMP-9, and MMP-13. In both cases, they derived models using 2D autocorrelation descriptors, Moran (MATS), Geary (GATS), and Moreau-Brato (ATS). These descriptors are calculated from molecular graph by summing the products of atomic masses (m), atomic van der Waals volumes (v), atomic polarizabilities (p), or atomic sanderson electronegativities (e) of the terminal atoms of all of the paths of the considered path length (the lag). Thus, a descriptor such as ATS5m will be called a Broto–Moreau autocorrelation of a topological structure-log 5/weighted by atomic masses.



For the series of HPSAAs (**30** and **31**), the multiple regression had revealed the following correlations:²⁰⁴

$$\begin{aligned} \log(1/\text{IC}_{50})_{\text{MMP-1}} &= 219.442 - 166.804 \text{ MATS4m} - 51.519 \text{ MATS8m} \\ &\quad - 13.020 \text{ MATS3v} + 4.817 \text{ GATS1e} - 6.913 \text{ GATS2e} \\ n &= 26, r^2 = 0.834, r^2_{cv} = 0.745, s = 0.383, p < 10^{-5} \end{aligned} \quad (17)$$

$$\begin{aligned} \log(1/\text{IC}_{50})_{\text{MMP-2}} &= 162.799 - 110.925 \text{ MATS4m} - 55.421 \text{ MATS8m} \\ &\quad - 8.431 \text{ MATS3v} + 2.379 \text{ GATS6e} + 5.227 \text{ GATS2p} - 0.042 \text{ ATS2v} \\ n &= 32, r^2 = 0.808, r^2_{cv} = 0.721, s = 0.420, p < 10^{-5} \end{aligned} \quad (18)$$

$$\begin{aligned} \log(1/\text{IC}_{50})_{\text{MMP-3}} &= 104.088 - 112.340 \text{ MATS4m} \\ &\quad - 15.666 \text{ MATS3v} + 8.716 \text{ MATS6e} + 2.379 \text{ GATS6e} \\ &\quad - 1.457 \text{ GATS8e} + 7.200 \text{ GATS2p} \\ n &= 30, r^2 = 0.750, r^2_{cv} = 0.581, s = 0.431, p < 10^{-5} \end{aligned} \quad (19)$$

$$\begin{aligned} \log(1/\text{IC}_{50})_{\text{MMP-9}} &= -72.742 + 109.844 \text{ MATS2m} - 51.167 \text{ MATS4m} \\ &\quad + 8.380 \text{ MATS2v} + 13.240 \text{ MATS6e} + 7.864 \text{ GATS6e} \\ &\quad + 13.015 \text{ GATS2p} \\ n &= 32, r^2 = 0.767, r^2_{cv} = 0.644, s = 0.478, p < 10^{-5} \end{aligned} \quad (20)$$

$$\begin{aligned} \log(1/\text{IC}_{50})_{\text{MMP-13}} &= 122.338 - 86.944 \text{ MATS4m} - 33.782 \text{ MATS8m} \\ &\quad - 5.375 \text{ MATS3v} + 8.188 \text{ MATS1p} + 1.103 \text{ GATS5e} \\ n &= 29, r^2 = 0.767, r^2_{cv} = 0.703, s = 0.397, p < 10^{-5} \end{aligned} \quad (21)$$

Similarly, for the analogues of **32** and **33** that constituted a large series, Fernández et al.²⁰⁵ had obtained the following correlations:

$$\begin{aligned} \log(1/\text{IC}_{50})_{\text{MMP-1}} &= 15.274 - 17.557 \text{ MATS4m} - 5.396 \text{ MATS3v} \\ &\quad + 17.908 \text{ MATS6v} - 4.396 \text{ MATS5e} - 4.375 \text{ MATS6e} \\ &\quad + 10.359 \text{ GATS6v} - 5.118 \text{ GATS7v} \\ n &= 63, r^2 = 0.736, r^2_{\text{cv}} = 0.559, s = 0.312, p < 10^{-5} \end{aligned} \quad (22)$$

$$\begin{aligned} \log(1/\text{IC}_{50})_{\text{MMP-9}} &= -4.571 + 8.881 \text{ MATS2e} - 7.718 \text{ MATS4e} \\ &\quad - 4.665 \text{ GATS1v} + 14.788 \text{ GATS1e} + 2.379 \text{ GATS6p} \\ &\quad - 0.005 \text{ ATS6m} + 0.018 \text{ ATS3e} \\ n &= 66, r^2 = 0.731, r^2_{\text{cv}} = 0.605, p < 10^{-5} \end{aligned} \quad (23)$$

$$\begin{aligned} \log(1/\text{IC}_{50})_{\text{MMP-13}} &= -11.139 + 11.363 \text{ MATS6v} \\ &\quad - 1.118 \text{ MATS6e} - 1.826 \text{ GATS1v} + 11.911 \text{ GATS6v} \\ &\quad + 6.097 \text{ GATS1e} + 1.297 \text{ GATS4e} \\ n &= 68, r^2 = 0.692, r^2_{\text{cv}} = 0.598, s = 0.376, p < 10^{-5} \end{aligned} \quad (24)$$

In all of these equations, p refers to the significance of the variables. However, all of these equations seem to us of only predictive value, and no conclusions can be drawn about the nature of interactions of these compounds with MMPs. Many of the descriptors used in these correlations were shown to be mutually correlated; even then Fernandez et al.²⁰⁴ extracted the following from eqs 17–21 for the derivatives of **30** and **31**.

- Atomic masses have high contributions in the inhibition of all MMPs ($C_m > 30\%$), except for MMP-3, and equally high contributions are made by Sanderson electronegativities in the inhibition of MMP-1, MMP-3, and MMP-9 ($C_e > 30\%$).
- In general, the atomic van der Waals volumes and polarizabilities have poor contributions.

These authors had, however, also obtained nonlinear models for these compounds using the Bayesian-regularized neural network (BRANN) approach.²⁰⁵ These models produced entirely different pictures as described below.

- Atomic van der Waals volumes have high contributions in the inhibition of all MMPs ($C_v > 30\%$) and are the key features in the inhibition of MMP-2 ($C_v = 43\%$), MMP-3 ($C_v = 41\%$), and MMP-9 ($C_v = 65\%$).
- Atomic Sanderson electronegativities influence only MMP-1 and MMP-3 inhibitions, and the atomic masses are important only in the inhibition of MMP-1.

Similarly, the linear and nonlinear models derived by Fernández and Caballero²⁰⁵ for the series of **32** and **33** gave somewhat conflicting conclusions as follows. From the linear models (eqs 22–24), they had concluded that inhibition of MMP-1 was greatly influenced by atomic van der Waals volumes ($C_v = 60\%$) and that of MMP-9 by atomic Sanderson electronegativities ($C_e = 56\%$). The inhibition of MMP-13 was almost equally influenced by these two descriptors ($C_v = 44\%$ and $C_e = 42\%$). On the other hand, the nonlinear models had indicated that MMP-1 inhibition was mainly influenced by atomic Sanderson electronegativities ($C_e = 59\%$) and that the inhibitions of MMP-9 and MMP-13 were equally influenced by atomic masses, van der Waals volumes, and Sanderson electronegativities, each producing an equal effect of approximately 30%.

Such differences in QSARs of inhibitors of different MMPs in case of both HPSAAs and HPSAs were accounted for by Fernández et al.^{204,205} from the structural differences among the active pockets, particularly S1', S1, and S2', of various MMPs as pointed out by Hanessian et al.^{206–208} The occupation of the pockets allows modulating the selectivity by steric, hydrophobic, and electronic differences among different MMPs.

It was pointed out by Welch et al.²⁰⁹ that the S1' pocket in MMPs is the most well-defined area of binding that consists of a hydrophobic pocket, varying in depth for different MMPs. As Figure 40 shows, S1' in MMP has a characteristic Arg (R),

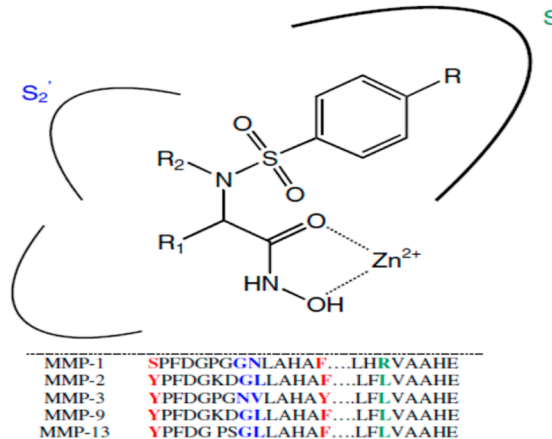


Figure 40. Position of *N*-hydroxy-2-[(phenylsulfonyl)amino]-acetamide derivatives inside MMP active site. Comparison of amino acids sequences of MMPs: colored letters indicate the amino acids of S1' (green), S1 (red), and S2' (blue) pockets that contribute to the ligand specificity. Reprinted with permission from ref 204. Copyright 2006 Elsevier.

whose long side chain extends to the bottom of S1' and forms a rather shallow pocket. In other MMPs, this Arg is replaced by a Leu (L), which causes a deep pocket. S2' subsite is essentially hydrophobic, and in MMP-2, MMP-9, and MMP-13 it is commonly constituted of Gly and Leu (G-L), but in MMP-1 it is constituted of Gly-Asn (G-N) and in MMP-3 of Asn-Val (N-V).^{210–212} Some mutations were found in S2 of all five MMPs, and thus Tyr (Y) and Phe (F) were found commonly in MMP-2, MMP-9, and MMP-13, Tyr (Y) is replaced by Ser (S) in MMP-1, and Phe (F) is replaced by Tyr (Y) in MMP-3. These constitutional differences in active sites of MMPs lead to hydrophobic and electronic differences in them, because of which they differ in inhibitor binding and enzymatic activity.

Gupta et al.²¹³ performed several 2D QSAR studies on different classes of hydroxamates acting as MMP inhibitors, and then in a comprehensive review Gupta¹⁷¹ summarized that, in addition to binding with catalytic Zn²⁺ ions, the hydroxamates also have hydrophobic, electrostatic, and steric interactions with MMPs and that the neutral ZBGs, such as hydroxamic acid function, are advantageous over ionized ZBGs, such as carboxylates and phosphates. The review by Gupta also summarized that the greatest potency with the MMP inhibitors can be associated with their ability to interact with S1, S1', and S2' subsites, where S1' differs most among the MMPs. A certain degree of specificity can be achieved by varying P1' residue of the inhibitors. Introduction of larger P1' substituent generally gives greater specificity for MMP-2, MMP-9, and MMP-13.²¹⁴ However, the increased activity for different

Table 8. Some Important 2D QSAR Models Developed by Various Authors^a

compd no.	QSAR type	MMP type	statistics				refs
			n	r^2	q^2	s	
QSAR models							
I	1	MMP-1	$\log \left(1/K_{\text{I}}\right) = 0.19(\pm 0.08)^1\chi' + 0.42(\pm 0.14)S_{\text{N}} - 0.86(\pm 0.24)S_{\text{S}} + 0.75(\pm 0.14)I + 8.86(\pm 1.61); I = 1 \text{ for } R = C_6F_3; \text{ otherwise } I = 0$	31	0.893	0.170	217
	2	MMP-2	$\log \left(1/K_{\text{I}}\right) = 0.20(\pm 0.08)^1\chi' + 0.20(\pm 0.13)S_{\text{S}} - 0.68(\pm 0.21)S_{\text{N}} + 0.62(\pm 0.14)I + 7.94(\pm 1.56); I = 1 \text{ for } R = C_6F_3; \text{ otherwise } I = 0$	39	0.929	0.210	217
	3	MMP-8	$\log \left(1/K_{\text{I}}\right) = 0.24(\pm 0.12)^1\chi' + 0.26(\pm 0.19)S_{\text{S}} - 0.76(\pm 0.32)S_{\text{N}} + 0.67(\pm 0.22)I + 7.93(\pm 2.37); I = 1 \text{ for } R = C_6F_3; \text{ otherwise } I = 0$	37	0.884	0.310	217
	4	MMP-9	$\log \left(1/K_{\text{I}}\right) = 0.28(\pm 0.11)^1\chi' + 0.43(\pm 0.14)S_{\text{N}} + 0.68(\pm 0.24)I + 5.51(\pm 0.95); I = 1 \text{ for } R = C_6F_3; \text{ otherwise } I = 0$	37	0.846	0.340	217
II	5	MMP-1	$\log \left(1/KC_{50}\right) = -0.40(\pm 0.26)C \log P + 0.09(\pm 0.05)(C \log P)^2 + 0.94(\pm 0.21)I_{\text{R}} + 0.39(\pm 0.20)I_{\text{R}} + 7.60(\pm 0.33)C \log P_{\text{o}} = 2.38; I_{\text{R}} = 1 \text{ for } R = c\text{-pentyl} \text{ and } 0 \text{ for } R = i\text{-Pr}; I_{\text{R}} = 1 \text{ for } R = t\text{-pentyl}; I_{\text{R}} = 1 \text{ for } R = i\text{-Pr} \text{ and } I_{\text{R}} = 0 \text{ for } R = t\text{-pentyl}; I_{\text{R}} = 1 \text{ for } R = c\text{-pentyl}; I_{\text{R}} = 0 \text{ for } R = i\text{-Pr} \text{ and } I_{\text{R}} = 0 \text{ for } R = t\text{-pentyl}; I_{\text{R}} = 0$	18	0.910	0.750	0.150
	6	MMP-2	$\log \left(1/KC_{50}\right) = 0.43(\pm 0.12)C \log P - 0.43(\pm 0.32)I_{\text{R}} + 1.09(\pm 0.34)I_{\text{R}} + 4.75(\pm 0.35); I_{\text{R}} = 1 \text{ for } R = c\text{-pentyl}, \text{ otherwise } I_{\text{R}} = 0$	20	0.893	0.821	0.270
	7	MMP-3	$\log \left(1/KC_{50}\right) = 0.50(\pm 0.17)C \log P + 1.27(\pm 0.46)I_{\text{R}} + 4.43(\pm 0.50); I_{\text{R}} = 1 \text{ for } R_1 = \text{methyl}, \text{ otherwise } I_{\text{R}} = 0$	19	0.836	0.745	0.380
	8	MMP-8	$\log \left(1/KC_{50}\right) = 0.35(\pm 0.19)C \log P - 1.18(\pm 0.47)I_{\text{R}2} + 7.29(\pm 0.51); I_{\text{R}2} = 1 \text{ for } R_2 = \text{methyl}, \text{ otherwise } I_{\text{R}2} = 0$	17	0.841	0.739	0.377
	9	MMP-13	$\log \left(1/KC_{50}\right) = 0.30(\pm 0.10)C \log P - 1.01(\pm 0.23)I_{\text{R}2} + 6.97(\pm 0.27); I_{\text{R}2} = 1 \text{ for } R_2 = \text{methyl}, \text{ otherwise } I_{\text{R}2} = 0$	14	0.959	0.925	0.164
III	10	MMP-1	$\log \left(1/KC_{50}\right) = -1.37(\pm 1.07)C \log P + 0.55(\pm 0.28)(C \log P)^2 0.67(\pm 0.46)I_{\text{NH}} - 0.79(\pm 0.32)I_{\text{2H}} + 6.87(\pm 0.975)C \log P_{\text{o}} = 1.24; I_{\text{LNH}} = 1 \text{ for } R_1 \text{ substituent with an NH- moiety, otherwise } I_{\text{1NH}} = 0; I_{\text{2H}} = 1 \text{ for } R_2 = H, \text{ otherwise } I_{\text{2H}} = 0$	15	0.924	0.860	0.270
	11	MMP-9	$\log \left(1/KC_{50}\right) = 0.61(\pm 0.22)C \log P + 1.56(\pm 0.50)I_{\text{R}-\text{CC}} - 0.94(\pm 0.34)I_{\text{2H}} + 4.95(\pm 0.68); I_{\text{2H}} = 1 \text{ for } R_2 = H, \text{ otherwise } I_{\text{2H}} = 0; I_{\text{R}-\text{CC}} = 1 \text{ for } R = OCH_2CCCH_3, \text{ otherwise } I_{\text{R}-\text{CC}} = 0$	17	0.891	0.800	0.290
	12	MMP-13	$\log \left(1/KC_{50}\right) = 0.64(\pm 0.25)C \log P + 1.27(\pm 0.56)I_{\text{R}-\text{CC}} + 5.09(\pm 0.77); I_{\text{R}-\text{CC}} = 1 \text{ for } R = OCH_2CCCH_3, \text{ otherwise } I_{\text{R}-\text{CC}} = 0$	15	0.792	0.680	0.330
IV	13	MMP-3	$\log \left(1/K_{\text{I}}\right) = 0.58(\pm 0.14)C \log P + 6.57(\pm 0.20)$	11	0.904	0.848	0.245
V	14	MMP-2	$\log \left(1/KC_{50}\right) = 11.24(\pm 8.14)^1\chi' - 1.06(\pm 0.72)(^1\chi'_{\text{X}})^2 + 2.68(\pm 0.96)I_{\text{Y}} - 1.47(\pm 1.38)\sigma_{\text{X}} - 22.79(\pm 22.88); \text{ optimum } (^1\chi'_{\text{X}}) = 5.29; I_{\text{Y}} = 1 \text{ for } Y = CH_3, \text{ otherwise } I_{\text{Y}} = 0$	14	0.859	0.680	0.510
	15	MMP-3	$\log \left(1/KC_{50}\right) = 14.71(\pm 6.46)(^1\chi'_{\text{X}}) - 1.33(\pm 0.57)(^1\chi'_{\text{X}})^2 + 1.39(\pm 0.76)I_{\text{Y}} - 1.17(\pm 1.10)\sigma_{\text{X}} - 32.36(\pm 18.14); \text{ optimum } (^1\chi'_{\text{X}}) = 5.52; I_{\text{Y}} = 1 \text{ for } Y = CH_3, \text{ otherwise } I_{\text{Y}} = 0$	14	0.846	0.680	0.410
	16	MMP-3	$\log \left(1/KC_{50}\right) = 30.54(\pm 7.06)\pi_{\text{X}} - 3.09(\pm 0.70)\pi_{\text{X}}^2 - 0.49(\pm 0.21)\pi_{\text{Y}} - 65.94(\pm 17.53); \text{ optimum } \pi_{\text{X}} = 4.94(4.87 - 4.99)$	15	0.906	0.842	0.296
	17	MMP-3	$\log \left(1/K_{\text{I}}\right) = 0.64(\pm 0.19)C \log P + 4.64(\pm 0.50)$	12	0.857	0.806	0.313
	18	MMP-1	$\log \left(1/KC_{50}\right) = -0.19(\pm 0.12)C \log P + 1.02(\pm 0.40)I_{\text{2}} + 0.60(\pm 0.49)I_{\text{3}} + 5.98(\pm 0.43); I_{\text{2}} = 1 \text{ for } R_2 = CH_2\text{-3-pyridyl}, \text{ otherwise } I_{\text{2}} = 0; I_{\text{3}} = 1 \text{ for } R_3 = \text{an aromatic substituent, otherwise } I_{\text{3}} = 0$	16	0.845	0.670	0.280
	19	MMP-9	$\log \left(1/KC_{50}\right) = -0.27(\pm 0.18)C \log P - 1.24(\pm 0.73)I_{\text{1}} + 1.18(\pm 0.69)I_{\text{4}} + 8.34(\pm 0.49)I_{\text{1}} = 1 \text{ for } R_1 = OCH_2Ph, \text{ otherwise } I_{\text{1}} = 0; I_{\text{4}} = 1 \text{ for } R_4 = \text{an aromatic moiety, otherwise } I_{\text{4}} = 0$	19	0.778	0.640	0.500
	20	MMP-13	$\log \left(1/KC_{50}\right) = -0.18(\pm 0.14)C \log P - 1.05(\pm 0.55)I_{\text{1}} + 1.08(\pm 0.63)I_{\text{3}} + 1.34(\pm 0.53)I_{\text{4}} + 7.90(\pm 0.37); I_{\text{1}} = 1 \text{ for } R_1 = OCH_2Ph, \text{ otherwise } I_{\text{1}} = 0; I_{\text{3}} = 1 \text{ for } R_3 = \text{an aromatic substituent, otherwise } I_{\text{3}} = 0; I_{\text{4}} = 1 \text{ for } R_4 = \text{an aromatic moiety, otherwise } I_{\text{4}} = 0$	22	0.845	0.750	0.380
	21	MMP-2	$\log \left(1/KC_{50}\right) = 3.53(\pm 2.40)C \log P - 0.89(\pm 0.59)(C \log P)^2 + 1.98(\pm 0.46)I_{\text{1,NH}} + 3.86(\pm 2.16)C \log P_{\text{o}} = 1.97; I_{\text{1}} = 1 \text{ for } R_1 = 4\text{-substituted phenyl group, otherwise } I_{\text{1}} = 0; I_{\text{1,NH}} = 1 \text{ for } R_1 \text{ with an NH- moiety, otherwise } I_{\text{1,NH}} = 0$	22	0.916	0.820	0.420
	22	MMP-13	$\log \left(1/KC_{50}\right) = 5.49(\pm 2.13)C \log P - 1.33(\pm 0.52)(C \log P)^2 + 1.87(\pm 0.41)I_{\text{1}} + 1.28(\pm 1.95)C \log P_{\text{o}} = 2.05; I_{\text{1}} = 1 \text{ for } R_1 = 4\text{-substituted phenoxypyridinyl group, otherwise } I_{\text{1}} = 0$	22	0.910	0.860	0.380
	23	MMP-1	$\log \left(1/K_{\text{I}}\right) = 0.55(\pm 0.26)\pi_{\text{t,nn}} - 0.58(\pm 0.33)I_{\text{ic}} + 0.59(\pm 0.37)\sigma_{\text{m}} - 0.63(\pm 0.38)MR_{\text{o}} + 1.75(\pm 0.48); I_{\text{ic}} = 1, \text{ if substituents having size larger than that of hydrogen are present on vicinal carbon atoms of the phenyl ring, and } 0, \text{ otherwise}$	19	0.771	0.172	0.225
	24	MMP-2	$\log \left(1/K_{\text{I}}\right) = 5.70(\pm 1.85)\sigma_{\text{m}} - 5.50(\pm 2.40)\sigma_{\text{m}}^2 - 1.52(\pm 0.62)MR_{\text{m}} - 0.36(\pm 0.33)\pi_{\text{o}} + 2.16(\pm 0.55)$	18	0.830	0.202	0.225
	25	MMP-8	$\log \left(1/K_{\text{I}}\right) = 7.68(\pm 2.22)\sigma_{\text{m}} - 6.57(\pm 2.88)\sigma_{\text{m}}^2 - 2.55(\pm 0.75)MR_{\text{m}} - 0.46(\pm 0.40)\pi_{\text{o}} + 2.34(\pm 0.66)$	18	0.882	0.242	0.225
	26	MMP-9	$\log \left(1/K_{\text{I}}\right) = 6.58(\pm 2.17)\sigma_{\text{m}} - 6.30(\pm 2.82)\sigma_{\text{m}}^2 - 1.80(\pm 0.73)MR_{\text{m}} - 0.53(\pm 0.39)\pi_{\text{o}} + 2.16(\pm 0.65)$	18	0.828	0.237	0.225
	27	MMP-1	$\log \left(1/KC_{50}\right) = -0.18(\pm 0.14)C \log P + 0.84(\pm 0.29)I_{\text{2,M}} + 6.58(\pm 0.60); I_{\text{2,M}} = 1 \text{ for } Y = OCH_3, \text{ otherwise } I_{\text{2,M}} = 0$	19	0.835	0.730	0.210
	28	MMP-1	$\log \left(1/KC_{50}\right) = 1.61(\pm 0.71)C \log P - 0.32(\pm 0.12)C \log P^2 + 0.95(\pm 0.96)C \log P_{\text{o}} = 2.48(2.17 - 2.66); I_{\text{Y}} = 1 \text{ for } Y = OCH_3,$	20	0.891	0.724	0.187
	29	MMP-13	$\log \left(1/KC_{50}\right) = -0.40(\pm 0.11)C \log P + 9.69(\pm 0.38)$	18	0.773	0.730	0.210

Table 8. continued

compd	Q SAR no.	MMP type	QSAR models	statistics				refs
				n	r^2	q^2	s	
XI	30	MMP-9	$\log \left(1/\text{IC}_{50}\right) = 2.19(\pm 0.34)\text{Pol} - 0.87(\pm 0.26)\text{I}_2 - 2.08(\pm 1.60); \text{I}_2 = 1 \text{ for } R_3 = \text{butynoxy group, otherwise } I_{2,CC} = 0$	10	0.982	0.950	0.150	226
	31	MMP-13	$\log \left(1/\text{IC}_{50}\right) = 1.73(\pm 0.60)\text{Pol} - 1.11(\pm 0.45)\text{I}_2 + 0.23(\pm 2.81); \text{I}_2 = 1 \text{ for } R_2 = \text{butynoxy group, otherwise } I_{2,CC} = 0$	10	0.943	0.880	0.260	226
XII	32	MMP-9	$\log \left(1/\text{IC}_{50}\right) = 0.34(\pm 0.15)\text{C log P} + 0.85(\pm 0.48)\text{I}_{\text{COPh}} + 7.22(\pm 0.33); \text{I}_{\text{COPh}} = 1 \text{ for } R_1 = \text{COPh, otherwise } I_{\text{COPh}} = 0$	10	0.887	0.700	0.250	227
	33	MMP-13	$\log \left(1/\text{IC}_{50}\right) = 0.17(\pm 0.14) \text{C log P} + 0.83(\pm 0.42)\text{I}_{\text{COPh}} + 7.57(\pm 0.30); \text{I}_{\text{COPh}} = 1 \text{ for } R_1 = \text{COPh, otherwise } I_{\text{COPh}} = 0$	10	0.835	0.710	0.220	227
XIII	34	MMP-13	$\log \left(1/\text{IC}_{50}\right) = -0.35(\pm 0.15) \pi_{R_1} + 1.03(\pm 0.27)\text{I} + 8.14(\pm 0.22); \text{I} = 1 \text{ for } R_1 = \text{COPh or its deriv, otherwise } I = 0$	10	0.925	0.824	0.159	227
	35	MMP-1	$\log \left(1/\text{IC}_{50}\right) = 0.53(\pm 0.18)\text{C log P} - 0.10(\pm 0.04) (\text{C log P})^2 + 0.59(\pm 0.17)I_{\text{OMe}} + 4.98(\pm 0.25) \text{C log P}_o = 2.61; I_{\text{OMe}} = 1 \text{ for } R_1 = \text{OCH}_3,$ otherwise $I_{\text{OMe}} = 0$	38	0.723	0.640	0.210	228
XIV	36	MMP-9	$\log \left(1/\text{IC}_{50}\right) = 0.91(\pm 0.26)\text{C log P} - 0.13(\pm 0.06) (\text{C log P})^2 + 0.77(\pm 0.29)I_{\text{PhCl}} + 6.69(\pm 0.28) \text{C log P}_o = 3.55; I_{\text{PhCl}} = 1 \text{ for } R_1 = \text{OC}_6\text{H}_4\text{-4-Cl},$ otherwise $I_{\text{PhCl}} = 0$	42	0.794	0.740	0.310	228
	37	MMP-13	$\log \left(1/\text{IC}_{50}\right) = 0.73(\pm 0.19)\text{C log P} - 0.14(\pm 0.05) (\text{C log P})^2 - 0.27(\pm 0.18)I_{\text{OMe}} + 8.00(\pm 0.265) \text{C log P}_o = 2.57; I_{\text{OMe}} = 1 \text{ for } R_1 = \text{OCH}_3,$ otherwise $I_{\text{OMe}} = 0$	41	0.723	0.630	0.230	228
XV	38	MMP-1	$\log \left(1/\text{IC}_{50}\right) = 0.88(\pm 0.32) \text{C log P} - 1.35(\pm 0.41) \text{CMR} + 0.82(\pm 0.41) \text{CMR} + 19.05(\pm 4.05); I_X = 1 \text{ for } X = \text{heterocyclic group, otherwise } I_X = 0$	16	0.846	0.761	0.226	229
	39	MMP-13	$\log \left(1/\text{IC}_{50}\right) = 0.62(\pm 0.21) \text{C log P} - 0.72(\pm 0.18) \text{CMR} + 15.30(\pm 1.73)$	10	0.925	0.842	0.157	230
XVI	40	MMP-1	$\log \left(1/\text{IC}_{50}\right) = -6.47(\pm 2.01) \text{MgVol} + 34.22(\pm 8.51)$	8	0.912	0.857	0.390	231

^a Adapted from ref 177.

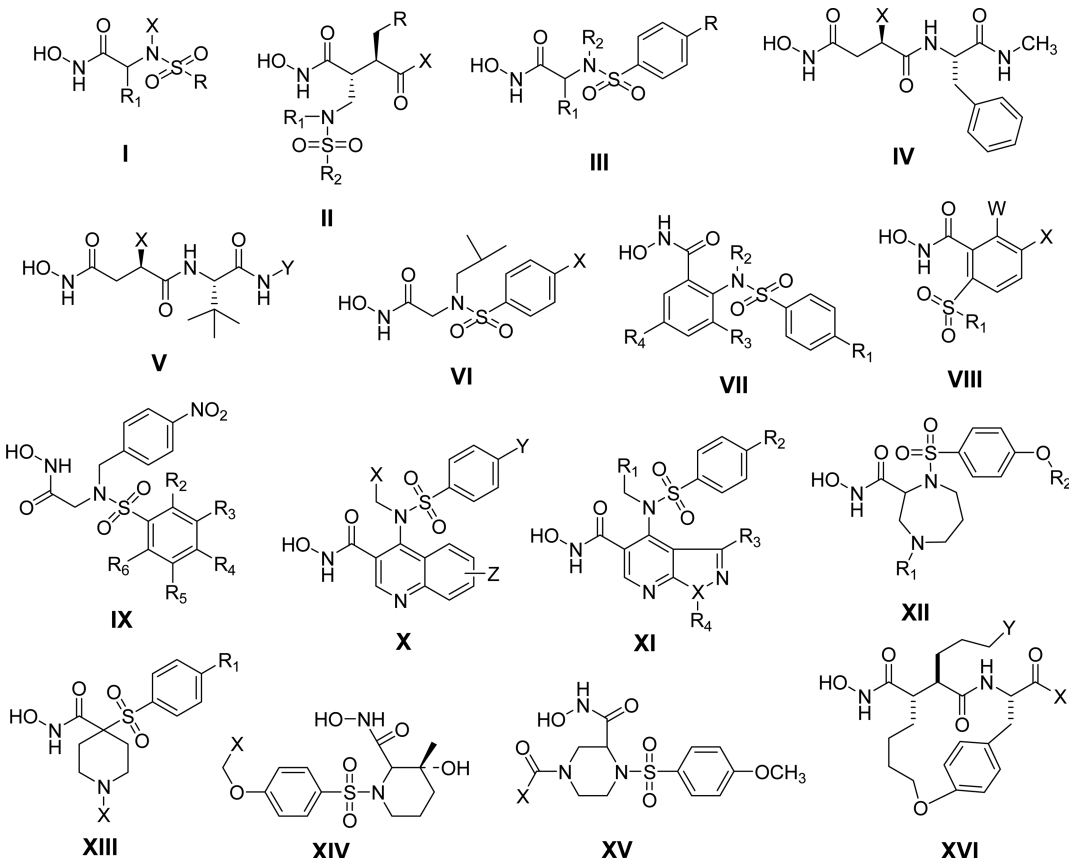


Figure 41. Various hydroxamates on which 2D QSARs are reported in Table 8.¹⁷⁷

MMPs can be achieved by designing molecules that can make noncovalent interactions at the S1 and S2 subsites as well as the usual S1'–S3' subsites.²¹⁵

That the hydrophobic, electrostatic, and steric interactions play important roles in MMP inhibition have been visualized by some molecular modeling studies.^{200,202,216} Verma and Hanch¹⁷² also reported 2D QSAR studies on several series of hydroxamates acting as MMP inhibitors just to conclude that hydrophobicity and molar refractivity of compounds play an important role in MMP inhibition. In his recent communication, Verma¹⁷⁷ beautifully summarized all 2D QSARs (Table 8) on different categories of hydroxamates (Figure 41) to have a comparative view of drug–receptor interactions of all hydroxamates and to conclude that among physicochemical properties, the greatest contribution in MMP inhibition is of hydrophobicity followed by the electronic properties of substituents. The relative contributions of all properties are very well shown in Figure 42. Topological parameters are also shown to have good contribution, but the indicator variables are shown to play as important roles as the hydrophobicity. Indicator variables are important in the sense that they specify the roles of some specific substituents with their specific physicochemical properties.

6.3.1. An Overview of MMP Inhibition. Hydroxamic acids fulfill all of the three basic requirements that are essential for a compound to be an effective MMP inhibitor, that is, a zinc-binding group, a functional group capable of forming hydrogen bonds with the enzyme backbone, and one or more side chains that can have van der Waals interactions with enzyme subsites. The greatest potency of MMP inhibitors, however, has been observed to be associated with their ability

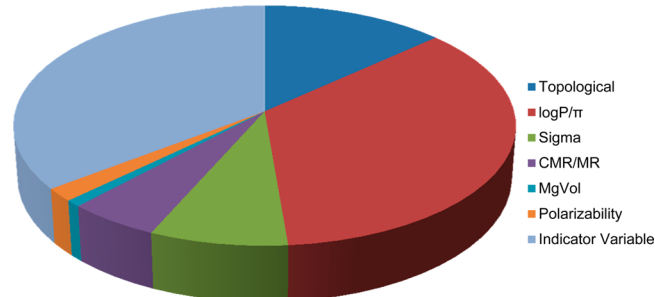
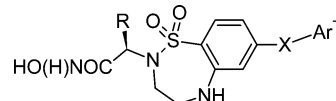


Figure 42. A graphical representation of the contributions of different parameters in 40 QSAR models as given in Table 8. Reprinted with permission from ref 177. Copyright 2012 Springer Basel AG.

to interact with S1, S1', and S2' subsites of MMPs. SAR studies have shown that the S1' subsite differs most among the MMPs, and a certain degree of specificity can be achieved by varying the P1' residue of the inhibitors. The P1' substituent should preferably be a long side chain for binding with MMP-2, MMP-3, and MMP-9. The COMFA model obtained by Amin and Welsh¹⁹⁸ for aryl sulfonylisoquinoline-based MMPs pointed out the narrow hydrophobic nature of S1' pocket and the necessity to avoid the steric bulk near the zinc-binding group, facts that were observed in X-ray and NMR structural studies.

Various COMFA and COMSIA studies have indicated the involvement of steric, electrostatic, hydrophobic, and H-bond interactions in the inhibition of MMPs by hydroxamic acids. Various QSAR studies by Gupta et al.²¹³ and others as shown in Table 8 have, however, shown that, in addition to binding with Zn²⁺ ion, the greatest contribution to the MMP inhibition

Table 9. Series of Benzothiazepine Derivatives and Their TACE Inhibition Activity²⁵⁰

compd	R	X	Ar	K_i	p K_i
1	Me	OMe		274	6.562
2	Me	H		484	6.315
3	iPr	OMe		71	7.148
4	Me	OH		391	6.407
5	Me	OCH ₂	phenyl	705	6.151
6	Me	OCH ₂	3,5-dimethylphenyl	229	6.640
7	Me	OCH ₂	3,5-dichlorophenyl	153	6.815
8	Me	OCH ₂	3,5-dimethoxyphenyl	27	7.568
9	Me	OCH ₂	3,5-diethoxyphenyl	81	7.091
10	Me	OCH ₂	2,6-dimethyl-4-pyridinyl	544	6.264
11	iBu	OH		89	7.050
12	iBu	OCH ₂	phenyl	177	6.752
13	iBu	OCH ₂	3,5-dimethoxyphenyl	17	7.792
14	iPr	OCH ₂	3,5-dimethoxyphenyl	10	8.00
15	iPr	OCH ₂	3,5-diethoxyphenyl	51	7.292
16	iPr	OCH ₂	4,5-dimethyl-2-thiazolyl	290	6.537
17	(CH ₂) ₂ CO ₂ Me	OCH ₂	3,5-diethoxyphenyl	177	6.752
18	(CH ₂) ₃ CO ₂ Me	OCH ₂	3,5-diethoxyphenyl	242	6.616
19	(CH ₂) ₃ CO ₂ Me	OCH ₂	3,5-dimethoxyphenyl	10	8.00
20	(CH ₂) ₃ CO ₂ Me	OCH ₂	3,5-diethoxyphenyl	13	7.886
21	(CH ₂) ₄ NHSO ₂ Me	OCH ₂	3,5-dimethoxyphenyl	5	8.301
22	(CH ₂) ₄ NHBoc	OCH ₂	3,5-dimethoxyphenyl	77	7.113
23	(CH ₂) ₄ NH ₂	OCH ₂	3,5-dimethoxyphenyl	31	7.508
24	iBu	NHCH ₂	3,5-dimethoxyphenyl	56	7.251
25	Me	O	4-(trifluoromethyl)phenyl	758	6.120
26	Me	O	4-methoxyphenyl	621	6.206
27	Me	O	phenyl	734	6.134
28	Me	O	3-nitrophenyl	129	6.889
29	Me	O	4-nitrophenyl	11	7.958

activity of hydroxamates is of their hydrophobic property followed by their electronic properties. Some differences in QSARs of inhibitors of different MMPs can be attributed to the structural differences among the active pockets, particularly S1', S1, and S2' of various MMPs. The occupation of pocket allows modulating the selectivity and hydrophobic and electronic property differences among various MMPs.

According to Welch et al.,²⁰⁹ the S1' pocket in MMPs is the most well-defined area of binding that consists of a hydrophobic pocket, varying in depth for different MMPs. The constitutional differences in active sites of MMPs lead to hydrophobic and electronic differences in them, because of which they differ in inhibitor binding and enzyme activity.

6.4. TACE Inhibition

Despite a low sequence homology and divergent structural elements, the TACE structure has excellent similarity with MMP structures, and more importantly the active site of TACE is reminiscent of the MMPs. As in MMPs, in TACE also there are three flat substrate subsites, S1, S2, and S3, to the left of catalytic Zn²⁺ ion and three deep subsites, S1', S2', and S3', to the right of catalytic Zn²⁺ ion. However, the active sites of TACE have a very interesting feature, where S1' and S3' subsites are merged to create an L-shaped S1' binding cleft that opens into the S3' pocket. Both S1' and S3' are hydrophobic but are connected by a polar entrance.^{233,234} Thus, the

characteristics of the TACE binding pocket are unique relative to MMPs so far examined.

So, as the catalytic sites of TACE and MMPs have excellent similarity, most of the MMP inhibitors have also been studied simultaneously for TACE inhibition. However, this structural similarity between the active sites of MMPs and TACE creates a serious problem for the design of specific TACE inhibitors with selectivity over MMPs. However, the fact that S1' and S3' pockets of TACE are merged and create an L-shaped S1' binding cleft that opens into the S3' pocket sets it apart from the S1' subsites of MMPs. Exploiting this difference, some novel, selective hydroxamic TACE inhibitors were designed and synthesized.^{235–238} However, hydroxamic acids often exhibited poor oral absorption *in vivo* and significant metabolic liabilities (rapid hydrolysis and glucuronidation).²³⁹ Therefore, attempts were made to develop some nonhydroxamate TACE inhibitors, such as thiol-containing aryl sulfones and sulfonamides, hydantoins, trizzolones, imidazolines, etc.^{241–244} However, to rationalize the observed activity of hydroxamate and non-hydroxamate TACE inhibitors, a highly plausible pharmacophore model was developed by Bristol-Myers Squibb Pharmaceutical Research Institute (BMSPRI).²⁴⁵

The TACE inhibitors from different classes have been found to have different interactions with TACE.²⁴⁵ Because of high sequence similarity in the active site regions of TACE and MMPs and among the various categories of TACE and MMP

inhibitors, the hydroxamic acid-based inhibitors have been most widely studied, and consequently most of the QSAR studies have been directed to only this class of MMP and TACE inhibitors. The 2D QSAR studies on hydroxamic acid TACE inhibitors have been vividly reported by Gupta,¹⁷¹ while various authors have paid attention to 3D QSAR studies as well.^{246–249}

For 3D QSAR studies, the structural information of proteins is essential. To date several crystal structures of TACE, cocrystallized with different inhibitors, are available in the PDB data bank. Scientists at BMSPRI designed and developed some benzothiadiazepine derivatives (Table 9) as selective TACE inhibitors, in which there were several very highly potent and more selective over MMP-1, MMP-2, and MMP-9.²⁵⁰ Among them, compound **21** (Table 9) was found to be the most active ($K_i = 5 \text{ nM}$) with over 75-fold higher selectivity over MMPs.

For this series of compounds (Table 9), Murumkar et al.²⁴⁶ performed CoMFA and CoMSIA study using different alignment rules in which database alignment option was found to give the best models. In database alignment, each analog was aligned to the template by rotation and translation so as to minimize the RMSD between atoms in template and the corresponding atom in the analogue. In this study, compound **21** was used as the template. Both CoMFA and CoMSIA models were found to have $r^2_{cv} > 0.5$, which indicated the stability of model as well as good predictive ability. However, CoMSIA had slightly better r^2_{cv} value (0.556) than CoMFA (0.510).

For both CoMFA and CoMSIA, contour maps were drawn for the template compound that showed favorable and unfavorable steric, electrostatic, hydrophobic, and H-bond donor regions. The CoMFA steric contour map indicated that the steric bulk would be preferred in the vicinity of substituted amino moiety of methane sulfonyl group, but any bulky substituent near the methane sulfonyl amino group may disfavor the potency. The electrostatic contours of CoMFA indicated that near the 5-methoxy phenyl group the high electron density might increase the activity and that in the vicinity of the 3-methoxy phenyl group the low electron density might increase the activity.

According to CoMSIA hydrophobic contours, the hydrophobic substituents might be favorable at the region surrounding the amino group, but in the vicinity of the 5-methoxy phenyl group hydrophobic substituents might be detrimental to the activity. In the H-bond donor CoMSIA contours, it was indicated that H-bond donor might be favorable in the vicinity of methane sulfonamide moiety but unfavorable near benzodiazepine ring.

An interaction study of this compound by Murumkar et al.²⁴⁶ with the crystal structure of TACE revealed that apart from binding with oxygen atoms of hydroxamic acid, the Zn^{2+} ion of the active site also binds strongly with the oxygen of SO_2Me group (Figure 43). It could be the reason why this compound was found to be the most active in the series. It was also predicted by Murumkar et al.²⁴⁶ that an aliphatic substitution (*n*-butyl or *n*-pentyl) at the 4-position of 3,5-dimethoxy phenyl ring of this compound could further improve its TACE inhibitory activity.

A CoMFA and CoMSIA study was also performed by Murumkar et al.²⁴⁷ on a series of constrained β -amino-hydroxamic acids as represented by general structures **34a–d**, acting as TACE inhibitors.²⁵¹ The study revealed that electrostatic field contribution for this series of compounds was more important than the steric contribution. The CoMFA contours

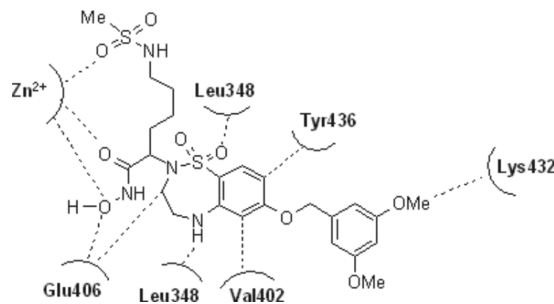


Figure 43. Interaction of active site of TACE with the template compound (21, Table 9). Reprinted with permission from ref 246. Copyright 2008 Blackwell Munksgaard.

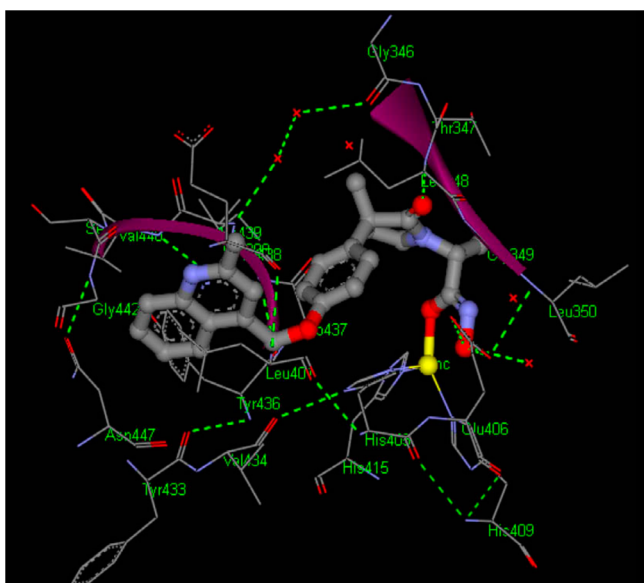
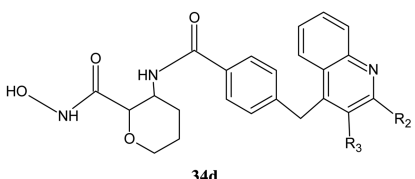
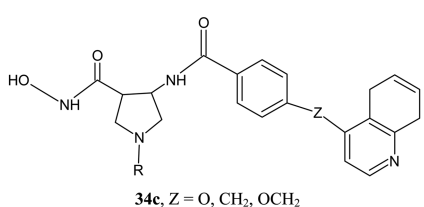
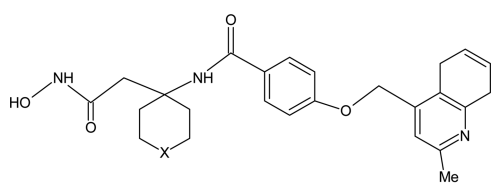
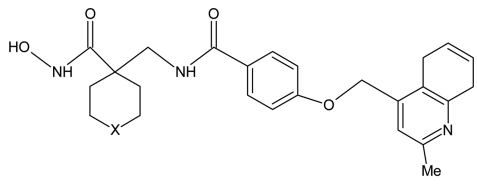
obtained by these authors for steric field had exhibited 80% regions of high steric tolerance and only 20% region of low steric tolerance. Similarly, the electrostatic contour map had exhibited that 80% of the regions was favorable to the increase in the negative charge on the atoms. A derivative of **34a** ($X = N-SO_2Me$), that had the highest activity in the series and had more than 5000 times higher selectivity over MMP-1 and MMP-13, was selected for getting the contour plots. In the steric contours, a region enclosing the quinoline ring of **34a** ($X = N-SO_2Me$) had indicated that a bulky group here would increase the TACE inhibitory activity of the compound. Similarly, a large region over the piperidine ring was also indicated to be favorable for the bulkier substituents. On the other hand, a region near quinolone ring was indicated to be unfavorable for bulky substituents.

The electrostatic contours indicated that a region surrounding the central benzamide ring might be favorable for high electron density, while low electron density may be favored in the vicinity of the central phenyl ring.

The CoMFA model derived by Murumkaret al.²⁴⁷ was found to have high predictive ability. It predicted the activity of IK-682 (**35**) ($pIC_{50} = 8.991$) very close to its experimental value ($pIC_{50} = 9.0$). This compound was designed by Duan et al.²⁵² at BMSPRI and was found to be a compound of choice with *in vitro* IC_{50} value of 1 nM. It is at least 1000 times more selective toward TACE over most of its MMPs. Its free fraction in human serum is relatively high (3.6%). It was cocrystallized with TACE (PDB code 2FV5), where it was found to interact with the active site of the enzyme as shown in Figure 44.²⁵³

Because the CoMSIA model was not found to be as good as CoMFA, its implication was not much discussed.

In their further communication, Murumkar et al.²⁵⁴ developed a five-point pharmacophore model having two H-bond acceptors (A), one H-bond donor (D), and two aromatic rings. The model was based on a large series of compounds similar to **36** imported from the project table in the "Develop Pharmacophore Model" panel. The model was based on common pharmacophore hypothesis (CPH) and alignment, using PHASE.²⁵⁵ Compound **36** was the most active compound in the whole data set, and with reference to this compound the pharmacophore model contained two aromatic ring features, one mapping on the central phenyl ring and the other on the phenyl part of the quinoline ring, two H-bond acceptor features, one mapping on the lone pair of oxygen of central carbonyl of the amide group and the other mapping on oxygen of the carbonyl group of the hydroxamate, and one H-bond donor, mapping on the NH of the hydroxamate moiety. This pharmacophore is shown in Figure 45 with compound **36**.



mapped on it, and mapping of the pharmacophore features in active site of TACE is shown in Figure 46. This figure shows that the aromatic ring can act as P1' group that can interact with S1' subsite of the enzyme, and the second aromatic ring acts as a linker between the zinc binding group and P1' side chain. The first H-bond acceptor lies in the vicinity of Leu348, and the second one is aligned toward the zinc motif. The H-

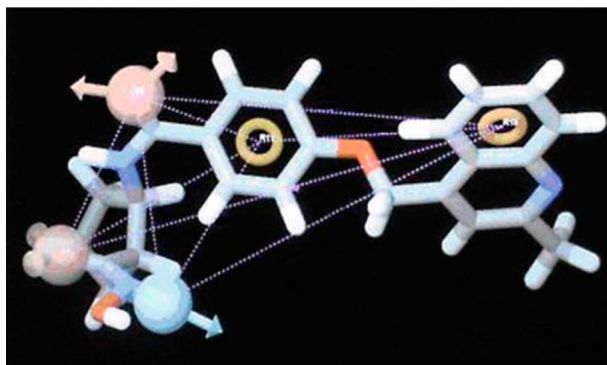
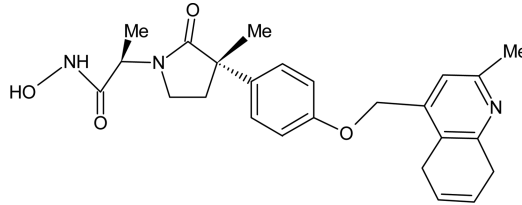


Figure 45. Mapping of active compound 36 on the pharmacophore features (CPH1). Reprinted with permission from ref 254. Copyright 2010 Springer.

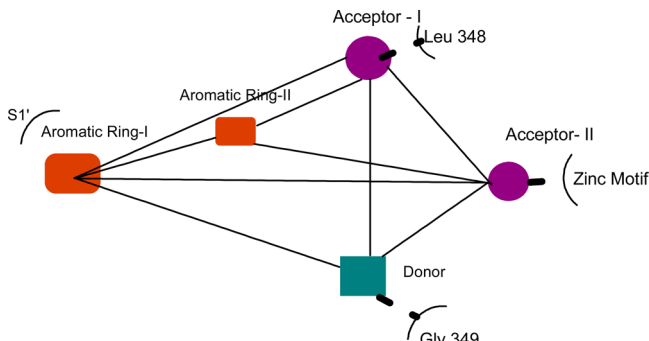
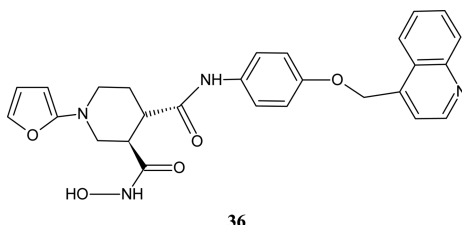


Figure 46. A 2D representation of pharmacophoric features interacting with TACE. Reprinted with permission from ref 254. Copyright 2010 Springer.

bond donor feature lies in the vicinity of Gly349. The features of H-bond acceptor-I and H-bond donor are important to have a bonding with NH group of Leu348 and CO of Gly349, respectively.



A series of 12 α -substituted chromen-core-based hydroxamic acids (37) were synthesized and evaluated for their TACE inhibition activity by Yang et al.²⁴⁹ These compounds were designed to fill in the S1' pocket of the enzyme. Almost all of the compounds were found to be highly potent against TACE as well as cellular TNF- α , but a compound (37a) was observed to be most promising in the in vitro and in vivo activity profiles. QSAR and docking studies were also performed on these

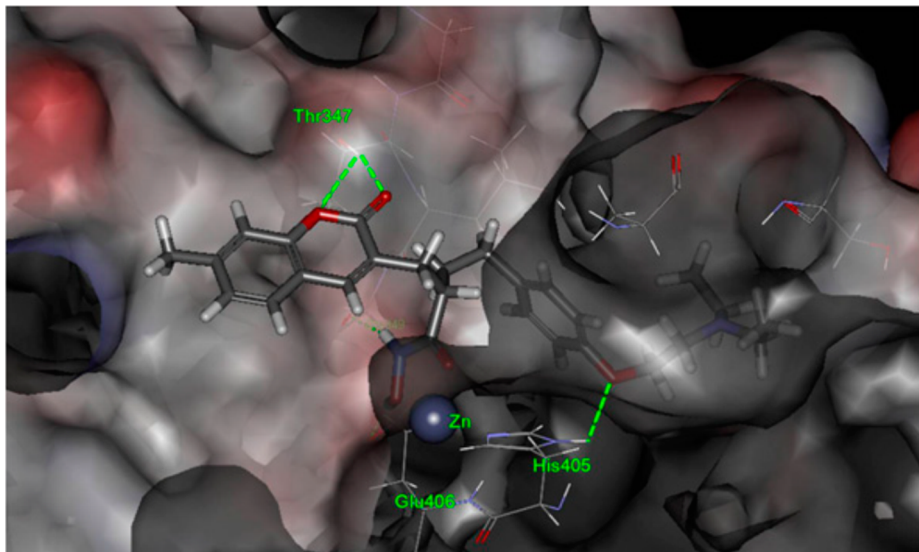
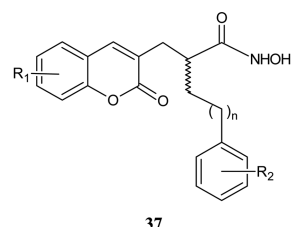


Figure 47. Docking model for the (S)- α -substituted chromen analogue (37a) binding to the binding pocket of TACE. Reprinted with permission from ref 249. Copyright 2010 Elsevier.

compounds. The docking study showed that α -substituent with long and bulky groups of coumarin core gets inside the S1' and S3' pockets of TACE and undergoes van der Waals interaction to increase the activity. Further, the docking study suggested that an α -alkoxyaryl alkyl group further stabilizes the receptor–ligand interaction by forming an extra hydrogen bond and thus leads to greater activity. A docking model showing the interaction of 37a is shown in Figure 47.²⁴⁹



37a: n = 1, R₁ = 7-Me, R₂ = 4-(2-dimethylamino-ethoxy)

A QSAR model for TACE inhibition was also generated for these compounds by Yang et al.²⁴⁹ using genetic function approximation technique with Discovery Studio 2.5. The model obtained was as shown in eq 25. This model has two

$$\begin{aligned} \log(1/\text{IC}_{50}) &= 12.369(\text{Balaban_index_JX}) \\ &- 736.95(\text{FNSA3}) - 0.85767 \log D \\ &+ 1.5867(\text{Num_Atoms}) + 1.0541(\text{Num_Chains}) \\ &+ 0.070294(\text{WNSA2}) - 120.91 \\ n &= 12, r^2 = 0.9214, r^2_{\text{pred}} = 0.7978, s = 0.2687 \end{aligned} \quad (25)$$

constitutional descriptors, Num_Atoms and Num_Chains, which define the size of the molecule. Thus, their positive coefficients may indicate the van der Waals interaction of the molecule with the receptor. FNSA3 and WNSA2 are electrostatic descriptors, denoting fractional negative surface area computed with quantum charges and weighted negatively charged partial surface area, respectively. Because, in the model, the coefficient of the former is very high and negative as

compared to that of the latter, the fractional negative surface would have the dominant effect on the activity. Simultaneously, the parameter log D, defining the lipophilicity of the molecule taking into consideration the ionization state of the molecule, also seems to be determinant to the activity. However, the Balaban_index_JX, which is a topological descriptor weighted on relative electronegativity, seems to be favorable to the activity, indicating that more electronegative atoms in the molecule will be conducive to TACE inhibition.

Because FNSA3 has negative value, increase in its value will lead to the increase in the activity, and this indicates the electrostatic interaction between the molecule and the active site of the receptor. This is also supported by the negative correlation of log D. However, eq 25 has a disproportionately large number of variables (6) as compared to the number of data points (12); hence caution should be observed to derive any meaning from it.

However, on the basis of several QSAR equations reported by his own group^{213c,d,g-i} (eqs 26–33) on different series of TACE inhibitors as shown in Figure 48, Gupta concluded in his review¹⁷¹ that, in most of the cases, the hydrophobic property of the molecules has been the most important controlling factor. In some cases (38–40), the activity had the parabolic correlation with C log P (eqs 26–28) and in some cases (41–43) negative linear correlations (eqs 29–31). Thus, the positive effect of hydrophobic property may be only up to a certain point, beyond which it would play a negative role. In the in vitro case, the parabolic dependence of activity on hydrophobicity is assumed to be due to the limited bulk tolerance of the active sites of the receptors, as there are no hydrophilic–lipophilic intervening barriers vis-à-vis cell membranes in the cells. This tantamounts to steric effects, and thus bulky molecules or bulky substituents in the molecules might produce steric effects in TACE inhibition. This steric effect is obviously shown by negative correlation of activity with C log P (eqs 29–31) and more obviously by its negative correlation with molecular volume (eq 32).

Acyclic hydroxamic acids (38):^{213c}

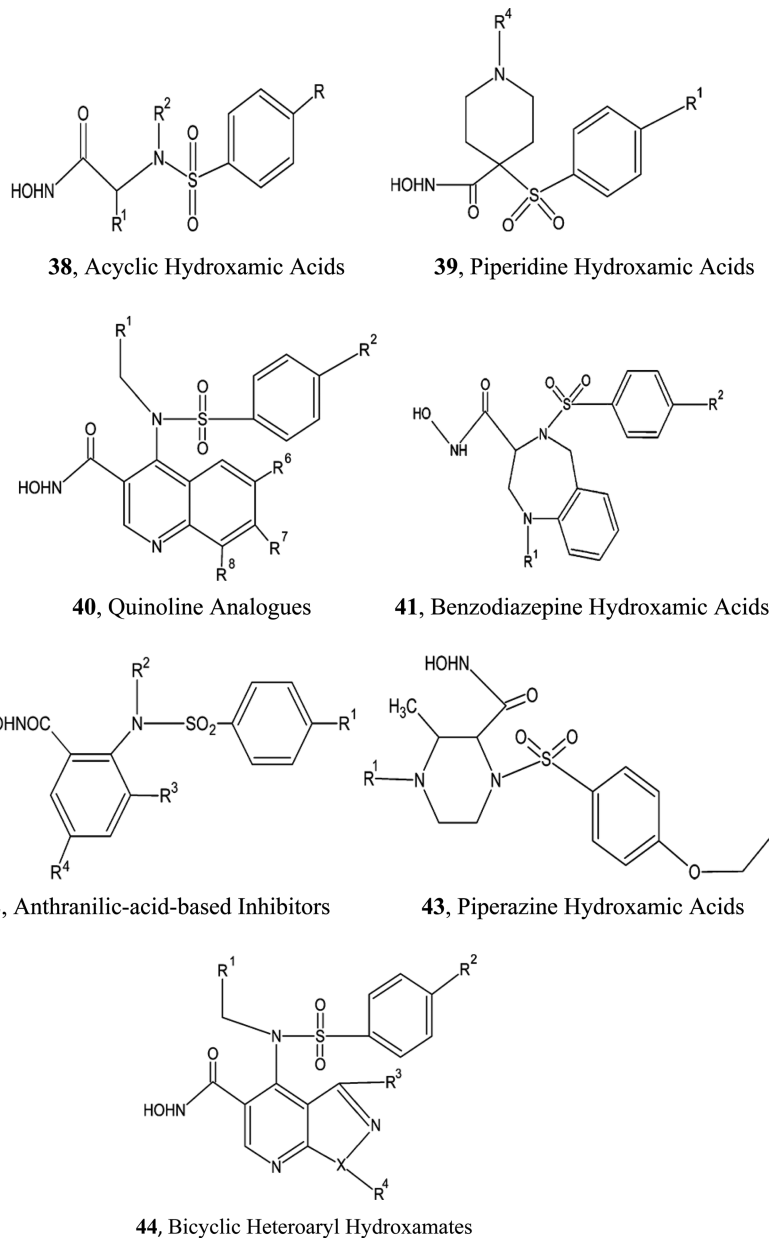


Figure 48. Different series of hydroxamic acid TACE inhibitors as subjected to QSAR by Gupta et al.^{213c,d,g-i}

$$\log(1/\text{IC}_{50}) = 0.895(\pm 0.492)(C \log P) - 0.368(\pm 0.143)(C \log P)^2 + 0.525(\pm 0.222)I_{1,\text{pyr}} + 7.708(\pm 0.396)$$

$$n = 17, r = 0.910, r_{\text{cv}}^2 = 0.71, s = 0.15, F_{3,13} = 20.89(5.74), C \log P_o = 1.22$$

(26)

$$\log(1/\text{IC}_{50}) = 0.800(\pm 0.657)(C \log P) - 0.155(\pm 0.109)(C \log P)^2 - 1.184(\pm 0.321)I_{2,\text{M}} - 0.746(\pm 0.303)I_7 + 6.965(\pm 0.303)$$

$$n = 16, r = 0.934, r_{\text{cv}}^2 = 0.67, s = 0.17, F_{4,11} = 18.87(5.67), C \log P_o = 2.58$$

(28)

Benzodiazepine hydroxamic acids (**41**):^{213d}

$$\log(1/\text{IC}_{50}) = 0.930(\pm 0.251)I_{\text{R2-CC}} - 0.133(\pm 0.112)(C \log P) + 7.143(\pm 0.299)$$

$$n = 17, r = 0.906, r_{\text{cv}}^2 = 0.71, s = 0.20, F_{2,14} = 31.97(6.51)$$

Anthranilic-acid-based inhibitors (**42**):^{213d}

$$\log(1/\text{IC}_{50}) = 0.637(\pm 0.229)I_{4,\text{Br}} - 0.163(\pm 0.084)(C \log P) + 7.156(\pm 0.248)$$

$$n = 16, r = 0.898, r_{\text{cv}}^2 = 0.69, s = 0.20, F_{2,13} = 27.14(6.70)$$

Piperazine hydroxamic acids (**43**):^{213g}

Piperidine hydroxamic acids (**39**):²¹³ⁱ

$$\log(1/\text{IC}_{50}) = 0.379(\pm 0.282)(C \log P) - 0.064(\pm 0.054)(C \log P)^2 - 0.306(\pm 0.140)\text{Pol} + 0.312(\pm 0.108)I_{4,\text{benz}} + 7.283(\pm 0.576)$$

$$n = 27, r = 0.840, r_{\text{cv}}^2 = 0.55, s = 0.11, F_{4,22} = 12.91(4.31), C \log P_o = 2.96$$

(27)

Quinoline analogues (**40**):^{213h}

$$\log(1/\text{IC}_{50}) = -0.299(\pm 0.086)(C \log P) + 8.888(\pm 0.300)$$

$$n = 14, r = 0.909, r_{cv}^2 = 0.72, s = 0.16, F_{1,12} = 57.35(9.33) \quad (31)$$

Bicyclic heteroaryl hydroxamates (**44**):^{213h}

$$\log(1/\text{IC}_{50}) = -3.880(\pm 2.122)\text{MV} + 19.576(\pm 6.749)$$

$$n = 7, r = 0.903, r_{cv}^2 = 0.73, s = 0.30, F_{1,5} = 22.09(16.26) \quad (32)$$

The positive effects on TACE inhibition were, however, shown of some specific substituents on the molecules as indicated by different indicator parameters in different equations; for example, in eq 26 the positive coefficient of the indicator variable $I_{1\text{-pyr}}$ showed the beneficial effect of R₁-substituent bearing a pyridyl ring, and so did $I_{4\text{-benz}}$ in eq 27 for the effect of a substituted or unsubstituted benzyl group in R⁴-substituent in **39**, $I_{R2\text{-cc}}$ for an acetylene derived R²-substituent in eq 29 for **41**, and $I_{4\text{-Br}}$ for the bromine as an R⁴-substituent in the series of **42**. However, a negative effect is shown of an R²-substituent being a methoxy group and an R⁷-substituent being a group other than a hydrogen in **40**.

6.4.1. An Overview of TACE Inhibition. Although the TACE structure has excellent similarity with MMP structures and like MMPs it also has three flat substrate subsites S1, S2, and S3 to the left of catalytic Zn²⁺ ion and three deep subsites S1', S2', and S3' to the right of catalytic Zn²⁺ ion, its active sites have very interesting features, where S1' and S3' subsites are merged to create an L-shaped S1' binding cleft that opens into the S3' pocket. Both S1' and S3' are hydrophobic but connected by a polar entrance. Thus, in many cases, the TACE inhibition activity was shown to depend on the hydrophobic property of molecules with the steric problem of bulky substituent (eqs 26–31). If the 2-D QSAR model derived by Yang et al.²⁴⁹ (eq 25) has any meaning, the involvement of some electrostatic interaction in TACE inhibition can also be assumed. However, different COMFA and COMSIA studies discussed here suggested involvement of all steric, electrostatic, hydrophobic, and H-bonding interactions at different points of molecular structure of inhibitors in TACE inhibition. A five-point pharmacophore model developed by Murmurkar et al.²⁵⁴ (Figures 45 and 46), however, showed the requirement of two H-bond acceptors, one H-bond donor, and two aromatic rings. The aromatic rings would necessarily be involved in the hydrophobic interaction, showing the importance of the hydrophobic interaction.

6.5. Clostridium Histolyticum Collagenase (ChC) Inhibition

Clostridium histolyticum collagenase (ChC) is one of the bacterial collagenases that belongs to the M-31 MMP family and that also degrades extracellular matrix.²⁵⁶ It is a 116 kDa protein (E.C.3.4.24.3) isolated from bacterium *C. histolyticum*.²⁵⁶ It hydrolyzes triple helical regions of collagen under physiological conditions and is able to hydrolyze an entire range of synthetic peptide substrates.^{256–258} Because the increase in bacterial collagenase activity has been reported to be responsible for bacterial corneal keratitis in humans as well as animals,^{259,260} it has been assumed that ChC inhibitors may be of great value for putative ophthalmologic applications.

Because ChC and MMPs have been found to bind with the substrate and inhibitor in a similar fashion,²⁶¹ hydroxamates were also studied for ChC inhibition activity. Thus, along with QSARs of MMP inhibition, Gupta also discussed QSARs on ChC inhibition.¹⁷¹ For the following four series of sulfonylated hydroxamates (**45a–d**) reported by ScozzaFava and Supuran,^{262–265} Gupta and Kumaran had obtained the correlations as shown by eqs 33a–33d, respectively.^{171,266}

$$\log(1/K_i) = 4.060(\pm 0.946)S_N - 2.312(\pm 0.524)S_s + 0.510(\pm 0.263)I - 9.633(\pm 3.962)$$

$$n = 31, r = 0.886, r_{cv}^2 = 0.60, s = 0.17, F_{3,27} = 32.92(4.60) \quad (33a)$$

$$\log(1/K_i) = 4.171(\pm 1.007)S_N - 2.374(\pm 0.554)S_s + 0.480(\pm 0.261)I - 10.763(\pm 4.358)$$

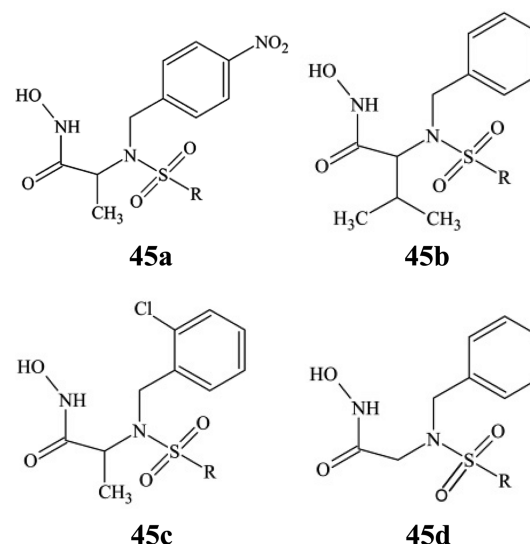
$$n = 29, r = 0.891, r_{cv}^2 = 0.75, s = 0.17, F_{3,25} = 32.06(4.68) \quad (33b)$$

$$\log(1/K_i) = 4.218(\pm 0.947)S_N - 2.404(\pm 0.523)S_s + 0.539(\pm 0.257)I - 10.718(\pm 4.041)$$

$$n = 30, r = 0.899, r_{cv}^2 = 0.77, s = 0.17, F_{3,26} = 36.69(4.64) \quad (33c)$$

$$\log(1/K_i) = 3.655(\pm 0.831)S_N - 2.102(\pm 0.459)S_s + 0.522(\pm 0.219)I - 7.960(\pm 3.432)$$

$$n = 27, r = 0.918, r_{cv}^2 = 0.81, s = 0.14, F_{3,33} = 40.85(4.76) \quad (33d)$$



In all of these equations, S_N and S_s refer to electropotential state (E-state) indices of N and S atoms, respectively. According to Kier and Hall,²⁶⁷ the E-state index of an atom is a measure of π or lone pair electrons at the atom and refers to

the ability of the atom to transfer the electron or to be involved in some electrostatic interactions. This led Gupta and Kumaran to suggest that the inhibitors may have either charge transfer interactions with the receptor in which nitrogen may act as a donor of charge to some active site of the receptor, and sulfur as an acceptor of the charge from some active site of the receptor, or both nitrogen and sulfur may have some electrostatic interactions with the active site of the receptor. However, these E-state indices should be treated more of predictive value than of diagnostic value. In all of these equations, the indicator parameter I was used for an R-substituent being C_6F_5 or $3-CF_3-C_6H_4$. For such an R-substituent, I was given a value of 1 and for others zero. A positive coefficient of I in all of the equations (eqs 33a–33d) indicated that these two types of R-substituents could be beneficial to the activity of compounds against *ChC*. In these substituents, the fluorine might be expected to have some electronic interaction with some residues in the active site of the receptor. However, it could also be assumed that a relatively better role of C_6F_5 or $3-CF_3-C_6H_4$ might be because of their steric effects, rather than any kind of electronic effects, due to their relatively better orientation toward the active site. The R-substituent is generally supposed to have hydrophobic interaction with S3' subsite of the *ChC* enzyme. In fact, in the design of all of these *ChC* inhibitors, Scozzafava and Supuran had opted the following structural information based on strong MMP inhibitory properties of some arylsulfonylaminohydroxamic acids studied by Jeng et al.²⁶⁸ and Hanessian et al.:²⁶⁹ (a) a strong zinc-binding group like $-COOH$ and $-CONHOH$, (b) a relatively compact spacer between ZBG and the rest of the molecule, that is, any amino acid moiety, (c) a variant of the already optimized benzyl group to interact with S2' subsite, and (d) an aryl sulfonamide moiety to interact with S3' subsite. All of these structural elements in a hydroxamate and their interactions with *ChC* are schematically shown in Figure 49.²⁶⁴

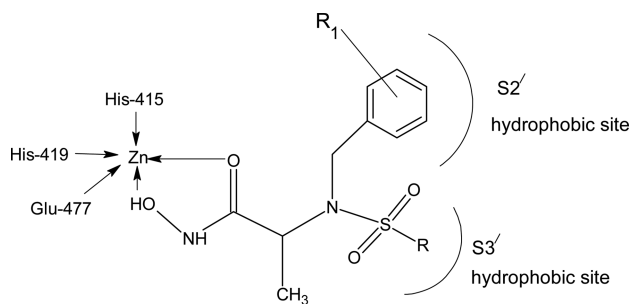


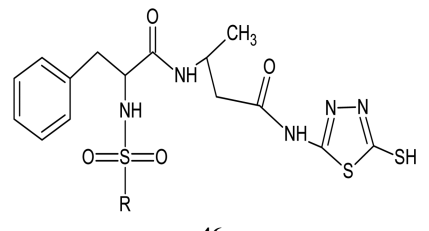
Figure 49. A model showing the binding features of a hydroxamate within *ChC*. Reprinted (with slight modification) with permission from ref 264. Copyright 2000 Elsevier.

It is to be noted that all four series of compounds (**45a–d**) differed from each other only in terms of the substituent at their aromatic ring or the alkyl substituent at the carbon adjacent to nitrogen of the $-NSO_2R$ moiety; otherwise the R-substituents were identical in all of them and that is why all of the correlations (eqs 33a–33d) are parallel to each other, showing no specific roles of variation at any other position.

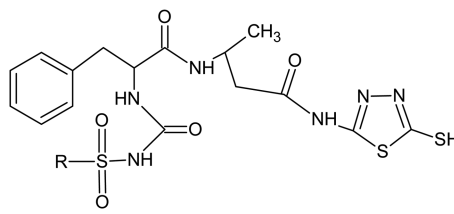
For an entirely different series of *ChC* inhibitors, 5-amino-2-mercaptop-1,3,4-thiadizole derivatives (**46a,b**) reported by Scozzafava and Supuran,²⁷⁰ Jamloki et al.²⁷¹ derived a correlation for a combination of **46a** and **46b** as shown by eq

34, where $^1\chi^v$ is Kier's first-order valence molecular connectivity index of the molecule and I is an indicator parameter for the derivatives of **46b** in which each compound has an amide function in the vicinity of sulfonamide moiety. Thus, while the negative coefficient of $^1\chi^v$, which defines the molecular size and shape of the molecule, indicated that the bulky molecule would not be conducive to the activity, the positive coefficient of I suggested that the amide function in the vicinity of the sulfonamide moiety would have an added advantage. This amide function might be assumed to be involved in H-bonding interactions with the receptor.

$$\begin{aligned} \log(1/K_i) = & 6.099(\pm 0.569) - 0.219(\pm 0.093)^1\chi^v \\ & + 0.575(\pm 0.20)I \\ n = 25, r = 0.858, r^2_{cv} = 0.626, s = 0.156, \\ F_{2,22} = 30.81(6.81) \end{aligned} \quad (34)$$



46a



46b

6.5.1. An Overview of *ChC* Inhibition. For *ChC* inhibition, an exclusive electronic role of nitrogen and sulfur of sulfonamide group has been exhibited by all of the correlations represented by eqs 33a–33d and 34 for all of the series of hydroxamates treated. Additionally, substituents such as C_6F_5 and $3-CF_3-C_6H_4$ have been shown to play an additional favorable role in compounds **45a–d**, but a possibility of hydrogen bonding has been indicated in **46a** and **b**.

6.6. 5-Lipoxygenase (5-LOX) Inhibition

As already mentioned in section 3.1.3, among all of the lipoxygenases, 5-LOX inhibition has been most studied. Among the various kinds of 5-LOX inhibitors, attention has been paid to mainly three kinds of inhibitors: (i) antioxidant agents that interfere with the redox catalytic site of the enzyme, (ii) nonchelating agents, and (iii) nonredox competitive inhibitors, which compete with the substrate to bind the active site.^{272,273} 5-LOX was found to be a cytosolic enzyme containing a nonheme iron atom (Fe^{2+}) and calcium. This iron atom is critical to determine the catalytic potential of the enzyme with oxidation to Fe^{3+} form conferring activity.²⁷⁴ The increase in Ca^{2+} concentration can activate 5-LOX, and with the absence of Ca^{2+} it may have minimal catalytic activity. This enzyme is expressed mainly in leukocytes, in line with the functions of leukotrienes as mediator of immune response.²⁷⁵

The function of any enzyme, however, depends on its structure. Therefore, attempts have been made to determine

the chemical and 3D structures of 5-LOX. Until recently, the exact crystal structure of 5-LOX was not known; hence many authors attempted homology modeling of its structure. However, structure information for three lipoxygenases from Research Collaboratory for Structural Bioinformatics (<http://www.rcsb.org/pdb>) was available. These LOXs were rabbit reticulocyte 15-LOX (1LOX),²⁷⁶ the soybean LOX, LOX-1 (1YGE²⁷⁷ and 2SBL²⁷⁸), and the soybean LOX, LOX-3 (1BYT²⁷⁹ and 1LNH²⁸⁰). The high similarity between the catalytic domains of human 5-LOX and rabbit 15-LOX indicated that the 15-LOX may be a good template for homology modeling of catalytic domain of 5-LOX. Using the resolved structure of 15-LOX (1LOX) as a template, Hemak et al.²⁸¹ theoretically developed the model for 5-LOX, in which they found, as shown in Figure 50, that the catalytic domain of

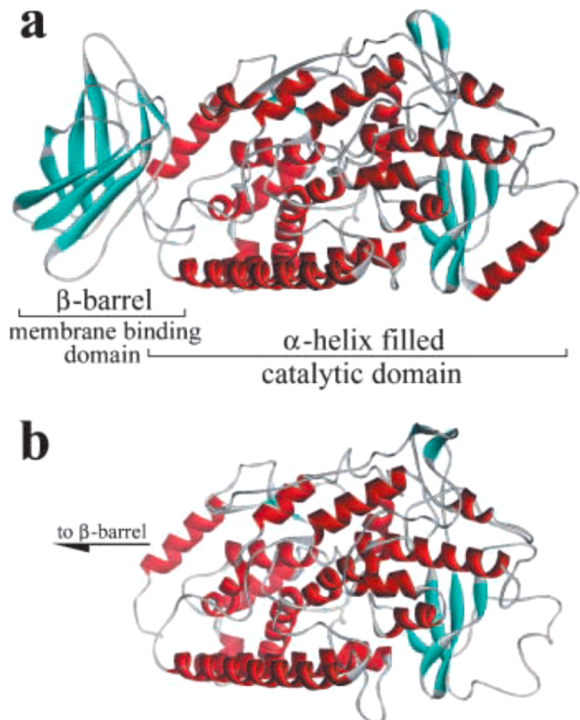


Figure 50. Comparison of theoretical model for the catalytic domain of 5-LOX with the resolved structure of 15-LOX. (a) Entire 15-LOX molecule, from 1LOX, and (b) theoretical model of the catalytic domain of human 5-LOX. Reprinted with permission from ref 281. Copyright 2002 Springer.

5-LOX superficially resembled that of 15-LOX. Like all lipoxygenases, 5-LOX also has a two-domain structure, the small N-terminal β -barrel domain and a larger catalytic domain, containing a single atom of nonheme iron coordinating with His525, His530, His716, and Ile864. According to the homology model of potato 5-LOX based on soybean LOX-3, obtained by Aporoy et al.,²⁸² the fifth coordination position of iron is occupied by Asn720, and the sixth one faces the open cavity occupied by docked ligand. Along the active site channel of 5-LOX are present the polar residues like Gln521, Glu787, His530, His525, His271, His783, Thr784, Arg782, Asp276, Arg559, Asp560, Asn563, Asn565, Asn720, Ser567, Ser863, and Thr279, of which the acidic amino acids, Asp276 and Asp560, and basic amino acids, His525 and His530, are present in the active site channel and play a vital role in ligand binding.

However, Charlier et al. had derived a homology model of human 5-LOX using rabbit 15-LOX as template.²⁸³ From this model, they characterized the active site of 5-LOX. As shown in Figure 51, the active site of human 5-LOX consists of a deep

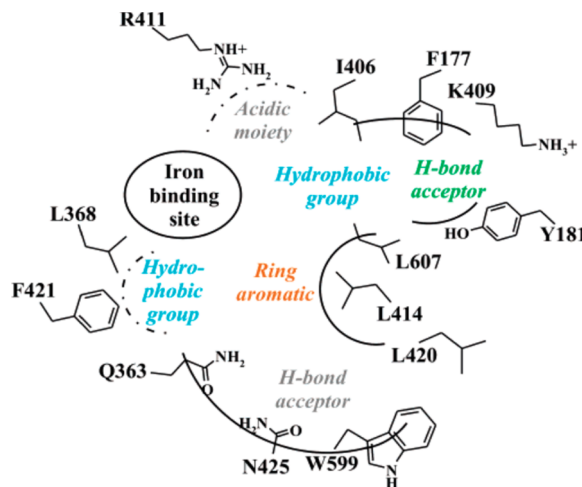


Figure 51. Target-based pharmacophore of 5-LOX nonredox inhibitors consisting of four major anchoring points (identified by pharmacophore modeling, colored accordingly) and two secondary ones (identified through docking, colored in gray). Reprinted with permission from ref 283. Copyright 2006 American Chemical Society.

bent-shaped cleft containing the nonheme iron cofactor. This modeled active site of human 5-LOX was found to be more spacious than that of rabbit 15-LOX, which agreed with the mutagenesis studies.²⁸⁴ In this model, there are two channels opening on the surface. The upper channel has on one side a positively charged K409 (Lys409) and on the other side Y181 (Tyr181) residue. The bottom channel has on the upper side L420 (Leu420) and on the lower side a cleft made of Q363 (Glu363), N425 (Asp425), and Q363 (Glu363) residues. The lower surface of the upper channel as well as that of the bottom one contain H-bond acceptor sites. Between these two channels the region constituted of L607, L414, and L420 (L = leucine) provides an active site that can interact with an aromatic moiety of the ligand. The model also contains two hydrophobic sites, one constituted of I406 (Ile406) and Phe177 on the upper side and one constituted of L368 (Leu368) and F421 (Phen421) on the left side. Additionally, there is one more region containing R411 (Arg411) that can interact with an acid moiety of the ligand.

Charlier et al.²⁸³ reported a pharmacophore model based on some nonredox inhibitors that can have optimum interactions with human 5-LOX. First, a pharmacophore model was generated for 16 nonredox 5-LOX inhibitors with catalyst (Hip Hop module) that included two hydrophobic (H) groups, two hydrogen-bond acceptors (A), and an aromatic ring (R). Yet when the 3D structure of 5-LOX was modeled and it was used to investigate the interactions with it of some selected inhibitors, such as 47, through docking, a slightly refined pharmacophore was proposed that consisted of four major and two secondary interactions points: two hydrophobic groups, an aromatic ring, and a hydrogen-bond acceptor as major points, and an acidic moiety and an additional hydrogen-bond acceptor as minor points. This refined pharmacophore with only four major interaction points along with the distances among them is shown in Figure 52. The interactions of all six points are

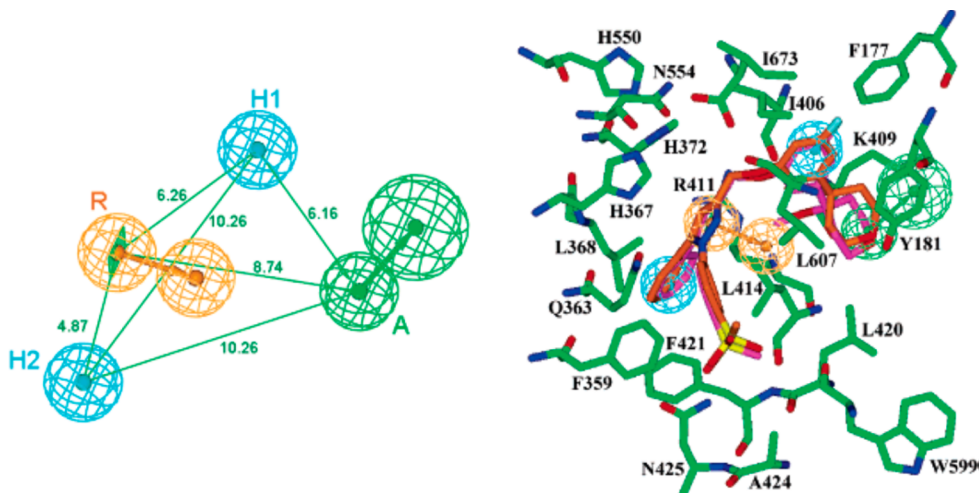
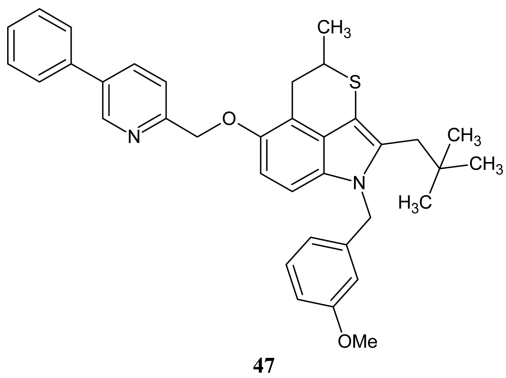


Figure 52. Left: Refined pharmacophore hypothesis. The pharmacophore features are color coded as follows: hydrogen-bond acceptor (A) in green, hydrophobic features (H) in cyan, and aromatic ring (R) in orange. Distances between the features are expressed in Å, with a tolerance of 0.8 Å. Right: Refined pharmacophore hypothesis mapped with 47 (in magenta) superimposed onto the docked conformation (in orange) of 47 inside the 5-LOX active site. Reprinted with permission from ref 283. Copyright 2006 American Chemical Society.

shown in Figure 51. The key anchoring points inside the binding cavity include among others Y181, L414, N425, R411, and F421.



A pharmacophore model of 5-LOX inhibitors was also reported recently by Kalva et al.²⁸⁵ that consisted of two H-bond acceptors and two hydrophobic groups (Hypo-1 model). A homology model of 5-LOX was also constructed by these authors using the X-ray crystal structure of soyabean lip-oxygenase-3 as template. However, when a set of 5-LOX inhibitors was docked to modeled 5-LOX protein using AutoDock, no significant correlation between the fitness scores and 5-LOX inhibitory activities of compounds was found.

However, an X-ray crystal structure of human 5-LOX was recently reported by Gilbert et al.²⁸⁶ with PDB code 308Y. In this structure, the active site is an elongated cavity with no clear access to bulk solvent, lined with both invariant and 5-LOX specific amino acids. The invariant amino acids that are conserved in all AA-metabolizing LOXs are Leu368, Leu373, Leu414, Leu607, and Ile406. They form a structurally similar constellation of branched hydrophobic side chains that envelops the region where the pentadiene moiety of the substrate is accommodated for catalysis. Specific to 5-LOX are the amino acids Tyr181, Thr364, His600, Ala603, Ala606, and Tryp599. These amino acids contribute to ligand binding. Small side chains of Ala603 and Ala606 are required for the conformation of Tyr181, which along with Phe177 corks the cavity at one end. This cork is designated as FY (Phe177-

Tyr181) cork, and from one side it is buttressed by Try599. There are two more residues, Asn407 and His432, that also appear to be the part of the active site. In this feature of 5-LOX, iron is coordinated by His367, His372, and His550 as well as the main carboxylate of the C-terminus Ile673.

With this X-ray structure of human 5-LOX, an interaction study was made by Eren et al.²⁸⁷ using 59 diverse nonredox competitive LOX inhibitors. These authors performed a QSAR study using molecular descriptors obtained from the QuaSAR module of MOE and a docking study using GOLD 5.0.1 software²⁸⁸ that uses genetic algorithm (GA). Compounds that were used in these studies had the general structure as shown in Figure 53. For a test set of 50 compounds of them, the best correlation that a multiple regression analysis (MRA) had revealed was as shown by eq 35, in which ASA P stands for

$$\begin{aligned} \log(1/\text{IC}_{S_0}) = & 43.6516 - 0.0024(\text{ASA}_P) - 0.0001(\text{pmi}) \\ & + 0.0001(\text{pmi}Y) - 15.9066(\text{vsurf_CW1}) \\ & + 4.8673(\text{vsurf_CW2}) + 1.0024(\text{vsurf_EDmin1}) \\ & + 0.4148(\text{vsurf_EWmin2}) + 0.0051(\text{vsurf_HB1}) \\ & + 0.1412(\text{vsurf_IW8}) \end{aligned}$$

total polar surface area, pmi for principal moment of inertia, $pmiY$ for principal momenta of inertia (Y), $vsurf_CW1$ for capacity factor at 0.2 kcal/mol, $vsurf_CW2$ for capacity factor at 0.5 kcal/mol, $vsurf_Edmin1$ for lowest hydrophobic energy, $vsurf_EWmin2$ for second lowest hydrophobic energy, $vsurf_HB1$ for H-bond donor capacity at -0.2, and $vsurf_IW8$ for hydrophilic entegy moment at -6.0. This equation does not show any obvious role of any physicochemical parameter in the drug-receptor interaction, but authors have extracted from $vsurf$ descriptors that surface polarity, H-bond donor properties, and hydrophilic contact surface of molecules would be important for their activity.

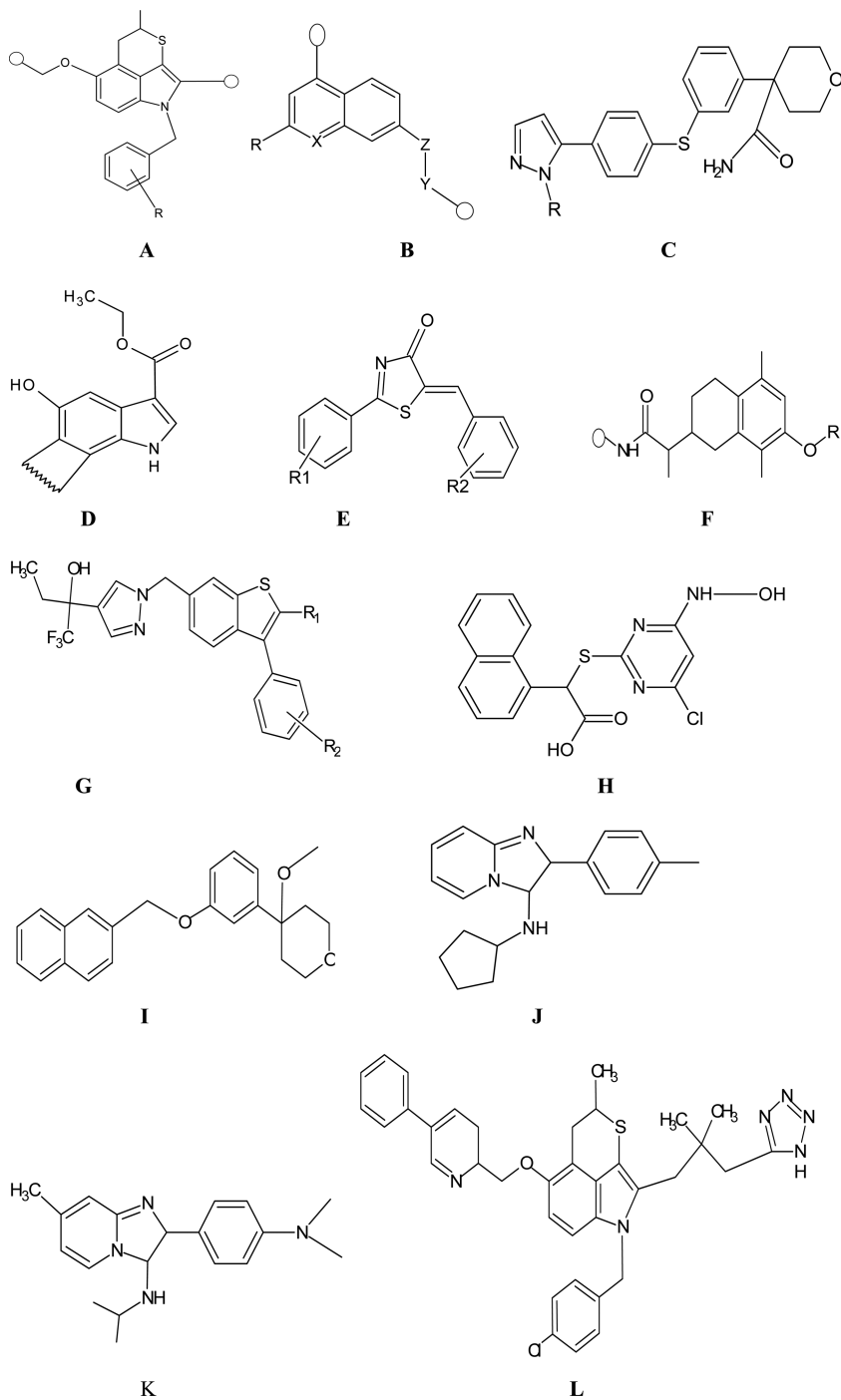


Figure 53. Nonredox competitive 5-LOX inhibitors used in the study by Eren et al.²⁸⁷

However, from their docking studies, Eren et al.²⁸⁷ found that CH- π and/or π - π contacts between the ligands and the side chain of Phe421 and Trp599 of 5-LOX were the most conserved interactions observed for the majority of the data set molecules. Another conserved interaction observed was hydrophobic contact with Leu420. Many molecules were observed to have hydrogen bonding or π - π contact interactions with Tyr181, Gln363, Thr364, Leu414, and His600. The most active compound of the data set was observed to form hydrogen bonds with a side chain of His600 and a backbone of Ile673 and to have CH- π and π - π contacts with Leu420, Phe421, and Trp599 (Figure 54). The CH- π and π - π contacts of the coumarin moiety of this compound with Phe421 are important,

as this residue is supposed to play a significant role in the catalytic activity of 5-LOX.

Now after a thorough discussion of 3D structure of 5-LOX, we must be concerned how hydroxamic acids interact with it. In fact, there has been no specific study on hydroxamic acids-5-LOX interaction, but some QSAR studies have been made on hydroxamic acids acting as 5-LOX inhibitors, in which it has been established that their inhibition activity is mainly governed by their hydrophobicity and molecular size. Summers et al.²⁸⁹ had taken four different groups of hydroxamic acids as shown in Charts 1–4 to make a QSAR study, where the R₁-substituent was mostly H or CH₃. For the compounds of Chart 1 that were 38 in total, the best correlation obtained was as

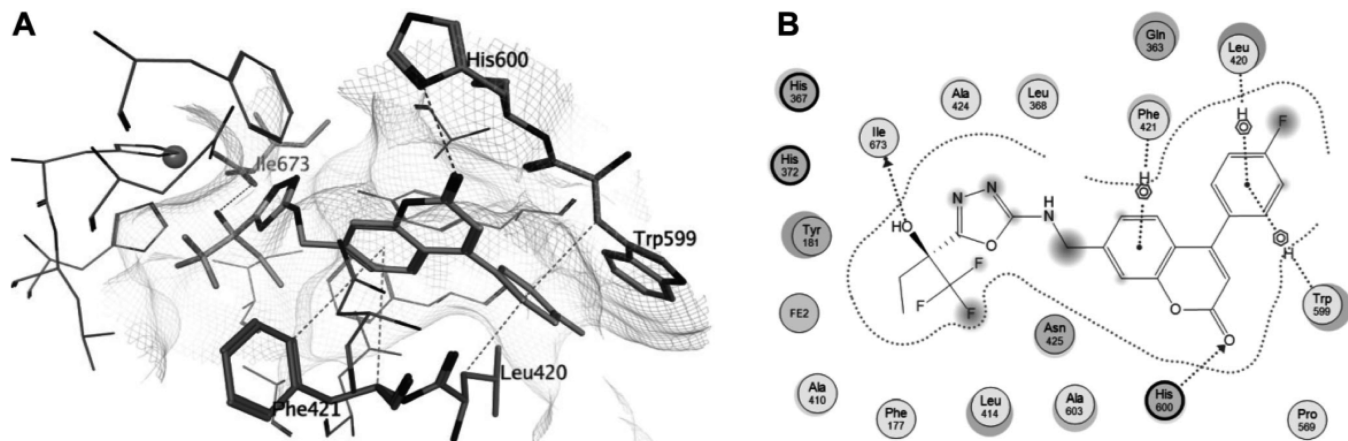


Figure 54. (A) Interactions of the most active compound with the amino acids at the active site of 5-LOX. (B) Ligand interaction diagram showing the most active compound docked. Reprinted with permission from ref 287. Copyright 2012 Wiley-VCH.

Chart 1

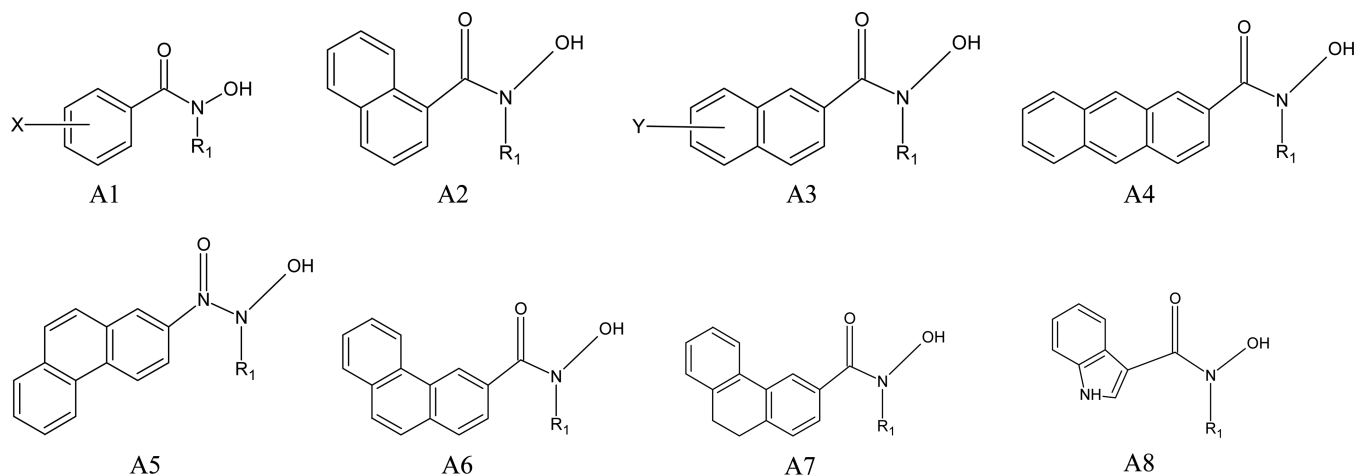


Chart 2

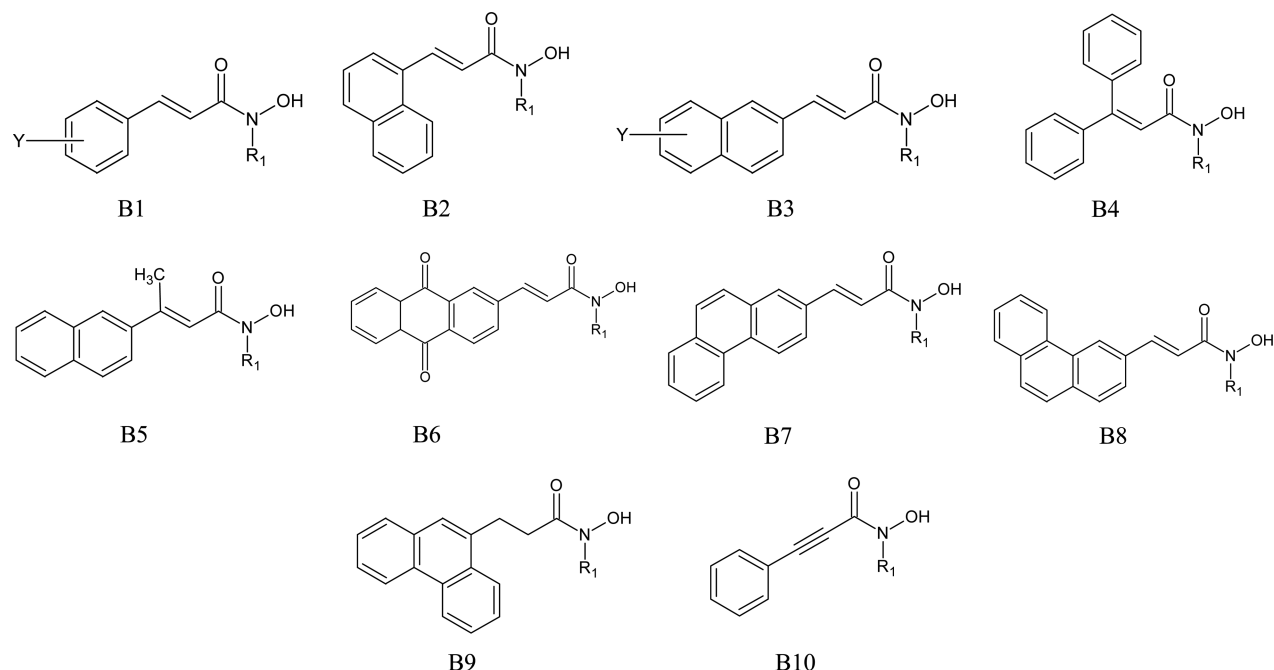


Chart 3

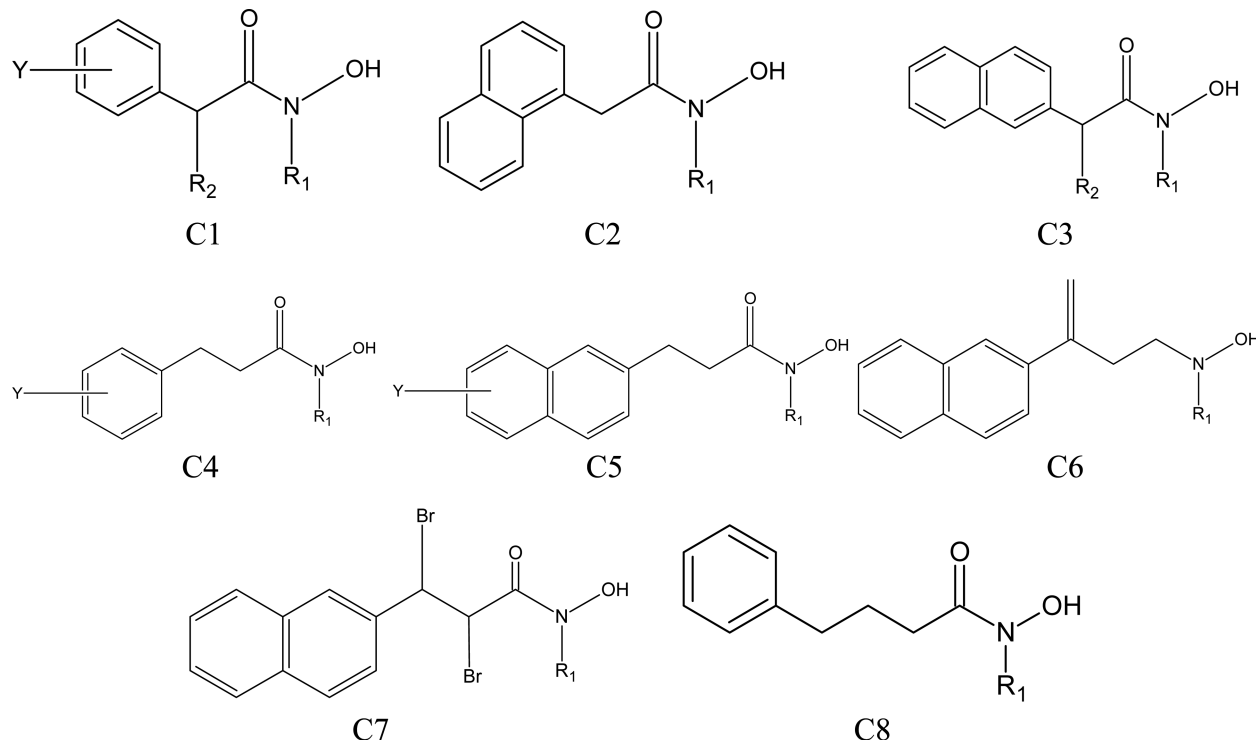
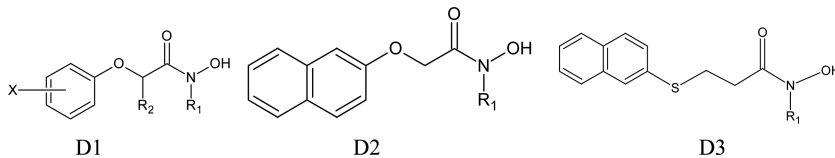


Chart 4



$$\log(1/\text{IC}_{50}) = 0.66(\pm 0.04)\pi' - 0.83I_{\text{NH}} + 3.68(\pm 0.21)$$

$$n = 38, r = 0.942, s = 0.301, F_{2,35} = 137.0 \quad (36)$$

where π' refers to the calculated hydrophobicity constant for the entire group attached to the carbonyl carbon of the hydroxamate group and I_{NH} is an indicator parameter having a value of 1 when the substituent on the hydroxamate nitrogen R_1 is H and zero when it is anything else. Thus, this correlation suggested that 5-LOX inhibition activity of these compounds was significantly controlled by the entire aryl moiety attached to the hydroxamate group, and any group other than hydrogen attached to its nitrogen would be beneficial to the activity. One can, therefore, assume that the entire aryl moiety attached to hydroxamate group might have strong hydrophobic interaction with the hydrophobic region of the enzyme, and any group attached to the nitrogen of hydroxamate, usually an alkyl group, might have a secondary hydrophobic interaction with any other hydrophobic site in the enzyme. The use of π' in place of π was a concern to Y -substituents of the naphthyl ring that were alkoxy groups. Long alkoxy chains at the naphthyl ring were observed to produce lesser activity. Summers et al.²⁸⁹ assumed that the bigger alkoxy substituents at the naphthyl ring might reach beyond the hydrophobic regions (e.g., open solvent) where their lipophilicity might not contribute to the binding. Hence, for such groups the lipophilicity of only the first three

carbon atoms was included and referred to as π' , which was essentially π for all other compounds.

For the 29 compounds of Chart 2, the correlation obtained was as

$$\log(1/\text{IC}_{50}) = 0.36(\pm 0.07)\pi' - 1.46(\pm 0.18)I_{\text{NH}} - 0.98(\pm 0.15)I_{\text{big2}} + 5.36(\pm 0.33)$$

$$n = 29, r = 0.944, s = 0.299, F = 67.8 \quad (37)$$

where π' was adjusted so as to omit the contribution of the hydrophobicity of all but the first carbon of the R_2 -substituent. The bigger R_2 -substituent might create some steric problem. This problem was accounted for by including the indicator parameter I_{big2} in the correlation. For a set of total 35 compounds of Chart 3, the correlation obtained (eq 38) was exactly parallel to that shown by eq 37, but the one obtained for eight compounds of Chart 4 had no I_{big2} parameter (eq 39), because none of these compounds had an R_2 -substituent bigger than CH_3 .

$$\log(1/\text{IC}_{50}) = 0.61(\pm 0.09)\pi' - 1.26(\pm 0.11)I_{\text{NH}} - 0.62(\pm 0.13)I_{\text{big2}} + 3.43(\pm 0.43)$$

$$n = 35, r = 0.950, s = 0.266, F_{3,31} = 95.7 \quad (38)$$

Table 10. ω -Phenylalkyl Hydroxamic Acids and Their 5-Lipoxygenase Inhibitory Activities and Physicochemical Parameters

no.	R ₁	R ₂	$V_w(R_1)$ (10^2 \AA^3)	$V_w(R_2)$ (10^2 \AA^3)	$\log P$	$\log(1/\text{IC}_{50})$	
						obsd	calcd, eq 41
1	H	CONHOH	0.056	0.442	-1.67	3.96	3.81
2	H	CH ₂ CONHOH	0.056	0.596	-2.03	3.52	4.12
3	H	CH ₂ CH ₂ CONHOH	0.056	0.750	-1.49	4.06	4.44
4	H	CH ₂ CH ₂ CH ₂ CONHOH	0.056	0.904	-0.95	4.57	4.75
5	H	CH=CHCONHOH(<i>trans</i>)	0.056	0.708	-2.04	4.92	4.35
6	H	CH=CHCONHOH(<i>cis</i>)	0.056	0.708	-2.04	4.51	4.35
7	H	C≡CCONHOH	0.056	0.675	-2.91	4.34	4.28
8	p-NO ₂	CONHOH	0.276	0.442	-2.15	4.64	4.33
9	p-CN	CONHOH	0.268	0.442	-2.46	4.22	4.31
10	p-CF ₃	CONHOH	0.383	0.442	-1.01	4.57	4.58
11	p-Br	CONHOH	0.287	0.442	-0.81	4.85	4.35
12	p-I	CONHOH	0.388	0.442	-0.55	4.82	4.59
13	p-C ₆ H ₅	CONHOH	0.809	0.442	-0.13	5.39	5.58
14	p-CH ₃	CONHOH	0.245	0.442	-1.14	4.19	4.25
15	p-OH	CONHOH	0.137	0.442	-2.56	3.72	4.00
16	m-C ₆ H ₅	CONHOH	0.809	0.442	-0.13	5.22	5.58
17	p-(2,4,6-trimethylphenyl)	CONHOH	1.271	0.442	1.45	6.54	6.67
18	p-(2,4,6-trimethylphenyl)	CON(CH ₃)OH	1.271	0.604	1.36	7.19	7.00
19	p-(1-naphthyl)	CONHOH	1.253	0.442	0.99	6.75	6.62
20	p-(2-naphthyl)	CONHOH	1.253	0.442	0.99	6.48	6.62
21	p-(2,4,6-trimethylphenyl)	CH=CHCON(CH ₃)OH	1.271	0.870	1.36	7.66	7.54

$$\begin{aligned}\log(1/\text{IC}_{50}) &= 0.57(\pm 0.21)\pi' - 0.80(\pm 0.27)I_{\text{NH}} \\ &\quad + 3.71(\pm 0.77) \\ n &= 8, r = 0.853, s = 0.319, F_{2,5} = 6.69\end{aligned}\quad (39)$$

When the compounds of all four charts were combined, the correlation obtained was as shown by eq 40 that had an additional indicator variable I_1 , used with a value of zero for Charts 1 and 2, where the hydroxamate moiety is directly attached to the aryl ring or through an unsaturated spacer unit, and with a value 1 for Charts 3 and 4, where it is attached to the aryl ring through one or more methylenes. The negative coefficient of this I_1 suggested that the methylene spacer would lead to less activity than an unsaturated spacer or no spacer. Summers et al. gave no explanation for this, but to us it seems that no spacer or an unsaturated spacer keeps the hydroxamate moiety in the plane of the ring, because of which it might have better interaction with the enzyme. The saturated spacer, because of its flexibility, might change the orientation of the hydroxamate group, and as a result it may not have the proper interaction with the enzyme.

$$\begin{aligned}\log(1/\text{IC}_{50}) &= 0.57(\pm 0.03)\pi' - 1.16(\pm 0.07)I_{\text{NH}} \\ &\quad - 0.69(\pm 0.11)I_{\text{big2}} - 0.64(\pm 0.07)I_1 \\ &\quad + 4.30(\pm 0.15) \\ n &= 111, r = 0.940, s = 0.323, F_{4,106} = 201.8\end{aligned}\quad (40)$$

From this study, Summers et al. concluded that for 5-LOX inhibition the hydrophobic property of compounds is important, but noticed that in these hydroxamic acids the hydrophobicity of portions of compounds in the immediate vicinity of hydroxamic acid functionality was not able to make any contribution to the activity and so was the case with the fragments beyond approximately 12 Å from the hydroxamate.

The study had, however, revealed that an alkyl group on the hydroxamate nitrogen was favorable to the activity and that activity could also increase when the hydroxamate was conjugated to an aromatic system. In all of these situations, a favorable hydrophobic interaction of compounds with the hydrophobic sites of the enzyme was assumed.

The above conclusion was well supported by Gupta and Gupta²⁹⁰ who performed a QSAR study on a small set of these hydroxamic acids as shown in Table 10. For these compounds, they correlated the 5-LOX inhibition activity with van der Waals volume of both R₁- and R₂-substituents as

$$\begin{aligned}\log(1/\text{IC}_{50}) &= 2.351(\pm 0.295)V_w(R_1) + 2.033(\pm 0.930)V_w(R_2) + 2.779 \\ n &= 21, r = 0.970, s = 0.305, F_{2,18} = 141.35\end{aligned}\quad (41)$$

Simultaneously, these authors also showed that the hydrophobicity of these molecules was very well correlated with the van der Waals volume of the substituents (eq 42), and, therefore, it was concluded that it is essentially the hydrophobic property of the molecules that governs the activity. In this study, it was also found that the major role in the drug–receptor interaction is played by the R₁-substituent and a little by the R₂-substituent, as the deletion of the $V_w(R_2)$ term from eq 41 had little effect on the significance of the correlation (eq 43), and not only this, even the hydrophobic property of the molecule was little affected by the R₂-substituent (compare eq 42 with eq 44). Thus, on the whole, the study of Gupta and Gupta supported the conclusion of Summers et al. Pontiki and Hadjipavlou-Litina²⁹¹ had made a comprehensive review on different classes of 5-LOX inhibitors other than hydroxamic acids to conclude that in almost all of the cases the hydrophobicity of the molecules played the most dominant role in their 5-LOX inhibition activity. Additionally, in some cases, a few steric factors were also found to play some roles.

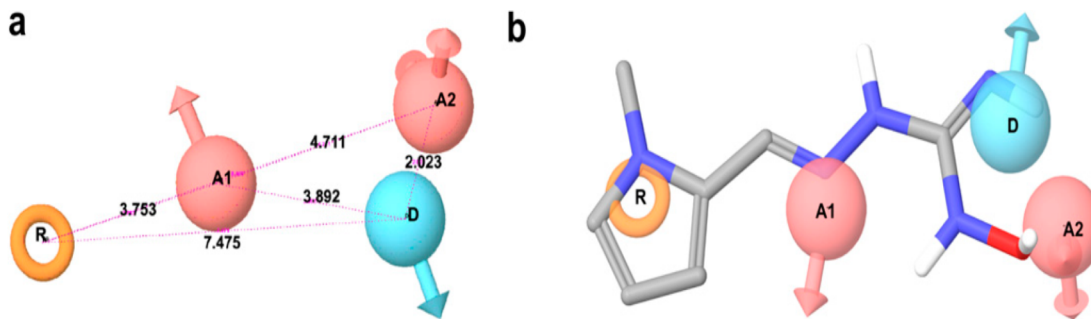


Figure 55. Pharmacophore map of the generated model for anticancer activity: A1, A2, H-bond acceptors; D, H-bond donor; R, an aromatic ring. (a) Distances between the various pharmacophoric features, and (b) the most active molecule (48) shown to be embedded in the map. Reprinted with permission from ref 304. Copyright 2011 Elsevier.

For a certain category of 5-LOX inhibitors, not belonging to hydroxamic acids, the activity was also found to be correlated with topological parameters.²⁹²

$$\log P = 2.719(\pm 0.507)V_w(R_1) + 1.062(\pm 1.598)V_w(R_2) - 2.773$$

$$n = 21, r = 0.936, s = 0.524, F_{2,8} = 63.54 \quad (42)$$

$$\log(1/IC_{50}) = 2.236(\pm 0.415)V_w(R_1) + 3.955$$

$$n = 21, r = 0.933, s = 0.437, F_{1,19} = 127.07 \quad (43)$$

$$\log P = 2.659(\pm 0.510)V_w(R_1) - 2.519$$

$$n = 21, r = 0.929, s = 0.537, F_{1,19} = 119.18 \quad (44)$$

6.6.1. An Overview of 5-LOX Inhibition. The human 5-LOX contains a heme iron atom (Fe^{2+}) and calcium. Before the X-ray crystal structure of 5-LOX was reported by Gilbert et al.²⁸⁶ in 2011, several authors had attempted the homology modeling of this enzyme. One such homology model was predicted to have a two-domain structure, the small N-terminal β -barrel domain and a larger catalytic domain, containing a single atom of nonheme iron coordinating with His525, His530, His716, and Ile864.²⁸¹ Yet, in the crystal structure of Gilbert et al., the active site was found to be an elongated cavity with no clear access to bulk solvent, lined with both invariant and 5-LOX specific amino acids. The invariant amino acids form a similar constellation of branched hydrophobic side chains that envelops the region where the pentadiene of the substrate is accommodated for catalysis, and specific amino acids contribute to the ligand binding. With this X-ray structure of human 5-LOX, an interaction study, performed by Eren et al.²⁸⁷ for some nonredox competitive inhibitors as shown in Figure 53, showed that for the majority of the molecules CH- π and/or $\pi-\pi$ contacts of molecules with side chains of Phen421 and Trp599 of 5-LOX were the most conserved interactions. Also, many molecules were observed to have hydrophobic interaction as well as hydrogen bonding with a few amino acid residues. The most active compound of the data set was observed to form hydrogen bonds with side chain of His600 and backbone of Ile673 and to have CH- π and $\pi-\pi$ contacts with many residues (Figure 54). Specifically for hydroxamic acids, the QSAR equations obtained by Summers et al.²⁸⁹ (eqs 36–40) for four different groups of compounds (Charts 1–4) suggested the involvement of only hydrophobic interaction of substituents, where some bigger substituents might create the

steric problems. Also, a dominant role of hydrophobicity in the interaction of hydroxamic acids with 5-LOX was shown by Gupta and Gupta.²⁹⁰ Pontiki and Hadjipavlav-Litina²⁹¹ showed the dominant role of hydrophobicity not only in the case of hydroxamic acids but also in the case of several other kinds of 5-LOX inhibitors.

6.7. Miscellaneous

6.7.1. Hydroxamic Acids as Anticancer Agents. Hydroxamic acids act as anticancer agents not only by inhibiting HDACs, but also inhibiting several other enzymes and different cell lines.²⁹³ They have been found to inhibit DNA synthesis by inhibiting specifically the R2 subunit of the enzyme ribonucleotide reductase,²⁹⁴ which is one of the most widely accepted targets for the development of anticancer agents.^{76,295} Hydroxamic acids contain pharmacophoric features similar to those of many other anticancer agents, such as hydroxyaminoguanidines (HAGs),^{296–298} hydroxysemicarbazide (HSs),²⁹⁹ and amidoximes,³⁰⁰ which have been widely studied for their anticancer activity. The common pharmacophoric feature in all of them is $\{-C(=X)NHOH, X = O, NH\}$, which has been identified as the basic pharmacophore for anticancer activity.^{301–303} For all of these groups of compounds, a common four-point pharmacophore was developed by Basu et al.³⁰⁴ that consisted of two H-bond acceptors (A₁, A₂), one H-bond donor (D), and one aromatic ring (R), in which an aminoguanidine (48) is shown to be embedded (Figure 55). The interpharmacophoric distances for this model are shown in Figure 55a as well as in Table 11.

Table 11. Interpharmacophoric Distances in Pharmacophoric Model (Figure 55)

site 1	site 2	distance (Å)
A1	A2	4.711
A1	D2	3.892
A1	R	3.753
A2	D	2.023
A2	R	8.463
D	R	7.475

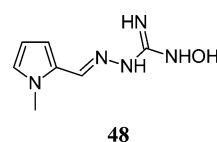
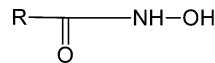


Table 12. A Series of Aryl Hydroxamic Acids and Their RDR Inhibitory Potency³⁰⁷

compd	R	${}^3\chi_p$	${}^0\chi^v$	${}^1\chi^v$	$\log(1/\text{IC}_{50})$	
					obsd	calcd, eq 45
1	pyridyl-2	3.099	5.112	2.698	3.30	3.23
2	pyridyl-3	3.099	5.112	2.688	3.10	3.17
3	unsubstituted phenyl	3.099	5.242	2.838	3.40	3.46
4	2-hydroxyphenyl	3.553	5.612	2.979	3.82	3.85
5	2-aminophenyl	3.553	5.742	3.044	3.92	3.71
6	3-hydroxyphenyl	3.426	5.612	2.973	3.46	3.52
7	3-aminophenyl	3.426	5.742	3.038	3.46	3.38
8	4-hydroxyphenyl	3.509	5.612	2.972	3.60	3.71
9	4-aminophenyl	3.509	5.742	3.038	3.82	3.57
10	4-methylaminophenyl	3.917	6.665	3.499	3.48	3.79
11	4-dimethylaminophenyl	4.208	7.612	3.867	3.30	3.33
12	4-methoxyphenyl	3.917	6.573	3.361	3.30	3.24
13	2,3-dihydroxyphenyl	4.145	5.982	3.119	5.10	4.60
14	2,4-dihydroxyphenyl	3.873	5.982	3.113	3.60	3.92
15	2,5-dihydroxyphenyl	3.895	5.982	3.113	3.70	3.98
16	2,6-dihydroxyphenyl	3.934	5.982	3.119	4.00	4.11
17	3,4-dihydroxyphenyl	4.087	5.982	3.113	4.52	4.43
18	3,5-dihydroxyphenyl	3.664	5.982	3.107	3.40	3.40
19	2-hydroxy-3-methylphenyl	4.145	6.535	3.395	3.82	4.15
20	2-hydroxy-4-methylphenyl	3.873	6.112	3.178	3.70	3.80
21	3,4-dimethylphenyl	4.087	7.088	3.666	3.52	3.67
22	3,4-diaminophenyl	4.087	6.242	3.243	4.40	4.20
23	3,4-dimethoxyphenyl	4.678	7.904	3.891	3.60	3.46
24	2,4-dichlorophenyl	3.873	7.478	3.861	3.35	3.03
25	3,4-dichlorophenyl	4.087	7.478	3.861	3.60	3.54
26	2,3,4-trihydroxyphenyl	4.732	6.352	3.259	5.46	5.38
27	3,4,5-trihydroxyphenyl	4.593	6.352	3.253	5.00	5.02
28	3,4,5-trimethoxyphenyl	5.391	9.235	4.420	4.00	4.10

The RDR is inhibited by hydroxyl urea, which was a primary clinical antitumor agent. Replacement of the amine group of hydroxyl urea by various aryl groups gives hydroxamic acids that were found to inhibit RDR at concentrations lower than those of hydroxyureas.³⁰⁵ Several aryl hydroxamic acids were found to also inhibit DNA synthesis^{306,307} as well as to prolong the life of mice with L1210 leukemia.^{308,309}

A series of such aryl hydroxamic acids (Table 12) was synthesized and tested for RDR inhibition by van't Riet et al.^{293,305} When these authors performed a QSAR study on these compounds, the activity was found to be significantly correlated with Kier's molecular connectivity indices (χ 's) as shown by eq 45.³¹⁰ In this equation, ${}^3\chi_p$ refers to a weighted count of contiguous three path fragments, ${}^0\chi^v$ is based on atom deltas, and ${}^1\chi^v$ is a weighted counts of bonds.³¹¹ The ${}^3\chi_p$ quantifies a structure fragment that plays a favorable role in the activity. It discriminates among compounds having the same number of substituents in different substitution patterns. It is derived from an additional subgraph wherever two substituents at a ring are ortho to each other. ${}^3\chi_p$, thus, in eq 45 describes a favorable role of this structural condition. The ${}^0\chi^v$ and ${}^1\chi^v$ are zero- and first-order valence molecular connectivity indices as defined by eqs 46 and 47, respectively, where δ^v is the vertex connectivity index of an atom of second or third row as defined by eq 48,³¹² in which Z^v is the number of valence electrons of the atom, N_H is the number of hydrogen atoms attached to it in the molecule, and Z^a is its atomic number. Now, as obvious, the value of δ^v will depend on the number of its valence electrons and its

unsaturation (less value of N_H), meaning thereby that atoms with a large number of valence electrons and highly unsaturated will lead to a high value of δ^v and consequently low value of ${}^0\chi^v$ and ${}^1\chi^v$. A high negative value of ${}^0\chi^v$ in eq 45 thus suggests that molecule with atoms of high valence electrons and high unsaturation will be advantageous to the activity. The reason of this may be that such molecules may be most prone to have electronic interaction with the receptor. A positive effect of ${}^1\chi^v$, as shown by eq 45, may however try to offset this effect, but because its coefficients are very low, it may have only a marginal effect.

$$\log(1/\text{IC}_{50}) = 2.36(\pm 0.04){}^3\chi_p - 3.98(\pm 0.53){}^0\chi^v + 0.97(\pm 0.05){}^1\chi^v)^2 + 9.20(\pm 5.50)$$

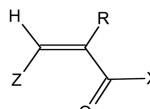
$$n = 28, r = 0.943, s = 0.21, F = 64 \quad (45)$$

$${}^0\chi^v = \Sigma(\delta_i^v)^{-1/2} \quad (46)$$

$${}^1\chi^v = \Sigma(\delta_i^v \delta_j^v)^{-1/2} \quad (47)$$

$$\delta = (Z^v - N_H)/(Z^a - Z^v - 1) \quad (48)$$

A series of aryl-acetic and hydroxamic acids, which were studied for their antioxidant and anti-inflammatory activities,³¹³ were also found to possess anticancer activity.³¹⁴ The compounds that were studied for their anticancer activity by

Table 13. Anticancer Activities of Aryl-acetic and Hydroxamic Acids³¹⁴


No	Z	R	X	Esp-min	MgVol	D	log(1/IC ₅₀) _{HT29}		log(1/IC ₅₀) _{A549}		log(1/IC ₅₀) _{OAW42}	
							Obsd eq 49	Calcd eq 49	Obsd eq 50	Calcd eq 50	Obsd eq 51	Calcd eq 51
1		Ph	-OH	-44.52	316.37	1.74	3.94	3.86	3.93	3.88	3.99	3.82
2		H	-OH	-44.71	240.27	1.97	3.90	3.88	3.92	4.01	3.67	3.82
3		Ph	-NHOH	-41.19	331.39	2.56	4.00	4.08	3.99	3.96	4.02	4.06
4		H	-NHOH	-47.32	255.29	3.14	3.87	3.88	3.98	3.90	3.73	3.76
5		Ph	-OH	-39.06	409.29	1.07	3.96	4.03	3.97	3.89	4.18	4.08
6		H	-OH	-42.93	333.19	1.91	3.85	3.95	3.80	3.90	3.79	3.92
7		Ph	-NHOH	-39.50	424.31	1.53	4.18	4.05	3.73	3.85	4.21	4.09
8		H	-NHOH	-43.14	348.21	1.54	3.83	3.90	3.98	3.87	3.31	3.88
9		Ph	-OH	-43.16	293.39	3.81	4.10	4.11	3.84	3.97	3.86	4.04
10		H	-OH	-47.02	217.29	2.17	3.87	3.80	3.95	3.98	3.59	3.71
11		Ph	-NHOH	-49.84	308.41	3.11	4.11	3.77	3.92	3.73	3.66	3.61
12		H	-NHOH	-44.04	232.31	5.66	4.32	4.25	4.08	4.05	4.19	4.12
13		Ph	-OH	-52.84	292.30	7.28	3.99	4.03	3.63	3.67	3.72	3.74
14		Ph	-NHOH	-50.54	307.32	4.62	3.88	3.88	3.73	3.72	3.86	3.68

Pontiki et al.,³¹⁴ using three human cancer cell lines, HT-29 (colon), A-549 (lung), and OAW-42 (ovarian), are given in Table 13. Pontiki et al.³¹⁴ then made a QSAR study on these compounds and found that their anticancer activities against these three cell lines were correlated with minimum electro-

static potential (Esp-min), dipole moment (D), and the McGowan volume (MgVol) of the molecules as

$$\begin{aligned} \log(1/\text{IC}_{50})_{\text{HT29}} &= 0.041(\pm 0.018)\text{Esp-min} \\ &\quad + 0.093(\pm 0.039)D + 5.543(\pm 0.728) \\ n &= 13, r = 0.872, r^2_{\text{cv}} = 0.573, s = 0.078, \\ F_{2,10} &= 15.74, \alpha = 0.01 \end{aligned} \quad (49)$$

Compound 11 was omitted.

$$\begin{aligned} \log(1/\text{IC}_{50})_{\text{A549}} &= 0.031(\pm 0.017)\text{Esp-min} \\ &\quad + 0.002(\pm 0.001)\text{MgVol} + 5.802(\pm 0.989) \\ n &= 12, r = 0.826, r^2_{\text{cv}} = 0.426, s = 0.083, \\ F_{2,9} &= 9.65, \alpha = 0.01 \end{aligned} \quad (50)$$

Compounds 9 and 11 were omitted.

$$\begin{aligned} \log(1/\text{IC}_{50})_{\text{OAW42}} &= 0.062(\pm 0.028)\text{Esp-min} \\ &\quad + 0.084(\pm 0.065)D + 6.647(\pm 1.142) \\ n &= 12, r = 0.862, r^2_{\text{cv}} = 0.602, \\ s &= 0.128, F_{2,9} = 13.04, \alpha = 0.01 \end{aligned} \quad (51)$$

Compounds 8 and 9 were omitted.

All of the three above equations, although not so highly significant, indicated that in cell line inhibition activities of these compounds, the minimum electrostatic potential and dipole moment play dominant roles, which is suggestive of the involvement of potential electrostatic interactions between the molecules and the receptors. However, in eq 50, the presence of MgVol in place of D with a negative coefficient suggested that the inhibition of A-549 cell lines might face some steric problem due to the bulk of the molecules.

For the inhibition of a PC-3 cell line, driven by a net contribution of a mixture of different HDACs, the activity of a series of TSA analogues (**10a**) was analyzed by Wang et al.¹⁴⁵ to obtain the equation:

$$\begin{aligned} \log(1/\text{IC}_{50}) &= 1.96 + 14.08Q_{\text{CO}} - 15.73\text{Golb} \\ &\quad + 0.05\text{FISA} \\ n &= 19, r = 0.96, F = 59.25, t\text{-value: } 4.33(Q_{\text{CO}}), \\ &\quad - 4.02(\text{Golb}), 9.70(\text{FISA}) \end{aligned} \quad (52)$$

where Q_{CO} is PM3 atomic charge on the carbon atom of CONHOH, Glob is globularity of compound defined as $4\pi r^2 / \text{total solvent-accessible surface area}$, and FISA is the hydrophilic component of the solvent-accessible surface area. This equation led Wang et al. to suggest that high charge on carbon reflected more polarization of C=O bond and thus strong polar interaction of this bond with the active site of the receptor.

However, eq 52 showed the negative effect of globularity of the compound, which is controlled by total solvent-accessible area (SASA). Thus, if SASA increases, Glob would decrease and the activity would increase. The positive coefficient of FISA suggests that if in SASA the hydrophilic component increases the activity could increase. Hydrophilicity in the molecules arises when it is charged. Thus, the molecule may have some charge-charge interaction with the active site of the receptor.

6.7.2. Hydroxamic Acids as Antibacterial Agents. Hydroxamic acids have also been studied for their antibacterial activity.³¹⁵ They elicit their antibacterial activity by inhibiting the enzyme peptide deformylase (PDF). PDF is an essential

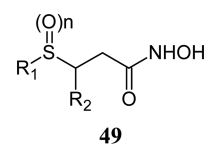
iron-containing metallo-enzyme that catalyzes the removal of N-formyl group from the N-formyl methionine of ribosome synthesized nascent polypeptide, which is an essential step in the maturation of proteins in eubacteria.^{316–320} Thus, PDF has been found to be a good target for development of antibacterial agents.

However, few QSAR studies have been made on hydroxamic acids as antibacterial agents. Nonetheless, on a series of β -sulfinyl ($n = 1$) and β -sulfonyl ($n = 2$) hydroxamic acids analogues (**49**) reported by Apfel et al.,³¹⁷ Gupta et al.³²¹ performed a QSAR study on their PDF inhibitory and antibacterial activities against *E. coli* DC2 and *Moraxella catarrhalis* RA21. For all three systems, the correlations obtained were as follows.

$$\begin{aligned} \log(1/\text{IC}_{50})_{\text{PDF}} &= 0.056(\pm 0.020)\text{MR}(R_1) \\ &\quad + 0.985(\pm 0.198)\text{Fr}(R_2) \\ &\quad - 3.386(\pm 0.727) \\ n &= 19, r = 0.86, s = 0.41, F = 21.7 \end{aligned} \quad (53)$$

$$\begin{aligned} \log(1/\text{IC}_{50})_{E. \text{coli}} &= 1.024(\pm 0.373)\text{Fr}(R_2) - 0.964(\pm 0.198)I_n \\ &\quad - 2.810(\pm 0.950) \\ n &= 17, r = 0.84, s = 0.37, F = 17.0 \end{aligned} \quad (54)$$

$$\begin{aligned} \log(1/\text{IC}_{50})_{M. \text{cata}} &= 0.075(\pm 0.022)\text{MR}(R_1) - 0.812(\pm 0.360)I_n \\ &\quad - 2.188(\pm 0.891) \\ n &= 10, r = 0.85, s = 0.34, F = 8.4 \end{aligned} \quad (55)$$



In these equations, MR refers to molar refractivity of substituents and Fr their hydrophobic constant. I_n is an indicator parameter used with a value of unity for sulfonyl derivatives ($n = 2$) and zero for sulfinyl derivatives ($n = 1$). Although these equations were marginally significant, they expressed that while cell free PDF inhibition was governed by the molar refractivity of R_1 -substituent and hydrophobicity of R_2 -substituents, the *M. cata* inhibition was controlled only by the former and *E. coli* inhibition by the latter. These differences may be attributed to the different conformations/orientations of the molecule in different system. However, in any case, while R_1 -substituent was indicated to have dispersion interaction, the R_2 -substituent was indicated to have hydrophobic interaction.

In eqs 54 and 55, the negative coefficient of I_n suggested that the sulfonyl group will be less effective than the sulfinyl group. This difference may be attributed to the involvement of lone pairs of electrons on oxygen in some repulsive interaction with the receptor, and obviously the two oxygen atoms in the sulfonyl group have more lone pairs of electrons than a single atom in the sulfinyl group.

6.7.3. Hydroxamic Acids as Mineral Collectors. One of the most interesting applications that utilizes the ability of

hydroxamic acids to form stable coordination compounds with several metal ions is in mineral collections in ore beneficiation by froth flotation. Froth flotation is a physical, chemical separation process used for the beneficiation of low-grade ores. This process involves forcing air bubbles through a suspension of ground mineral in water. These rising air bubbles pick up the mineral particles and bring them to the surface to form froth. Before the mineral particles are attached to the air bubble, they are hydrophobicized by a surface active reagent called a collector. A collector imparts hydrophobicity to a mineral by selective absorption on its surface. A collector is adsorbed on a mineral either by physisorption or by chemisorption.³²² Chemisorption involves strong interaction between the collector and the mineral in which there can be the formation of chelates between the mineral and the collector. Therefore, several kinds of chelating agents have been used for this purpose, among which hydroxamic acids have been the most important. The efficiency of mineral collection of compound will however depend on their structure and physicochemical properties. Therefore, few authors have attempted QSAR studies on hydroxamic acids as mineral collectors.

The flotation performance of a collector is evaluated by its separation efficiency (E_s) defined as

$$E_s = R_m - R_g \quad (56)$$

where R_m is % recovery of valuable mineral and R_g is % recovery of gangue mineral into the concentrate. For a series of 17 hydroxamic acids as given in Table 14, Natarajan and

Table 14. Hydroxamic Acids and Their Physicochemical Property ($\log K_{oc}$) and Separation Efficiency (E_s)

compd	substituents		$\log K_{oc}$	E_s
	R	R'		
1	Ph	H	2.770	29.0
2	Ph	4-Me	2.979	60.7
3	Ph	4-Et	3.264	63.4
4	Ph	4-Pr	3.529	28.7
5	Ph	4-i-Pr	3.462	37.0
6	Ph	4-Bu	3.794	15.9
7	Ph	4-t-Bu	3.621	32.4
8	Ph	4-MeO	2.630	56.7
9	Ph	4-F	2.979	57.4
10	Ph	2,6-Me	3.206	46.1
11	Me	H	1.796	20.1
12	Pr	H	2.346	59.9
13	Pen	H	2.876	56.9
14	Hep	H	3.406	38.7
15	Non	H	3.936	14.0
16	Udec	H	4.466	7.9
17	Pr	2,6-Me	2.782	54.4

Nirdosh³²³ evaluated their E_s values and correlated them with the soil–water partition coefficient ($\log K_{oc}$) as

$$E_s = 198.26(\log K_{oc}) - 36.03(\log K_{oc})^2 - 215.41 \quad (57)$$

$$n = 14, r^2 = 0.915, s = 4.95, F = 71.31$$

In the derivation of eq 57, compounds **1**, **3**, and **16** were, however, not included. These compounds were outliers, but no reason could be assigned to the deviation of these compounds. This equation represented a very significant correlation. Several other variables were also tried, but $\log K_{oc}$ was found to be the best parameter to describe the flotation efficiency of the compounds. This was probably due to the close similarity in the fundamental principle involved in flotation and the measurement of the soil–water partition coefficient. The use of $\log K_{oc}$ for flotation is thus analogous to the popular use of $\log P$ for drug activity.

In fact, in a previous communication, Natarajan et al.³²⁴ had shown that the separation efficiency of a series of substituted cupferrons (**50**) (Table 15) could be well correlated with equal significance with both $\log K_{oc}$ and $\log P$ as shown by eqs 58 and 59. However, in both of the equations, the five derivatives, 4-chloro, 4-floro, 4-bromo, 4-methoxy, and 4-phenyl, were not included as they were outliers. For all of them, the experimental E_s values were much higher than the corresponding predicted values from these equations. All of the cupferrons were synthesized and tested for their separation efficiency by Natarajan et al.³²⁵ According to Natarajan et al.,³²⁴ these five outliers might have different flotation kinetics because of the interactions of their halogens, methoxy group, or phenyl ring at their 4-position. It however seems that they influenced the electronic character of the molecules, as when these authors included Mulliken charge (Q) of one of the two chelating oxygen atoms (O_1) and the electronic parameter σ of the substituents, along with an indicator variable IP with a value of 1 for each of these outliers, a highly significant correlation was obtained as shown by eq 60.

$$E_s = 9.86(\pm 2.61) \log K_{oc}(\text{ACD}) + 9.358(\pm 8.09) \quad (58)$$

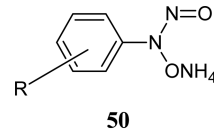
$$n = 17, r = 0.901, s = 3.86, F = 64.48$$

$$E_s = 5.74(\pm 1.52) \log P(\text{SRC}) + 24.89(\pm 4.21) \quad (59)$$

$$n = 17, r = 0.902, s = 3.85, F = 65.12$$

$$E_s = 13.04(\pm 2.163) \log K_{oc}(\text{TK}) + 1669.56(\pm 682.03) Q_{O_1} + 18.724(\pm 9.124) \sigma + 17.60(\pm 4.11) \text{IP} - 1066.88(\pm 438.85) \quad (60)$$

$$n = 22, r = 0.963, s = 2.50, F = 53.61$$

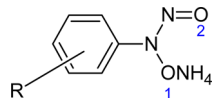


This equation suggested some electronic interaction also between the collectors and the frother in which the O_1 atom and electron-withdrawing substituents might play significant roles.

In eq 58, $\log K_{oc}(\text{ACD})$ refers to $\log K_{oc}$ values calculated using the ACD/I LAB program,³²⁶ and in eq 60, $\log K_{oc}(\text{TK})$ refers to $\log K_{oc}$ values calculated using the TOOLKIT program,³²⁷ while in eq 59 $\log P(\text{SRC})$ means the $\log P$ values calculated using the LOGKOW program.³²⁸

However, for the same series of cupferrons (Table 15), Natarajan et al.³²⁹ found that for the prediction of separation efficiency, a good model could be had by principal components analysis for which the principal components (PCs) were

Table 15. Substituted Cupferrons and Their Separation Efficiency and Physicochemical Parameters



compd	R	E_s^a	$\log K_{oc}$ (ACD) ^b	$\log P$ (SRC) ^c	$\log K_{oc}$ (TK) ^d	Q_1	σ
1	H	27.1	2.41	0.90	2.17	-0.6389	0.00
2	<i>p</i> -methyl	36.3	2.62	1.45	2.42	-0.6385	-0.14
3	<i>m</i> -methyl	36.4	2.62	1.45	2.42	-0.6394	-0.06
4	<i>p</i> -ethyl	30.6	2.90	1.95	2.71	-0.6384	-0.15
5	<i>p</i> -propyl	33.4	3.17	2.43	3.00	-0.6378	-0.15
6	<i>p</i> - <i>i</i> -opropyl	37.4	3.10	2.36	2.90	-0.6377	-0.15
7	<i>p</i> - <i>t</i> -butyl	37.3	3.26	2.81	3.01	-0.6383	-0.15
8	<i>p</i> -pentyl	42.5	3.70	3.42	3.59	-0.6377	-0.15
9	<i>p</i> -heptyl	52.3	4.23	4.40	4.18	-0.6376	-0.15
10	<i>p</i> -octyl	51.7	4.49	4.89	4.47	-0.6376	-0.15
11	<i>p</i> -nonyl	58.7	4.76	5.38	4.76	-0.6376	-0.15
12	2,6-dimethyl	32.5	3.84	2.00	2.68	-0.6342	0.20
13	3,5-dimethyl	40.7	2.83	2.00	2.68	-0.6390	0.22
14	2,4,6-trimethyl	44.8	3.05	2.55	2.93	-0.6418	0.06
15	<i>p</i> -phenyl	52.4	3.98	2.67	3.31	-0.6296	-0.01
16	<i>p</i> -fluoro	43.5	2.62	1.10	2.27	-0.6327	0.06
17	<i>m</i> -fluoro	36.3	2.62	1.10	2.33	-0.6354	0.34
18	<i>p</i> -chloro	47.1	2.62	1.55	2.43	-0.6334	0.24
19	<i>m</i> -chloro	31.1	2.62	1.55	2.57	-0.6340	0.37
20	<i>p</i> -bromo	44.2	2.62	1.79	2.72	-0.6318	0.22
21	<i>p</i> -methoxy	42.5	2.26	0.98	1.68	-0.6398	-0.28
22	<i>m</i> -methoxy	32.9	2.26	0.98	2.21	-0.6394	0.11

^aSee ref 317. ^b $\log K_{oc}$ values calculated using ACD/I-LAB. ^c $\log P$ values calculated using LOGKOW. ^d $\log K_{oc}$ values calculated using TOOLKIT.

obtained using 35 topological parameters.³²⁹ A two-parameter model with a correlation coefficient of 0.889 (eq 61) and a three-parameter model with a correlation coefficient of 0.913 (eq 62) were obtained, but these models had only predictive ability and no mechanistic value.

$$\begin{aligned} E_s &= 5.66(\pm 1.76)PC_1 + 4.23(\pm 1.75)PC_7 \\ &\quad + 40.69(\pm 1.78) \\ n &= 22, \quad r = 0.889, \quad s = 3.98 \end{aligned} \quad (61)$$

$$\begin{aligned} E_s &= 5.61(\pm 1.62)PC_1 + 4.25(\pm 1.65)PC_7 \\ &\quad + 1.68(\pm 1.64)PC_3 + 40.59(\pm 1.64) \\ n &= 22, \quad r = 0.913, \quad s = 3.65 \end{aligned} \quad (62)$$

6.7.4. An Overview of Mechanisms of Miscellaneous Activities of HAs. Among miscellaneous activities of HAs discussed here are their anticancer, antibacterial, and mineral collection activities. Their anticancer activities have been associated with their ability to inhibit ribonucleotide reductase (RDR) and some cancer cell lines. For RDR inhibition, a four-point pharmacophore developed by Basu et al.³⁰⁴ (Figure 55) indicated the involvement of only hydrogen bonding and hydrophobic interactions between the compounds and the enzyme. However, in cell line inhibitions, eqs 49–51 derived by Pontiki et al.³¹⁴ suggested the involvement of only electrostatic interactions. Supporting this, in the inhibition of a cell line driven by a mixture of HDACs, Wang et al.¹⁴⁵ showed the involvement of electrostatic interaction where the polarization of the C=O bond of CONHOH moiety was a governing factor (eq 52).

For antibacterial activity of HAs, which may be due to peptide defomylase (PDF) inhibition, or otherwise, the involvement of the dispersion interaction between the molecules and the receptor was shown by some authors³²³ (eqs 53–55).

The mineral collection ability of HAs, that is measured by their separation efficiency, E_s , was however shown to depend only on their soil–water partition coefficient $\log K_{oc}$ (eq 57). For other types of mineral collectors, $\log K_{oc}$ was found to play major role with some minor role of electronic characteristics of compounds (eq 60).

7. AN OVERVIEW OF DRUG–RECEPTOR INTERACTIONS OF MULTIFARIOUS ACTIONS OF HYDROXAMIC ACIDS

Because hydroxamic acids have a CONHOH moiety, they are able to form the hydrogen bonds with the active sites of any enzyme that contains H-bond donor or acceptor residues. If the active site of any enzyme contains any metal ion, the CONHOH moiety also undergoes chelation with the metal ion. Also, both the oxygen atoms and the nitrogen atom can participate in electrostatic interaction with the active site. Thus, these kinds of forces have been found to be commonly involved in the inhibition of all of the enzymes discussed. The other portions of hydroxamic acids can be involved in hydrophobic, steric, and electronic interactions, depending upon the nature and orientation of substituents and those of residues in active sites of the enzyme. For example, in urease inhibition, the ortho and meta substituents of the phenyl ring of HAs have been shown to be sterically and hydrophobically favorable. In urease inhibition, the hydrophobic interaction has been found to play a special role, because the active region of the enzyme has a

cavity, surrounded by hydrophobic amino acid residues, Met366, Met316, and Ala365, that warrants an interaction with a large hydrophobic group on the ligand. Similarly, potent HDAC inhibitors must possess a hydrophobic group (cap group) to have interaction at the entrance of the catalytic domain of the enzyme. Similarly, the greatest potency of MMP inhibitors has been observed to be associated with their ability to interact with S1, S1', and S2' subsites where they can have usually hydrophobic interactions. According to Welch et al.,²²⁷ the S1' pocket in MMPs is the most well-defined area of binding that consists of a hydrophobic pocket, varying in depth for different MMPs. Similarly in TACE inhibition, S1' and S3' are hydrophobic, but connected by a polar entrance, so that in many cases the activity of TACE inhibitors was shown to depend on the hydrophobic property of molecules, however, with steric problem of bulky substituents.

For ChC inhibition, however, only the electronic interaction has been found to be prominent, but for 5-LOX inhibition, the CH- π and/or π - π contacts of molecules with the side chain of some residues were found to be the most conservative interactions. Many 5-LOX inhibitors were found to have only hydrophobic interactions, and for hydroxamic acids, specifically, some QSAR studies (eqs 36–44) had suggested the involvement of only hydrophobic interactions.

In the miscellaneous activities, the RDR inhibition prominently involved the H-bonding and hydrophobic interactions. The cell inhibition involved only the electronic interaction, where the major effect might be produced by the polarizability of the C=O bond of CONHOH group. The antibacterial activity involved only the dispersion interaction, and the mineral collection ability of HAAs was found to depend only on the soil–water partition coefficient, $\log K_{oc}$, which is equivalent to $\log P$ in drug action.

Thus, hydroxamic acids effectively involve primarily their CONHOH moiety, which can have hydrogen bonding and metal chelation, and the remaining portions participate in other kinds of interactions, mainly hydrophobic and electronic.

AUTHOR INFORMATION

Corresponding Author

*E-mail: spgbits@gmail.com.

Notes

The authors declare no competing financial interest.

Biography



Satya P. Gupta is presently a Professor in the Department of Applied Sciences at the National Institute of Technical Teachers' Training and Research (NITTTR), Bhopal, India. He obtained his M.Sc. and D.Phil.

degrees from University of Allahabad, Allahabad, in 1967 and 1971, respectively. For his doctoral degree, he worked with Professor Bal Krishna in Quantum Chemistry, leading to the development of a new molecular orbital method, known as IOC- ω -Technique (inclusion of overlap charges in ω -technique). The method was found at that time very useful in dealing with the problems of π -electron systems. After his doctorate, Gupta spent a couple of years at Tata Institute of Fundamental Research (TIFR), Mumbai, working with Professor Girjesh Govil on the structure and functions of biomembranes. In 1973, he joined Birla Institute of Technology and Science (BITS), Pilani, from where he retired in 2008, and joined as a Distinguished Professor the Meerut Institute of Engineering and Technology (MIET) at Meert, from where he shifted to NITTTR in 2013. Ever since he joined BITS, he has been working on the theoretical aspects of drug design. He has made notable contributions in this area, for which he was bestowed upon, in 1990, the Ranbaxy Research Foundation Award, a coveted national award, and made, in 1985, the Fellow of the National Academy of Sciences, India (F.N. A. Sc.). In the past, he has been an advisory member of the Technical Resource Group on Research and Development on HIV/AIDS, constituted by the Ministry of Health and Welfare, Government of India. He has acted as a Guest Editor of *Current Medicinal Chemistry* and *Combinatorial Chemistry & High Throughput Screening*, both published by Bentham Science Publishers BV, The Netherlands and U.S., and acted as the Editor-in-Chief of the four journals from the same publishers, *Cardiovascular and Hematological Agents in Medicinal Chemistry*, *Current Computer-Aided Drug Design*, *Current Enzyme Inhibition*, and *Current Bioinformatics*. Regarding authoring and editing the books, he has authored a book entitled "Quantum Biology", New Age International Publishers, New Delhi, 1996, and a book entitled "QSAR and Molecular Modeling", Anamaya Publishers, New Delhi and Springer, Dordrecht, The Netherlands, 2011, and edited four books, "Ion Channels and Their Inhibitors", Springer-Verlag GmbH, Berlin, Heidelberg, 2011; "Hydroxamic Acids: A Unique Family of Chemicals with Multiple Biological Activities", Springer-Verlag GmbH, Berlin, Heidelberg, 2011; "Matrix Metalloproteinase Inhibitors: Specificity of Binding and Structure–Activity Relationships", Springer DE, 2012; and "Cancer Causing Viruses and Their Inhibitors", CRC Press, Taylor and Francis, U.S., 2014. He also guest-edited two volumes of *Topics in Heterocyclic Drugs* (Springer-Verlag Heidelberg Germany), 2006. Dr. Gupta has also been on the Editorial Board of *Indian Journal of Chemistry, Section B* (CSIR, New Delhi) and presently is at the editorial board of several international journals such as *Letters in Drug Design and Discovery* (Bentham Science, The Netherlands), *Online Journal of Organic Chemistry* (Bentham Science, The Netherlands), *BenSci Journal* (Bentham Science, The Netherlands), *Research and Reports in Medicinal Chemistry* (Dove Press, New Zealand), *Journal of Modern Medicinal Chemistry* (Synergy Publishers, Karachi), *Journal of Applied Biopharmaceutics and Pharmacokinetics* (Pharma Publishers), etc. Dr. Gupta has around two dozen reviews to his credit in highly esteemed journals, such as *Chemical Reviews* (American Chemical Society), *Progress in Drug Research* (Birkhauser Verlag), and *Current Medicinal Chemistry* (Bentham Science), in addition to hundreds of excellent original research publications in various internationally reputed journals.

ACKNOWLEDGMENTS

I express my sincere thanks to one of my senior co-workers and the former director of the NITTTR, Dr. Vijay K. Agrawal, for several thoughtful discussions of the subject matter. I acknowledge the assistance rendered by some of my colleagues, Abhilash Thakur, Bashirullah Shaik, and Izhar Ahmad, and

some of my co-workers, Neha, Neelu Singh, Shweta, Anita K., Tripti, and Shailendra Agrawal, in the preparation of this manuscript and drawing several figures and structures.

REFERENCES

- (1) Muri, E. M.; Nieto, M. J.; Sindelar, R. D.; Williamson, J. S. Hydroxamic Acids as Pharmacological Agents. *Curr. Med. Chem.* **2002**, *9*, 1631–1653.
- (2) Steward, W. P. Marimastat (BB2516): Current Status of Development. *Cancer Chemother. Pharmacol.* **1999**, *43*, S56–60.
- (3) Botos, I.; Scapozza, L.; Zhang, D.; Liotta, L. A.; Meyer, E. F.; Batimastat, A Potent Matrix Metalloproteinase Inhibitor, Exhibits an Unexpected Mode of Binding. *Proc. Natl. Acad. Sci. U.S.A.* **1996**, *93*, 2749–2754.
- (4) Sani, M.; Belotti, D.; Giavazzi, R.; Panzeri, W.; Volonterio, A.; Zanda, M. Synthesis and Evaluation of Stereopure α -Trifluoromethylmalic Hydroxamates as Inhibitors of Matrix Metalloproteinases. *Tetrahedron Lett.* **2004**, *45*, 1611–1615.
- (5) Tegoni, M.; Dallavalle, F.; Santos, A. Succinylhydroxamic Derivatives of α -Amino Acids as MMP Inhibitors. Study of Complex-formation Equilibria with Cu^{2+} , Ni^{2+} and Zn^{2+} . *J. Inorg. Biochem.* **2004**, *98*, 209–218.
- (6) Indiani, C.; Santoni, E.; Becucci, M.; Boffi, A.; Fukuyama, K.; Smulevich, G. New Insight into the Peroxidase-hydroxamic Acid Interaction Revealed by the Combination of Spectroscopic and Crystallographic Studies. *Biochemistry* **2003**, *42*, 14066–14074.
- (7) O'Brien, E. C.; Farkas, E.; Gil, M. J.; Fitzgerald, D.; Castineras, A.; Nolan, K. B.. Metal Complexes of Salicylhydroxamic Acid (H2Sha), Anthranilic Hydroxamic Acid and Benzohydroxamic Acid. Crystal and Molecular Structure of $[\text{Cu}(\text{phen})_2\text{Cl}] \text{Cl} \times \text{H2Sha}$, a Model for a Peroxidase-Inhibitor Complex. *J. Inorg. Biochem.* **2000**, *79*, 47–51.
- (8) Tsukamoto, K.; Itakura, H.; Sato, K.; Fukuyama, K.; Miura, S.; Takahashi, S.; Ikezawa, H.; Hosoya, T. *Biochemistry* **2007**, *38*, 12558–12568.
- (9) Brown, D. A.; Cuffe, L. P.; Fitzpatrick, N. J.; Ryan, A. T. A DFT Study of Model Complexes of Zinc Hydrolases and Their Inhibition by Hydroxamic Acids. *Inorg. Chem.* **2004**, *43*, 297–302.
- (10) Brown, D. A.; Glass, W. K.; Fitzpatrick, N. J.; Kemp, T. J.; Errington, W.; Clarkson, G. J.; Haase, W.; Karsten, F.; Mahdy, A. H. Structural Variations in Dinuclear Model Hydrolases and Hydroxamate Inhibitor Models: Synthetic, Spectroscopic and Structural Studies. *Inorg. Chim. Acta* **2004**, *357*, 1411–1436.
- (11) Brown, D. A.; Cuffe, L. P.; Fitzpatrick, N. J.; Glass, W. K.; Herlihy, K.; Namir, H.; Deeg, O.; Errington, W.; Kemp, T. J. Novel Elimination of Hydroxylamine and Formation of a Nickel Tetramer on Reaction of Glutarodihydroxamic Acid with Model Dinickel Hydrolases. *Chem. Commun.* **1998**, 2433–2434.
- (12) Amtul, Z.; Rahman, A. U.; Siddiqui, R. A.; Choudhry, M. I. Chemistry and Mechanism of Urease Inhibition. *Curr. Med. Chem.* **2002**, *9*, 1323–1342.
- (13) Benini, S.; Rypniewski, W. R.; Wilson, K. S.; Milette, S.; Ciurli, S.; Mangani, S. The Complex of *Bacillus pasteurii* Urease with Acetohydroxamate Anion from X-ray Data at 1.55 Å Resolution. *J. Biol. Inorg. Chem.* **2000**, *5*, 110–118.
- (14) Arnold, M.; Brown, D. A.; Deeg, O.; Errington, W.; Haase, W.; Herlihy, K.; Kemp, T. J.; Nimir, H.; Werner, R. Hydroxamate-Bridged Dinuclear Nickel Complexes as Models for Urease Inhibition. *Inorg. Chem.* **1998**, *37*, 2920–2925.
- (15) Connolly, P. J.; Wetter, S. K.; Beers, K. N.; Hamel, S. C.; Chen, R. H. K.; Wachter, M. P.; Ansell, J.; Singer, M. M.; Steber, M.; Ritchie, D. M.; Argentieri, D. C. N-Hydroxyurea and Hydroxamic Acid Inhibitors of Cyclooxygenase and 5-Lipoxygenase. *Bioorg. Med. Chem. Lett.* **1999**, *9*, 979–984.
- (16) Dooley, C. M.; Devocelle, M.; McLaughlin, B.; Nolan, K. B.; Fitzgerald, D. J.; Sharkey, C. T. A Novel Family of Hydroxamate-based Acylating Inhibitors of Cyclooxygenase. *Mol. Pharmacol.* **2003**, *63*, 450–455.
- (17) Marks, P. A.; Richon, V. M.; Rifkind, R. A. Histone Deacetylase Inhibitors: Inducers of Differentiation or Apoptosis of Transformed Cells. *J. Natl. Cancer Inst.* **2000**, *92*, 1210–1216.
- (18) Johnstone, R. W. Histone-Deacetylase Inhibitors: Novel Drugs for the Treatment of Cancer. *Nat. Rev. Drug Discovery* **2002**, *1*, 287–299.
- (19) Jung, M. Inhibitors of Histone Deacetylase as New Anticancer Agents. *Curr. Med. Chem.* **2001**, *8*, 1505–11.
- (20) Kelly, W. K.; Connor, O. A.; Marks, P. A. Histone Deacetylase Inhibitors: from Target to Clinical Trials. *Expert Op. Invest. Drugs* **2002**, *11*, 1695–713.
- (21) Chen, D.; Hackbarth, C.; Ni, Z. J.; Wu, C.; Wang, W.; Jain, R.; He, Y.; Bracken, K.; Weidmann, B.; Patel, D. V.; Trias, J.; White, R. J.; Yuan, Z. Peptide Deformylase Inhibitors as Antibacterial Agents: Identification of VRC337S, a Proline-3-Alkylsuccinyl Hydroxamate Derivative, by Using an Integrated Combinatorial and Medicinal Chemistry Approach. *Antimicrob. Agents Chemother.* **2004**, *48*, 250–61.
- (22) Lou, B.; Yang, K. Molecular Diversity of Hydroxamic Acids: Part II. Potential Therapeutic Applications. *Mini-Rev. Med. Chem.* **2003**, *3*, 609–620.
- (23) Zamora, R.; Grzesiok, A.; Weber, H.; Feelisch, M. Oxidative Release of Nitric Oxide Accounts for Guanylyl Cyclase Stimulating, Vasodilator and Anti-Platelet Activity of Piloty's Acid: a Comparison with Angeli's Salt. *Biochem. J.* **1995**, *312*, 333–39.
- (24) Steward, W. P.; Thomas, A. L. Marimastat: the Clinical Development of a Matrix Metalloproteinase Inhibitor. *Expert Opin. Invest. Drugs* **2000**, *9*, 2913–22.
- (25) Brammer, R.; Buckels, J.; Bramhall, S. Advances in non-operative therapy in pancreatic cancer. *Int. J. Clin. Pract.* **2000**, *54*, 373–381.
- (26) Bouchain, G.; Delorme, D. Novel Hydroxamate and Anilide Derivatives as Potent Histone Deacetylase Inhibitors: Synthesis and Antiproliferative Evaluation. *Curr. Med. Chem.* **2003**, *10*, 2359–2372.
- (27) Holmes, J.; Mast, K.; Marcotte, P.; Elmore, I.; Li, J.; Pease, L.; Glaser, K.; Morgan, D.; Michaelides, M.; Davidsen, S. Discovery of Selective Hydroxamic Acid Inhibitors of Tumor Necrosis Factor-Alpha Converting Enzyme. *Bioorg. Med. Chem. Lett.* **2001**, *11*, 2907–2910.
- (28) Holland, K. P.; Elford, H. L.; Bracchi, V. Antimalarial Activities of Polyhydroxyphenyl and Hydroxamic Acid Derivatives. *Antimicrob. Agents Chemother.* **1998**, *42*, 2456–2458.
- (29) Apfel, C. M.; Banner, D. W.; Bur, D.; Dietz, M.; Hirata, T.; Hubschwerlen, C.; Locher, H.; Page, M. G. P.; Pirson, W.; Rosse, G.; Specklin, J. L. Hydroxamic Acid Derivatives as Potent Peptide Deformylase Inhibitors and Antibacterial Agents. *J. Med. Chem.* **2000**, *43*, 2324–2331.
- (30) Golenser, J.; Tsafack, A.; Amichai, Y.; Libman, A.; Shanzer, J.; Cabantchik, Z. I. Antimalarial Action of Hydroxamate-Based Iron Chelators and Potentiation of Desferrioxamine Action by Reversed Siderophores. *Antimicrob. Agents Chemother.* **1995**, *39*, 61–65.
- (31) Mishra, R. C.; Tripathi, R.; Katiyar, D.; Tewari, N.; Singh, D.; Tripathi, R. P. Synthesis of Beta-Amino Hydroxamates as New Class of Antimalarial Agents. *Bioorg. Med. Chem.* **2003**, *11*, 5363–5374.
- (32) Tsafack, A.; Golenser, J.; Libman, J.; Shanzer, A.; Cabantchik, Z. I. Mode of Action of Iron(III) Chelators as Antimalarials. III. Over Additive Effects in the Combined Action of Hydroxamate-Based Agents on In-vitro Growth of *Plasmodium falciparum*. *Mol. Pharmacol.* **1995**, *47*, 403–409.
- (33) Miller, M. J. Syntheses and Therapeutic Potential of Hydroxamic Acid Based Siderophores and Analogs. *Chem. Rev.* **1989**, *89*, 1563–1579.
- (34) El Yazal, J.; Pang, Y. P. Novel Stable Configurations and Tautomers of the Neutral and Deprotonated Hydroxamic Acids Predicted from High-Level *ab initio* Calculations. *J. Phys. Chem. A* **1999**, *103*, 8346–8350.
- (35) El Yazal, J.; Pang, Y. P. Proton Dissociation Energies of Zinc-Coordinated Hydroxamic Acids and Their Relative Affinities for Zinc: Insight into Design of Inhibitors of Zinc-Containing Proteinases. *J. Phys. Chem. B* **2000**, *104*, 6499–6504.

- (36) Marmion, C. J.; Griffith, D.; Nolan, K. B. Hydroxamic Acids -An Intriguing Family of Enzyme Inhibitors and Biomedical Ligands. *Eur. J. Inorg. Chem.* **2004**, *15*, 3003–3016.
- (37) Scolnick, L. R.; Clements, A. M.; Liao, J. C.; Hellberg, L. M.; May, J.; Dean, T. R.; Christianson, D. W. Novel Binding Mode of Hydroxamate Inhibitors to Human Carbonic Anhydrase II. *J. Am. Chem. Soc.* **1997**, *119*, 850–851.
- (38) Kurzak, B.; Kurzak, K.; Jeziorska, J. Solution Properties of Cu(II)-L- α -alaninehydroxamic Acid. *Inorg. Chim. Acta* **1986**, *125*, 77–88.
- (39) Kurzak, B.; Kurzak, K.; Jeziorska, J. Solution Properties of Cu(II)-L- α Leucinehydroxamic Acid. *Inorg. Chim. Acta* **1987**, *130*, 189–93.
- (40) Kurzak, B.; Farkas, E.; Glowik, T. X-Ray and Potentiometric Studies on a Pentanuclear Copper (II) Complex with β -Alaninehydroxamic Acid. *J. Chem. Soc., Dalton Trans.* **1991**, 163–67.
- (41) Adams, D. R.; Bchrowicz-Lewinski, M.; Butler, A. R. Nitric Oxide: Physiological Roles, Biosynthesis and Medical Uses. *Fortschr. Chem. Org. Naturst.* **1999**, *76*, 1–211.
- (42) Stuehr, D. J. Mammalian Nitric Oxide Synthases. *Biochim. Biophys. Acta, Bioenerg.* **1999**, *1411*, 217–230.
- (43) Saavedra, J.; Keefer, L. K. NO Better Pharmaceuticals. *Chem. Br.* **2000**, *36*, 30–33.
- (44) Kumar, H.; Gupta, S. P.; Siddiqui, A.; Kumar, V. Advances in Design and Development of Inhibitors of Nitric Oxide Synthases. *Curr. Enzyme Inhib.* **2013**, *9*, 117–141.
- (45) Muri, E. M.; Nieto, M. J.; Williamson, J. S. Hydroxamic Acids as Pharmacological Agents: An Update. *Med. Chem. Rev.* **2004**, *1*, 385–394.
- (46) Sidebotham, R. L.; Batten, J. J.; Karim, Q. N.; Spencer, J.; Baron, J. H. Breakdown of Gastric Mucus in Presence of *Helicobacter pylori*. *J. Clin. Pathol.* **1991**, *44*, 52–57.
- (47) Tsujii, M.; Kawano, S.; Tsuji, S.; Fusamoto, H.; Kameda, T.; Sato, N. Mechanism of Gastric Mucosal Damage Induced by Ammonia. *Gastroenterology* **1992**, *102*, 1881–1888.
- (48) Kouzarides, T. Histone Acetylases and Deacetylases in Cell Proliferation. *Curr. Opin. Genet. Dev.* **1999**, *9*, 40–48.
- (49) Marks, P. A.; Richon, V. M.; Breslow, A.; Rifkind, R. A. Histone Deacetylase Inhibitors as New Cancer Drugs. *Curr. Opin. Oncol.* **2001**, *13*, 477–483.
- (50) Gray, G. G.; Ekstrom, T. J. The Human Histone Deacetylase Family. *Exp. Cell Res.* **2001**, *262*, 75–83.
- (51) Rokach, J. *Bioactive Molecules*, Vol. 11, *Leukotrienes and Lipoxygenases: Chemical, Biological, and Clinical Aspects*; Elsevier: Amsterdam, 1989.
- (52) Summers, J. B.; Kim, K. H.; Mazdiyasni, H.; Holmes, J. H.; Ratajczyk, J. D.; Stewart, A. O.; Dyer, R. D.; Carter, G. W. Hydroxamic Acid Inhibitors of S-Lipoxygenase: Quantitative Structure-Activity Relationships. *J. Med. Chem.* **1990**, *33*, 992–998.
- (53) Brinckerhoff, C. E.; Matrisian, L. M. Matrix Metalloproteinases: a Tail of a Frog that Became a Prince. *Nat. Rev. Mol. Cell Biol.* **2002**, *3*, 207–214.
- (54) Burzlaff, N. In *Concepts and Models in Bioinorganic Chemistry*; Douglas, B., McDaniel, D. H., Alexander, J. J., Eds.; Wiley: New York, 2006; Vol 17, pp 397–429.
- (55) Gupta, S. P. Quantitative Structure-Activity Relationship Studies on Zinc-Containing Metalloproteinase Inhibitors. *Chem. Rev.* **2007**, *107*, 3042–3087.
- (56) Sternlicht, M.; Werb, Z. How Matrix Metalloproteinases Regulate Cell Behavior. *Annu. Rev. Cell Dev. Biol.* **2001**, *17*, 463–516.
- (57) Brew, K.; Dinakarpandian, D.; Nagase, H. Tissue Inhibitors of Metalloproteinases: Evolution, Structure and Functions. *Biochim. Biophys. Acta* **2000**, *1477*, 267–283.
- (58) Yadav, M. R.; Murumkar, P. R.; Zambre, V. P. Advances in Studies on Collagenase Inhibitors. In *Matrix Metalloproteinase Inhibitors: Specificity of Binding and Structure Activity Relationships*; Gupta, S. P., Ed.; Springer: Basel AG, 2012; pp 83–135.
- (59) Whittaker, M.; Flyod, C. D.; Brown, P.; Gearing, A. J. H. Design and Therapeutic Application of Matrix Metalloproteinase Inhibitors. *Chem. Rev.* **1999**, *99*, 2735–2776.
- (60) Verma, R. P. Hydroxamic Acids as Matrix Metalloproteinase Inhibitors. In *Matrix Metalloproteinase Inhibitors: Specificity of Binding and Structure Activity Relationships*; Gupta, S. P., Ed.; Springer: Basel AG, 2012; pp 137–176.
- (61) Heath, E. I.; Grochow, L. B. Clinical Potential of Matrix Metalloprotease Inhibitors in Cancer Therapy. *Drugs* **2000**, *59*, 1043–1055.
- (62) Skiles, J. W.; Monovich, L. G.; Jeng, A. Y. Matrix Metalloproteinase Inhibitors for Treatment of Cancer. *Annu. Rep. Med. Chem.* **2000**, *35*, 167–176.
- (63) Elliott, S.; Cawston, T. The Clinical Potential of Matrix Metalloproteinase Inhibitors in the Rheumatic Disorders. *Drugs Aging* **2001**, *18*, 87–99.
- (64) Leff, R. L. Clinical Trials of a Stromelysin Inhibitor. Osteoarthritis, Matrix Metalloproteinase Inhibition, Cartilage Loss, Surrogate Markers, and Clinical Implications. *Ann. N. Y. Acad. Sci.* **1999**, *878*, 201–207.
- (65) Shlopov, B. V.; Lie, W. R.; Mainardi, C. L.; Cole, A. A.; Chubinskaya, S.; Hasty, K. A. Osteoarthritic Lesions: Involvement of Three Different Collagenases. *Arthritis Rheum.* **1997**, *40*, 2065–2074.
- (66) Overall, C. M.; Wiebkin, O. W.; Thonard, J. C. Demonstration of Tissue Collagenase Activity *in vivo* and its Relationship to Inflammation Severity in Human Gingiva. *J. Periodontal Res.* **1987**, *22*, 81–88.
- (67) Yong, V. W.; Krekoski, C. A.; Forsyth, P. A.; Bell, R.; Edwards, D. R. Matrix Metalloproteinases and Diseases of the CNS. *Trends Neurosci.* **1998**, *21*, 75–80.
- (68) Li, Y. Y.; Feldman, A. M. Matrix Metalloproteinases in the Progression of Heart Failure: Potential Therapeutic Implications. *Drugs* **2001**, *61*, 1239–1252.
- (69) Skotnicki, J. S.; Zask, A.; Nelson, F. C. Design and Synthetic Considerations of Matrix Metalloproteinase Inhibitors. *Ann. N. Y. Acad. Sci.* **1999**, *878*, 61–72.
- (70) (a) Black, R. A.; Rauch, C. T.; Kozlosky, C. J.; Peschon, J. J.; Slack, J. L.; Wolfson, M. F.; Castner, B. J.; Stocking, K. L.; Reddy, P.; Srinivasan, S.; Nelson, N.; Boiani, N.; Schooley, K. A.; Gerhart, M.; Davis, R.; Fitzner, J. N.; Johnson, R. S.; Paxton, R. J.; March, C. J.; Cerretti, D. P. A Metalloproteinase Disintegrin That Releases Tumour-necrosis Factor-alpha from Cells. *Nature* **1997**, *385*, 729–733. (b) Losken, H. Ueber die Oxalohydroxamsaure. *Ann. Chem.* **1869**, *150*, 314–320.
- (71) Moss, M. L.; White, J. M.; Lambert, M. H.; Andrews, R. C. TACE and Other ADAM Proteases as Targets for Drug Discovery. *Drug Discovery Today* **2001**, *6*, 417–426.
- (72) Vassali, P. The Pathophysiology of Tumor Necrosis Factors. *Annu. Rev. Immunol.* **1992**, *10*, 411–452.
- (73) Nelson, F. C.; Zask, A. The Therapeutic Potential of Small Molecule TACE Inhibitors. *Expert Opin. Invest. Drugs* **1999**, *8*, 383–392.
- (74) Newton, R. C.; Decicco, C. P. Therapeutic Potential and Strategies for Inhibiting Tumor Necrosis Factor-Alpha. *J. Med. Chem.* **1999**, *42*, 2295–2314.
- (75) (a) Supuran, C. T., Scozzafava, A., Conway, J., Eds. *Expert Opin. Ther. Pat.* **2004**, *10*, 575. (b) Supuran, C. T.; Scozzafava, A. *Expert Opin. Ther. Pat.* **2000**, *10*, 575–600.
- (76) Hooper, N. M. *Zinc Metalloproteases in Health and Disease*; Taylor & Francis: London, 1996.
- (77) Hackbarth, C. J.; Chen, D. Z.; Lewis, J. G.; Clark, K.; Mangold, J. B.; Cramer, J. A.; Margolis, P. S.; Wang, W.; Koehn, J.; Wu, C.; Lopez, S.; Withers, I. G.; Gu, H.; Dunn, E.; Kulathila, R.; Pan, S. H.; Porter, W. L.; Jacobs, J.; Trias, J.; Patel, D. V.; Weidmann, B.; White, R. J.; Yuan, Z. N-alkyl Urea Hydroxamic Acids as a New Class of Peptide Deformylase Inhibitors with Antibacterial Activity. *Antimicrob. Agents Chemother.* **2002**, *46*, 2752–2764.
- (78) Hogg, J. H.; Ollmann, I. R.; Haeggstrom, J.; Wetterholm, A.; Samuelsson, B.; Wong, C. Amino Hydroxamic Acids as Potent

- Inhibitors of Leukotriene A4 Hydrolase. *Bioorg. Med. Chem.* **1995**, *3*, 1405–1415.
- (79) Ollmann, I. R.; Hogg, J. H.; Munoz, B.; Haeggstroem, J. Z.; Samuelsson, B.; Wong, C. Investigation of the Inhibition of Leukotriene A4 Hydrolase. *Bioorg. Med. Chem.* **1995**, *3*, 969–995.
- (80) Hogg, J. H.; Ollmann, I. R.; Wetterholm, A.; Andberg, M. B.; Haeggstrom, J.; Samuelsson, B.; Wong, C.-H. Probing the Activities and Mechanisms of Leukotriene A₄ Hydrolase with Synthetic Inhibitors. *Chem.—Eur. J.* **1998**, *4*, 1698–1713.
- (81) Onishi, H. R.; Pelak, B. A.; Gerckens, L. S.; Silver, L. L.; Kahan, F. M.; Chen, M. H.; Patchett, A. A.; Galloway, S. M.; Hyland, S. A.; Anderson, M. S.; Raetz, C. R. H. Antibacterial Agents That Inhibit Lipid A Biosynthesis. *Science* **1996**, *274*, 980–982.
- (82) Arner, E. C.; Pratta, M. A.; Decicco, C. P.; Xue, C. B.; Newton, R. C.; Trzaskos, J. M.; Magolda, R. L.; Tortorella, M. D. Aggrecanase: A Target for the Design of Inhibitors of Cartilage Degradation. *Ann. N. Y. Acad. Sci.* **1999**, *878*, 92–107.
- (83) Browner, M. F.; Smith, W. W.; Castelhano, A. L. Matrilysin-Inhibitor Complexes: Common Themes Among Metalloproteases. *Biochemistry* **1995**, *34*, 6602–6610.
- (84) Hansch, C.; Fujita, T. A Method for the Correlation of Biological Activity and Chemical Structure. *J. Am. Chem. Soc.* **1964**, *86*, 1616–1626.
- (85) (a) Hansch, C.; Leo, A. Exploring QSAR. *Fundamentals and Applications in Chemistry and Biology*; American Chemical Society: Washington, DC, 1995. (b) Comparative QSAR; Devillers, J., Ed.; Taylor and Francis Publishers: Washington, DC, 1998. (c) QSAR and Strategies in Design of Bioactive Compounds; Seydel, J. K., Ed.; VCH: Weinheim, Germany, 1985. (d) Gupta, S. P. QSAR and Molecular Modeling; Anamaya Publishers: New Delhi (copublished with Springer, AH Dordrecht, The Netherlands), 2011.
- (86) Hansch, C. Quantitative Approach to Biochemical Structure–Activity Relationships. *Acc. Chem. Res.* **1969**, *2*, 232–239.
- (87) Wiener, H. Structural Determination of Paraffin Boiling Points. *J. Am. Chem. Soc.* **1947**, *69*, 17–20.
- (88) Hosoya, H. Topological Index. A Newly Proposed Quantity Characterizing the Topological Nature of Structural Isomers of Saturated Hydrocarbons. *Bull. Chem. Soc. Jpn.* **1971**, *44*, 2332–2339.
- (89) (a) Randic, M. Characterization of Molecular Branching. *J. Am. Chem. Soc.* **1975**, *97*, 6609–6615. (b) Kier, L. B.; Hall, L. H. *Molecular Connectivity in Structure-Activity Analysis*; Wiley: New York, 1986. (c) Kier, L. B.; Hall, L. H. *Molecular Structure Description: The Electropotential State*; Academic: San Diego, CA, 1999.
- (90) (a) Balaban, A. T. *From Chemical Topology to Three-Dimensional Geometry*; Plenum Press: New York, 1997. (b) Randic, M. Topological Indices. In *Encyclopedia of Computational Chemistry*; Schleyer, P.V. R., Allinger, N. L., Clark, T., Gasteiger, J., Kollman, P. A., Schaefer, H. F., III, Schreiner, P. R., Eds.; John-Wiley and Sons: Chichester, 1998; p 3018. (c) *Topological Indices and Related Descriptors in QSAR and QSPR*; Devillers, J., Balaban, A. T., Eds.; Taylor and Francis: New York, 2000. (d) Todeschini, R.; Consonni, V. *Molecular Descriptors for Chemoinformatics*, (2 volumes); Wiley-VCH: New York, 2009.
- (91) Free, S. M., Jr.; Wilson, J. W. A Mathematical Contribution to Structure-Activity Studies. *J. Med. Chem.* **1964**, *7*, 395–399.
- (92) Fujita, T.; Ban, T. Structure-Activity Study of Phenethylamines as Substrates of Biosynthetic Enzymes of Sympathetic Transmitters. *J. Med. Chem.* **1971**, *14*, 148–152.
- (93) Martin, Y. C.; Holland, J. B.; Jarboe, C. H.; Plotnikoff, N. Discriminant Analysis of the Relationship between Physical Properties and the Inhibition of Monoamine Oxidase by Aminotetralins and Aminoindans. *J. Med. Chem.* **1974**, *17*, 409–413.
- (94) (a) Kowalski, B. R.; Bonder, C. F. Pattern Recognition. Powerful Approach to Interpreting Chemical Data. *J. Am. Chem. Soc.* **1972**, *94*, 5632–5639. (b) Chu, K. C. Applications of Artificial Intelligence to Chemistry. Use of Pattern Recognition and Cluster Analysis to Determine the Pharmacological Activity of some Organic Compounds. *Anal. Chem.* **1974**, *46*, 1181–1187.
- (95) Topliss, J. G. Utilization of Operational Schemes for Analog Synthesis in Drug Design. *J. Med. Chem.* **1972**, *15*, 1006–1011.
- (96) Craig, P. N. Interdependence between Physical Parameters and Selection of Substituent Groups for Correlation Studies. *J. Med. Chem.* **1971**, *14*, 680–684.
- (97) (a) Bustard, T. M. Optimization of Alkyl Modifications by Fibonacci Search. *J. Med. Chem.* **1974**, *17*, 777–778. (b) Santora, N. J.; Auyang, K. Non-computer Approach to Structure-Activity Study. An Expanded Fibonacci Search Applied to Structurally Diverse Types of Compounds. *J. Med. Chem.* **1975**, *18*, 959–963. (c) Deming, S. N. On the Use of Fibonacci Searches in Structure-Activity Studies. *J. Med. Chem.* **1976**, *19*, 977–978.
- (98) Darvas, F. Application of the Sequential Simplex Method in Designing Drug Analogs. *J. Med. Chem.* **1974**, *17*, 799–804.
- (99) Wold, S. PLS for Multivariate Linear Modeling. In *Chemometric Methods in Molecular Design. Methods and Principle in Medicinal Chemistry*; van de Waterbeemd, H., Ed.; Verlag-Chemie: New York, 1994; pp 523–550.
- (100) (a) Crippen, G. M. Distance Geometry Approach to Rationalizing Binding Data. *J. Med. Chem.* **1979**, *22*, 988–997. (b) Ghose, A. K.; Crippen, G. M. Quantitative Structure-Activity Relationship by Distance Geometry: Quinazolines as Dihydrofolate Reductase Inhibitors. *J. Med. Chem.* **1982**, *25*, 892–899. (c) Crippen, G. M. *Distance Geometry and Conformational Calculations*; Research Studies Press: New York, 1981. (d) Srivastava, S.; Richardson, W. W.; Bradley, M. P.; Crippen, G. M. Three Dimensional QSAR Using Distance Geometry and Voronoi Polyhedra. In *3D-QSAR in Drug Design: Theory, Methods and Applications*; Kubinyi, H., Ed.; ESCOM: Leiden, 1993; pp 409–430.
- (101) (a) Cramer, R. D., III; Patterson, D. E.; Bunce, J. D. Comparative Molecular Field Analysis (CoMFA). 1. Effect of Shape on Binding of Steroids to Carrier Proteins. *J. Am. Chem. Soc.* **1988**, *110*, 5959–5967. (b) Kim, K. H.; Grecco, G.; Novellino, E. A Critical Review of Recent CoMFA Applications. In *3D QSAR in Drug Design*; Kubinyi, H., Folkers, G., Martin, Y. C., Eds.; Kluwer Academic: Dordrecht, 1998; Vol. 3, pp 257–315.
- (102) Klebo, G.; Abraham, U.; Mietzner, T. Molecular Similarity Indices in a Comparative Analysis (CoMSIA) of Drug Molecules to Correlate and Predict their Biological Activity. *J. Med. Chem.* **1994**, *37*, 4130–4146.
- (103) Doweyko, A. M. The Hypothetical Active Site Lattice. An Approach to Modelling Active Sites from Data on Inhibitor Molecules. *J. Med. Chem.* **1988**, *31*, 1396–1406.
- (104) (a) *Trends in QSAR and Molecular Modelling*; Wermuth, C. G., Ed.; ESCOM: Leiden, 1993. (b) Kubinyi, H. *QSAR: Hansch Analysis and Related Approaches*; VCH: New York, 1993.
- (105) Kintz, I. D.; Blaney, J. M.; Oatley, S. J.; Langridge, R.; Ferrin, T. E. A Geometric Approach to Macromolecule-Ligand Interactions. *J. Mol. Biol.* **1982**, *161*, 269–288.
- (106) Kobashi, K.; Kumara, K.; Hase, J. Effect of Acyl Residues of Hydroxamic Acids on Urease Inhibition. *Biochim. Biophys. Acta* **1971**, *227*, 429–441.
- (107) Kumaki, K.; Tomioka, S.; Kobashi, K.; Kumara, K.; Hase, J. Structure-Activity Correlations Between Hydroxamic Acids and Their Inhibitory Power on Urease Activity. I. A Quantitative Approach to the Effect of Hydrophobic Character of Acyl Residue. *Chem. Pharm. Bull.* **1972**, *20*, 1599–1606.
- (108) Munakata, K.; Kobashi, K.; Hase, J. Quantitative Structure-Activity Relationship between Hydroxamic Acids and Their Urease Inhibitory Potency. *J. Pharm. Dyn.* **1980**, *3*, 457–462.
- (109) Kanoda, M.; Shinoda, H.; Kobashi, K.; Hase, J.; Nagahara, S. Studies on Hydroxamic Acids and Their Urease Inhibition Potency by Quantum Chemistry Calculation. *J. Pharm. Dyn.* **1983**, *6*, 61–67.
- (110) Zaheer-ul-Haq; Wadood, A.; Reazuddin. CoMFA and CoMSIA 3D-QSAR Analysis on Hydroxamic Acids as Urease Inhibitors. *J. Enzyme Inhib. Med. Chem.* **2009**, *24*, 272–278.
- (111) Zaheer-ul-Haq; Wadood, A. Prediction of Binding Affinities for Hydroxamic Acid Derivatives as Urease Inhibitors by Molecular Docking and 3D-QSAR Studies. *Lett. Drug Des. Discovery* **2009**, *6*, 93–100.

- (112) Zareen, A.; Atta-ur-Rahman; Siddiquie, R. A.; Choudhary, M. I. Chemistry and Mechanism of Urease Inhibition. *Curr. Med. Chem.* **2002**, *9*, 1323–1348.
- (113) Clark, M.; Cramer, R. D., III; Van Opdenbosch, N. Validation of the General Purpose Tripos 5.2 Force Field. *J. Comput. Chem.* **1989**, *10*, 982–1012.
- (114) Jabri, E.; Car, M. B.; Hausinger, R. P.; Karplus, P. A. The Crystal Structure of Urease from *Klebsiella Aerogenes*. *Science* **1995**, *268*, 998–1004.
- (115) Langenberg, M. L.; Tytgat, G. N. J.; Schipper, M. E. L. Campylobacter-like Organisms in the Stomach of Patients and Healthy Individuals. *Lancet* **1984**, *332*, 1348–1349.
- (116) Todd, M. J.; Hausinger, R. P. Fluoride Inhibition of *Klebsiella Aerogenes* Urease: Mechanistic Implications of a Pseudo-Uncompetitive, Slow-Binding Inhibitor. *Biochemistry* **2000**, *38*, 5389–5396.
- (117) Todd, M. J.; Hausinger, R. P. Competitive Inhibitors of *Klebsiella Aerogenes* Urease. Mechanisms of Interaction with the Nickel Active Site. *Biol. Chem.* **1989**, *264*, 15835–15842.
- (118) Kobashi, K.; Hase, J.; Uehara, K. Specific Inhibition of Urease by Hydroxamic Acids. *Biochim. Biophys. Acta* **1962**, *65*, 380–383.
- (119) Odake, S.; Morikawa, T.; Tsuchiya, M.; Imamura, L.; Kobashi, K. Inhibition of *Helicobacter Pylori* Urease Activity by Hydroxamic Acid Derivatives. *Biol. Pharm. Bull.* **1994**, *17*, 1329–1332.
- (120) Mishra, H.; Parill, A. L.; Williamson, J. S. Three-Dimensional Quantitative Structure-Activity Relationship and Comparative Molecular Field Analysis of Dipeptide Hydroxamic Acid *Helicobacter Pylori* Urease Inhibitors. *Antimicrob. Agents Chemother.* **2002**, *46*, 2613–2618.
- (121) Abid, O.; Babar, T. M.; Ali, F. I.; Ahmed, S.; Wadood, A.; Rama, N. H.; Reazuddin; Zaheer- ul-Haq; Khan, A.; Choudhury, M. I. Identification of Novel Urease Inhibitors by High-Throughput Virtual and *in vitro* Screening. *ACS Med. Chem. Lett.* **2010**, *1*, 145–149.
- (122) Zaheer-ul-Haq; Lodhi, A.; Nawaj, S. A.; Iqbal, S.; Khan, K. M.; Rode, B. M.; Atta-ur- Rahman; Choudhary, M. I. 3D-QSAR CoMFA Studies on Bis-Coumarine Analogues as Urease Inhibitors: a Strategic Design in Anti-Urease Agents. *Bioorg. Med. Chem.* **2008**, *16*, 3456–3461.
- (123) Khan, K. M.; Iqbal, S.; Lodhi, M. X.; Maharvi, G. M.; Ullah, Z.; Choudhary, M. I. Atta-ur-Rahman; Perveen, S. *Bioorg. Med. Chem.* **2008**, *16*, 3456–3461.
- (124) Ito, Y.; Onoda, Y.; Nakamura, S.; Tagakawa, K.; Fukushima, T.; Sugawara, Y.; Takaiti, O. Effects of the New Anti-Ulcer Drug Ecabet Sodium (TA-2711) on Pepsin Activity. II. Interaction with Substrate Protein. *Jpn. J. Pharmacol.* **1993**, *62*, 175–181.
- (125) Amtul, Z.; Atta-ur-Rahman; Siddiqui, R. A.; Choudhary, M. I. Chemistry and Mechanism of Urease Inhibition. *Curr. Med. Chem.* **2002**, *9*, 1323–1348.
- (126) Rashid, U.; Batool, T.; Wadood, A.; Khan, A.; Zaheer-ul-Haq; Choudhary, M. I.; Ansari, F. L. Structure Based Virtual Screening-Driven Identification of Monastrol as a Potent Urease Inhibitor. *J. Mol. Graphics Modell.* **2013**, *43*, 47–57.
- (127) Benini, S.; Rypniewski, W. R.; Wilson, K. S.; Milette, S.; Ciurli, S.; Mangani, S. The Complex of *Bacillus Pasteurii* Urease with Acetohydroxamate Anion from X-ray Data at 1.55 Å Resolution. *J. Biol. Inorg. Chem.* **2000**, *5*, 110–118.
- (128) Benini, S.; Rypniewski, W. R.; Wilson, K. S.; Milette, S.; Ciurli, S. Molecular Details of Urease Inhibition by Boric Acid: Insights into the Catalytic Mechanism. *J. Am. Chem. Soc.* **2004**, *126*, 3714–3715.
- (129) Benini, S.; Rypniewski, W. R.; Wilson, K. S.; Milette, S.; Ciurli, S.; Mangani, S. A New Proposal for Urease Mechanism Based on the Crystal Structures of the Native and Inhibited Enzyme from *Bacillus Pasteurii*: Why Urea Hydrolysis Costs Two Nickels. *Structure* **1999**, *15*, 205–216.
- (130) Musiani, F.; Arnofic, R.; Casadio, R.; Ciurli, S. Structure-Based Computational Study of the Catalytic and Inhibition Mechanisms of Urease. *J. Biol. Inorg. Chem.* **2001**, *6*, 300–314.
- (131) Khan, K. M.; Ali, M.; Wadood, A.; Zaheer-ul-Haq; Khan, M.; Lodhi, M. A.; Parveen, S.; Choudhary, M. I.; Voelter, W. Molecular Modeling-Based Antioxidant Arylidene Barbiturates as Urease Inhibitors. *J. Mol. Graphics Modell.* **2011**, *30*, 153–156.
- (132) Khan, K. M.; Zia-ullah; Lodhi, M. A.; Ali, M.; Choudhary, M. I.; Atta-u-Rahman; Zaheer-ul-Haq. Successful Computer Guided Planned Synthesis of (4R)-Thiazolidine Carboxylic Acid and its 2-Substituted Analogues as Urease Inhibitors. *Mol. Diversity* **2006**, *10*, 223–231.
- (133) Khan, K. M.; Wadood, A.; Ali, M.; Zia-ullah; Zaheer-ul-Haq; Lodhi, M. A.; Parveen, S.; Choudhary, M. I.; Voelter, W. Identification of Potent Urease Inhibitors via Ligand- and Structure-Based Virtual Screening and *in vitro* Assays. *J. Mol. Graphics. Modell.* **2010**, *28*, 792–798.
- (134) Benini, S.; Rypniewski, W. R.; Wilson, K. S.; Ciurli, S.; Mangani, S. Structure-Based Rationalization of Urease Inhibition by Phosphate: Novel Insights into the Enzyme Mechanism. *J. Biol. Inorg. Chem.* **2001**, *6*, 778–790.
- (135) Jung, M. Inhibitors of Histone Deacetylase as New Anticancer Agents. *Curr. Med. Chem.* **2001**, *8*, 1505–1511.
- (136) Chen, J. S.; Faller, D. V.; Spanjaard, R. A. Short-Chain Fatty Acid Inhibitors of Histone Deacetylases: Promising Anticancer Therapeutics? *Curr. Cancer Drug Targets* **2003**, *3*, 219–236.
- (137) Suzuki, T.; Ando, T.; Tsuchiya, K.; Fukazawa, N.; Saito, A.; Mariko, Y.; Yamashita, T.; Nakanishi, O. Synthesis and Histone Deacetylase Inhibitory Activity of New Benzamide Derivatives. *J. Med. Chem.* **1999**, *42*, 3001–3003.
- (138) Breslow, R. B. S.; Gershell, L.; Miller, T. A.; Marks, P. A.; et al. U.S. Patent 51,990B1, 2003.
- (139) Marshall, J. L.; Rizvi, N.; Kauh, J.; Dahut, W.; Figuera, M.; Kang, M. H.; Fig, W. D.; Wainer, I.; Chassang, C.; Li, M. Z.; Hawkins, M. J. A Phase I Trial of Depsiteptide (FR901228) in Patients with Advanced Cancer. *J. Exp. Ther. Oncol.* **2002**, *2*, 325–332.
- (140) Finnin, M. S.; Donigian, J. R.; Cohen, A.; Richon, V. M.; Rifkind, R. A.; Marks, P. A.; Breslow, R.; Pavletich, N. P. Structures of a Histone Deacetylase Homologue Bound to the TSA and SAHA Inhibitors. *Nature* **1999**, *401*, 188–193.
- (141) (a) Miller, T. A.; Witter, D. J.; Belvedere, S. Histone Deacetylase Inhibitors. *J. Med. Chem.* **2003**, *46*, 5097–5116. (b) Thangapandian, S.; John, S.; Sakkiah, S.; Lee, K. W. Ligand and Structure Based Pharmacophore Modeling to Facilitate Novel Histone Deacetylase 8 Inhibitor Design. *Eur. J. Med. Chem.* **2010**, *45*, 4409–4417.
- (142) Monneret, C. Histone Deacetylase Inhibitors. *Eur. J. Med. Chem.* **2005**, *40*, 1–13.
- (143) Nobuko, M.; Yashunari, T.; Masaya, K.; Seiji, T.; Masamichi, I.; Takeo, N.; Minoru, T. Involvement of the Virulence Gene Products of *Yersinia Enterocolitica* in the Immune Response of Infected Mice. *Genes Cells* **2005**, *10*, 321–329.
- (144) (a) Brodeur, G. M. Neuroblastoma: Biological Insights into a Clinical Enigma. *Nat. Rev. Cancer* **2003**, *3*, 203–216. (b) Oehme, I.; Deubzer, H. E.; Wegener, D.; Pickert, D.; Linke, J. P.; Hero, B.; Kopp-Schneider, A.; Westerman, F.; Ulrich, S. M.; von Deimling, A.; Fischer, M.; Witt, O. Histone Deacetylase 8 in Neuroblastoma Tumorigenesis. *Clin. Cancer Res.* **2009**, *15*, 91–99.
- (145) Wang, D. F.; Helquist, P.; Wiech, N. L.; Wiest, O. Toward Selective Histone Deacetylase Inhibitor Design: Homology Modeling, Docking Studies, and Molecular Dynamics Simulations of Human Class I Histone Deacetylases. *J. Med. Chem.* **2005**, *48*, 6936–6947.
- (146) Sundarapandian, T.; Shalini, J.; Sugundevi, S.; Woo, L. K. Docking-Enabled Pharmacophore Model for Histone Deacetylase 8 Inhibitors and its Application in Anti-Cancer Drug Discovery. *J. Mol. Graphics Modell.* **2010**, *29*, 382–395.
- (147) Bozorgi, A. H.; Bagheri, M.; Aslebagh, R.; Rajabi, M. S. A Structure-Activity Relationship Survey of Histone Deacetylase (HDAC) Inhibitors. *Chemom. Intell. Lab. Syst.* **2013**, *125*, 132–138.
- (148) Bertand, P. Inside HDAC with HDAC Inhibitors. *Eur. J. Med. Chem.* **2010**, *45*, 2095–2116.
- (149) Vanommeslaeghe, K.; Loverix, S.; Geerlings, P.; Tourwe, D. DFT-based Ranking of Zinc-binding Groups in Histone Deacetylase Inhibitors. *Bioorg. Med. Chem.* **2005**, *13*, 6070–6082.

- (150) Chen, Y.; Jiang, Y. J.; Zhou, J. W.; Yu, Q. S.; You, Q.-D. Identification of Ligand Features Essential for HDACs Inhibitors by Pharmacophore Modeling. *J. Mol. Graphics Modell.* **2008**, *26*, 1160–1168.
- (151) Chen, Y.; Li, H.; Tang, W.; Zhu, C.; Jiang, Y.; Zou, J.; You, Q. 3D-QSAR Studies of HDACs Inhibitors using Pharmacophore-Based Alignment. *Eur. J. Med. Chem.* **2009**, *44*, 2868–2876.
- (152) Vadivelan, S.; Sinha, B. N.; Rambabu, G.; Bopanna, K.; Jagarlapudi, S. A. R. P. Pharmacophore Modeling and Virtual Screening Studies to Design Some Potential Histone Deacetylase Inhibitors as New Leads. *J. Mol. Graphics Modell.* **2008**, *26*, 935–946.
- (153) Nair, S. B.; Teli, M. K.; Pradeep, H.; Rajnikant, G. K. Computational Identification of Novel Histone Deacetylase Inhibitors by Docking Based QSAR. *Comput. Biol. Med.* **2012**, *42*, 697–705.
- (154) Juvale, D. C.; Kulkarni, V. V.; Deokar, H. S.; Wagh, N. K.; Padhye, S. B.; Kulkarni, V. M. 3D-QSAR of Histone Deacetylase Inhibitors: Hydroxamate Analogues. *Org. Biomol. Chem.* **2006**, *4*, 2858–2868.
- (155) Wagh, N. K.; Deokar, H. S.; Juvale, D. C.; Kadam, S. S.; Kulkarni, V. M. 3D-QSAR of Histone Deacetylase Inhibitors as Anticancer Agents by Genetic Function Approximation. *Indian J. Biochem. Biophys.* **2006**, *43*, 360–371.
- (156) Xie, A.; Lio, C.; Li, Z.; Ning, Z.; Hu, W.; Lu, X.; Shi, L.; Zhou, J. Quantitative Structure-Activity Relationship Study of Histone Deacetylase Inhibitors. *Curr. Med. Chem.: Anti-Cancer Agents* **2004**, *4*, 273–299.
- (157) Kalyaanamurthy, S.; Phoebe Chen, Y. P. Quantum Polarized Ligand Docking Investigation to Understand the Significance of Protonation States in Histone Deacetylase Inhibitors. *J. Mol. Graphics Modell.* **2013**, *44*, 44–53.
- (158) Wu, R.; Wang, N.; Zhou, N.; Cao, Z.; Zhang, Y. A Proton-Shuttle Reaction Mechanism for Histone Deacetylase 8 and the Catalytic Role of Metal Ions. *J. Am. Chem. Soc.* **2010**, *132*, 9471–9479.
- (159) Wang, D.; Helquist, P.; Wiest, O. Zinc Binding in HDAC Inhibitors: a DFT study. *J. Org. Chem.* **2007**, *72*, 5446–5449.
- (160) Tavakol, H. Computational Study of Simple and Water-assisted Tautomerism of Hydroxamic Acids. *J. Mol. Struct. (THEOCHEM)* **2009**, *916*, 172–179.
- (161) Wu, R.; Lu, Z.; Cao, Z.; Zhang, Y. Zinc Chelation with Hydroxamate in Histone Deacetylases Modulated by Water Access to the Linker Binding Channel. *J. Am. Chem. Soc.* **2011**, *133*, 6110–6113.
- (162) Guo, Y.; Xio, J.; Guo, Z.; Chu, F.; Cheng, Y.; Wu, S. Exploration of a Binding Mode of Indole Amide Analogue as Potent Histone Deacetylase Inhibitors and 3D-QSAR Analyses. *Bioorg. Med. Chem.* **2005**, *13*, 5424–5434.
- (163) Xiang, Y.; Zhang, L.; Zhang, Z. QSAR and Docking Studies on Different Series of Histone Deacetylase Inhibitors. *Lett. Drug Des. Discovery* **2012**, *9*, 367–378.
- (164) (a) Pontiki, A.; Hadjipavlou-Litina, D. Histone Deacetylase Inhibitors (HDACs). Structure-Activity Relationships: History and New QSAR Perspectives. *Med. Res. Rev.* **2012**, *32*, 1–165. (b) Hadjipavlou-Litina, D.; Pontiki, E. Hydroxamic Acids in Cancer and Inflammation. In *Hydroxamic Acids: A Unique Family of Chemicals with Multiple Biological Activities*; Gupta, S. P., Ed.; Springer-Verlag: Berlin Heidelberg, 2013; pp 205–240.
- (165) Kozokowski, A. P.; Chen, Y.; Gasin, A. M.; Savoy, D. N.; Billadeau, D. D.; Kim, K. H. Chemistry, Biology, and QSAR Studies of Substituted Biaryl Hydroxamates and Mercaptoacetamides as HDAC Inhibitors: Nanomolar-Potency Inhibitors of Pancreatic Cancer Cell Growth. *ChemMedChem* **2008**, *3*, 487–501.
- (166) Lan-Hargest, H.-Y.; Kaufman, R. J.; Wiech, N. L. U.S. Patent Appl. US2002143196.
- (167) Wang, D. F.; Wiest, O.; Helquist, P.; Lan-Hargest, H.-Y.; Wiech, N. L. QSAR Studies of PC-3 Cell Line Inhibition Activity of TSA and SAHA-like Hydroxamic Acids. *Bioorg. Med. Chem. Lett.* **2004**, *14*, 707–711.
- (168) Wang, D.-F.; Helquist, P.; Wiech, N. L.; Wiest, O. Toward Selective Histone Deacetylase Inhibitor Design: Homology Modeling, Docking Studies, and Molecular Dynamics Simulations of Human Class I Histone Deacetylases. *J. Med. Chem.* **2005**, *48*, 6936–6947.
- (169) Bajpai, A.; Agrawal, N.; Gupta, S. P. A Comparative 2D QSAR Study on a Series of Hydroxamic-acid Based Histone Deacetylase Inhibitors *vis-à-vis* Comparative Molecular Field Analysis (CoMFA) and Comparative Molecular Similarity Indices Analysis (CoMSIA). *Indian J. Biochem. Biophys.* **2014**, *S1*, 244–252.
- (170) Whittakar, M.; Floyd, C. D.; Brown, P.; Gearing, A. J. Design and Therapeutic Application of Matrix Metalloproteinase Inhibitors. *Chem. Rev.* **1999**, *99*, 2735–2776.
- (171) Gupta, S. P. Quantitative Structure-Activity Relationship Studies on Zinc-Containing Metalloproteinase Inhibitors. *Chem. Rev.* **2007**, *107*, 3042–3087.
- (172) Verma, R. P.; Hansch, C. Matrix Metalloproteinases (MMPs): Chemical-Biological Functions and (Q)SARs. *Bioorg. Med. Chem.* **2007**, *15*, 2223–2268 Repeated 57.
- (173) Yadav, R. K.; Gupta, S. P.; Sharma, P. K.; Patil, V. M. Recent Advances in Studies on Hydroxamates as Matrix Metalloproteinase Inhibitors: A Review. *Curr. Med. Chem.* **2011**, *18*, 1704–1722.
- (174) Gupta, S. P., Ed. *Matrix Metalloproteinase Inhibitors: Specificity of Binding and Structure-Activity Relationships: Experientia Supplementum*; Springer: Basel AG, 2012; Vol. 103.
- (175) Vargova, V.; Pytliaik, M.; Mechirova, V. Matrix Metalloproteinases. *Matrix Metalloproteinase Inhibitors: Specificity of Binding and Structure-Activity Relationships: Experientia Supplementum*; Springer: Basel AG, 2012; pp 1–34.
- (176) (a) Gupta, S. P.; Patil, V. M. Specificity of Binding with Matrix Metalloproteinases. *Matrix Metalloproteinase Inhibitors: Specificity of Binding and Structure-Activity Relationships: Experientia Supplementum*; Springer: Basel AG, 2012; pp 35–56. (b) Patil, V. M.; Gupta, S. P. Quantitative Structure-Activity Relationship Studies on Sulfonamide-based MMP Inhibitors. *Matrix Metalloproteinase Inhibitors: Specificity of Binding and Structure-Activity Relationships: Experientia Supplementum*; Springer: Basel AG, 2012; pp 177–208.
- (177) Verma, R. P. Hydroxamic Acids as Matrix Metalloproteinase Inhibitors. *Matrix Metalloproteinase Inhibitors: Specificity of Binding and Structure-Activity Relationships: Experientia Supplementum*; Springer: Basel AG, 2012; pp 137–176.
- (178) Babine, R. E.; Bender, S. L. Molecular Recognition of Protein-Ligand Complexes: Applications to Drug Design. *Chem. Rev.* **1997**, *97*, 1359–1472.
- (179) Nagase, H.; Visse, R.; Murphy, G. Structure and Function of Matrix Metalloproteinases and TIMPs. *Cardiovasc. Res.* **2006**, *69*, 562–573.
- (180) Overall, C. M.; Kleifeld, O. Towards Third Generation Matrix Metalloproteinase Inhibitors for Cancer Therapy. *Br. J. Cancer* **2006**, *94*, 941–946.
- (181) Tallant, C.; Marrero, A.; Gomis-Ruth, F. X. Matrix Metalloproteinases: Fold and Function of Their Catalytic Domains. *Biochim. Biophys. Acta* **2010**, *1803*, 20–28.
- (182) Park, H. I.; Jin, Y.; Hurst, D. R.; Monroe, C. A.; Lee, S.; Schwartz, M. A.; Sang, O. X. The Intermediate S1' Pocket of the Endometase/Matrilysin-2 Active Site Revealed by Enzyme Inhibition Kinetic Studies, Protein Sequence Analyses, and Homology Modeling. *J. Biol. Chem.* **2003**, *278*, 51646–51653.
- (183) Aureli, L.; Gioia, M.; Cerbara, I.; Monaco, S.; Fasciglione, G. F.; Marini, S.; Ascenzi, P.; Topai, A.; Coletta, M. Structural Bases for Substrate and Inhibitor Recognition by Matrix Metalloproteinases. *Curr. Med. Chem.* **2008**, *15*, 2192–2222.
- (184) Jacobson, J. A.; Jourden, J. L. M.; Miller, M. T.; Cohen, S. M. To Bind Zinc or Not to Bind Zinc: An Examination of Innovative Approaches to Improved Metalloproteinase Inhibition. *Biochim. Biophys. Acta* **2010**, *1803*, 72–94.
- (185) Gall, A.-L.; Ruff, M.; Kannan, R.; Cuniase, P.; Yiotakis, A.; Dive, V.; Rio, C. M.; Basset, P.; Moras, D. Crystal Structure of the Stromelysin-3 (MMP-11) Catalytic Domain Complexed with a Phosphinic Inhibitor Mimicking the Transition-State. *J. Mol. Biol.* **2001**, *307*, 577–586.

- (186) Johnson, A. R.; Pavlovsky, A. G.; Ortwin, D. F.; Prior, F.; Man, C. F.; Bornmeir, D. A.; Banoti, C. A.; Mueller, W. T.; McConnell, K.; Guzman, R.; Han, H. K.; Dyer, R. D. Discovery and Characterization of a Novel Inhibitor of Matrix Metalloproteinase-13 that Reduces Cartilage Damage *in vivo* Without Joint Fibroplasia Side Effects. *J. Biol. Chem.* **2007**, *282*, 27781–27791.
- (187) Supuran, C. T.; Scozzafava, A. Matrix Metalloproteinases (MMPs). In *Proteinase and Peptidase Inhibition; Recent Potential Targets for Drug Development*; Smith, H. J., Simons, C., Eds.; Taylor and Francis: London and New York, 2002; pp 35–61.
- (188) Pirard, B. Insight into the Structural Determinants for Selective Inhibition of Matrix Metalloproteinases. *Drug Discovery Today* **2007**, *15/16*, 640–646.
- (189) Terp, G. E.; Cruciani, G.; Christensen, I. T.; Jørgensen, F. S. Structural Differences of Matrix Metalloproteinases with Potential Implications for Inhibitor selectivity Examined by the GRID/CPCA Approach. *J. Med. Chem.* **2002**, *45*, 2675–2684.
- (190) Lukacova, V.; Zhang, Y.; Mackov, M.; Baricic, P.; Raha, S.; Calvo, J. A.; Balaz, S. Similarity of Binding Sites of Human Matrix Metalloproteinases. *J. Biol. Chem.* **2004**, *279*, 14194–14200.
- (191) Yang, S. M.; Scannevin, R. H.; Wang, B.; Burke, S. L.; Wilson, L. J.; Karnachi, P.; Rhodes, K. J.; Lagu, B.; Murray, W. V. Beta-N-Biaryl Ether Sulfonamide Hydroxamates as Potent Gelatinase Inhibitors: Part 1. Design, Synthesis, and Lead Identification. *Bioorg. Med. Chem. Lett.* **2008**, *18*, 1135–1139.
- (192) Tuccinardi, T.; Nuti, E.; Ortore, G.; Rossello, A.; Auramova, S. I.; Martinelli, A. Development of a Receptor-Based 3D-QSAR Study for the Analysis of MMP2, MMP3, and MMP9 Inhibitors. *Bioorg. Med. Chem.* **2008**, *16*, 7749–7758.
- (193) Xi, L.; Du, J.; Li, S.; Li, J.; Liu, H.; Yao, X. A Combined Molecular Modeling Study on Gelatinases and Their Potent Inhibitors. *J. Comput. Chem.* **2010**, *31*, 24–42.
- (194) Nicolotti, O.; Miscioscia, T. F.; Leonetti, F.; Muncipinto, G.; Carotti, A. Screening of Matrix Metalloproteinases Available from the Protein Data Bank: Insights into Biological Functions, Domain Organization, and Zinc Binding Groups. *J. Chem. Inf. Model.* **2007**, *47*, 2439–2448.
- (195) Consonni, V.; Todeschini, R.; Pavan, M.; Gramitica, P. Structure/Response Correlations and Similarity/Diversity Analysis by GETAWAY Descriptors. 2. Application of the Novel 3D Molecular Descriptors to QSAR/QSPR Studies. *J. Chem. Inf. Comput. Sci.* **2002**, *42*, 693–705.
- (196) O'Brien, P. M.; Ortwin, D. F.; Pavlovsky, A. G.; Picard, J. A.; Sliskovic, D. R.; Roth, B. D.; Dyer, R. D.; Johnson, L. L.; Man, C. F.; Hallak, H. Structure-Activity Relationships and Pharmacokinetic Analysis for a Series of Potent, Systemically Available Biphenylsulfonamide Matrix Metalloproteinase Inhibitors. *J. Med. Chem.* **2000**, *43*, 156–166.
- (197) Amin, E. A.; Welsh, W. J. Three-Dimensional Quantitative Structure-Activity Relationship (3D-QSAR) Models for a Novel Class of Piperazine-Based Stromelysin-1 (MMP-3) Inhibitors: Applying a “Divide and Conquer” Strategy. *J. Med. Chem.* **2001**, *44*, 3849–3855.
- (198) Amin, E. A.; Welsh, W. J. Highly Predictive CoMFA and CoMSIA Models for Two Series of Stromelysin-1 (MMP-3) Inhibitors Elucidate S1' and S1-S2' Binding Modes. *J. Chem. Inf. Model.* **2006**, *46*, 1775–1783.
- (199) Cheng, M.; De, B.; Pikul, S.; Almstead, N. G.; Natchus, M. G.; Anastasio, M. V.; McPhall, S. J.; Snider, C. E.; Taiwo, Y. O.; Chen, L.; Dunaway, C. M.; Gu, F.; Dowty, M. E.; Mieling, G. E.; Janusz, M. J.; Wang-Weigand, S. Design and Synthesis of Piperazine-Based Matrix Metalloproteinase Inhibitors. *J. Med. Chem.* **2000**, *43*, 369–380.
- (200) Tsai, K.-C.; Lin, T.-H. A Ligand-Based Molecular Modeling Study on some Matrix Metalloproteinase-1 Inhibitors Using Several 3D QSAR Techniques. *J. Chem. Inf. Comput. Sci.* **2004**, *44*, 1857–71.
- (201) Cheng, M.; De, B.; Almstead, N. G.; Pikul, S.; Dowty, M. E.; Dietsch, C. R.; Dunaway, C. M.; Gu, F.; Hsieh, L. C.; Janusz, M. J.; Taiwo, Y. O.; Natschus, M. G.; Hudlicky, T.; Mandel, M. Design, Synthesis, and Biological Evaluation of Matrix Metalloproteinase Inhibitors Derived from a Modified Proline Scaffold. *J. Med. Chem.* **1999**, *42*, 5426–5436.
- (202) Matter, H.; Schwab, W.; Barbier, D.; Billen, G.; Haase, B.; Neises, B.; Schudok, M.; Thorwat, W.; Schreuder, H.; Brachvogel, V.; Lönze, P.; Weithman, K. U. Quantitative Structure-Activity Relationship of Human Neutrophil Collagenase (MMP-8) Inhibitors Using Comparative Molecular Field Analysis and X-ray Structure Analysis. *J. Med. Chem.* **1999**, *42*, 1908–1920.
- (203) Natchus, M. G.; Bookland, R. G.; De, B.; Almstead, N. G.; Pikul, S.; Janusz, M. J.; Heitmeyer, S. A.; Hookfin, E. B.; Hsieh, L. C.; Dowty, M. E.; Dietsch, C. R.; Patel, V. S.; Garver, S. M.; Gu, F.; Pokross, M. E.; Meiling, G. E.; Baker, T. R.; Foltz, D. J.; Peng, S. X.; Borne, D. M.; Strojnowski, M. J.; Taiwo, Y. O. Development of New Hydroxamate Matrix Metalloproteinase Inhibitors Derived from Functionalized 4-Aminoprolines. *J. Med. Chem.* **2000**, *43*, 4948–4963.
- (204) Fernández, M.; Caballero, J.; Tundidor-Camba, A. Linear and Nonlinear QSAR Studies of N-Hydroxy-2-[(Phenylsulfonyl) Amino]-Acetamide Derivatives as Matrix Metalloproteinase Inhibitors. *Bioorg. Med. Chem.* **2006**, *14*, 4137–4150.
- (205) Fernández, M.; Caballero, J. QSAR Modeling of Matrix Metalloproteinase Inhibition by N-Hydroxy-Alpha-Phenylsulfonylacetamide Derivatives. *Bioorg. Med. Chem.* **2007**, *15*, 6298–6310.
- (206) Hanessian, S.; Bouzbouz, S.; Boudon, A.; Tucker, G. C.; Payroulan, D. Picking the S1, S1' and S2' Pockets of Matrix Metalloproteinases. A Niche for Potent Acyclic Sulfonamide Inhibitors. *Bioorg. Med. Chem. Lett.* **1999**, *9*, 1691–1696.
- (207) Hanessian, S.; Moitessier, N.; Gauchet, C.; Viau, M. N-Aryl Sulfonyl Homocysteine Hydroxamate Inhibitors of Matrix Metalloproteinases: Further Probing of the S(1), S(1)', and S(2)' Pockets. *J. Med. Chem.* **2001**, *44*, 3066–3073.
- (208) Hanessian, S.; Mackay, D. B.; Moitessier, N. Design and Synthesis of Matrix Metalloproteinase Inhibitors Guided by Molecular Modeling. Picking the S (1) Pocket Using Conformationally Constrained Inhibitors. *J. Med. Chem.* **2001**, *44*, 3074–3082.
- (209) Welch, A. R.; Holman, C. M.; Huber, M.; Brenner, M. C.; Browner, M. F.; Van Wart, H. E. Understanding the P1' Specificity of the Matrix Metalloproteinases: Effect of S1' Pocket Mutations in Matrilysin and Stromelysin-1. *Biochemistry* **1996**, *35*, 10103–10109.
- (210) Chen, L.; Rydel, T. J.; Gu, F.; Dunaway, M.; Pikul, S.; McDow Dunham, K.; Barnett, B. L. Crystal Structure of the Stromelysin Catalytic Domain at 2.0 Å Resolution: Inhibitor-Induced Conformational Changes. *J. Mol. Biol.* **1999**, *293*, 545–557.
- (211) Lovejoy, B.; Welch, A. R.; Carr, S.; Luong, C.; Broka, C.; Hendricks, R. T.; Campbell, J. A.; Walker, K. A. M.; Martin, R.; Van Wart, H.; Browner, M. F. Crystal Structures of MMP-1 and -13 Reveal the Structural Basis for Selectivity of Collagenase Inhibitors. *Nat. Struct. Biol.* **1999**, *3*, 217–221.
- (212) Rowsell, S.; Hawtin, P.; Minshull, C. A.; Jepson, H.; Brockbank, S. M. V.; Barrat, D. G.; Slater, A. M.; McPheat, W. L.; Waterson, D.; Henney, A. M.; Paupit, R. A. Crystal Structure of Human MMP9 in Complex with a Reverse Hydroxamate Inhibitor. *J. Mol. Biol.* **2002**, *319*, 173–181.
- (213) (a) Gupta, S. P.; Maheshwaran, B.; Pande, V.; Kumar, D. A Comparative QSAR Study on Carbonic Anhydrase and Matrix Metalloproteinase Inhibition by Sulfonylated Amino Acid Hydroxamates. *J. Enzyme Inhib. Med. Chem.* **2003**, *18*, 7–13. (b) Kumar, D.; Gupta, S. P. A Quantitative Structure-Activity Relationship Study on Some Matrix Metalloproteinase and Collagenase Inhibitors. *Bioorg. Med. Chem.* **2003**, *11*, 421–426. (c) Gupta, S. P.; Kumaran, S. Quantitative Structure-Activity Relationship Studies on Matrix Metalloproteinase Inhibitors: Hydroxamic Acid Analogs. *Med. Chem.* **2006**, *2*, 243–250. (d) Gupta, S. P.; Kumaran, S. A Quantitative Structure-Activity Relationship Study on Some Series of Anthranilic Acid-Based Matrix Metalloproteinase Inhibitors. *Bioorg. Med. Chem.* **2005**, *13*, 5454–5462. (e) Kumaran, S.; Gupta, S. P. A Quantitative Structure-Activity Relationship Study on Matrix Metalloproteinase Inhibitors: Piperidine Sulfonamide Aryl Hydroxamic Acid Analogs. *J. Enzyme Inhib. Med. Chem.* **2007**, *22*, 23–27. (f) Kumaran, S.; Gupta, S. P. A Quantitative Structure-Activity Relationship Study on Some Novel

- Series of Hydroxamic Acid Analogs Acting as Matrix Metalloproteinase Inhibitors. *Med. Chem.* **2007**, *3*, 167–173. (g) Gupta, S. P.; Kumaran, S. Quantitative Structure-Activity Relationship Studies on Benzodiazepine Hydroxamic Acid Inhibitors of Matrix Metalloproteinases and Tumor Necrosis Factor- α Converting Enzyme. *Asian J. Biochem.* **2006**, *1*, 47–56. (h) Gupta, S. P.; Kumaran, S. Quantitative Structure-Activity Relationship Studies on Matrix Metalloproteinase Inhibitors: Bicyclic Heteroaryl Hydroxamic Acid Analogs. *Lett. Drug Des. Discovery* **2005**, *2*, 522–528. (i) Gupta, S. P.; Kumaran, S. Quantitative Structure-Activity Relationship Studies on Matrix Metalloproteinase Inhibitors: Piperazine, Piperidine and Diazepine Hydroxamic Acid Analogs. *Asian J. Biochem.* **2006**, *1*, 211–223. (j) Gupta, S. P.; Bagaria, P.; Kumar Satuluri, V. S. A Quantitative Structure-Activity Relationship Study on a Series of Hydroxamic Acid Analogs Acting as Matrix Metalloproteinase Inhibitors. *Lett. Drug. Des. Discovery* **2008**, *5*, 281–285.
- (214) Becker, J. W.; Marcy, A. I.; Rokosz, L. L.; Axel, M. G.; Burbbaum, J. J.; Fitzgerald, P. M.; Cameron, P. M.; Esser, C. K.; Hagman, W. K.; Hermes, J. D. Stromelysin-1: Three-Dimensional Structure of the Inhibited Catalytic Domain and of the C-Truncated Proenzyme. *Protein Sci.* **1995**, *4*, 1966–1976.
- (215) Leung, D.; Abbenante, G.; Fairlie, D. P. Protease Inhibitors: Current Status and Future Prospects. *J. Med. Chem.* **2000**, *43*, 305–341.
- (216) Matter, H.; Schwab, W. Affinity and Selectivity of Matrix Metalloproteinase Inhibitors: A Chemometrical Study from the Perspective of Ligands and Proteins. *J. Med. Chem.* **1999**, *42*, 4506–4523.
- (217) Scozzafava, A.; Supuran, C. T. Carbonic Anhydrase and Matrix Metalloproteinase Inhibitors: Sulfonated Amino Acid Hydroxamates with MMP Inhibitory Properties Act as Efficient Inhibitors of CA Isozymes I, II, and IV, and N-Hydroxysulfonamides Inhibit Both These Zinc Enzymes. *J. Med. Chem.* **2000**, *43*, 3677–3687.
- (218) Martin, M. F.; Beckett, R. P.; Bellamy, C. L.; Courtney, P. F.; Davies, S. J.; Drummond, A. H.; Dodd, R.; Pratt, L. M.; Patel, S. R.; Ricketts, M. L.; Todd, R. S.; Tuffnell, A. R.; Ward, J. W. S.; Whittaker, M. The Synthesis and Biological Evaluation of Non-Peptidic Matrix Metalloproteinase Inhibitors. *Bioorg. Med. Chem. Lett.* **1999**, *9*, 2887–2892.
- (219) Levin, J. I.; Chen, J. M.; Cheung, K.; Cole, D.; Crago, C.; Santos, E. D.; Du, X.; Khafizova, G.; MacEwan, G.; Niu, C.; Salaski, E. J.; Zask, A.; Cummons, T.; Sung, A.; Xu, W.; Ayral-Kaloustian, S.; Jin, G.; Cowling, R.; Barone, D.; Mohler, K. M.; Black, R. A.; Skotnicki, J. S. Acetylenic TACE inhibitors. Part 1. SAR of the Acyclic Sulfonamide Hydroxamates. *Bioorg. Med. Chem. Lett.* **2003**, *13*, 2799–2803.
- (220) Gowravaram, M. R.; Tomczuk, B. E.; Johnson, J. S.; Delecki, D.; Cook, E. R.; Ghose, A. K.; Mathiowitz, A. M.; Spurlino, J. C.; Rubin, B.; Smith, D. L.; Pulvino, T.; Wahl, R. C. Inhibition of Matrix Metalloproteinases by Hydroxamates Containing Heteroatom-Based Modifications of the P1' Group. *J. Med. Chem.* **1995**, *38*, 2570–2581.
- (221) Fray, M. J.; Dickinson, R. P. Discovery of Potent and Selective Succinyl Hydroxamate Inhibitors of Matrix Metalloprotease-3 (Stromelysin-1). *Bioorg. Med. Chem. Lett.* **2001**, *11*, 571–574.
- (222) MacPherson, L. J.; Bayburt, E. K.; Capparelli, M. P.; Carroll, B. J.; Goldstein, R.; Justice, M. R.; Zhu, L.; Hu, S.-L.; Melton, R. A.; Fryer, L.; Goldberg, R. L.; Doughty, J. R.; Spirito, S.; Blancuzzi, V.; Wilson, D.; O'Byrne, E. M.; Ganu, V.; Parker, D. T. Discovery of CGS 27023A, a Non-Peptidic, Potent, and Orally Active Stromelysin Inhibitor That Blocks Cartilage Degradation in Rabbits. *J. Med. Chem.* **1997**, *40*, 2525–2532.
- (223) Levin, J. I.; Chen, J.; Du, M.; Hogan, M.; Kincaid, S.; Nelson, F. C.; Venkatesh, A. M.; Wehr, T.; Zask, A.; DiJoseph, J.; Killar, L. M.; Skala, S.; Sung, A.; Sharr, M.; Roth, C.; Jin, G.; Cowling, R.; Mohler, K. M.; Black, R. A.; March, C. J.; Skotnicki, J. S. The Discovery of Anthranilic Acid-Based MMP Inhibitors. Part 2: SAR of the S-Position and P1(1) Groups. *Bioorg. Med. Chem. Lett.* **2001**, *11*, 2189–2192.
- (224) (a) Barta, T. E.; Becker, D. P.; Bedell, L. J.; De Crescenzo, G. A.; McDonald, J. J.; Munie, G. E.; Rao, S.; Shieh, H. S.; Stegeman, R.; Stevens, A. M.; Villamil, C. I. Synthesis and Activity of Selective MMP Inhibitors with an Aryl Backbone. *Bioorg. Med. Chem. Lett.* **2000**, *10*, 2815–2817. (b) Barta, T. E.; Becker, D. P.; Bedell, L. J.; De Crescenzo, G. A.; McDonald, J. J.; Mehta, P.; Munie, G. E.; Villamil, C. I. Selective, Orally Active MMP Inhibitors with an Aryl Backbone. *Bioorg. Med. Chem. Lett.* **2001**, *11*, 2481–2483.
- (225) Scozzafava, A.; Supuran, C. T. Protease Inhibitors: Synthesis of Potent Bacterial Collagenase and Matrix Metalloproteinase Inhibitors Incorporating N-4-Nitrobenzylsulfonylglycine Hydroxamate Moieties. *J. Med. Chem.* **2000**, *43*, 1858–1865.
- (226) Zask, A.; Gu, Y.; Albright, J. D.; Du, X.; Hogan, M.; Levin, J. I.; Chen, J. M.; Killar, L. M.; Sung, A.; DiJoseph, J. F.; Sharr, M. A.; Roth, C. E.; Skala, S.; Jin, G.; Cowling, R.; Mohler, K. M.; Barone, D.; Black, R.; March, C.; Skotnicki, J. S. Synthesis and SAR of Bicyclic Heteroaryl Hydroxamic Acid MMP and TACE Inhibitors. *Bioorg. Med. Chem. Lett.* **2003**, *13*, 1487–1490.
- (227) Levin, J. I.; DiJoseph, J. F.; Killar, L. M.; Sung, A.; Walter, T.; Sharr, M. A.; Roth, C. E.; Skotnicki, J. S.; Albright, J. D. The Synthesis and Biological Activity of a Novel Series of Diazepine MMP Inhibitors. *Bioorg. Med. Chem. Lett.* **1998**, *8*, 2657–2662.
- (228) Aranapakam, V.; Davis, J. M.; Grosu, G. T.; Baker, J.; Ellingboe, J.; Zask, A.; Levin, J. I.; Sandanayaka, V. P.; Du, M.; Skotnicki, J. S.; DiJoseph, J. F.; Sung, A.; Sharr, M. A.; Killar, L. M.; Walter, T.; Jin, G.; Cowling, R.; Tillett, J.; Zhao, W.; McDevitt, J.; Xu, Z. B. Synthesis and Structure-Activity Relationship of N-Substituted 4-Arylsulfonylpiperidine-4-Hydroxamic Acids as Novel, Orally Active Matrix Metalloproteinase Inhibitors for the Treatment of Osteoarthritis. *J. Med. Chem.* **2003**, *46*, 2376–2396.
- (229) Noe, M. C.; Natarajan, V.; Snow, S. L.; Wolf-Gouveia, L. A.; Mitchell, P. G.; Lopresti Morrow, L.; Reeves, L. M.; Yocum, S. A.; Oterness, I.; Bliven, M. A.; Carty, T. J.; Barberia, J. T.; Sweeney, F. J.; Liras, J. L.; Vaughn, M. Discovery of 3-OH-3-Methylpiperolic Hydroxamates: Potent Orally Active Inhibitors of Aggrecanase and MMP-13. *Bioorg. Med. Chem. Lett.* **2005**, *15*, 3385–3388.
- (230) Cheng, M.; De, B.; Pikul, S.; Almstead, N. G.; Natchus, M. G.; Anastasio, M. V.; Mcphail, S. J.; Snider, C. E.; Taiwo, Y. O.; Chen, L.; Dunaway, C. M.; Gu, F.; Dowty, M. E.; Mieling, G. E.; Janusz, M. J.; Wang-Weigand, S. Design and Synthesis of Piperazine-Based Matrix Metalloproteinase Inhibitors. *J. Med. Chem.* **2000**, *43*, 369–380.
- (231) Holmes, J.; Mast, K.; Marcotte, P.; Elmore, I.; Li, J.; Pease, L.; Glaser, K.; Morgan, D.; Michaelides, M.; Davidsen, S. Discovery of Selective Hydroxamic Acid Inhibitors of Tumor Necrosis Factor-Alpha Converting Enzyme. *Bioorg. Med. Chem. Lett.* **2001**, *11*, 2907–10.
- (232) Roy, K.; Pal, D. K.; De, A. U.; Sengupta, C. QSAR of Matrix Metalloproteinase Inhibitor N-[*Substituted Phenyl*]Sulfonyl-N-4-Nitrobenzylglycine Hydroxamates Using LFER Model. *Drug. Des. Discovery* **2001**, *17*, 315–23.
- (233) Wasserman, Z. R.; Duan, J. J.; Voss, M. E.; Xue, C. B.; Cherney, R. J.; Nelson, D. J.; Hardman, K. D.; Deccico, C. P. Identification of a Selectivity Determinant for Inhibition of Tumor Necrosis Factor-Alpha Converting Enzyme by Comparative Modeling. *Chem. Biol.* **2003**, *10*, 215–223.
- (234) Maskos, K.; Fernandez-Catalan, C.; Huber, R.; Bourenkov, G. P.; Bartnik, H.; Elestad, G. A.; Reddy, P.; Wolfson, M. F.; Rauch, C. T.; Castner, B. J.; Davis, R.; Clarke, H. R. G.; Petersen, M.; Fitzner, J. N.; Ceretti, D. P.; March, C. J.; Paxton, R. J.; Black, R. A.; Bode, W. Crystal Structure of the Catalytic Domain of Human Tumor Necrosis Factor-Alpha-Converting Enzyme. *Proc. Natl. Acad. Sci. U.S.A.* **1998**, *95*, 3408–3412.
- (235) Park, K.; Aplaska, A.; Du, M. T.; Sun, L.; Zhu, Y.; Zhang, Y.; Levin, J. I. Design and Synthesis of Butynyoxyphenyl β -Sulfone Piperidine Hydroxamates as TACE Inhibitors. *Bioorg. Med. Chem. Lett.* **2006**, *16*, 3927–3931.
- (236) Levin, J. I.; Chen, J. M.; Laasko, L. M.; Du, M.; Schmid, J.; Xu, W.; Cummons, T.; Xu, J.; Jin, G.; Barone, D.; Skotnicki, J. S. Acetylenic TACE Inhibitors. Part 3: Thiomorpholine Sulfonamide Hydroxamates. *Bioorg. Med. Chem. Lett.* **2006**, *16*, 1605–1609.
- (237) Levin, J. I.; Chen, J. M.; Laasko, L. M.; Du, M.; Du, X.; Venkatesan, A. M.; Sandanayaka, V.; Zask, A.; Xu, J.; Xu, W.; Zhang, Y.; Skotnicki, J. S. Acetylenic TACE Inhibitors. Part 2: SAR of Six-

- membered Cyclic Sulfonamide Hydroxamates. *Bioorg. Med. Chem. Lett.* **2005**, *15*, 4345–4349.
- (238) Tsukida, T.; Moriyana, H.; Inoue, Y.; Kondo, H.; Yoshino, K.; Nishimura, S. Synthesis and Biological Activity of Selective Azasugar-based TACE Inhibitors. *Bioorg. Med. Chem. Lett.* **2004**, *14*, 1569–1572.
- (239) Fisher, J. F.; Mobashery, S. Recent Advances in MMP Inhibitor Design. *Cancer Metastasis Rev.* **2006**, *25*, 115–136.
- (240) Bandarage, U. K.; Wang, T.; Come, J. H.; Perola, E.; Wei, Y.; Rao, B. G. Novel Thiol-Based TACE Inhibitors. Part 2: Rational Design, Synthesis, and SAR of Thiol-Containing Aryl Sulfones. *Bioorg. Med. Chem. Lett.* **2008**, *18*, 44–48.
- (241) Rao, B. G.; Bandarage, U. K.; Wang, T.; Come, J. H.; Perola, E.; Wei, Y.; Trian, S. K.; Saunders, J. O. Novel Thiol-based TACE Inhibitors: Rational Design, Synthesis, and SAR of Thiol-containing Aryl Sulfonamides. *Bioorg. Med. Chem. Lett.* **2007**, *17*, 2250–2253.
- (242) Shepek, J. E., II; Gilmore, J. L.; Tebben, A.; Xue, C. B.; Liu, R. Q.; Decicco, C. P.; Duan, J. J. Hydantoins, Triazolones, and Imidazolones as Selective Non-hydroxamate Inhibitors of Tumor Necrosis Factor-Alpha Converting Enzyme (TACE). *Bioorg. Med. Chem. Lett.* **2007**, *17*, 2769–2774.
- (243) Duan, J. J.; Chen, L.; Lu, Z.; Jiang, B.; Asakawa, N.; Shepek, J. E., II; Liu, R. Q.; Covington, M. B.; Pitts, W.; Kim, S. H.; Decicco, C. P. Discovery of Low Nanomolar Non-hydroxamate Inhibitors of Tumor Necrosis Factor-Alpha Converting Enzyme (TACE). *Bioorg. Med. Chem. Lett.* **2007**, *17*, 266–271.
- (244) Shepek, J. E., II; Gilmore, J. L.; Yang, A.; Chen, X. T.; Xue, C. B.; Roderick, J.; Liu, R. Q.; Covington, M. B.; Decicco, C. P.; Duan, J. J. Discovery of Novel Hydantoins as Selective Non-hydroxamate Inhibitors of Tumor Necrosis Factor-Alpha Converting Enzyme (TACE). *Bioorg. Med. Chem. Lett.* **2007**, *17*, 1413–1417.
- (245) Shepek, J. E., II; Tebben, A.; Gilmore, J. L.; Yang, A.; Washeman, Z. R.; Decicco, C. P.; Duan, J. J. A Molecular Modeling Analysis of Novel Non-hydroxamate Inhibitors of TACE. *Bioorg. Med. Chem. Lett.* **2007**, *17*, 1408–1412.
- (246) Murumkar, P. R.; Giridhar, R.; Yadav, M. R. 3D-Quantitative Structure-Activity Relationship Studies on Benzothiadiazepine Hydroxamates as Inhibitors of Tumor Necrosis Factor-Alpha Converting Enzyme. *Chem. Biol. Drug Des.* **2008**, *71*, 363–373.
- (247) Murumkar, P. R.; DasGupta, S.; Zambre, V. P.; Giridhar, R.; Yadav, M. R. Development of Predictive 3D-QSAR CoMFA and CoMSIA Models for Beta-Aminohydroxamic Acid-Derived Tumor Necrosis Factor-Alpha Converting Enzyme Inhibitors. *Chem. Biol. Drug Des.* **2009**, *73*, 97–107.
- (248) Cong, Y.; Yang, X.; Lu, W.; Xue, Y. Prediction of Novel and Selective TNF-Alpha Converting Enzyme (TACE) Inhibitors and Characterization of Correlative Molecular Descriptors by Machine Learning Approaches. *J. Mol. Graphics Modell.* **2009**, *28*, 236–244.
- (249) Yang, J. S.; Chun, K.; Park, J. E.; Cho, M.; Seo, J.; Song, D.; Yoon, H.; Park, C.-H.; Joe, B.-Y.; Choi, J.-H.; Kim, M.-H.; Han, G. Structure Based Optimization of Chromen-Based TNF- α Converting Enzyme (TACE) Inhibitors on S1' Pocket and Their Quantitative Structure-Activity Relationship (QSAR) Study. *Bioorg. Med. Chem.* **2010**, *18*, 8618–8629.
- (250) Cherney, R. J.; Duan, J. J.; Voss, M. E.; Chen, L.; Wang, L.; Meyer, D. T.; Wasserman, Z. R.; Hardman, K. D.; Liu, R. Q.; Covington, M. B.; Qian, M.; Mandlekar, S.; Christ, D. D.; Trzasokos, J. M.; Newton, R. C.; Magolda, R. L.; Wexler, R. R.; Decicco, C. P. Design, Synthesis, and Evaluation of Benzothiadiazepine Hydroxamates as Selective Tumor Necrosis Factor-Alpha Converting Enzyme Inhibitors. *J. Med. Chem.* **2003**, *46*, 1811–1823.
- (251) (a) Gilmore, J. L.; King, B. W.; Harris, C.; Maduskuie, T.; Mercer, S. E.; Liu, R. Q.; Covington, M. B.; Qian, M.; Ribadeneria, M. D.; Vaddi, K.; Trzaskos, J. M.; Newton, R. C.; Decicco, C. P.; Duan, J. J. W. Synthesis and Structure-Activity Relationship of a Novel, Achiral Series of TNF-Alpha Converting Enzyme Inhibitors. *Bioorg. Med. Chem. Lett.* **2006**, *16*, 2699–2704. (b) Chen, X. T.; Ghavimi, B.; Corbett, R. L.; Xue, C. B.; Liu, R. Q.; Covington, M. B.; Qian, M.; Vaddi, K. G.; Christ, D. D.; Hartman, K. D.; Ribadeneria, M. D.;
- Trzaskos, J. M.; Newton, R. C.; Decicco, C. P.; Duan, J. J. W. A New 4-(2-Methylquinolin-4-ylmethyl)phenyl P1' Group for the Beta-Amino Hydroxamic Acid Derived TACE Inhibitors. *Bioorg. Med. Chem. Lett.* **2007**, *17*, 1865–1870.
- (252) Duan, J. J. W.; Chen, L.; Wasserman, J. R.; Lu, Z.; Liu, R. Q.; Covington, M. B.; Qian, M.; Hardman, K. D.; Magolda, R. L.; Newton, R. C.; Christ, D. D.; Wexler, R. R.; Decicco, C. P. Discovery of Gamma-Lactam Hydroxamic Acids as Selective Inhibitors of Tumor Necrosis Factor Alpha Converting Enzyme: Design, Synthesis, and Structure-Activity Relationships. *J. Med. Chem.* **2002**, *45*, 4954–4957.
- (253) Niu, X.; Umland, S.; Ingram, R.; Beyer, B. M.; Liu, Y. H.; Sun, J.; Lundell, D.; Orth, P. IK682, a Tight Binding Inhibitor of TACE. *Arch. Biochem. Biophys.* **2006**, *451*, 43–50.
- (254) Murumkar, P. R.; Zambre, V. P.; Yadav, M. R. Development of Predictive Pharmacophore Model for in Silico Screening and 3D QSAR CoMFA and CoMSIA Studies for Lead Optimization for Designing of Potent Tumor Necrosis Factor-Alpha Converting Enzyme Inhibitors. *J. Comput.-Aided Mol. Des.* **2010**, *24*, 143–156.
- (255) Dixon, S. L.; Smolyrev, A. M.; Knoll, E. H.; Rao, S. N.; Shaw, D. E.; Friesner, R. A. PHASE: a New Engine for Pharmacophore Perception, 3D QSAR Model Development, and 3D Database Screening: 1. Methodology and Preliminary Results. *J. Comput.-Aided Mol. Des.* **2006**, *20*, 647–671.
- (256) Bond, M. D.; Van Wart, H. E. Characterization of the Individual Collagenases from *Clostridium histolyticum*. *Biochemistry* **1984**, *23*, 3085–3071.
- (257) Matsushita, O.; Jung, C. M.; Minami, J.; Katayama, S.; Nishi, N.; Okable, A. A Study of the Collagen-Binding Domain of a 116-kDa *Clostridium histolyticum* Collagenase. *J. Biol. Chem.* **1998**, *273*, 3643–3648.
- (258) Matsushita, O.; Jung, C. M.; Minami, J.; Katayama, S.; Nishi, N.; Okable, A. Gene Duplication and Multiplicity of Collagenases in *Clostridium histolyticum*. *J. Bacteriol.* **1999**, *181*, 923–933.
- (259) Groos, E. B. In *Cornea: Fundamentals of Corneals and External Disease*; Kracher, J. H., Mannis, M. J., Holland, E. J., Eds.; Mosby-Year Book: St. Louis, MO, 1997; Vol. 6, pp 105–142.
- (260) Reidy, J. J.; Gebhardt, B. M.; Kaufman, H. E. The Collagen Shield. A New Vehicle for Delivery of Cyclosporin A to the Eye. *Cornea* **1990**, *9*, 196–199.
- (261) Van Wart, H. E. Clostridium Collagenases. In *Handbook of Proteolytic Enzymes*; Barret, A. J., Rawlings, N. D., Woessner, J. F., Eds.; Academic Press: London (CD-ROM), 1998; Chapter 368.
- (262) Scozzafava, A.; Supuran, C. T. Protease Inhibitors: Synthesis of *Clostridium Histolyticum* Collagenase Inhibitors Incorporating Sulfonyl-L-Alanine Hydroxamate Moieties. *Bioorg. Med. Chem. Lett.* **2000**, *10*, 499–502.
- (263) Scozzafava, A.; Supuran, C. T. Protease Inhibitors. Part 7. Inhibition of *Clostridium Histolyticum* Collagenase with Sulfonated Derivatives of L-Valine Hydroxamate. *Eur. J. Pharm. Sci.* **2000**, *10*, 67–76.
- (264) Scozzafava, A.; Supuran, C. T. Protease Inhibitors. Part 8: Synthesis of Potent *Clostridium Histolyticum* Collagenase Inhibitors Incorporating Sulfonated L-Alanine Hydroxamate Moieties. *Bioorg. Med. Chem.* **2000**, *8*, 637–645.
- (265) Scozzafava, A.; Supuran, C. T. Protease Inhibitors - Part 5. Alkyl/Arylsulfonyl- and Arylsulfonylureido-/Arylureido-Glycine Hydroxamate Inhibitors of *Clostridium Histolyticum* Collagenase. *Eur. J. Med. Chem.* **2000**, *35*, 299–307.
- (266) Gupta, S. P.; Kumaran, S. A Quantitative Structure-Activity Relationship Study on *Clostridium Histolyticum* Collagenase Inhibitors: Roles of Electropotential State Indices. *Bioorg. Med. Chem.* **2003**, *11*, 3065–3071.
- (267) Kier, L. B.; Hall, L. H. *Molecular Structure Descriptors: Electropotential State Indices*; Academic Press: San Diego, CA, 1999.
- (268) Jeng, A. Y.; Chou, M.; Parker, D. T. Sulfonamide-Based Hydroxamic Acids as Potent Inhibitors of Mouse Macrophage Metalloelastase. *Bioorg. Med. Chem. Lett.* **1998**, *8*, 897–902.
- (269) Hannessian, S.; Bouzbouz, S.; Boudan, A.; Tucker, G. C.; Payroulan, D. Picking the S1, S1' and S2' Pockets of Matrix

- Metalloproteinases. A Niche for Potent Acyclic Sulfonamide Inhibitors. *Bioorg. Med. Chem. Lett.* **1999**, *9*, 1691–1696.
- (270) Scozzafava, A.; Supuran, C. T. Protease Inhibitors: Synthesis of Matrix Metalloproteinase and Bacterial Collagenase Inhibitors Incorporating 5-Amino-2-Mercapto-1,3,4-Thiadiazole Zinc Binding Functions. *Bioorg. Med. Chem. Lett.* **2002**, *12*, 2667–2672.
- (271) Jamlok, A.; Karthikeyan, C.; Hari Narayan Murthy, N. S.; Trivedi, P. QSAR Analysis of Some 5-Amino-2-Mercapto-1,3,4-Thiadiazole Based Inhibitors of Matrix Metalloproteinases and Bacterial Collagenase. *Bioorg. Med. Chem. Lett.* **2006**, *16*, 3847–3854.
- (272) Young, R. N. Dual Inhibition of Cyclooxygenase-2 (COX-2) and 5-Lipoxygenase (5-LOX) as a New Strategy to Provide Safer Non-steroidal Anti-inflammatory Drugs. *Eur. J. Med. Chem.* **2003**, *38*, 645–659.
- (273) Julemont, F.; Dogne, J. M.; Laeckmann, D.; Pirotte, B.; de Leval, X. Recent Developments in 5-Lipoxygenase Inhibitors. *Expert Opin. Ther. Pat.* **2003**, *13*, 1–13.
- (274) Peters-Golden, M.; Brock, T. G. 5-Lipoxygenase and FLAP. *Prostaglandins, Leukotrienes and Essential Fatty Acids* **2003**, *69*, 99–109.
- (275) Werz, O.; Steinhilber, D. Development of 5-Lipoxygenase Inhibitors—Lessons from Cellular Enzyme Regulation. *Biochem. Pharmacol.* **2005**, *70*, 327–333.
- (276) Gillmor, S.; Villasenor, A.; Fetherick, R.; Sigal, E.; Browner, M. The structure of Mammalian 15-Lipoxygenase Reveals Similarity to the Lipases and the Determinants of Substrate Specificity. *Nat. Struct. Biol.* **1997**, *4*, 1003–1009.
- (277) Minor, W.; Steczko, J.; Stec, B.; Otwinowski, Z.; Bolin, J.; Walter, R.; Axelrod, B. Crystal Structure of Soybean Lipoxygenase L-1 at 1.4 Å Resolution. *Biochemistry* **1996**, *35*, 10687–10701.
- (278) Boyington, J.; Gaffney, B.; Amzel, L. The Three-dimensional Structure of an Arachidonic Acid 15-Lipoxygenase. *Science* **1993**, *260*, 1482–1486.
- (279) Pham, C.; Jankun, J.; Skrzypczak-Jankun, E.; Flowers, R.; Funk, M. Structural and Thermochemical Characterization of Lipoxygenase-catechol Complexes. *Biochemistry* **1998**, *37*, 17952–17957.
- (280) Skrzypczak-Jankun, E.; Amzel, L.; Kroha, B.; Funk, M. Structure of Soybean Lipoxygenase L3 and a Comparison with its L1 Isoenzyme. *Proteins* **1997**, *29*, 15–31.
- (281) Hemak, J.; Gale, D.; Brock, T. J. Structural Characterization of the Catalytic Domain of the Human 5-Lipoxygenase Enzyme. *J. Mol. Model.* **2002**, *8*, 102–112.
- (282) Aparoy, P.; Reddy, R. N.; Guruparasad, L.; Reddy, M. R.; Reddanna, P. Homology Modeling of 5-Lipoxygenase and Hints for Better Inhibitor Design. *J. Comput.-Aided Mol. Des.* **2008**, *22*, 611–9.
- (283) Charlier, C.; Hinichart, J.-P.; Durant, F.; Wouters, J. Structural Insights into Human 5-Lipoxygenase Inhibition: Combined Ligand-based and Target-based Approach. *J. Med. Chem.* **2006**, *49*, 186–195.
- (284) Schwarz, K.; Walter, M.; Anton, M.; Gerth, C.; Feussner, I.; Kuha, H. Structural Basis for Lipoxygenase Specificity. Conversion of the Human Leukocyte 5-Lipoxygenase to a 15-Lipoxygenating Enzyme Species by Site-directed Mutagenesis. *J. Biol. Chem.* **2001**, *276*, 773–779.
- (285) Kalva, S.; Saleena L. M.; Vadivelan, S.; Sarma, A. R. P. J. *International Conference on Biophysics, Biochemistry and Bioinformatics; IPCBEE*, 2011; Vol. S.
- (286) Gilbert, N. C.; Bartlett, S. G.; Waugh, M. T.; Neau, D. B.; Boegl, W. E.; Brash, A. R.; Newcomer, M. E. The Structure of Human 5-Lipoxygenase. *Science* **2011**, *331*, 217–219.
- (287) Eren, G.; Maccharulo, A.; Banoglu, E. From Molecular Docking to 3D-Quantitative Structure-Activity Relationships (3D-QSAR): Insights into the Binding Mode of 5-Lipoxygenase Inhibitors. *Mol. Inf.* **2012**, *31*, 123–134.
- (288) Verdonk, M. L.; Cole, J. C.; Hartshorn, M. J.; Murray, C. W.; Taylor, R. D. Improved Protein-Ligand Docking Using GOLD. *Proteins* **2003**, *52*, 609–623.
- (289) Summers, J. B.; Kim, K. H.; Mazdiyasni, H.; Holmes, J. H.; Ratajczyk, J. D.; Stewart, A. O.; Dyer, R. D.; Carter, G. W. Hydroxamic Acid Inhibitors of 5-Lipoxygenase: Quantitative Structure-Activity Relationships. *J. Med. Chem.* **1990**, *33*, 992–998.
- (290) Gupta, S. P.; Gupta, J. K. Quantitative Structure-Activity Relationship Study on Some 5-Lipoxygenase Inhibitors. *J. Enzyme Inhib.* **1990**, *3*, 179–188.
- (291) Pontiki, E.; Hadjipavlou-Litina, D. Lipoxygenase Inhibitors: a Comparative QSAR Study Review and Evaluation of New QSARs. *Med. Res. Rev.* **2008**, *28*, 39–117.
- (292) Agrawal, V. K.; Bano, S.; Khadikar, P. V. QSAR Study on 5-Lipoxygenase Inhibitors Using Distance-based Topological Indices. *Bioorg. Med. Chem.* **2003**, *11*, 5519–5527.
- (293) Van't Riet, B.; Wampler, G. L.; Elford, H. L. Synthesis of Hydroxy- and Amino-substituted Benzohydroxamic Acids: Inhibition of Ribonucleotide Reductase and Antitumor Activity. *J. Med. Chem.* **1979**, *22*, 589–592.
- (294) Shao, J.; Zhoce, B.; Zhu, L.; Bilbo, A. J.; Su, L.; Yuan, Y. C.; Ren, S.; Lien, E. J.; Shih, J.; Yen, Y. Determination of the Potency and Subunit-Selectivity of Ribonucleotide Reductase Inhibitors with a Recombinant-Holoenzyme-based *in vitro* Assay. *Biochem. Pharmacol.* **2005**, *69*, 627–634.
- (295) Shao, J.; Zhou, B.; Chu, B.; Yen, Y. Ribonucleotide Reductase Inhibitors and Future Drug Design. *Curr. Cancer Drug Targets* **2006**, *6*, 409–431.
- (296) Koneru, P. B.; Lien, E. J.; Avramis, B. I. Synthesis and Testing of New Antileukemic Schiff Bases of N-Hydroxy-N'-Aminoguanidine Against CCRF-CEM/0 Human Leukemia Cells *in vitro* and Synergism Studies with Cytarabine (Ara-C). *Pharm. Res.* **1993**, *10*, 515–520.
- (297) Tang, A.; Lien, E. J.; Lia, M. M. Optimization of the Schiff Bases of N-Hydroxy-N'-Aminoguanidine as Anticancer and Antiviral Agents. *J. Med. Chem.* **1985**, *28*, 1103–1106.
- (298) Tang, A.; Lien, E. J.; Lia, M. M. Optimization of the Schiff Bases of N-Hydroxy-N'-Aminoguanidine as Anticancer and Antiviral Agents. *J. Med. Chem.* **1985**, *28*, 1103–1106.
- (299) Ren, S.; Wang, R.; Komatsu, K.; Bonaz-Krause, P.; Zyrianov, Y.; McKenna, C. E.; Csiple, C.; Tokes, Z. A.; Lien, E. J. Synthesis, Biological Evaluation, and Quantitative Structure-Activity Relationship Analysis of New Schiff Bases of Hydroxysemicarbazide as Potential Antitumor Agents. *J. Med. Chem.* **2002**, *45*, 410–419.
- (300) Fylaktakidou, K. C.; Hadjipavlou-Litina, D. J.; Litinas, K. E.; Varelle, E. A.; Nicolaides, D. N. Recent Developments in the Chemistry and in the Biological Applications of Amidoximes. *Curr. Pharm. Des.* **2008**, *14*, 1001–1047.
- (301) Nocentini, G. Ribonucleotide Reductase Inhibitors: New Strategies for Cancer Chemotherapy. *Crit. Rev. Concol. Hematol.* **1996**, *22*, 89–126.
- (302) Tsimberidou, A. M.; Alvarado, Y.; Giles, F. J. Evolving Role of Ribonucleotide Reductase Inhibitors in Hematologic Malignancies. *Expert Rev. Anticancer Ther.* **2002**, *2*, 437–448.
- (303) Cerqueira, N. M.; Pereira, S.; Fernandes, P. A.; Ramos, M. J. Overview of Ribonucleotide Reductase Inhibitors: An Appealing Target in Anti-tumour Therapy. *Curr. Med. Chem.* **2005**, *12*, 1283–1294.
- (304) Basu, A.; Sinha, B. N.; Saiko, P.; Graser, G.; Szekeres, T. N-Hydroxy-N'-Aminoguanidines as Anti-cancer Lead Molecule: QSAR, Synthesis and Biological Evaluation. *Bioorg. Med. Chem. Lett.* **2011**, *21*, 3324–3328.
- (305) van't Riet, B.; Wampler, G. L.; Elford, H. L. Synthesis of Hydroxy and Amino-Substituted Benzohydroxamic Acids: Inhibition of Ribonucleotide Reductase and Antitumor Activity. *J. Med. Chem.* **1979**, *22*, 589–592.
- (306) Gale, G. R.; Hynes, J. B. Effects of Certain Arylhydroxamic Acids on Deoxyribonucleic Acid Synthesis by Ehrlich Ascites Tumor Cells *In-vitro*. *J. Med. Chem.* **1968**, *11*, 191–194.
- (307) Gale, G. R.; Hynes, J. B.; Smith, A. B. Synthesis of Additional Arylhydroxamic Acids which Inhibit Nucleic Acid Biosynthesis *In-vitro*. *J. Med. Chem.* **1970**, *13*, 571–574.
- (308) Elford, H. L. Inhibition of Ribonucleotide Reductase by Analogs of Hydroxyurea and Their Effect on L1210 Leukemia. *Proc. Am. Assoc. Cancer Res.* **1977**, *18*, 177–177.

- (309) Elford, H. L.; Wamper, G. L.; van't Riet, B. New Ribonucleotide Reductase Inhibitors with Anti-neoplastic Activity. *Cancer Res.* **1979**, *39*, 844–851.
- (310) Van't Riet, B.; Kier, L. B.; Elford, H. L. Structure-activity Relationships of Benzohydroxamic Acid Inhibitors of Ribonucleotide Reductase. *J. Pharm. Sci.* **1980**, *69*, 856–857.
- (311) Kier, L. B.; Hall, L. H. *Molecular Connectivity in Chemistry and Drug Research*; Academic Press: New York, 1976.
- (312) Kier, L. B.; Hall, L. H. General Definition of Valence Delta-values for Molecular Connectivity. *J. Pharm. Sci.* **1983**, *72*, 1170–1173.
- (313) Pontiki, E.; Hadjipavlou-Litina, D. Synthesis, Antioxidant and Antiinflammatory Activity of Novel Aryl-acetic and Aryl-hydroxamic Acids. *Arzneim.-Forsch./Drug Res.* **2003**, *53*, 780–785.
- (314) Pontiki, E.; Hadjipavlou-Litina, D.; Geromichalos, G.; Papageorgiou, A. Anticancer Activity and Quantitative-Structure Activity Relationship (QSAR) Studies of a Series of Antioxidant/Anti-inflammatory Aryl-acetic and Hydroxamic Acids. *Chem. Biol. Drug Des.* **2009**, *74*, 266–275.
- (315) Apfel, C.; Banner, D. W.; Bur, D.; Dietz, M.; Hirata, T.; Hubschwerlen, C.; Cher, H.; Page, M. G. P.; Pirson, W.; Rosse, G.; Speckin, J. L. Hydroxamic Acid Derivatives as Potent Peptide Deformylase Inhibitors and Antibacterial Agents. *J. Med. Chem.* **2000**, *43*, 2324–31.
- (316) Adams, J. M. On the Release of the Formyl Group from Nascent Protein. *J. Mol. Biol.* **1968**, *33*, 571–589.
- (317) Mazel, D.; Pochet, S.; Marliere, P. Genetic Characterization of Polypeptide Deformylase, a Distinctive Enzyme of Eubacterial Translation. *EMBO J.* **1994**, *13*, 914–23.
- (318) Mienel, T.; Blanquet, S. Characterization of the *Thermus Thermophilus* Locus Encoding Peptide Deformylase and Methionyl-tRNA (fMet) Formyltransferase. *J. Bacteriol.* **1994**, *176*, 7387–7390.
- (319) Adams, J. M.; Capecchi, M. N-formylmethionine-tRNA as Initiator of Protein Syntheses. *Proc. Natl. Acad. Sci. U.S.A.* **1996**, *93*, 147–155.
- (320) Takeda, M.; Webster, R. E. Protein Chain Initiation and Deformylation in *B. Subtilis* Homogenates. *Proc. Natl. Acad. Sci. U.S.A.* **1968**, *60*, 1487–1494.
- (321) Gupta, M. K.; Mishra, P.; Prathipati, P.; Saxena, A. K. 2D-QSAR in Hydroxamic Acid Derivatives as Peptide Deformylase Inhibitors and Antibacterial Agents. *Bioorg. Med. Chem.* **2002**, *10*, 3713–3716.
- (322) Fuerstenau, D. W.; Herra-Urbina, R. Mineral Separation by Froth Flotation. *Surfactant Sci. Ser.* **1989**, *33*, 259–320.
- (323) Natarajan, R.; Nirdosh, I. Application of Topochemical, Topostructural, Physicochemical and Geometrical Parameters to Model the Flotation Efficiencies of N-Arylhydroxamic Acids. *Int. J. Miner. Process.* **2003**, *71*, 113–129.
- (324) Natarajan, R.; Nirdosh, I.; Venuvanalingam, P.; Ramalingum, M. Quantitative Property-Property Relationship (QPPR) Approach in Predicting Flotation Efficiency of Chelating Agents as Mineral Collectors. *SAR QSAR Environ. Res.* **2002**, *13*, 499–508.
- (325) Natarajan, R.; Nirdosh, I.; Muthuswami, S. V.; Jeyaraman, R. Effect of Substituent on the Performance of Cupferron as a Collector for Uranium. *Dev. Chem. Eng. Miner. Process.* **1994**, *4*, 202–217.
- (326) www.acdlabs.com/ilab.
- (327) *The Toolkit for Estimating Physicochemical Properties of Organic Compounds*; John Wiley: New York.
- (328) LOGKOW Version 1.54b; Syracuse Research Corp.: Syracuse, NY
- (329) Natarajan, R.; Nirdosh, I.; Basak, S. C.; Mills, D. R. QSAR Modeling of Flotation Collectors Using Principal Components Extracted from Topological Indices. *J. Chem. Inf. Compt. Sci.* **2002**, *42*, 1425–1430.